Institute of Cancer and Genetics

School of Medicine

Cardiff University

Examining Telomere Dysfunction in Multiple Myeloma

A thesis submitted to the School of Medicine, Cardiff University in partial fulfilment for the degree of Doctor of Philosophy

Sam Hyatt

2017

NOTICE OF SUBMISSION OF THESIS FORM:
POSTGRADUATE RESEARCH

DECLARATION

This work has not been submitted in substance for any other degree or award at this or any other university or place of learning, nor is being submitted concurrently in candidature for any degree or other award.

Signed …… Date ……

STATEMENT 1

This thesis is being submitted in partial fulfillment of the requirements for the degree of PhD

Signed …… Date ……

STATEMENT 2

This thesis is the result of my own independent work/investigation, except where otherwise stated, and the thesis has not been edited by a third party beyond what is permitted by Cardiff University's Policy on the Use of Third Party Editors by Research Degree Students. Other sources are acknowledged by explicit references. The views expressed are my own.

Signed …… Date ……

STATEMENT 3

I hereby give consent for my thesis, if accepted, to be available online in the University's Open Access repository and for inter-library loan, and for the title and summary to be made available to outside organisations.

Signed …… Date ……

STATEMENT 4: PREVIOUSLY APPROVED BAR ON ACCESS

I hereby give consent for my thesis, if accepted, to be available online in the University's Open Access repository and for inter-library loans **after expiry of a bar on access previously approved by the Academic Standards & Quality Committee.**

Signed …… Date ……

Acknowledgements

I would like to thank my supervisors, Prof. Duncan Baird and Prof. Chris Pepper for giving me the opportunity to undertake this PhD, as well as for all their support and guidance over the past four years.

I would also like to thank Julia Grimstead and Rhiannon Robinson. Without their hard work and patience, this PhD would not have been possible. I will never understand how they put up with me for so long. Seriously, they are saints.

Thank you to everyone involved with the STELA research group: Kez Cleal, Ceri Jones, Kate Liddiard, Thet Thet Lin, Greg Ngo and Kevin Norris. I'm not going to miss the lab meetings, but I will miss all of you. Also, good luck to Alys Evans and Hélène Geiller. Remember, it's never too late to turn back.

There are also a considerable number of friends that I have made during this project, with each of them contributing to this thesis in their own way: Marie Clarke, Kayleigh Dodd, Lauren Elston, Katie Evans, Shimaz Hashimdeen, Stefan Holzhauser, Melanie Hurtz, Charlotte Johnson, Isabel Martin, Jens Mattern, James Murray, Tom Lewis, Victoria Proctor, Ellie Rad, Reiss Reid, Sara Seifan, Mel Varley and Beth Walsby. I definitely owe each of you a drink.

Thank you to my family for pretending to take an interest in my work. I know, I can't believe that it's finally over either. Now I'm going to make you read this entire thesis. Every. Last. Page.

Thank you to Amy Whittaker for reminding me that there is life outside of academia.

And most importantly, thank you to Laura Escudero. You were the best friend that I could have asked for and a tolerable housemate. I'm not sure that I could have survived this process without you. I promise that one day I will learn Spanish, right after I'm done learning Welsh.

Summary

Telomeres are repetitive nucleotide sequences of TTAGGG that cap the ends of linear eukaryotic chromosomes. Short dysfunctional telomeres have previously been identified as a driving force in cancer, resulting in chromosomal fusion and rearrangement that acts to facilitate progression of the malignancy. As it has recently been demonstrated that telomere length is an accurate predictor of clinical outcome in patients with chronic lymphocytic leukaemia (CLL), we aimed to determine whether a similar relationship existed in multiple myeloma (MM). Having used single telomere length analysis (STELA) to measure the mean XpYp telomere length of whole bone marrow aspirates from 141 MM patients, a telomere length threshold of 3.92kb was identified which could be used to stratify patients as either low- or high-risk. Incorporation of this threshold into the international staging system (ISS) for MM increased its prognostic resolution, allowing each prognostic subset to be further risk-stratified.

Having demonstrated that a shorter mean XpYp telomere length (<3.92kb) was associated with inferior patient outcome in MM, we next sought to identify a potential cause for this observation. Using clonal populations of the JJN-3 cell line, each expressing DN-hTERT, we observed that telomeric shortening resulted in a greater frequency of fusion and the initiation of a telomere-driven crisis. Cells were eventually able to escape crisis, driven by the spontaneous reactivation of telomerase which led to increasing telomere length and decreasing fusion frequency. Finally, we sought use the PARP inhibitors Rucaparib and Olaparib to prevent the escape of these clonal JJN-3 populations from a telomere-driven crisis. It was thought that PARP inhibition would interfere with the DNA repair pathways that are known to be responsible for processing telomere-deficient chromosomes. It was established that treating JJN-3 cells with either 7.50μM Rucaparib or 3.75μM Olaparib prevented their escape from a telomere-driven crisis.

Publications

Hyatt S, Jones RE, Heppel NH, Grimstead JW, Fegan C, Jackson GH, Hills R, Allan JM, Pratt G, Pepper C, Baird DM. **Telomere length is a critical determinant for survival in multiple myeloma.** Br J Haematol. 2017 Jul;178(1):94-98. doi:10.1111/bjh.14643. Epub 2017 Mar 24. PubMed PMID: 28342200.

List of Abbreviations

AEBSF	4-(2-aminoethyl)benzenesulfonyl fluoride hydrochloride
ALT	Alternative Lengthening of Telomeres
Alt-NHEJ	Alternative Non-Homologous End Joining
ANOVA	Analysis of Variance
APE1	AP-Endonuclease
APLF	Aprataxin-and-PNK-like Factor
ATM	Ataxia Telangiectasia Mutated
ATRIP	ATR-interactive protein
ATRX	Alpha Thalassemia/Mental Retardation Syndrome X-Linked
BER	Base Excision Repair
BFB	Breakage-Fusion-Bridge
bp	Base Pairs
BRCA1	Breast Cancer Type 1 Susceptibility
BRCA2	Breast Cancer Type 2 Susceptibility
BSA	Bovine Serum Albumin
CDC	Cell Division Cycle
CDK	Cyclin-Dependent Kinase
CHIP	C-Terminus of Hsc70-Interacting Protein
Chk-1	Checkpoint Kinase 1
Chk-2	Checkpoint Kinase 2
C-NHEJ	Classical Non-Homologous End Joining
CLL	Chronic Lymphocytic Leukaemia
CSB	Cockayne Syndrome B
CTE	C-Terminal Extension
DAPI	4',6-diamidino-2-phenylindole
DAXX	Death-Domain Associated
DKC	Dyskeratosis Congenita
D-Loop	Displacement Loop
DMEM	Dulbecco’s Modified Eagle’s Medium
DMSO	Dimethyl Sulfoxide
DNA	Deoxyribonucleic acid
DNA-PKcs	DNA-Dependent Protein Kinase
DN-hTERT	Dominant Negative Human Telomerase Reverse Transcriptase

dNTP	Deoxyribonucleotide
DSB	Double-Strand Break
DSBR	Double-Strand Break Repair
EDTA	Ethylenediaminetetraacetic Acid
EXO1	Exonuclease 1
FCS	Foetal Calf Serum
FDG-PET	Fluorine 18 Fluorodeoxyglucose Positron Emission Tomography
FGFR	Fibroblast Growth Factor Receptor
FEN1	Flap Endonuclease 1
FISH	Fluorescence *in situ* Hybridisation
GFP	Green Fluorescent Protein
GGR	Global Genome Repair
HCl	Hydrochloric Acid
HDAC	Histone Deacetylase
HT Q-FISH	High Throughput Quantitative Fluorescent *in situ* Hybridisation
HR	Homologous Recombination
HR	Hazard Ratio
kb	Kilobases
LDH	Lactate Dehydrogenase
Ig	Immunoglobulin
IL	Interleukin
ISS	International Staging System
mAB	Monoclonal Antibody
MAR	Mono (ADP-Ribose)
MGUS	Monoclonal Gammopathy of Undetermined Significance
MHC	Major Histocompatibility Complex
MHL1	MutL Homolog 1
MIP-1α	Macrophage Inflammatory Protein-1α
MM	Multiple Myeloma
MMQ-PCR	Monochrome Multiplex Quantitative Polymerase Chain Reaction
MR	Magnetic Resonance
MRN	MRE11-RAD50-NBS1
MZ	Marginal Zone
NaOH	Sodium Hydroxide
NER	Nucleotide Excision Repair

NHEJ	Non-Homologous End Joining
NICE	National Institute for Health and Care Excellence
OB	oligonucleotide/oligosaccharide-binding
ORC1	Origin Recognition Complex
PAR	Poly (ADP-Ribose)
PARP	Poly (ADP-Ribose) Polymerase
PBMC	Peripheral Blood Mononuclear Cells
PBS	Phosphate-Buffered Saline
PCR	Polymerase Chain Reaction
PD	Population Doubling
PCL	Plasma Cell Leukaemia
PCNA	Proliferating Cell Nuclear Antigen
PI3K	Phosphoinositide 3-Kinase
PMS2	Post-Meiotic Segregation Protein-2
PMSF	Phenylmethylsulfonyl fluoride
POT1	Protection of Telomeres 1
Q-FISH	Quantitative Fluorescent *in situ* Hybridisation
Q-PCR	Quantitative Polymerase Chain Reaction
RANKL	Receptor Activator of NF-κB ligand
RAP1	Repressor Activator Protein 1
Rb	Retinoblastoma
RFC	Replication Factor C
R-ISS	Revised International Staging System
ROS	Reactive Oxygen Species
RPMI	Roswell Park Memorial Institute
RNA	Ribonucleic Acid
RPA	Replication Protein A
RT	Reverse Transcriptase
SDS	Sodium Dodecyl Sulfate
SDSA	Synthesis-Dependent Strand Annealing
Sir	Silent Information Regulator
SNP	Single-Nucleotide Polymorphism
STELA	Single Telomere Length Analysis
TAE	Tris-acetate-EDTA
TCR	Transcript Coupled Repair

TEN	Telomerase Essential N-Terminal
TERC	Telomerase RNA Component
TERRA	Telomeric Repeat-Containing RNA
TERT	Telomerase Reverse Transcriptase
TFIIH	Transcription Factor IIH
T_H	T Helper
TIN2	TRF1-interacting Nuclear Factor 2
T-Loop	Telomere Loop
TNK1	Tankyrase-1
TNK2	Tankyrase-2
TOPBP1	Topoisomerase 2-Binding Protein 1
TPE	Telomeric Position Effect
TPG	Total Product Generated
TPP1	TIN2/PTOP/PIP1
TRBD	Telomerase RNA Binding
TRF	Terminal Restriction Fragment
TRF1	Telomeric Repeat-Binding Factor 1
TRF2	Telomeric Repeat-Binding Factor 2
TVR	Telomeric Variant Repeat
UV-DDB	UV-Damaged DNA-Binding
VCD	Velcade, Cyclophosphamide and Dexamethasone
VD	Velcade and Dexamethasone
VTD	Velcade, Thalidomide and Dexamethasone
WM	Waldenstrom’s Macroglobulinemia
WT1	Wilm’s Tumour Suppressor

Table of Contents

Chapter 2 – Materials and Methods

Chapter 3 – Using the Mean XpYp Telomere Length of Whole Bone Marrow Aspirates as a Prognostic Indicator in Multiple Myeloma

Chapter 4 – The Role of a Telomere-Driven Crisis in Generating Chromosomal Instability in Multiple Myeloma

Chapter 1

Introduction

1.1 Telomere Structure and Function

The telomere was first described by Hermann Muller in 1938. Using *Drosophila melanogaster*, it was demonstrated that a structure existed at the chromosomal ends which offered protection from genetic alteration. Unlike the rest of the genome, chromosomal ends did not undergo translocations or inversions when exposed to ionising radiation (Muller, 1938). Soon after this, Barbara McClintock utilised *Zea mays* as a model to identify the telomere as a protective cap which was necessary for preventing the fusion of chromosomal ends (McClintock 1941). Since then, it has been established that the telomere is a repetitive double-stranded nucleotide sequence which terminates in a short single-stranded overhang. This sequence recruits a protein complex to the telomere, initiating the formation of a looped structure. It is in this way that the telomere prevents a DNA damage response from being triggered, inhibiting the erroneous repair of chromosomal ends which would otherwise result in genetic rearrangement and instability.

1.1.1 The Telomeric Sequence

In humans, the repetitive nucleotide sequence that makes up the telomere is primarily composed of the hexameric sequence TTAGGG and tandemly repeated into arrays extending for up to 25kb depending on the tissue analysed (Capper et al. 2007; Griffith et al. 1999). However, telomeres vary in both sequence and length depending on the organism being examined. For example, most plants share the telomeric sequence TTTAGGG which can range from 2-4kb (Adams et al. 2001; Bundock, van Attikum, and Hooykaas 2002). Meanwhile, the budding yeast telomeric sequence is an irregular

structure of T(G_{1-3}) repeats which stretches for ~350bp (McEachern and Blackburn 1994; Kupiec 2014).

In humans, telomeres are found at both the short p-arm and long q-arm of the chromosome (***see figure 1.1***). The telomeric sequence of TTAGGG is well conserved throughout vertebrates, although this is not the only nucleotide sequence that can be found within a telomere. Telomeric variant repeats (TVRs) exist which are primarily localised to the most centromeric 2kb region of the telomere. Examples of nucleotide sequences that make up the human TVR include TGAGGG, TTGGGG and TCAGGG (Coleman, Baird, and Royle 1999; Baird et al. 2000). These TVR sequences are not thought to provide the same telomeric function as TTAGGG, with studies showing that telomeres lose their protective capacity once a telomere has shortened to within the TVR region (Capper et al. 2007). The presence of certain TVR sequences, most notably CTAGGG, has also been associated with telomeric instability (Mendez-Bermudez et al. 2009). However, the telomere is not simply defined by its nucleotide sequence. Various proteins are bound to the telomere, most notably those comprising the shelterin complex, which are crucial for shaping its structure and maintaining its protective function.

1.1.2 The Shelterin Complex

The human shelterin complex is a collection of six telomere-associated proteins; TRF1, TRF2, TIN2, RAP1, TPP1 and POT1. Together, these proteins induce the formation of the t-loop structure (***see figure 1.1***) which ensures that chromosomal ends are not mistakenly recognised as double-strand DNA breaks (Liu et al. 2004).

1.1.2.1 Telomeric Repeat-binding Factor 1 (TRF1)

TRF1 exists as a homodimer and localises to double-stranded telomeric sequences. Its main function is to regulate telomere length by blocking the binding of telomerase, a ribonucleoprotein which is responsible for the synthesis of telomeric repeats at the 3′ end

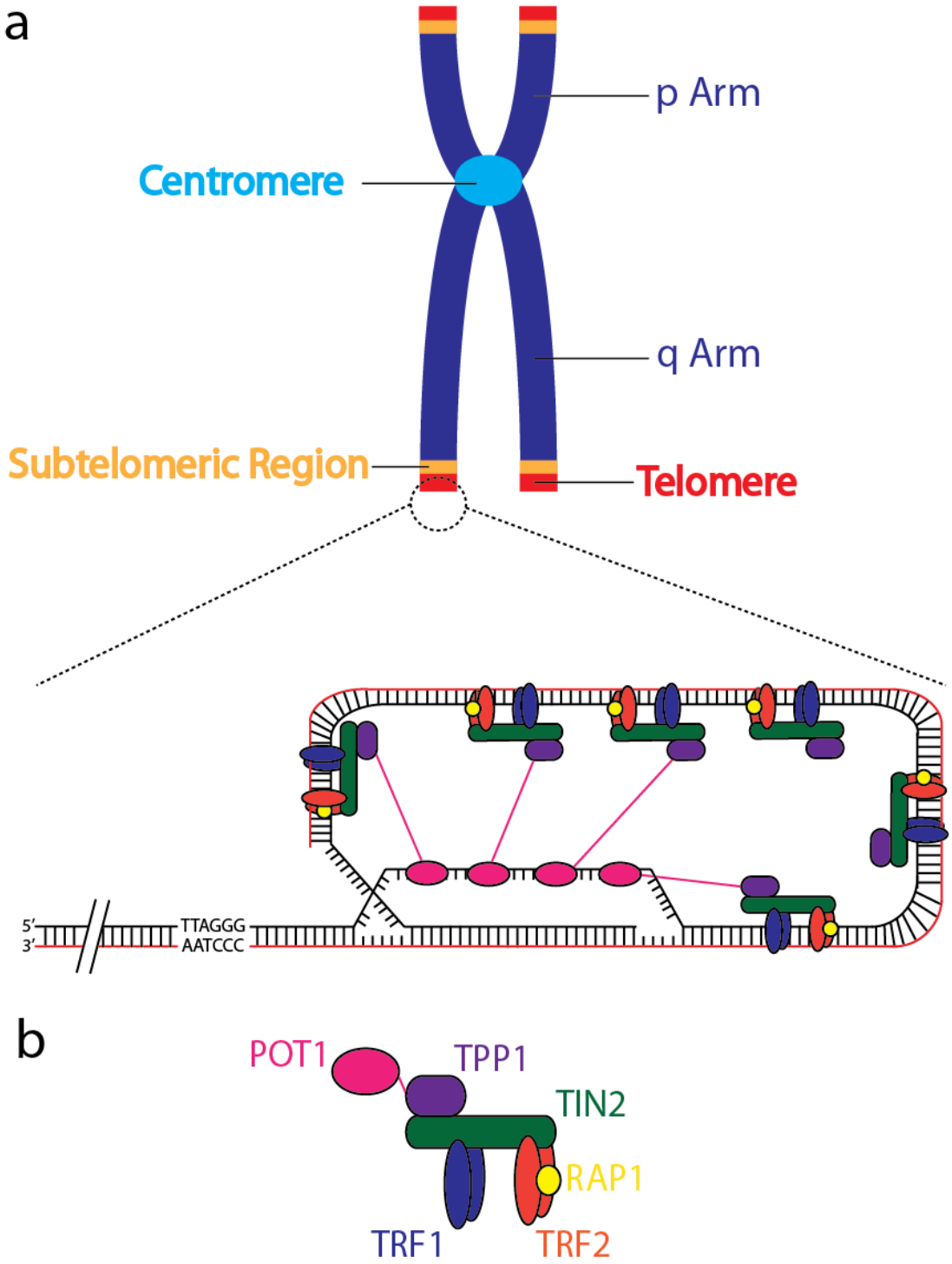

Figure 1.1 - The Telomere and Shelterin Complex
(a) Telomeres are repetative nucleotide sequences of TTAGGG which cap the ends of linear chromosomes. The 3′ end forms an overhang which can fold back and insert itself within the double-stranded section of the telomere (T-loop). This structure is stabalised by the shelterin complex and acts to prevent the chromosomal ends from being recognised as a double-strand break. **(b)** Shelterin is a complex of proteins which binds to double-stranded telomeric repeats; Telomeric Repeat-binding Factor 1 (TRF1), Telomeric Repeat-binding Factor 2 (TRF2), TRF1-interacting Nuclear Factor 2 (TIN2), Repressor Activator Protein 1 (RAP1), TIN2/PTOP/PIP1 (TPP1) and Protection of Telomeres 1 (POT1). These induce the formation of the T-loop structure which prevents the activation of an ATR- and ATM-mediated DNA damage response. The pink line between POT1 and TPP1 simply demonstrates that these two structures are directly linked. *Adapted from 'T-loops and the origin of telomeres' DeLange, Nature Reviews Molecular Cell Biology 5, 324 (2004)*

of a telomere (Ancelin et al. 2002). This is likely achieved via the recruitment of POT1 to the telomere which is known to inhibit telomerase activity (Xin et al. 2007). Artificially reducing the expression of TRF1 has been shown to cause telomere lengthening, while TRF1 overexpression results in telomere shortening (van Steensel and de Lange 1997). The binding of TRF1 at the telomere is thought to be regulated by PARP5a and PARP5b, also known as tankyrase-1 (TNK1) and tankyrase-2 (TNK2) respectively. These proteins act to positively regulate telomere length by modifying TRF1, preventing its binding to the telomere and instead allowing telomere synthesis by telomerase (Smith and de Lange 2000). It is this way that telomere length is maintained, with a homeostasis existing between TRF1 binding and TRF1 dissociation at the telomere.

1.1.2.2 Telomeric Repeat-binding Factor 2 (TRF2)

Like TRF1, TRF2 also exists as a homodimer and localises to double-stranded telomeric sequences. However, TRF2 is responsible for stabilising the t-loop structure which sequesters the single-stranded telomeric end and prevents it from being mistakenly identified as double-strand DNA breaks (Doksani et al. 2013). It is in this way that TRF2 also acts as a negative regulator of telomere length, shielding the telomere from elongation by telomerase (Smogorzewska et al. 2000). TRF2 works to inhibit signalling by the ATM-mediated DNA damage response pathway which would otherwise trigger non-homologous end joining (NHEJ) at the chromosomal ends (Herbig et al. 2004). Deletion of TRF2 results in the formation of chromosomal fusion events, effectively eliminating the end-capping function of the telomere (van Steensel, Smogorzewska, and de Lange 1998). These fusion events are not dependent on telomere length, with even long telomeres generating a ATM-mediated DNA damage response if TRF2 is not present (Celli and de Lange 2005).

1.1.2.3 TRF1-interacting Nuclear Factor 2 (TIN2)

TIN2 does not directly bind DNA, but instead acts as a bridge between the TRF1 and TRF2 subunits. It also binds to the TPP1 subunit, which is itself bound to POT1 (Kim et

al. 2004). Overexpression of TIN2 results in telomere shortening, while TIN2 suppression causes telomere elongation (Kim, Kaminker, and Campisi 1999; Ye and de Lange 2004). This may be explained by the ability of TIN2 to prevent the modification of TRF1 by tankyrase proteins, thus prohibiting TRF1 dissociation from the telomere and inhibiting the binding of telomerase (Ye and de Lange 2004).

1.1.2.4 Repressor Activator Protein 1 (RAP1)

RAP1 binds to the TRF2 protein, although its purpose within the shelterin complex is disputed. Deletion of the gene encoding RAP1 failed to induce genomic abnormalities or generate significant telomere dysfunction in human cell lines. Data also exists which appears to suggest that RAP1 does not play a role in telomere length regulation (Kabir, Hockemeyer, and de Lange 2014). However, contradictory reports demonstrate that overexpressing RAP1 results in telomere elongation (Li, Oestreich, and de Lange 2000). RAP1 is also thought to play a role in preventing NHEJ in telomere-deficient senescent cells (Benarroch-Popivker et al. 2016). Furthermore, it has been suggested that RAP1 reduces the binding affinity of TRF2 for DNA, acting to regulate the selectivity of TRF2 to specific areas within the telomere (Janouskova et al. 2015).

1.1.2.5 TIN2/PTOP/PIP1 (TPP1)

TPP1 is necessary for linking together POT1 and TIN2, as well as localising POT1 to the telomere. Knockout studies identify TPP1 as a negative regulator of telomere length, likely due to the ability of TPP1-bound POT1 to inhibit telomerase activity (Ye et al. 2004). However, phosphorylation of TPP1 was shown to be responsible for the direct recruitment of telomerase to telomeres. It is thought that this mechanism of TPP1-modification acts to regulate telomere length by recruiting either POT1 or telomerase when necessary (Zhang et al. 2013; Zhong et al. 2012).

1.1.2.6 Protection of Telomeres 1 (POT1)

POT1 rarely binds to the double-stranded telomeric sequence, instead binding almost exclusively to the single-stranded 3′-overhang of TTAGGG repeats at the end of a telomere (Takai et al. 2010). While it is recruited to the shelterin complex by TPP1, this association is not strictly necessary for POT1 binding to the telomere. However, TPP1 is known to significantly increase the affinity of POT1 for telomeric DNA (Colgin et al. 2003; Xin et al. 2007). Around 50-100 copies of POT1 are thought to be present at each telomere, with this shelterin subunit being responsible for stabilising the t-loop structure that protects the telomeric ends from being recognised as double-strand DNA breaks (Takai et al. 2010). It has been demonstrated in knockdown studies that loss of POT1 results in telomere elongation and chromosomal fusion (Kelleher, Kurth, and Lingner 2005; Veldman, Etheridge, and Counter 2004). As a negative regulator of telomere length, POT1 preferentially binds to the telomeric sequence 5′-TTAGGGTTAG-3′ at the 3′-overhang. This limits the access of telomerase to the terminal G residue of a telomere and inhibits elongation (Lei, Podell, and Cech 2004). POT1 also plays a role in preventing an ATR-mediated DNA damage response which would otherwise trigger aberrant homologous recombination at the telomere end (Thanasoula et al. 2012).

1.1.2.7 Mutations in Shelterin Components

Germline and somatic mutations involving shelterin proteins have been associated with predisposition to various cancers and diseases. For example, a single amino acid deletion in the TPP1 protein has been associated with compromised telomerase recruitment and the development of Hoyeraal-Hreidarsson syndrome (Kocak et al. 2014), a severe form of dyskeratosis congenita (***see section 1.4.2 – Critically Shortened Telomeres***). A R282H mutation in TIN2 has also been associated with dyskeratosis congenita and Revesz syndrome (Savage et al. 2008).

Meanwhile, POT1 germline mutations have mostly been associated with the increased incidence of cancer. Familial glioma has been associated with a D617E mutation in POT1 which disrupts the binding of TPP1, as have G95C and E450X mutations (Bainbridge et al. 2015). A rare S270N mutation in POT1 has also been observed in a small number of familial cutaneous malignant melanoma cases, resulting in carriers having an increased telomere length and more fragile telomeres (Shi et al. 2014). Familial chronic lymphocytic leukaemia (CLL) is associated with loss-of-function mutations in POT1, with a Y36C mutation disrupting the interaction between POT1 and the telomeric overhang (Speedy et al. 2016).

1.1.3 The T-Loop Structure

Although much of the telomere is comprised of double-stranded DNA, the most distal 50-200bp are single-stranded (Wright et al. 1997; Makarov, Hirose, and Langmore 1997). These TTAGGG repeats make up the G-rich 3′-overhang (otherwise known as the G-tail) which is able to fold back and insert itself, utilising a TRF2-dependent mechanism, within the upstream double-stranded section of the telomere. This sequesters the G-tail away from cellular repair pathways that would otherwise seek to trigger a DNA damage response after detecting an unprotected chromosomal end (Griffith et al. 1999; Doksani et al. 2013). The displaced strand of the previously-double-stranded telomere is known as the D-loop and is stabilised by the binding of POT1 (Lei, Podell, and Cech 2004; Loayza et al. 2004). Unwinding of the t-loop in preparation of DNA replication is performed by RTEL1, a helicase which is recruited to the telomere during S-phase by TRF2 (Sarek et al. 2015).

1.1.4 The Subtelomeric Region

A subtelomeric region exists between each telomere and the chromosome-specific sequence, ranging from 10-300kb in humans (***see figure 1.2***). These regions are comprised of diverse ‘blocks’ of nucleotide sequences whose order varies between the

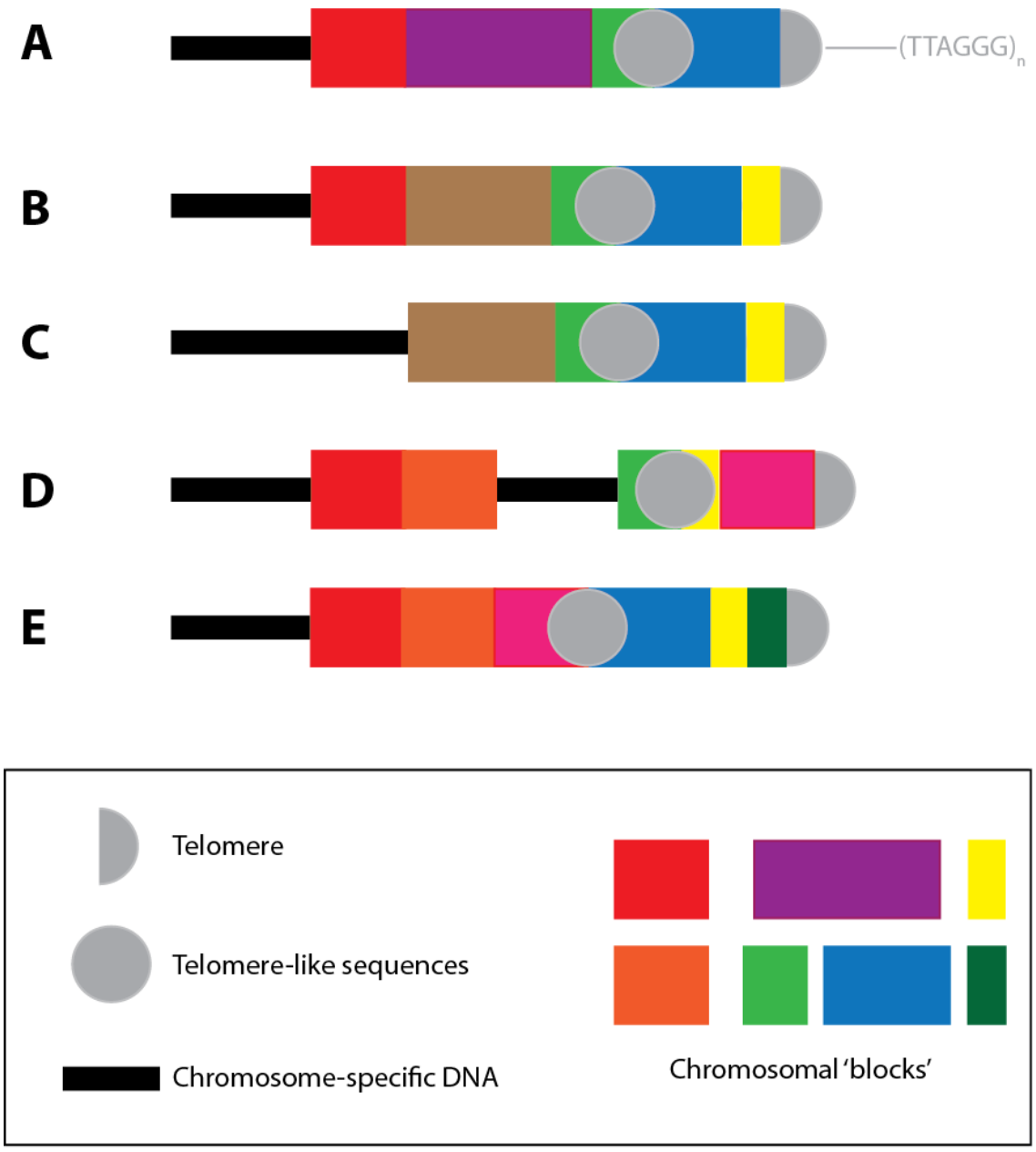

Figure 1.2 - The Subtelomeric Region
Examples of the different ways in which subtelomeric regions can be structured. These regions of diverse 'blocks' of nucleotide sequences can vary greatly. $(TTAGGG)_n$-like regions are common and range in size from 24-823 base pairs. Chromosomes B and C are examples of homologues which differ in subtelomeric content. Chromosome E is an example of subtelomeric region which contains a unique sequence, a feature which has been exploited during the development of STELA. *Adapted from 'The complex structure and dynamic evolution of human subtelomeres' Mafford and Trask, Nature Reviews Genetics 3, 91-102 (February 2002)*

subtelomeric regions of each chromosome (Mefford and Trask 2002). Certain sequences may even be unique to a specific subtelomeric region, a feature which has been exploited to allow the development of a novel PCR-based technique for measuring telomere length *(**see section 1.3.5 - Single Telomere Length Analysis***). Mapping data for the subtelomeric regions of each chromosome has also identified several $(TTAGGG)_n$-like sequences which range in size from 24 to 823bp (Riethman et al. 2004).

1.1.5 Telomere Function

The telomeres cap the ends of linear chromosomes and act to protect genomic DNA from erroneous DNA repair, rearrangement and erosion. They also function as a biological clock, triggering senescence after a set number of cell divisions. It is in this way that the telomeres are thought of as a tumour suppressive mechanism.

1.1.5.1 Protection from DNA Repair Pathways

The sources of DNA damage are multiple, but their effects are almost universally identical. From ionising radiation to chemical carcinogens, each causes the bonds between nucleotides in double-stranded DNA to break. Without a targeted repair mechanism, these DNA ends are at risk of undergoing fusion with other damaged sections of the genome. This can then result in genomic rearrangement and chromosomal instability (Helleday, Eshtad, and Nik-Zainal 2014). In humans, the homologous recombination and non-homologous end joining pathways (***see section 1.6.2 – Double-strand DNA breaks***) are responsible for the recognition and repair of double-strand DNA breaks (Chapman, Taylor, and Boulton 2012). However, these pathways are unable to distinguish between a legitimate double-strand DNA break and the unprotected ends of linear chromosomes. To avoid the erroneous repair of each chromosomal ends, each is capped with a repeating TTAGGG nucleotide sequence called the telomere. Along with the shelterin complex, the telomere works to sequester the G-tail of chromosomal ends within the upstream double-stranded DNA. This

prevents the activation of an ATM- or ATR-mediated DNA damage response (***see section 1.6 – DNA Repair and PARP Inhibition***). In cases where either the telomere or subunits of the shelterin complex are removed, significant chromosomal end-end fusion is observed (Diotti and Loayza 2011; van Steensel, Smogorzewska, and de Lange 1998; Capper et al. 2007; Veldman, Etheridge, and Counter 2004).

Inhibition of a DNA damage response at chromosomal ends is not thought to be solely due to binding of the G-tail within the double-stranded section of the telomere. Subunits of the shelterin complex have also been observed interacting with members of the ATM- and ATR-mediated signalling pathways which trigger DNA damage repair. TRF2 can directly bind the ATM-kinase and prevent its phosphorylation, thus inhibiting the dissociation of inactive ATM dimers into active monomers (Karlseder et al. 2004). This process blocks the phosphorylation of proteins by ATM-kinase, an action which is necessary for initiating the non-homologous end joining pathway (Okamoto et al. 2013). Meanwhile, POT1 prevents the activation of an ATR-mediated DNA damage response by coating the single-stranded DNA within the telomere. This prevents the binding of replication protein A (RPA) which would otherwise activate the homologous recombination pathway (Denchi and de Lange 2007; Guo et al. 2007).

1.1.5.2 The End-Replication Problem

The end-replication problem occurs during the semi-conservative replication of DNA in preparation of cell division (***see figure 1.3***). It exists due to the inability of cells to completely replicate all the DNA in a chromosome, with a small number of nucleotides lost from each chromosomal end after every cell division. The reason for this lies primarily in the method used to replicate the lagging strand, whereby DNA cannot be copied in a 3′ to 5′ direction due to the nature of DNA polymerase. While the leading strand is synthesised continuously in the 5′ to 3′ direction, RNA primers are necessary for the discontinuous synthesis of the lagging strand in the 5′ to 3′ direction. These are added to the lagging strand and allow short sequences of complementary DNA, called

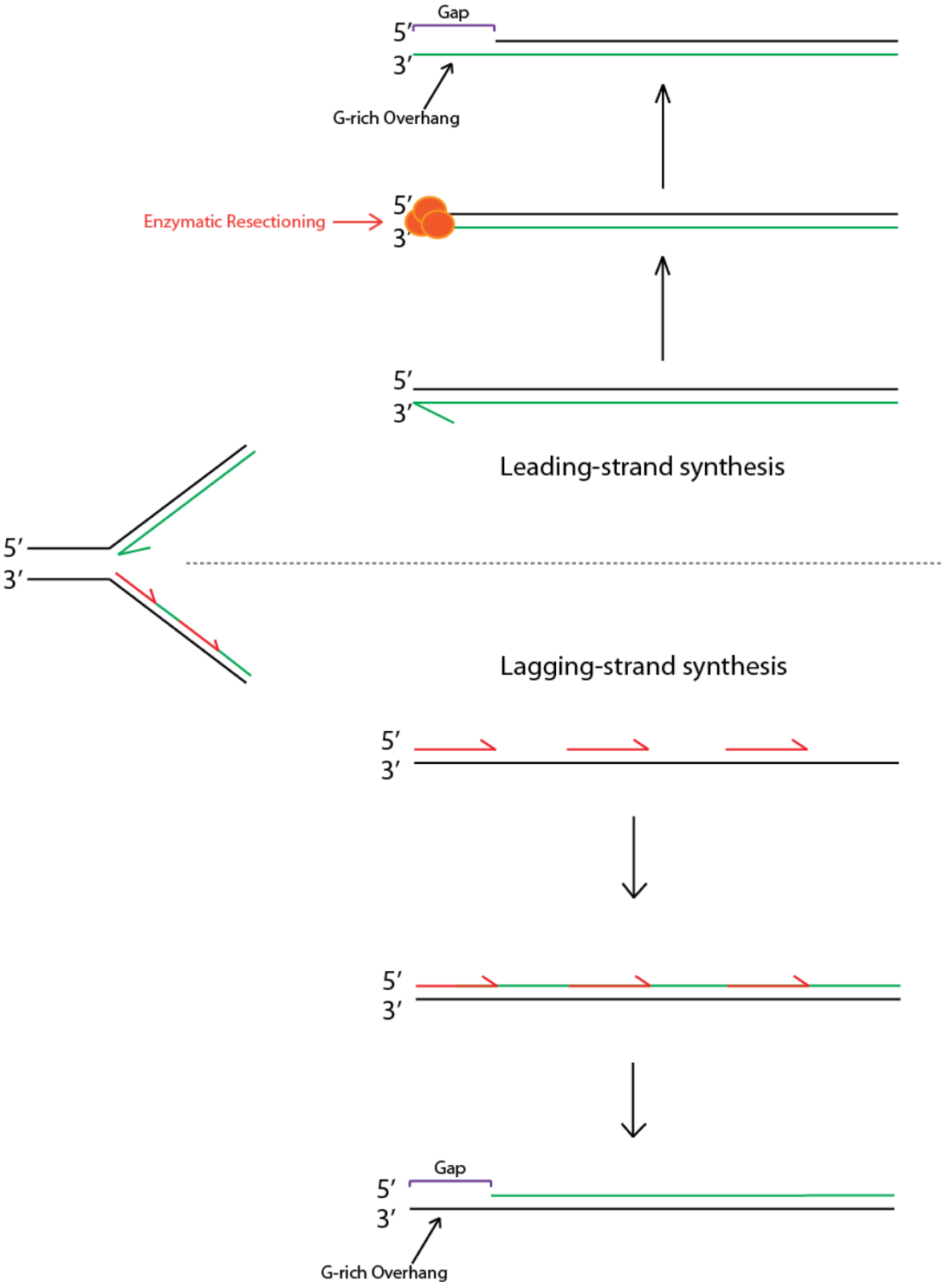

Figure 1.3 - The End Replication Problem
During DNA replication, the leading strand is fully replicated 5′ to 3′ by DNA polymerase. The G-rich overhang is then generated by enzymatic resectioning. This cannot occur at the lagging strand as DNA cannot be replicated 3′ to 5′. Instead, RNA primers are used to generate short nucleotide sequences in the 5′ to 3′ direction. The RNA primers are degraded during this process. However, nucleotide sequences cannot be generated at the position of the terminal RNA primer. This creates a gap which forms part of the G-rich overhang. *Adapted from 'Getting to the end: telomerase access in yeast and humans' Vega et al, Nature Reviews Molecular Cell Biology 4, 948-959 (December 2003)*

Okazaki fragments, to be synthesised. The RNA primers are then degraded, the resulting gaps are filled, and the Okazaki fragments are ligated (Gilson and Geli 2007; O'Sullivan and Karlseder 2010; Burgers 2009).

However, the terminal primer is added 70-100 nucleotides from the end of the chromosome. This results in a section of the lagging strand not being synthesised, producing a single-stranded DNA overhang that will eventually become the G-tail (Chow et al. 2012; Lundblad 2012). On the blunt-ended leading strand, resectioning of the chromosomal end produces the corresponding G-tail. This is initiated by TRF2 which recruits the exonuclease Apollo, resulting in 5' cleavage that is eventually blocked by POT1 binding (Wright et al. 1997; Arnoult and Karlseder 2015). Chromosomal shortening occurs during each cell division, with telomeres acting to absorb the loss of nucleotides. Without the telomere acting as a buffer, genomic DNA would instead be eroded which would result in the gradual loss of the most distal genes. This periodic shortening of the telomere also contributes to the Hayflick limit and the eventual triggering of senescence (***see section 1.1.5.4 - Senescence***). The rate of telomeric erosion varies depending on the cell type under examination and whether the cell is healthy or diseased, but is thought to be ~99bp/PD in healthy human fibroblasts. In comparison, the rate of telomeric erosion in the fibroblasts of patients with Werner syndrome can be up to 355bp/PD (Baird et al. 2004).

1.1.5.3 Telomeric Position Effect

The telomeric position effect (TPE) is described as the epigenetic silencing of telomere-proximal genes in relation to telomere length. This mechanism is thought to involve the spread of telomeric heterochromatin towards the subtelomeric DNA, as telomere length increases. The result is a silencing of the telomere-proximal genes via the modification of chromatin structure. Conversely, shorter telomeres lead to a more 'open' chromatin structure and the expression of these telomere-proximal genes (Doheny, Mottus, and Grigliatti 2008).

Little is known about this mechanism in humans, with most research being conducted in yeast cells, *Saccharomyces cerevisiae*. Here, the mechanism involves the recruitment of silent information regulator (Sir) proteins to the telomere by Rap1 and Ku70/80. A Sir2/Sir3/Sir4 complex is then responsible for initiating the formation of heterochromatin. The *spread* of this heterochromatin, towards the subtelomeric region, is catalysed by the histone deacetylase activity of Sir2 (Ottaviani, Gilson, and Magdinier 2008; Boulton and Jackson 1998). It is thought that this mechanism can be regulated by the expression of Rif1 and Rif2, proteins which compete with the Sir proteins for binding at the telomere. This was demonstrated experimentally by the inactivation of the Rif proteins in *Saccharomyces cerevisiae* which increased the efficiency of TPE (Mishra and Shore 1999).

Although it has been demonstrated that TPE can occur in human cells *in vitro*, the extent to which TPE influences human gene expression is not known (Robin et al. 2014). It has even been suggested that TPE does not occur in human cells, with experiments involving human fibroblasts failing to show a change in the expression of a reporter gene when telomere length was reduced from 25kb to 0.5kb (Sprung, Sabatier, and Murnane 1996). However, this has not stopped TPE from being suggested as the mechanism underlying various observations in several rare disease types (van Karnebeek et al. 2002; Inoue et al. 2002).

New research has even been presented that suggests TPE is responsible for the increased transcription of hTERT when telomere length decreases significantly. This involves the telomeric position effect over long distances (TPE-OLD), a process by which telomere length can change the expression of genes which are up to 10Mb away due to telomere looping (Robin et al. 2014). It has been observed that longer telomeres result in the 5p sub-telomeric region co-localising with the hTERT locus, repressing its expression. Contrary to this, telomeric shortening causes the hTERT locus to dissociate

from the subtelomeric region, triggering a change in chromatin structure which leads to increased hTERT expression and telomere lengthening (Kim et al. 2016).

1.1.5.4 Senescence

Cellular senescence is the process by which a normal cell ceases to divide, despite remaining metabolically active. The Hayflick limit, described by Leonard Hayflick, defines the number of times a normal telomerase-deficient somatic cell can undergo division before becoming senescent. This was identified as being 50±10 cell divisions by Hayflick (1965), but is thought to vary between 20-90 cell divisions depending on the age of the individual and the disease state of the cell (Rubin 2002). The cause of this replicative limit is the telomere, whereby successive rounds of genomic erosion after cell division result in telomeric shortening. When a telomere becomes critically shortened, the protective functions of the shelterin complex are lost and a DNA damage response is triggered. This commonly occurs through the ATM- and ATR-mediated signalling pathways (***see section 1.6 – DNA Repair and PARP Inhibition***), both of which culminate in the activation of a p53-driven irreversible cell cycle arrest in G_1 phase (Herbig et al. 2004). It has been demonstrated that the loss of p53, p21 or Rb (but not p16) can allow fibroblasts to bypass the cell cycle arrest that would normally be triggered by the loss of a telomere (Wei et al. 2003).

It is in this way that telomeres act as a 'biological clock' and confer a tumour suppressive mechanism. Cells acquire genetic damage over time, with senescence triggered by telomeric shortening preventing abnormal cells from growing indefinitely (Shay and Wright 2000). It is known that replicative senescence is triggered by the shortest telomere, not the average telomere length (Hemann et al. 2001). Most cancers are able overcome this process (***see section 1.4.1 – Abnormal Senescent-Signalling Pathways***), dividing beyond the Hayflick limit by elongating telomeres and avoiding cell cycle arrest (Shay and Wright 2005). However, it is not just cancerous cells that are able

to lengthen telomeres. Most stem and germline cells contain telomerase, a ribonucleoprotein which elongates telomeres and allows cell division beyond the Hayflick limit without the accompanying genomic erosion.

1.1.5.5 TERRA

Although it was originally thought that telomeres were transcriptionally inactive, it is now known that they produce a long non-coding RNA. Referred to as telomeric repeat-containing RNA (TERRA), it is made up of varying stretches of 5′-UUAGGG-3′ repeats which are transcribed from the C-rich strand of the telomere (Xu et al. 2010). The transcription of TERRA is performed by DNA-dependent RNA polymerase II and facilitated by TRF1 (Schoeftner and Blasco 2008). It is thought that the primary function of TERRA is to act as a regulator of telomerase activity, blocking the enzyme's active site by base pairing with the RNA template sequence within the TERC subunit (***see section 1.2.1 – Telomerase Structure***). In this way, TERRA acts as a competitive inhibitor of telomerase and prevents the elongation of telomeres (Redon, Reichenbach, and Lingner 2010).

However, this is not the only function of TERRA. It can also alter the expression of genes involved with the innate immune system, including STAT1 and ISG15 (Hirashima and Seimiya 2015). TERRA also directly interacts with the TRF2 Shelterin component, triggering the recruitment of the origin recognition complex (ORC1) which is responsible for the formation of heterochromatin at the telomeres (Deng et al. 2009). It also recruits LSD1 to uncapped chromosomal ends, which in turn recruits MRE11 and triggers their erroneous repair by the NHEJ pathway (Porro, Feuerhahn, and Lingner 2014). The depletion of TERRA is known to result in telomere dysfunction, aberrations in metaphase telomeres, and the loss of histone H3 K9me3 at the telomere (Deng et al. 2009).

1.2 Telomerase and Telomere Elongation

The telomerase enzyme is responsible for adding GTTAGG repeats to the 3′ end of the telomere, thereby increasing the capacity of a cell to divide without triggering senescence. Telomerase is not normally found in somatic cells, with its expression localised to stem and germline cells. However, its routine expression in cancer has made it a novel therapeutic target.

1.2.1 Telomerase Structure

Telomerase is a reverse transcriptase which uses an internal RNA template to generate GTTAGG repeats at the telomeric ends. It is mainly comprised of a telomerase reverse transcriptase (TERT) subunit and a telomerase RNA component (TERC) subunit (Wenz et al. 2001). TERT forms the catalytic domain of telomerase and includes four conserved structural domains; the telomerase essential N-terminal (TEN), telomerase RNA binding (TRBD), reverse transcriptase (RT) and C-terminal extension (CTE) domains. The TEN domain binds to the single-stranded DNA that makes up the telomeric G-tail, while the TRBD has been implicated in telomerase assembly and GTTAGG repeat processing (Sealey et al. 2010; Moriarty, Marie-Egyptienne, and Autexier 2004).

Partially embedded within the TERT subunit is the non-coding RNA that makes up the TERC subunit. It includes three extremely well-conserved domains; the template domain, the CR4/5 domain and the H/ACA domain. The template and CR4/5 domains bind to the TERT subunit and are sufficient for the enzymatic activity of telomerase (Tesmer et al. 1999; Mitchell and Collins 2000). While the H/ACA domain is not strictly necessary for telomerase activity *in vitro*, it binds to several telomerase-associated proteins; dyskerin, NOP10, NHP2 and GAR1 (Egan and Collins 2010). These proteins form a complex which are responsible for the stability and accumulation of the TERC subunit in adult stem cells (Schmidt and Cech 2015). The loss of functional dyskerin, NOP10 or NHP2 is known to cause dyskeratosis congenita, a rare disorder which is

characterised by a reduction in telomerase activity and significantly reduced telomere length (Mitchell, Wood, and Collins 1999; Walne et al. 2007; Vulliamy et al. 2008).

1.2.2 Telomerase Mechanism of Action

The telomerase TERC subunit contains a small RNA template sequence of 3′-AAUCCC-5′ repeats which can be divided into an 'alignment' and 'sequencing' section (***see figure 1.4***). The alignment section binds to the 5′-TTAGGG-3′ repeats at the most distal end of the telomere, the single-stranded G-tail, to form a DNA/RNA hybrid. The sequencing section is then used as a template with which to reverse transcribe 5′-GGTTAG-3′ onto the 3′-end of the telomere. The RT domain of the TERT subunit is responsible for catalysing this reaction. After the addition of these six nucleotides, the RNA template will dissociate from the telomere and reposition itself so that another round of telomeric synthesis can begin (Podlevsky and Chen 2012; Blackburn and Collins 2011). This template-translocation step is thought to take place outside of the telomerase active site (Qi et al. 2012). It has been demonstrated that each episode of elongation results in the addition of ~60 nucleotides or ~10 telomeric repeats (Zhao et al. 2011).

1.2.3 Regulation of Telomerase Activity

Specificity protein 1 (SP1) is a zinc finger transcription factor that upregulates the expression of the *TERT* gene. It binds to one of the five CG-boxes that exist within the *TERT* promotor, with mutations in these CG-boxes significantly inhibiting promotor activity (Kyo et al. 2000). c-MYC is also known to upregulate TERT expression by binding to the E-boxes that are present within the *TERT* promotor (Kyo et al. 2008). Many cancers that overexpress c-MYC are also known to have an increased TERT expression (Sagawa et al. 2001). It is therefore unsurprising that c-MYC inhibition has been explored as a potential mechanism by which to target cancer cell immortality (Kretzner et al. 2011; Xu, Popov, et al. 2001).

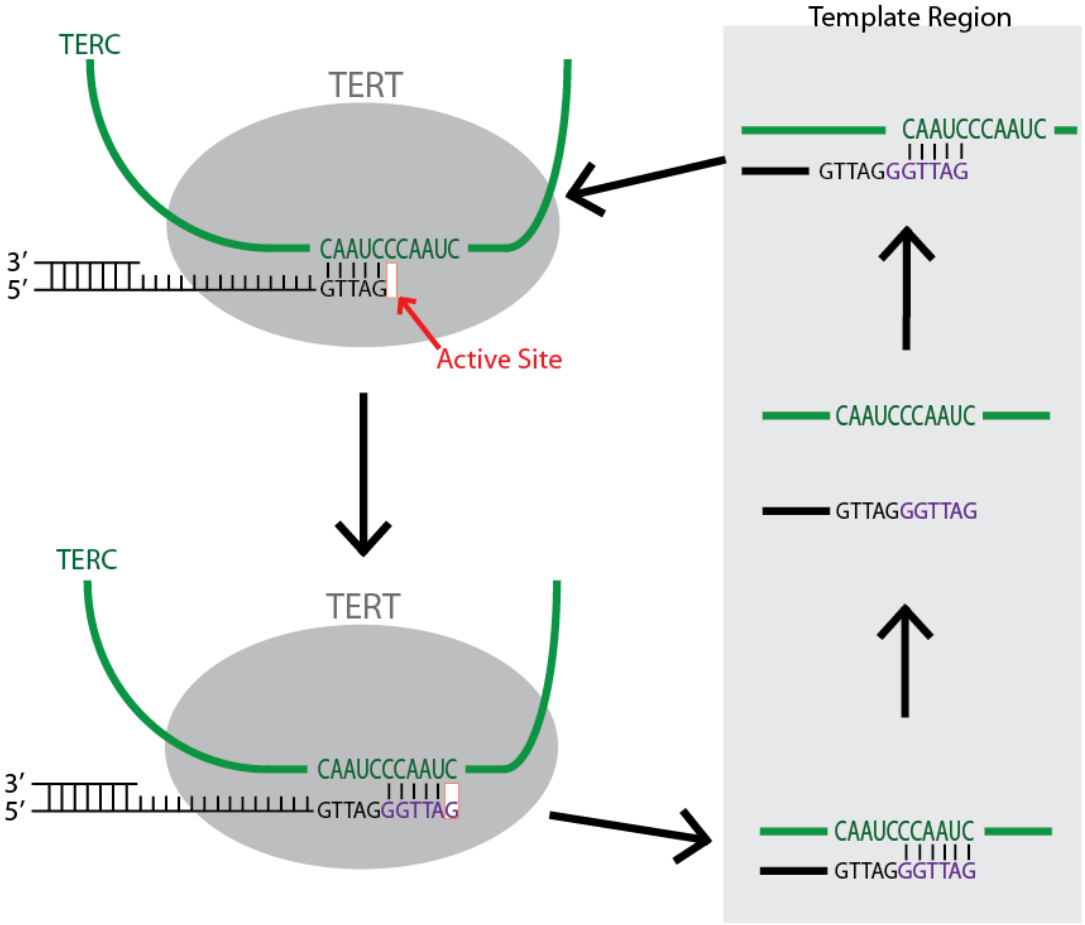

Figure 1.4 - A Symplified Model of Telomere Elongation by Telomerase
Telomerase is composed of two main subunits; TERT and TERC. The TERC subunit contains an RNA sequence which binds to the single-stranded telomeric sequence and acts as a template for DNA synthesis. The addition of nucleotides at the 3′ end of the telomere is catalysed by the TERT subunit. After synthesising a 5′-GGTTAG-3′ sequence, the telomere is repositioned. This allows further rounds of telomeric elongation to be performed before telomerase dissociates. *Adapted from 'It all comes together at the ends: Telomerase structure, function, and biogenesis' Podlevsky and Chen, Mutation Research/Fundamental and Molecular Mechanisms of Mutagenesis 730, 3-11 (2012)*

Wilm's tumour suppressor (WT1) can act as a negative regulator of TERT expression by binding to its promotor and inhibiting transcription (Oh et al. 1999). Mad1 has also been identified as a repressor of TERT, binding to the E-boxes and preventing the association of c-MYC (Oh et al. 2000). However, not all telomerase regulation takes place at the genetic level. Telomeres produce a non-coding RNA called TERRA that is made up of 5′-UUAGGG-3′ repeats (Azzalin and Lingner 2015). They are transcribed from the C-rich strand and have been shown *in vitro* to block the activity of telomerase by base-pairing with the RNA template sequence within the TERC subunit. As would be expected, cells with longer telomeres produce a greater number of transcripts (Schoeftner and Blasco 2008). It has also been demonstrated that TERRA levels significantly decrease in S-phase, when telomerase is most active (Porro et al. 2010). The activity of telomerase outside of the S-phase is also thought to be negatively regulated by the C-terminus of Hsc70-interacting protein (CHIP). This prevents nuclear translocation of TERT by dissociating the p21 chaperone, resulting in the degradation of TERT in the cytoplasm before it can reach the telomere (Lee et al. 2010).

It has been demonstrated that the TERT subunit can directly bind to an oligonucleotide/oligosaccharide-binding (OB)-fold of the TPP1 shelterin subunit, delaying the release of telomerase from the telomere. It is in this way that TPP1 can positively regulate telomere length, by increasing the number of telomeric repeats synthesised by telomerase before its dissociation (Zhong et al. 2012). Other shelterin subunits, such as TRF1 and POT1, inhibit the binding of telomerase by competitively binding at the telomere (Smith and de Lange 2000; Lei, Podell, and Cech 2004).

1.2.4 Alternative Lengthening of Telomeres

Alternative lengthening of telomeres (ALT) is a process by which a cell can elongate its telomeres without the need for telomerase. It is almost exclusive to abnormal cells, with around 10% of cancers thought to avoid senescence in this way (Henson et al. 2009).

So far, two potential mechanisms have been described by which ALT may occur. The first involves the presence of telomeric DNA which exists separately from the chromosome. This extrachromosomal telomere can be double-stranded and circular (t-circles), partially single-stranded and circular (C-circles), or double-stranded and linear (Cesare and Griffith 2004; Nabetani and Ishikawa 2009).

While t-circles have also been identified in ALT-negative cells, C-circles are thought to be localised almost exclusively to ALT-positive cells (Wang, Smogorzewska, and de Lange 2004; Henson et al. 2009). It is thought that t-circles are produced by the telomeric trimming that occurs during 3′-overhang formation, a process which is known to rely on the HR proteins XRCC3 and NBS1 (Wang, Smogorzewska, and de Lange 2004). How C-circles are generated is not known, but it has been proposed that they are simply formed by the nucleolytic degradation of t-circles (Cesare and Reddel 2010).

Telomeric recombinational events act to join this extrachromosomal DNA to the telomere, allowing it to be used as a template for telomeric repeat synthesis (Dunham et al. 2000; Henson et al. 2002). It has also been suggested that this mechanism can occur without the need for extrachromosomal DNA, with a chromosome utilising either its own telomere or the telomere of a second chromosome as a template (Muntoni et al. 2009). It was expected that this mechanism would be suppressed in normal cells by the action of TRF2 and POT1, subunits of the shelterin complex which are responsible for the formation of the telomeric t-loop structure that would insulate the chromosomal ends from this recombination-mediated synthesis. However, experiments have demonstrated that preventing TRF2 expression triggers telomeric erosion and senescence in ALT-positive cell lines (Stagno D'Alcontres et al. 2007). This begs the question of whether subunits of the shelterin complex are either directly or indirectly involved in maintaining the ALT pathway?

The second ALT mechanism is considered to utilise unequal telomere sister chromatid exchange (T-SCE) and occurs during cell division. Abnormal regions of unrepaired single-stranded DNA have been commonly observed within the telomeres of ALT-positive cells (Nabetani and Ishikawa 2009). These structural faults are unstable and result in the uneven separation of sister chromatids during anaphase. As a consequence, one daughter cell will have a longer telomere length and increased replicative capacity when compared to the other daughter cell (Bailey, Brenneman, and Goodwin 2004). However, this mechanism is thought to occur less frequently. Not only is it known that the amplification of telomeric DNA occurs during ALT, but a population of cells that predominantly utilised the T-SCE mechanism would still eventually succumb to cellular senescence as no new telomere was being generated (Muntoni et al. 2009; Henson and Reddel 2010).

Inactivating mutations in the alpha thalassemia/mental retardation syndrome X-linked (*ATRX*) and death-domain associated (*DAXX*) proteins have commonly been observed in ALT-positive cells (Bower et al. 2012). ATRX is a chromatin-remodelling protein which contains both a zinc finger domain and an ATPase/helicase domain (Xue et al. 2003). It colocalises with DAXX, a histone H3.3 chaperone, acting to incorporate this histone variant into telomeric chromatin (Goldberg et al. 2010). It is in this way that ATRX is thought to supress ALT, condensing chromatin and inhibiting the formation of telomeric G-quadruplex structures which allow adjacent telomeres to be used as templates for telomere synthesis (Napier et al. 2015). It is also thought that ATRX might facilitate the replication and resolution of G-quadruplex structures, preventing the HR-mediated repair of double-strand DNA breaks which can result in extrachromosomal DNA being ligated to the telomere (Amorim et al. 2016). In this way, ATRX expression acts as a suppressor of ALT. ATRX mutations have been identified 11% of high-risk neuroblastoma cases, resulting in telomere elongation via ALT (Valentijn et al. 2015).

1.3 Measuring Telomere Length

Due to the repetitive sequences that make up the telomere, attempting to measure telomere length using a PCR-based technique had always proved to be difficult. Of the techniques that have been developed, each varies in both accuracy and ability to recognise the telomere lengths of specific chromosomal ends.

1.3.1 Terminal Restriction Fragment (TRF) Analysis

TRF employs several restriction enzymes to digest non-telomeric DNA, whilst leaving the telomeres intact. The resulting genomic fragments and telomeric DNA are resolved by agarose gel electrophoresis. After southern blotting, a telomere-repeat containing labelled probe is used to hybridise to the telomeric repeats. Due to the heterogeneous nature of telomere lengths between different chromosomes and cells, the labelled telomeric DNA produces a smear which can then be used to estimate average telomere length. This estimation is based on comparisons to a ladder of standardised DNA sizes, as well as normalisation to a reference sample (Baird et al. 2003).

The disadvantages of using this technique are numerous, with the most obvious being that the estimated average length generated is too inaccurate for subtle changes in telomere length to be observed. Even if the accuracy of the estimation was improved, TRF analysis fails to distinguish between the different telomeric lengths of each chromosomal end. Substantial quantities of DNA are also required for this technique, with the need for a minimum of 10^6 cells restricting its ability to be used when the genetic material being analysed is scarce. Also, the quantity of probe that binds to a telomere is proportional to the length of that telomere. This makes shorter telomeres difficult to detect and places a lower limit on the telomeric lengths that can be measured (Aubert, Hills, and Lansdorp 2012).

1.3.2 Quantitative Polymerase Chain Reaction (Q-PCR)

A standard Q-PCR uses a machine which can perform PCR, but that also has the ability to detect fluorescence emitted by an excited fluorophore. Fluorescent probes are added to the PCR mixture which fluoresce only when bound to a target DNA sequence. As the PCR amplifies the target DNA sequence, greater quantities of probe can bind. This produces a fluorescent signal that is in proportion to the quantity of target DNA present. The signal emitted is recorded after each round of PCR. The quantity of template present at the start of the reaction can then be calculated, based on the intensity of the fluorescent signal throughout the reaction.

For use in telomere length measurements, primers are designed to both the G-rich and C-rich strands of the telomere. These primers have mismatches across their length which prevents primer dimerization. For the first two rounds of PCR, a low annealing temperature is used to allow mismatched-primer binding to the telomere. After this, a higher annealing temperature is used which ensures that the primers only bind to the amplified telomeric sequence (which contains the mismatched sequence) and not to the template telomeric sequence. Telomere-specific fluorescent probes then bind to the amplified telomeric-sequence, allowing a signal to be recorded. The longer the telomere, the greater the quantity of probe that binds and so the greater the fluorescent signal. Signal intensity is then compared to that of a standard gene, allowing the ratio of telomere signal vs standard gene signal intensity to be calculated. This yields a value which correlates with that of a known average telomere length (Cawthon 2002).

Although this technique requires less DNA to perform than TRF analysis, Q-PCR is not flawless and is also less accurate than TRF analysis (Aviv et al. 2011). Small pipetting volume discrepancies between the wells containing the telomeric template and standard gene template samples are known to lead to significant errors. For this reason, a revised technique called monochrome multiplex quantitative PCR (MMQ-PCR) was developed.

	Advantages	Disadvantages
TRF Analysis	• Widely used • No special requirements	• Estimated average telomere length is inaccurate. Does not allow subtle changes in telomere length to be observed • Cannot distinguish between different telomeric ends • Substantial quantities of DNA required (10^6 cells) • Shorter telomeres are difficult to detect, relative to longer telomeres
Q-PCR	• High throughput • Little DNA required (50ng)	• Small pipetting volume discrepancies can lead to significant errors • Cannot quantify individual length of individual telomeres
Q-FISH	• Allows telomere length of specific chromosomal ends in individual cells to be observed • Small number of cells required • Can be used to measure critically shortened telomeres	• Low throughput/time consuming • Labour intensive • Cannot be used to observe non-dividing cells (e.g. senescent)
Dot Blot	• Little DNA required (20ng) • Inexpensive	• Requires a unique dye (SYBR Dx) which is costly
STELA	• Most accurate technique • Can be used to measure length of individual telomeres • Can be used to measure specific telomere ends • Requires little DNA (<2ng)	• Use is restricted to several chromosomal ends: XpYp, 17p, 2p, 11q and 12q • Labour Intensive • Low throughput • Bias towards shorter telomeres • Cannot detect telomeres >25kb

Table 1.1 – Table detailing the advantages and disadvantages of each telomere-measurement technique (Nussey et al. 2014; Vera and Blasco, 2012)

This measures the signal intensity of the telomeric template and standard gene template from a single PCR well. Differences between the concentration of DNA in the telomeric template and standard gene template wells can then be avoided (Cawthon 2009).

1.3.3 Fluorescence *in Situ* Hybridisation

Quantitative fluorescence *in situ* hybridisation (Q-FISH) utilises fluorescently-labelled nucleic acid probes to visualise the individual telomeres of metaphase chromosomes. These probes carry a $(CCCTAA)_3$ sequence that can hybridise to the telomeric regions of single-stranded denatured DNA. A fluorescence microscope is then used to visualise the chromosomes, allowing the average telomere length to be estimated by comparing the intensity of the telomeric fluorescent signal to that of known standards (Lansdorp et al. 1996). This technique carries a number advantages over both TRF and Q-PCR methods, such as the small number of cells required for analysis. It also allows the telomere length of specific chromosomal ends to be observed, as well as providing a method of measuring the length of telomeres which are critically shortened (up to 0.2kb). However, the need for metaphase cells means that this technique cannot be employed for those populations which are senescent or otherwise unable to divide. As well as this, Q-FISH is both labour and time intensive which allows only a small number of metaphase cells to be analysed (Aubert, Hills, and Lansdorp 2012; Montpetit et al. 2014).

Several variations of this technique exist, the first of which is called high throughput quantitative fluorescent *in situ* hybridisation (HT Q-FISH). Here, the fluorescent signal emitted by the telomeric probe is normalised to that of a second probe at the centromere. This automated process allows interphase cells to be analysed, as well as increasing the number of cells being examined and so improving the accuracy of the technique. However, neither specific telomeric ends or telomere-deficient chromosomes can be recognised using this method (Canela et al. 2007).

The second variation is called flow-FISH and requires that the cells being examined are in suspension. This is in comparison to Q-FISH and HT Q-FISH, whereby the cells are fixed in place before the probe is added. The cells are then treated with a fluorescently labelled $(CCCTAA)_3$ probe, before being analysed using flow cytometry. Although flow-FISH is both fast and accurate, the need for a cell suspension limits its use to fresh blood samples. Also, this technique cannot be used to analyse the telomere length of individual chromosomes. As with all variations of FISH, the $(CCCTAA)_3$ probe cannot bind to the telomeric variant repeats that exist within the most proximal end of the telomere. This reduces the accuracy of the technique (Hultdin et al. 1998; Rufer et al. 1998; Aubert, Hills, and Lansdorp 2012).

1.3.4 Dot Blot Analysis

Dot blot analysis uses the intensity of a luminescent probe to calculate the average telomere length of a sample, based on the luminescent intensity of known standards. First, DNA from each sample is loaded onto a nylon membrane. A dye called SYBR Dx is then added which fluoresces when bound to double-stranded DNA. Fluorescent intensity is measured to identify the concentration of DNA bound to each part of the membrane. After washing, a digoxigenin-labelled telomeric probe is added to the samples which then undergo a luminescent detection procedure. An image is produced by exposing the samples to X-ray film. Average telomere length is then calculated from the ratio of DNA concentration vs luminescent intensity (Kimura and Aviv 2011).

1.3.5 Single Telomere Length Analysis

Single telomere length analysis (STELA) is a single-molecule PCR-based technique which allows individual telomeres from specific chromosomal ends to be measured (***see figure 1.5***). It uses a primer which contains a TTAGGG-binding sequence, as well as a unique nucleotide sequence. By exploiting the fact that the G-rich strand of a telomere ends with a 3′ single-stranded overhang, this primer is able to anneal via complementary

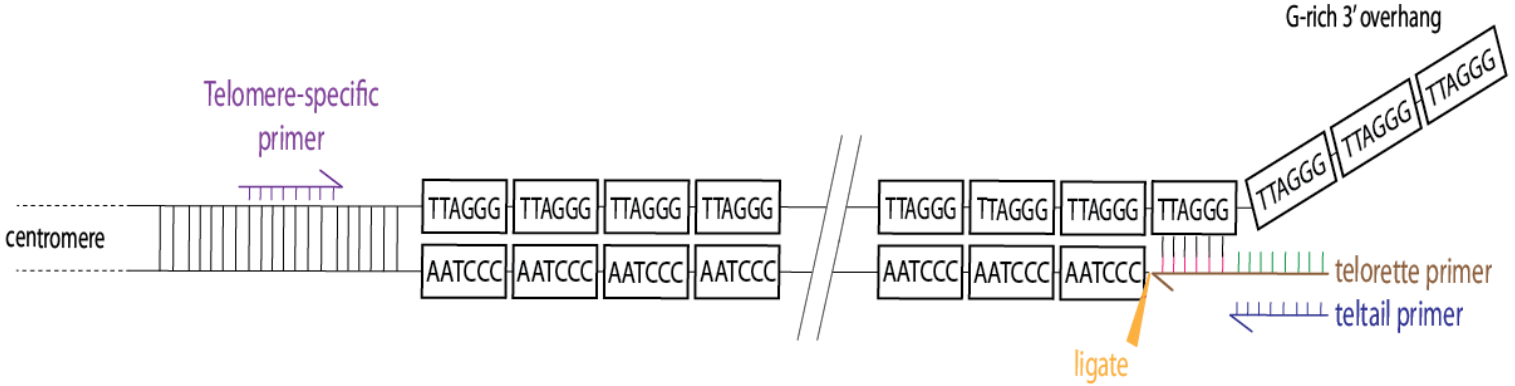

Figure 1.5 - Single Telomere Length Analysis (STELA)
A telomere-specific primer is designed which binds to a sequence within the subtelomeric region. A second 'telorette primer' is designed which is comprised of a sequence complementory to the telomeric sequence, as well as a having its own unique sequence of nucleotides. This binds at the end of the telomere via complementary base pairing. It is then ligated to the telomere, providing the most distal end of the chromosome a specific nucleotide sequence. A single PCR cycle is then initiated, at which point the teltail primer (a primer containing only the specific nucleotide sequence from the telorette primer) takes over from the telorette primer. *Adapted from 'Extensive allelic variation and ultrashort telomeres in senescent human cells' Baird et al. Nature Genetics 33, 203-207 (2003)*

base pairing before the chromosome has undergone the dissociation stage of PCR. Ligation of the primer to the C-rich telomeric end then endows the telomere with a unique sequence at its most distal point. Combined with a unique sequence within the subtelomeric region, this provides two primer-binding sites which flank the telomere and generate a targeted PCR. The sequence of the subtelomeric primer can also be changed, allowing STELA to be performed at specific telomeric ends. After this PCR step, the products are resolved using agarose gel electrophoresis and imaged by a southern blot procedure which utilises a telomere-specific radiolabelled probe (Baird et al. 2003).

STELA has the advantage of being one of the most accurate techniques for measuring telomere length, as well as being able to analyse individual chromosomal ends and critically shortened telomeres. STELA can also be carried out when starting material is scarce, with less than 10^5 cells necessary to generate a mean telomere length measurement. However, it is limited only to those chromosomal ends for which a specific sub-telomeric primer can be designed. The sub-telomeric regions of many chromosomes do not contain a unique binding site and so STELA is currently limited to the XpYp, 17p, 2p, 11q and 12q chromosomal ends (Britt-Compton et al. 2006).

There is also the issue that the analysis of a single chromosomal end may not be representative of all the telomeres within a cell. While this could be mitigated by measuring the telomere length at multiple chromosomal ends, STELA is a very labour-intensive process and this option would not be realistic for a large number of samples. A further limitation is that telomeres larger than 25kb cannot be detected using STELA, creating a bias towards the measurement of shorter telomeres (Aubert, Hills, and Lansdorp 2012; Montpetit et al. 2014; Nussey et al. 2014; Martin-Ruiz et al. 2015).

1.4 Telomeres and Disease

As with any tumour suppressive mechanism, the absence of a functional telomere-driven senescent pathway has been implicated in cancer. Critically shortened telomeres are thought to play a role in chromosomal fusion and rearrangement, driving progression of the disease. Meanwhile, unregulated lengthening by telomerase is known to be partially responsible for the immortality of cancer cells.

1.4.1 Abnormal Senescent-Signalling Pathways

Telomeric shortening acts to limit the replicative capacity of a cell, activating the ATR and ATM signalling pathways once a critical length is reached. This triggers cellular senescence, a process which exists to prevent the unrestrained growth of abnormal cells. Defects in these pathways diminish the effectiveness of the cell cycle checkpoints, as well as contributing to the continued division of a cell beyond the Hayflick limit (Chin et al. 1999). Due to the complexity of these pathways, inactivation can occur via several mechanisms. The loss of a functional p53 protein is possibly the most well characterised of these, with mutations in the TP53 gene thought to be present in around 50% of all cancers (Merkel *et al*., 2017).

Disruption of the ATR signalling pathway alone may also be enough to lead to the formation of cancer, with $ATR^{+/-}$ mice displaying a slight increase in tumour incidence (Brown and Baltimore 2000). The complete loss of ATR in adult mice also results in stem cell depletion, limited capacity for tissue renewal, and an ageing phenotype (Ruzankina et al. 2007). In humans, disruption of this signalling pathway is known to cause Seckel syndrome, a disease characterised by dwarfism and intellectual disability (Alderton et al. 2004). A limited number of cases have also presented with leukaemia or lymphoma, leading to the suggestion that this syndrome may be associated with a slightly increased risk of developing cancer (Hayani et al. 1994; Chanan-Khan et al. 2003).

The importance of ATM signalling in response to critically shortened telomeres is highlighted by the disease ataxia-telangiectasia. This is caused by a failure to produce a functioning ATM protein, resulting in cells being unable to efficiently respond to DNA damage. As well as being characterised by neurodegeneration and a weakened immune system, the disease is also known to confer a sensitivity to ionising radiation and a significantly increased risk of developing cancer (Chun and Gatti 2004).

1.4.2 Critically Shortened Telomeres

In the absence of a functioning senescent pathway, the telomeric erosion that occurs during cell division can result in the loss of the telomere and the protection that it confers. This often proves disastrous for genomic stability, with the ends of chromosomes now being recognised as double-strand DNA breaks (Murnane 2006). Erroneous repair can occur via the non-homologous end joining pathways (***see section 1.6.2.2 – Non-Homologous End Joining***), causing two ends to be fused together and creating a dicentric chromosome (Capper et al. 2007). This structure is inherently unstable, eventually breaking apart in an unequal manner. As the new chromosomal ends produced by this break are also unprotected, the response by the various DNA repair mechanisms is a further attempt at fusion. These cycles of breakage-fusion-bridge are known to cause genomic rearrangements that help to drive cancer progression (Maciejowski and de Lange 2017).

Dicentric chromosomes, generated during a telomere driven crisis, have also been implicated in chromothripsis. This is a process by which localised areas within a chromosome shatter, with the associated repair of these regions resulting in the significant rearrangement and deletion of genetic material (Ernst et al. 2016). The process by which this occurs begins with the joining together of two telomere-deficient chromosomal ends. During anaphase, the resulting dicentric chromosome is pulled to opposite ends of the cell, spanning the gap between the two daughter nuclei. To resolve

this, the exonuclease TREX1 generates single-stranded DNA within the chromatin bridge which eventually causes it to break. Each half of the dicentric chromosome then retreats to a corresponding daughter nuclei, where an attempt is made to repair the shattered ends by ligating random DNA segments (Maciejowski et al. 2015).

Dyskeratosis congenita (DKC) is an example of a condition which is characterised by critically shortened telomeres and genetic instability. Its symptoms may include a progressive bone marrow failure, lacey reticular pigmentation, aplastic anaemia, dystrophy of the nails and oral leukoplakia (Alter et al. 2007). It is the result of several possible defects in telomere maintenance biology, with the specific cause of DKC partially dependent on the mode of inheritance. For example, X-linked DKC is due to mutations in the DKC1 gene which encodes dyskerin, a telomerase-associated protein which works as part of a protein complex to stabilise TERC. Autosomal dominant DKC is caused by mutations in either the TERT or TERC subunits of telomerase, or the TIN2 subunit of the shelterin complex (Savage et al. 2008). While autosomal recessive DKC is due to mutations in TCAB1, a protein which is responsible for localising telomerase to Cajal bodies (Batista et al. 2011). In any case, the result is an inability of stem cells to elongate telomeres, leading to critically shortened telomeres and chromosomal instability. DKC is also associated with an increased risk of developing cancer, most frequently acute myeloid leukaemia and squamous cell carcinomas (Alter et al. 2009).

Critically shortened telomeres have been observed in a significant number of cancers. Colorectal, prostate, renal and bladder cancers have all been shown to express a mean telomere length that was significantly shorter than healthy cellular controls (Roger et al. 2013; Sommerfeld et al. 1996; Mehle, Ljungberg, and Roos 1994; Broberg et al. 2005). Studies into the dynamics of telomere length in breast cancer and chronic lymphocytic leukaemia (CLL) have not only demonstrated that mean telomere length is reduced in the diseased cells, but that the extent of telomeric shortening can be used as a prognostic

indicator. In both breast cancer and CLL, a shorter mean telomere length correlates with a reduced median overall survival (Simpson et al. 2015; Strefford et al. 2015).

This is unsurprising, as telomeric shortening has also been observed to correlate with an increased frequency of chromosomal end-end fusion in CLL. Fusion events were only observed in those patients whose mean telomere length fell below a 3.81kb threshold, with cells below this threshold being at a significantly increased risk of undergoing a telomere-driven crisis (Lin et al. 2014). For most cancerous cells, the chromosomal rearrangements that underpin crisis will be catastrophic. However, the potential exists for a small number of cells to survive this process and escape from crisis with a survival advantage (Jones et al. 2014). Although this can include the further disruption of apoptotic mechanisms, one of the most important and pervasive stages of cancer development is the reactivation of telomerase.

1.4.3 Unregulated Telomeric Lengthening

Lung cancer, breast cancer and multiple myeloma are just a small number of malignancies where telomerase is known to be reactivated (Albanell et al. 1997; Hayani et al. 1994; Wu et al. 2003). In total, telomerase is thought to be expressed in around 85% of all cancers (Buseman, Wright, and Shay 2012). This is unsurprising given that gain of the 5p chromosomal arm is one of the most common genetic events that occurs in the early stages of solid tumour development, with the 5p arm being host to the gene encoding the TERT subunit of telomerase (Rooney et al. 1999; Cao, Bryan, and Reddel 2008; Kang et al. 2008). Translocations that place enhancer elements close to the TERT locus have also been identified, with 21% of all high-risk neuroblastoma cases thought to involve 5p15.33 rearrangements (Peifer et al. 2015). Telomerase reactivation is also frequently accompanied by mutations in the TERT promoter, leading to its upregulation (Vinagre *et al*., 2013). Telomeres in the remaining 15% of cancers are elongated using

ALT. Regardless of which mechanism is utilised, the result is the immortalisation and limitless replicative capacity of cancer cells (Mocellin, Pooley, and Nitti 2013).

Due to the prevalence of telomerase reactivation in cancer, as well as the fact that telomerase is not normally expressed in healthy somatic cells, telomerase inhibition as a selective cancer treatment has become a significant area of research. Imetelstat is a promising example of an inhibitor which binds to the TERC subunit and supresses the reverse transcriptase activity of telomerase. Phase III clinical trials in pancreatic cancer, as well as phase II clinical trials in multiple myeloma, leukaemia, melanoma, breast cancer and lung cancer have recently been completed (Buseman, Wright, and Shay 2012; Barata, Sood, and Hong 2016; Arndt and MacKenzie 2016). However, a failure to improve progression free survival in several of these trials suggests that telomerase inhibition may not always be the most effective approach (Chiappori et al. 2015; Tefferi et al. 2015).

Telomerase-targeted immunotherapy has also been explored as a method of preventing telomere elongation in cancer. This process involves sensitising the patient's own immune system against cells which express TERT peptides as a surface antigen. The result should be an expansion of cytotoxic T lymphocytes which selectively target the telomerase-producing cancerous cells (Khalil et al. 2016). Promising phase II clinical trials have been described, with each targeting a number of solid tumours (Kotsakis et al. 2012; Ellebaek et al. 2012; Fenoglio et al. 2013). Unfortunately, disappointing phase III clinical trials in pancreatic cancer and phase II clinical trials in hepatocellular carcinoma have also been described, suggesting that telomerase inhibition may not be the universal cure that was hoped for (Middleton et al. 2014; Greten et al. 2010).

1.5 Multiple Myeloma

Multiple myeloma (MM) is a disease characterised by the accumulation of abnormal plasma cells within the bone marrow. It is commonly preceded by a related disorder which is known as monoclonal gammopathy of undetermined significance (MGUS). The first stages of MM are asymptomatic, eventually becoming symptomatic as the disease progresses. In more aggressive cases, MM may evolve into plasma cell leukaemia (PCL).

1.5.1 Plasma Cell Development

The plasma cell is the antibody-producing, terminally differentiated form of the B-lymphocyte. Maturation begins with the development of an immature B cell from the hematopoietic stem cells that reside within the bone marrow. Here, B cells undergo V(D)J recombination to produce the immunoglobulin heavy (Variable-Diversity-Joining) and light (Variable-Joining) chains. Selection occurs between 44 variable, 27 diversity, and 6 joining gene segments, resulting in roughly $3x10^{11}$ possible antibody combinations. This process, along with somatic hypermutation which drives a controlled process of mutation within the variable-region genes, acts to generate a high-affinity immunoglobulin binding site. B cells are tested for autoreactivity against the host, with those cells that elicit a response being subject to apoptosis. Meanwhile, unresponsive cells migrate from the bone marrow to the spleen and lymph nodes. In rare cases, autoreactive or low-affinity B cells may escape the bone marrow, but are unable to mature further and are eventually destroyed (Shapiro-Shelef and Calame 2005; Halverson, Torres, and Pelanda 2004).

Immature B cells are activated in either a T cell-independent or T cell-dependent manner. The independent route involves a subset of B cells called marginal zone (MZ) B cells, which are activated after coming into direct contact with a specific antigen. This causes the MZ B cells to undergo class switching, a process by which the constant regions of

the immunoglobulins produced by the B cells switch from IgM and IgD to either IgA, IgG or IgE (Stavnezer, Guikema and Schrader, 2009). The B cells also undergo rapid proliferation and antibody secretion, forming a primary response which lasts for around 14 days (Lopes-Carvalho and Kearney 2004; Smith et al. 1996). Meanwhile, T cell-dependent activation is a slower process that produces a more targeted and long-term response. After encountering an antigen, the B cell internalises and degrades it. Antigen peptides are then displayed on the surface of the B cell, awaiting recognition by T helper (T_H) cells. Upon sensing the MHCII-bound peptide, the T_H cell releases the interleukins IL-2, IL-4, IL-10 and IL-21. This, along with contact between the CD40 protein on the B cell and CD40 ligand on the T cell, causes the B cell to become activated (Oracki et al. 2010; Kuchen et al. 2007).

The activated B cells proliferate, with a small number forming germinal centres within the spleen and lymph nodes. The remaining B cells terminally differentiate to form short-lived, antibody-secreting plasma cells (Allen, Okada, and Cyster 2007). In the germinal centres, activated B cells undergo further rounds of proliferation, as well as affinity maturation. This process involves somatic hypermutation of the immunoglobulin variable region and clonal selection, resulting in the formation of plasma cells which secrete a high-affinity antibody against the antigen (Jacob et al. 1991). This process also produces memory B cells which remain dormant until being activated by the original antigen, facilitating the rapid production of high-affinity antibody-producing plasma cells (Shlomchik and Weisel 2012).

1.5.2 Monoclonal Gammopathy of Undetermined Significance

MGUS is an asymptomatic disorder, characterised by the presence of abnormal plasma cells within the bone marrow. Non-functioning antibodies can also be detected within the blood serum, a product of the clonal populations of these abnormal cells. Known as paraproteins or M proteins, these antibodies can either be IgA, IgD, IgE, IgG, IgM or free

light chains (Dispenzieri et al. 2009). Diagnostic criteria for MGUS includes the presence of less than 10% clonal plasma cells within the bone marrow; a paraprotein concentration of less than 30g/L in the blood serum; and an absence of hypercalcaemia, renal insufficiency, anaemia, bone lesions and amyloidosis that can be attributed to the abnormal plasma cells (Rajkumar et al. 2014).

As MGUS is asymptomatic, treatment is not usually advised. However, it is necessary to continually monitor the disease for the remaining life of the patient. This requires a measurement of the serum paraprotein concentration every 2-3 years for low-risk MGUS (defined as having a serum paraprotein concentration <15g/L), or every 6 months for intermediate- and high-risk MGUS (defined as either an IgA- or IgM-producing subtype, or having a serum paraprotein concentration >15g/L) (Kyle et al. 2010). Monitoring is necessary due to the possibility of progression to either MM or Waldenstrom's macroglobulinemia (WM). The risk to a patient that their MGUS will develop into MM is around 1% per year for that individual. This raises to 1.5% per year for those individuals harbouring the IgM subtype. Meanwhile, approximately 1.5% of MGUS patients harbouring the IgM-subtype will develop WM, a lymphoproliferative disorder which is characterised by lymphadenopathy and elevated serum globulin levels (International Myeloma Working 2003; Ghobrial, Gertz, and Fonseca 2003).

It is estimated that around 3.2% of people over the age of 50 have MGUS (Wadhera and Rajkumar 2010). In fact, one of the greatest risk factors for developing MGUS is aging. The average age at diagnosis is 70, with less than 2% of all cases being linked to people younger than 40 (Therneau et al. 2012; Cheema et al. 2009). Gender also plays a role, with men being slightly more likely than women to develop MGUS. Other risk factors include race, family history and environmental factors such as radiation and pesticide exposure (Landgren et al. 2006; Vachon et al. 2009; Iwanaga et al. 2009; Landgren et al. 2009).

1.5.3 Smouldering Multiple Myeloma

Although MGUS does not always develop into MM, it is thought that MM almost always develops from cases of MGUS (Landgren et al. 2009). MM can be categorised as either smouldering (asymptomatic) or symptomatic. Smouldering MM shares a significant number of its characteristics with MGUS, but is identified as having a greater plasma cell presence within the bone marrow and larger quantities of paraprotein within the blood serum. Officially, the diagnostic criteria for smouldering MM includes the presence of between 10-60% plasma cells within the bone marrow; and/or a paraprotein concentration >30g/L in the blood serum; and an absence of hypercalcaemia, renal insufficiency, anaemia, bone lesions and amyloidosis that can be attributed to the abnormal plasma cells (Rajkumar et al. 2014). The risk of progression to malignancy is also greater than MGUS, with each smouldering MM patient having around a 10% chance of developing symptomatic MM per year in the first five years following diagnosis. After this, the risk of progression diminishes to 3% per year for the next five years, followed by 1% per year thereafter (Kyle, Remstein, et al. 2007).

The risk of smouldering MM progression can be subcategorised as either low, intermediate, or high. This is based on three factors; plasma cell bone marrow infiltration >10%, paraprotein concentration >30g/L, and a serum free light chain ratio <0.125 or >8. Low risk patients display one of these factors, intermediate risk patients display any two of these factors, while high risk patients display all three factors (Dispenzieri et al. 2008). However, an ultra-high risk group of smouldering MM patients have also been identified which demonstrate a plasma cell bone marrow infiltration >60%. In these cases, it is recommended that patients begin treatment immediately, regardless of whether symptoms are present (Rajkumar, Larson, and Kyle 2011).

Other than this, treatment for smouldering MM is not normally recommended. The standard procedure is to continue monitoring plasma cell and paraprotein levels, as well

as blood calcium and creatinine values which measure bone loss and renal function respectively. X-rays are also performed to determine whether bone lesions are present. Measurements should continue for 2-3 months to determine baseline values. If stable, monitoring can be repeated every 3 months thereafter (Kyle et al. 2010). However, recent phase III clinical trials have suggested that earlier treatment of high risk smouldering MM with lenalidomide and dexamethasone has a positive impact on overall patient survival when compared to observation alone (Mateos et al. 2016).

1.5.4 Symptomatic Multiple Myeloma

Symptomatic MM is primary differentiated from smouldering MM by the presence of organ damage, clonal bone marrow plasma cell infiltration ≥60%, serum free light chain (SFLC) ≥100mg/L, or more than one focal lesion ≥5mm in size on a magnetic resonance imaging (MRI) scan. As MM is incurable, the onset of symptoms usually confers a heterogeneous but poor prognosis, with 25% of individuals living less than 3 years (Rajkumar et al. 2010). Even with treatment, the 5-year overall survival rate was shown to be 82% for low risk MM and 40% for high risk MM (Palumbo et al. 2015).

1.5.4.1 Bone Pain and Lesions

Symptoms usually begin with lower back pain, one of the most common symptoms which is a result of the loss of bone density in the spine and ribs. Bone reabsorption is facilitated by osteoclasts whose activity is stimulated by the presence of MM cells in the bone marrow (Roodman 2004). These abnormal plasma cells produce macrophage inflammatory protein-1α (MIP-1α), a chemokine which has been shown to promote osteoclastogenesis (Choi et al. 2000). MM cells also interact with bone marrow stromal cells via the integrin VLA-4, resulting in the release of receptor activator of NF-κB ligand (RANKL) from these stromal cells (Giuliani et al. 2001). RANKL directly promotes osteoclastogenesis while simultaneously inhibiting osteoclast apoptosis. MM cells also inhibit the production of a decoy receptor for RANKL called osteoprotegerin (OPG) by

osteoblastic cells, further increasing the activation of osteoclasts and the shift from bone formation to bone reabsorption (Giuliani, Colla, and Rizzoli 2004; Qiang et al. 2008).

For this reason, serum calcium levels are an important indicator of MM progression. Hypercalcaemia (>2.75mmol/L serum calcium) is primarily treated by administering bisphosphonates which encourage osteoclast apoptosis (Kyle, Yee, et al. 2007). MRI scans are also commonly performed to observe the presence and severity of bone lesions that result from the breakdown of bone by osteoclasts (Rajkumar et al. 2014). In severe cases, compression fractures can cause chronic pain, deformity or poor mobility, and may necessitate repair using a technique known as kyphoplasty. This fills the fracture with a viscous polymethylmethacrylate cement which has been shown to reduce the pain associated with vertebral compression fractures. However, there is a risk of the procedure causing nerve injury, spinal cord compression or paralysis (Berenson et al. 2011).

1.5.4.2 Renal Failure

Renal impairment is thought to affect around 50% of MM patients during the course of their disease (Dimopoulos et al. 2010). It is measured using serum creatinine levels and defined as having a creatinine concentration greater than 2mg/dL (Dimopoulos et al. 2008). Renal impairment is caused by the excess free light chains that are produced by abnormal plasma cells, overwhelming the ability of the kidneys to filter out this protein from the blood (Mead et al. 2004). The free light chains bind to Tamm-Horsfall glycoproteins in the loop of Henley, forming aggregates that obstruct distal parts of the nephron (Ying and Sanders 2001). In a small number of patients, increased concentrations of free light chains in the serum can lead to light-chain amyloidosis. This is characterised by the deposition of monoclonal light chain fibres within various tissues throughout the body. Deposits of these fibres in the kidneys can contribute to renal failure (Dimopoulos et al. 2010). Around 10% of MM patients require long-term dialysis (Yadav et al. 2015).

Dialysis is commonly used to treat renal impairment, acting to remove excess free light chains as well as replacing kidney function after failure (Hutchison et al. 2007). As hypercalcaemia is also known to negatively impact renal function, reducing calcium concentrations in the blood though hydration and bisphosphonate administration is also recommended (Dimopoulos et al. 2008). However, bisphosphonates themselves may cause further renal impairment and so an assessment of the risk to the patient must first be made (Faiman et al. 2011). The effective management of renal impairment significantly improves the overall survival of patients with MM. Unfortunately, patients who present with renal impairment at diagnosis are known to have an inferior survival when compared to those who do not (Gonsalves et al. 2015).

1.5.4.3 Anaemia and Infection

The growth of abnormal plasma cells throughout the bone marrow reduces the quantity of healthy stromal cells. This leads to a decrease in the production of red blood cells, resulting in anaemia (Mittelman 2003). However, it has also been observed that hepcidin is upregulated in cases of MM. This protein inhibits ferroportin, an iron export channel which is responsible allowing iron to pass into the bloodstream from the interior of a cell. While the cause for this increase in hepcidin has yet to be fully elucidated, it is nevertheless thought to play a role in the cellular retention of iron and the development of anaemia during MM (Sharma et al. 2008; Maes et al. 2010). The definition of anaemia in the case of MM is either a haemoglobin value >20g/L below the lower limit of normal, or simply <100g/L (Rajkumar et al. 2014). It is thought that anaemia presents in around 73% of all MM cases, resulting in the characteristic tiredness and weakness of the disease (Kyle et al. 2003).

As well as disrupting red blood cell production, immunodeficiency is also a common feature of MM. The immunodeficiency in MM is not due to a lack of neutrophils but is due to a more global effect on function of B and T cells, normal antibody production, dendritic cells, antigen presentation and function of innate immune cells. There are

increases in a range of immunosuppressive cytokines, inhibitory signalling pathways and an increase in immunosuppressive cells. This increases the risk of developing infections, with one UK study suggesting that bacterial infection directly causes 45% of all MM deaths observed within 6 months of diagnosis (Augustson et al. 2005). Further studies have observed that the risk of infection in MM patients, particularly from pneumonia and septicaemia, is seven times higher than in matched controls (Blimark et al. 2015). It has been suggested that recurrent infections may play a role in promoting the proliferation and survival of abnormal plasma cell populations. This is due to the presence of toll-like receptors on the surface of B cells, membrane-spanning proteins which act as sensors for the innate immune system and initiators of the adaptive immune system. The expression of these receptors, particularly that of toll-like receptors 4 and 9, is known to be upregulated in MM when compared to the plasma cells of healthy donors (Bohnhorst et al. 2006). Activation of these toll-like receptors during infection is thought to promote abnormal plasma cell proliferation and the avoidance of serum-deprivation induced apoptosis (Xu et al. 2010).

1.5.5 Plasma Cell Leukaemia

Plasma cell leukaemia (PCL) is a lymphoproliferative disorder which can either occur de novo, or evolve from an existing case of MM. It is characterised by the significant presence of abnormal plasma cells within the circulating blood, and officially defined as having $>2x10^9$ plasma cells/litre of blood or >20% plasma cells in the peripheral blood differential white cell count (Kyle et al. 2003). Although it is estimated that up to 4% of MM patients will eventually develop PCL, it is highly aggressive and confers an overall median survival of 2-15 months depending on the chemotherapeutic regimens used during treatment (Jimenez-Zepeda and Dominguez-Martinez 2009). Many of the symptoms displayed are identical to that of MM; bone lesions, hypercalcaemia, renal impairment and anaemia. However, around 11% of PCL cases that develop from MM

will present with hepatomegaly (enlargement of the liver), while 8% of cases will present with splenomegaly (enlargement of the spleen) (Tiedemann et al. 2008).

1.5.6 MM Staging Systems

Two different staging systems exist which are used to measure the extent of MM progression. The oldest of these was developed in 1975 by Brian Durie and Sydney Salmon and is known as the Durie-Salmon staging system. This categorises patients by analysing the concentrations of serum calcium, haemoglobin, paraprotein and urinary light chains (Durie and Salmon 1975). A competing model was developed in 2005 which is known as the international staging system (ISS) for MM. This simply measures serum β2 microglobulin and albumin levels (Greipp et al. 2005). An updated version of the ISS was released in 2015 which sought to improve prognostic resolution by combining these measurements with the presence or absence of high-risk chromosomal abnormalities, as well as measurements of serum lactate dehydrogenase concentration (Palumbo et al. 2015).

1.5.6.1 The Durie-Salmon Staging System

Although the Durie-Salmon staging system is still employed as a method of predicting an individual's prognosis, its use has become limited since the development of the ISS for MM. Patients are categorised as either stage I, II, or III (***see Table 1.2***). The main drawback of the Durie-Salmon staging system is the requirement to locate and identify lytic bone lesions from X-rays, a process which can be subjective and lacks sensitivity. To combat this, an updated system was published in 2003 (Durie-Salmon PLUS) which utilises magnetic resonance (MR) imaging and fluorine 18 fluorodeoxyglucose positron emission tomography (FDG-PET) to more accurately quantify the number of bone lesions present (Durie et al. 2003). Measurements of haemoglobin, serum calcium and paraprotein concentrations are also substituted for creatinine levels, allowing each stage to be further subdivided into either A or B (***see Table 1.3***).

Stage I	All of the following must be present: • Haemoglobin >10g/dL • Serum calcium <12mg/dL • No evidence of bone lesions • IgG paraprotein <5g/dL or IgA paraprotein <3g/dL or urine light chain M-component on electrophoresis <4g/24 hours
Stage II	Neither stage I or III
Stage III	One or more of the following must be present: • Haemoglobin <8.5g/dL • Serum calcium >12mg/dL • Three or more bone lesions • IgA paraprotein >5g/dL or IgG paraprotein >7g/dL or urine light chain M-component on electrophoresis >12g/24 hours

Table 1.2 – Staging Criteria for the Durie-Salmon staging system

Stage I	**A**	0 – 4 bone lesions; <2mg/dL serum creatinine
	B	0 – 4 bone lesions; >2mg/dL serum creatinine
Stage II	**A**	5 - 10 bone lesions; <2mg/dL serum creatinine
	B	5 - 10 bone lesions; >2mg/dL serum creatinine
Stage III	**A**	>20 bone lesions; <2mg/dL serum creatinine
	B	>20 bone lesions; >2mg/dL serum creatinine

Table 1.3 – Staging Criteria for the Durie-Salmon PLUS staging system

Stage I	β2 microglobulin < 3.5mg/dL and albumin >3.5g/dL
Stage II	Either: • β2 microglobulin < 3.5mg/dL and albumin < 3.5g/dL • β2 microglobulin between 3.5 and 5.5mg/dL
Stage III	β2 microglobulin > 5.5mg/dL

Table 1.4 – Staging Criteria for the MM ISS

R-Stage I	All of the following criteria must be met: • ISS stage I • No high-risk chromosomal abnormalities present • Normal LDH
R-Stage II	Neither R-ISS stage I or III
R-Stage III	All of the following criteria must be met: • ISS stage III • Presence of high-risk chromosomal abnormalities • High LDH

Table 1.5 – Staging Criteria for the Revised ISS

Studies comparing the original and updated systems have found that patients stratified using Durie-Salmon PLUS are commonly upstaged if the original Durie-Salmon staging system is used instead. Fechtner et al. (2010) observed that only 45% of a cohort of MGUS and MM patients remained in the same staging category when analysed using both systems. This was thought to be due to the removal of important clinical data (haemoglobin, serum calcium and paraprotein concentrations) in the Durie-Salmon PLUS system which is known to hold significant prognostic information. However, a small number of patients would also have been upstaged when using Durie-Salmon PLUS due to the greater sensitivity of MR imaging in detecting bone lesions when compared to X-rays.

1.5.6.2 The International Staging System for MM

The international myeloma working group, a collection of IMF scientific advisors, devised the ISS in 2005. It is more cost-effective than the Durie-Salmon staging system, relying on two blood tests to measure the concentration of serum β2 microglobulin and albumin. β2 microglobulin is a component of the MHC class I molecule, with higher concentrations reflecting a larger tumour mass and a greater impairment of renal function. Meanwhile a reduction in the concentration of serum albumin is caused by cytokine release from the myeloma microenvironment. Again, patients are categorised as either stage I, II or III (***see Table 1.4***).

Median overall survival for each stage was found to be 62 months, 44 months and 29 months respectfully (Greipp et al. 2005). A revision to the ISS in 2015 sought to include chromosomal abnormalities in the staging criteria, as well as measurements of serum lactate dehydrogenase (LDH). High-risk chromosomal abnormalities included the presence of del(17p), translocation t(4;14) or translocation t(14;16). The revised ISS patients were also categorised as either R-stage I, II or III (***see Table 1.5***). 5-year overall survival rates for R-stage I, II and III patients were 82%, 62% and 40% respectfully. The revised ISS also resulted in a significant number of patients being reclassified as higher-

risk, with 26% of patients being given a better prognosis when compared to the original ISS staging system (Palumbo et al. 2015). No matter which system is used, it must be recognised that both the ISS and revised ISS can lack accuracy for individual patients. Some patients may do better/worse than their ISS stage would suggest. Therefore, there still remains significant unpredictability.

1.5.7 Genetic Aberrations in MM

Translocations involving the immunoglobulin heavy locus (IgH), located on chromosome 14, are thought to be some of the earliest initiating events in the development of plasma cell disorders (***see figure 1.6***). These translocations most commonly occur during class switch recombination, with oncogenes being placed under the influence of the IgH enhancer. Studies have suggested that IgH translocations involving chromosome 14q32 exist in around 47% of MGUS and 73% of symptomatic MM patients, reaching as high as 84% in patients with plasma cell leukaemia (Nishida et al. 1997; Avet-Loiseau et al. 2002). This can result in the IgH enhancers Eμ, Eα1 and Eα2 being placed into the proximity of oncogenes (Bergsagel and Kuehl 2001). One such set of genes, commonly overexpressed in the early stages of MGUS, are the cyclin D proteins. These act to drive cells though the G1/S phase by forming a complex with cyclin-dependent kinases (CDKs), resulting in the phosphorylation and inactivation of the retinoblastoma protein (Musgrove et al. 2011). The upregulation of cyclin D1 or cyclin D3, caused by t(11;14)(q13;q32) and t(6;14)(p21;q32) translocations respectively, is thought to occur in around 20% of MM cases (Zhan et al. 2006).

IgH translocations are also involved in each of the high-risk chromosomal abnormalities outlined in the revised ISS for MM (Palumbo et al. 2015). A t(4;14)(p16;q32) translocation is thought to be present in around 15% of MM patients, resulting in overexpression of the FGFR3 and MMSET genes. This event is known to indirectly lead to the upregulation of cyclin D2 (Kuehl and Bergsagel 2005). Meanwhile, around 10%

of patients are thought to express a t(14;16)(q32;q23) translocation which results in the upregulation of the c-MAF proto-oncogene (Zhan et al. 2006).

Hyperdiploidy is also a common initiating event in MM, with around 50% of all MGUS and MM patients thought to present with multiple copies of chromosomes 3, 5, 7, 9, 11, 15, 19 and/or 21 (Smadja et al. 2001). Again, cyclin D1 expression can be upregulated due to an increased copy number of chromosome 11. However, it has been suggested that hyperdiploidy of some chromosomes may confer a significantly better prognosis than others. One study identified patients with trisomy 3 and 5 as having an improved overall survival, even in patients with the high-risk t(4;14) translocation. Conversely, trisomy 21 and gain of the 1q arm significantly worsened overall survival (Chretien et al. 2015).

Chromosome 13 deletions, arising either from loss of the q arm or monosomy, are further events that are thought to be present in around 50% of MM patients (Chiecchio et al. 2006). Recent studies have suggested that loss of chromosome 13 confers a significantly reduced overall survival (Shaughnessy et al. 2003; Chiecchio et al. 2006). One possible explanation for this is that the loss of the q arm also results in the loss of the gene encoding the retinoblastoma protein. However, chromosome 13 encodes a significant number of other genes and so this is unlikely to be to only reason (Walker et al. 2010). Deletion of the 17p arm is also a significant event in MM, leading to its inclusion in the revised ISS as a high-risk abnormality. This deletion is thought to be present in around 11% of MM patients, resulting in loss of the TP53 gene and disruption to apoptotic and senescent pathways (Avet-Loiseau et al. 2007).

Further secondary genetic events include the dysregulation of the genes encoding MYC and RAS-family proteins. In one study, the c-myc locus was shown to be rearranged in 3% of MGUS, 4% of smouldering MM, and 15% of symptomatic MM patients (Avet-Loiseau et al. 2001). Around 10% of these rearrangements are thought to occur via a

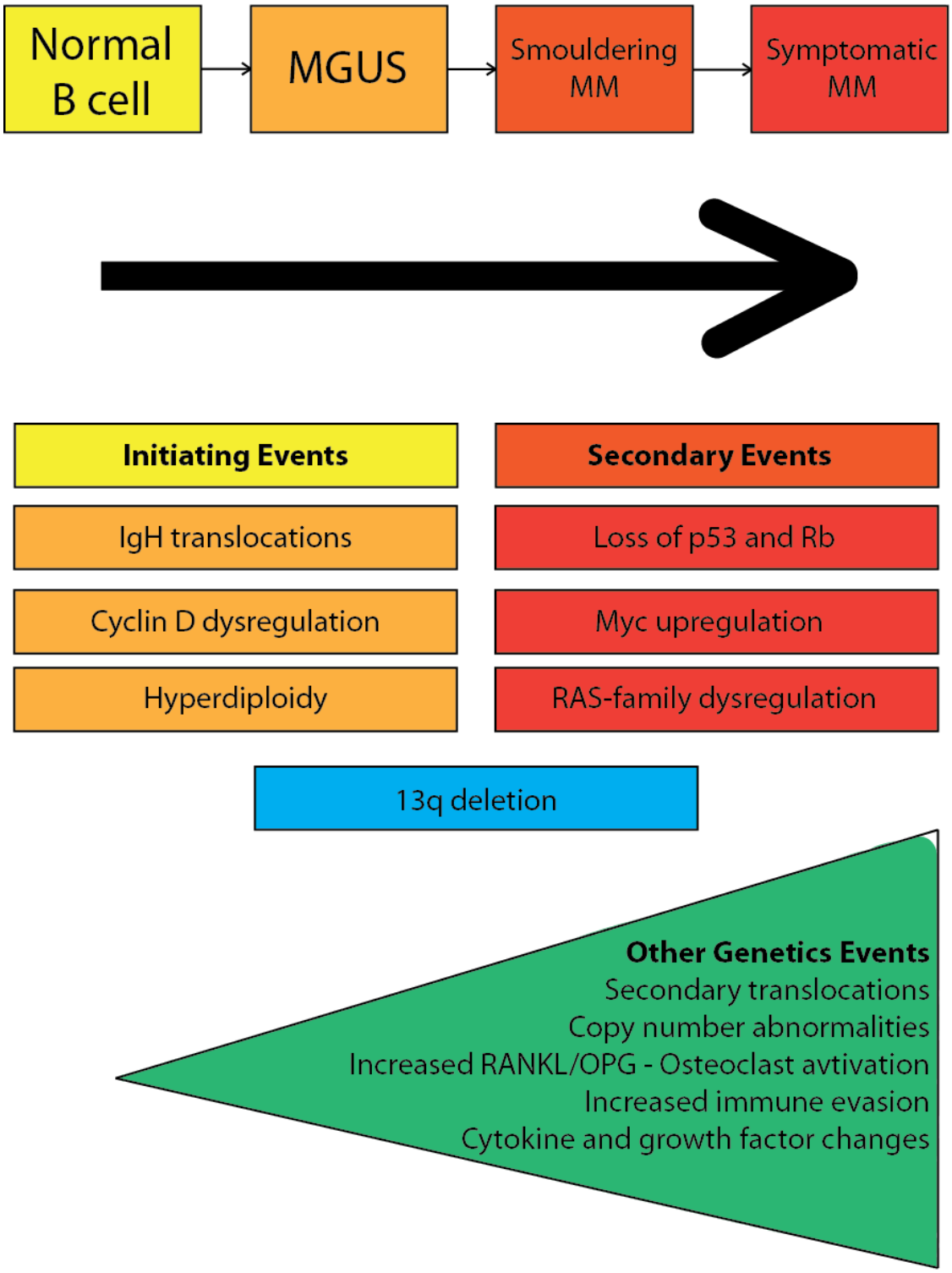

Figure 1.6 - Genetic Aberrations in Multiple Myeloma
Genetic dysregulation in MM varies depending on the stage of the disease. Primary initiating events are those which are commonly observed in the early stages of MGUS or smouldering MM. These are thought to be the main causes of the malignancy. Secondary events are those that commonly occur at a later stage in the disease and are thought to drive progression. *Adapted from 'Monoclonal Gammopathy of Undetermined Significance and Smoldering Multiple Myeloma: A Review of the Current Understanding of Epidemiology, Biology, Risk Stratification, and Management of Myeloma Precursor Disease' Agarwal and Ghobrial, Clinical Cancer Research 19, 985-994 (2013)*

t(8;14) translocation, again involving the IgH locus on chromosome 14 (Bergsagel and Kuehl 2003). Meanwhile, Chng et al. (2008) demonstrated that 7% of MGUS patients analysed during their study had mutations in RAS-family genes (RAS, KRAS and HRAS). This increased to 25% for patients with newly diagnosed MM and 45% of patients with relapsed MM. Those patients in which a RAS mutation was identified had a significantly reduced overall survival when compared to those without.

Telomeric shortening is also known to occur in the $CD138^+$ plasma cells of MM patients, acting as a possible explanation for the genetic instability that drives disease progression. Wu et al. (2003) used TRF analysis to compare the mean telomere lengths of abnormal plasma cells with normal leukocytes isolated from the same patient. They not only observed that mean telomere length was significantly reduced in the abnormal plasma cells, relative to the leukocyte population, but that the mean telomere lengths of those plasma cells were also reduced when compared to normal $CD138^+$ plasma cells isolated from healthy patients. Cottliar et al. (2003) appeared to verify this discovery, demonstrating that the mean telomere lengths of MM patient whole bone marrow aspirates were significantly shorter than normal controls. They also showed that a negative correlation exists between mean telomere length and the percentage of plasma cells within the bone marrow.

1.5.8 Treating MM

MM is an incurable disease, with treatments focusing on the relief of symptoms and reducing the population of abnormal plasma cells. As well as the treatment of individual symptoms mentioned earlier, a significant number of drugs have been devolved which are prescribed in the case of symptomatic MM. However, treatments vary depending on the current health of the patient and whether the disease has relapsed. Treatment is normally initiated either when myeloma-defining events are detected or if the

concentration of paraprotein in the blood increases significantly during several clinic visits.

1.5.8.1 Current Treatments

After being diagnosed, MGUS and smouldering MM are rarely treated. It is not until symptoms begin to appear that treatment is initiated. The national institute for health and care excellence (NICE) currently recommends bortezomib (marketed as Velcade), thalidomide and dexamethasone as an induction treatment for previously untreated patients. This is also known as VTD (NICE, 2016). Bortezomib is a proteasome inhibitor that causes cellular apoptosis by preventing the degradation of misfolded proteins, thalidomide is an immunomodulatory drug which prevents angiogenesis, and dexamethasone is a corticosteroid (Richardson et al. 2005; Palumbo et al. 2008). This combination is known to be more effective as an induction therapy than thalidomide and dexamethasone (VD) alone, or bortezomib-cyclophosphamide-dexamethasone (VCD). Instead, the use of cyclophosphamide is usually reserved for the treatment of relapsed MM (Cavo et al. 2010; Cavo et al. 2015).

If a patient is healthy and suitable enough, autologous stem cell transplantation can be considered. This involves first reducing the number of abnormal plasma cells in bone marrow by prescribing several cycles of VTD induction therapy. Stem cells are then harvested from the patient's bone marrow, at which point treatment with high-dose chemotherapy (and sometimes radiation) is used to kill most of the plasma cells. The harvested bone marrow is then infused back into the patient (Kyle and Rajkumar 2008). A second autologous stem cell transplantation can be performed once the patient relapses, with one phase III study suggesting that this can improve progression free survival and overall survival when compared to cyclophosphamide alone (Cook et al. 2014).

A small number of patients may benefit from myeloablative allogenic stem cell transplants, whereby the patient is given donor stem cells after high-dose chemotherapy. This method remains the only potential cure for MM, possibly due to the anti-MM effects of the immune cells within the allograft (Lokhorst et al. 2010). However, a high transplant-related mortality has been recorded, with around 29% of patients in one study eventually succumbing to either infection or graft versus host disease (Vekemans et al. 2014). Outcomes can be improved by having a patient undergo a reduced-intensity allograft, with less chemotherapy being administered. This does not suppress the patient's immune system to the same extent, but still allows the donor cells to mount an immune response against the cancer. Although Crawley et al. (2007) demonstrated that reduced-intensity allografts result in a reduced mortality when compared to myeloablative allografts (24% vs 37% at two years respectively), progression-free survival was also reduced (18.9% vs 34.5% at 2 years).

Autologous and allogenic stem cell transplants are unsuitable for frail patients who would not be expected to survive the high-risk procedure. Instead, NICE recommends treating with a combination of bortezomib and an alkylating agent such as melphalan (*NICE, 2016*). Facon et al. (2007) also recommend combining this treatment option with thalidomide to further increase overall survival. Regardless of how MM is treated, almost all cases will inevitably relapse. This is due to subclonal evolution, with the genetic landscape of the various plasma cell clones becoming more heterogeneous during disease progression and treatment (Bolli et al., 2014). At this point, NICE recommends bortezomib and dexamethasone, followed by the second autologous stem cell transplant where possible. After two or more relapses, lenalidomide should be administered in combination with dexamethasone and cyclophosphamide (NICE, 2016).

As well as direct treatment of the cancer, patients will also require their symptoms to be addressed and managed as the myeloma develops. For example, bisphosphonates are commonly administered to slow osteoclast-mediated bone resorption and prevent

hypercalcemia (Papapoulos, 2008). Dialysis may also be used to when renal impairment or failure occurs. As a chronic disease, supportive management is critical and involves focussing on preventing anaemia (blood transfusion) and thrombosis formation (plasma exchange), an impaired immune system, managing neuropathy, reducing pain and fatigue, and dealing with the psychologic effects of cancer formation and chemotherapy (NICE, 2016).

1.5.8.2 Future Treatments

Although the next generation of immunomodulators (Pomalidomide) and proteasome inhibitors (Carfilzomib and Ixazomib) have now been approved for treatment in cases of MM, novel treatments are also beginning to show promise (San Miguel et al. 2013; Stewart et al. 2015; Moreau et al. 2016). The histone deacetylase (HDAC) inhibitor panobinostat has recently been approved for use in cases of relapsed MM, with the clinical trials performed by San-Miguel et al. (2014) suggesting that panobinostat-bortezomib-dexamethasone results in a significantly increased progression-free survival when compared to bortezomib-dexamethasone alone (median 11.99 months against 8.08 months respectfully). Meanwhile, a HDAC-6 inhibitor called riclinostat has recently completed phase I clinical trials in refractory MM and has been shown to enhance the effects of carfilzomib *in vitro* (Yee et al. 2016; Mishima et al. 2015).

In patients where current therapeutic options have been exhausted, monoclonal antibodies (mAb) have emerged as a novel and effective treatment. One of the advantages of this therapy is its ability to selectively target the abnormal plasma cells in MM. Daratumumab is one such anti-CD38 mAb which induces cell death via antibody-dependent cell-mediated cytotoxicity, antibody-dependent cellular phagocytosis and complement-dependent cytotoxicity (Lonial et al. 2016). Palumbo et al. (2016) demonstrated during phase III clinical trials that the use of daratumumab-bortezomib-dexamethasone in relapsed MM patients improves progression-free survival when

compared to bortezomib-dexamethasone alone (60.7% vs 26.9% after 12 months respectfully).

Elotuzumab is another mAb which was recently approved for the treatment of relapsed MM. It targets the SLAMF7 (otherwise known as CD319) surface antigen on normal and abnormal plasma cells, inducing cell death by antibody-dependent cell-mediated cytotoxicity, as well as inhibition of the SLAMF7-mediated adhesion of MM cells to bone marrow stromal cells (Lonial et al., 2016). Phase III clinical trials by Lonial et al. (2015) demonstrated that elotuzumab-lenalidomide-dexamethasone treatment in relapsed MM resulted in an increased progression-free survival when compared to lenalidomide-dexamethasone alone (41% vs 27% after 24 months).

Novel treatments which target abnormal signalling pathways have also been proposed, with cyclin-dependent kinase (CDK) inhibitors currently being explored as an option to overcome the upregulation of cyclin D family proteins that have commonly been identified in MM. Dinaciclib is one such CDK inhibitor which has recently undergone successful phase II clinical trials in relapsed MM as a single agent (Kumar et al. 2015). It has also been demonstrated that dinaciclib is capable of sensitising MM cell lines to the effects of PARP inhibition (Alagpulinsa et al. 2016). However, PARP inhibitors are not currently recommended as a treatment for MM and little work has been carried out to explore their role in preventing a telomere-driven crisis within abnormal plasma cells.

1.6 DNA Repair and PARP Inhibition

Critical telomeric shortening may not always trigger senescence. Genetic abnormalities, such as the loss of functional retinoblastoma or p53 proteins described in MM, sometimes permit a cell to continue dividing beyond the Hayflick limit which eliminates the protective capacity of the telomere. In these cases, chromosomal fusion is thought

to drive the genomic rearrangement and instability that underpins a significant number of cancers (Lin et al. 2014; Roger et al. 2013; Gisselsson et al. 2001). As a method of identifying novel cancer treatments, it is necessary to understand and target the DNA damage repair mechanisms which play a role in the aberrant repair of telomere-deficient chromosomal ends. One such target is the poly(ADP-ribose) polymerase (PARP) family. Comprised of 17 members, each uses NAD^+ as a substrate with which to catalyse the addition of ADP-ribose to target proteins. PARP1 and PARP2 are both known to play various roles in the repair of DNA damage, making them attractive targets in the treatment of genetically-unstable cancers (Vyas and Chang 2014). PARP inhibitors have already been approved for use in BRCA-mutated breast and ovarian cancers, but little is known about their capacity to treat MM (Kaufman et al. 2015).

1.6.1 Single-Strand DNA Breaks

Common causes of single-strand DNA breaks include oxidative attack by endogenous reactive oxygen species (ROS), external factors such as UV light and cigarette smoke, and even aborted DNA repair mechanisms (Mello Filho and Meneghini 1984; Nelson and Kastan 1994; Caldecott 2008). The result is an inability to replicate DNA during S-phase, with replication forks becoming blocked or collapsing. Because of this, an inevitable consequence is that any unrepaired single-strand DNA breaks will eventually become double-strand breaks. Cells therefore require the ability to delay cell cycle progression whilst the damage is repaired by one of several mechanisms (Cimprich and Cortez 2008)

The process of cell cycle arrest is initiated by an ATR-mediated pathway. Replicative stress causes replication protein A (RPA) to bind at the site of single-strand DNA damage (Unsal-Kacmaz and Sancar 2004). RPA is a complex of three proteins (RPA14, RPA32 and RPA70) which are responsible for recruiting ATR via the ATR-interactive protein (ATRIP). It has been observed that the loss of ATRIP activity prevents ATR binding at the single-strand break, thus inhibiting the initiation of cell cycle arrest (Cortez et al.

2001). Once bound to DNA, ATR is activated by topoisomerase 2-binding protein 1 (TOPBP1) and the Rad9-Hus1-Rad1 (9-1-1) complex (Kumagai et al. 2006). This activation results in the phosphorylation of several signalling proteins, most notably checkpoint kinase 1 (CHK-1). CHK-1 then targets the cell division cycle (CDC) proteins CDC25a and CDC25b for ubiquitin-mediated degradation, preventing the cells from transitioning thought the S-phase or G2-M checkpoints (Mailand et al. 2000; Nam and Cortez 2011; Zhou and Bartek 2004). However, this pathway only seeks to prevent cell cycle progression. The repair of a single-strand DNA break is carried out by one of several different mechanisms.

1.6.1.1 Base Excision Repair

Base excision repair (BER) is primarily responsible for correcting base lesions which do not significantly distort the helical DNA structure (***see figure 1.7***). This mostly includes deaminated bases and abasic (AP) sites. The removal of the damaged base is carried out by a glycosylase enzyme, leaving behind an empty deoxyribose residue. An AP-endonuclease (APE1) then cleaves the deoxyribose residue, generating 5′-deoxyribose phosphate and 3′-hydroxyl ends at the site (Hegde, Hazra, and Mitra 2008). Before the repair of this single nucleotide-free gap, otherwise known as short-patch repair, PARP1 and PARP2 homo- and heterodimers bind to the site of the break. Their activity recruits XRCC1, a protein which ensures efficient gap-filling and nucleotide ligation by polymerase β and DNA ligase III (Schreiber et al. 2002). It has been demonstrated that inhibition of PARP1 and PARP2 prevents the recruitment of XRCC1, leading to elevated frequencies of genetic damage (Reynolds et al. 2015; Breslin et al. 2015).

A variation of this process exists whereby several nucleotides are removed from the area downstream of the base lesion. Known as long-patch repair, this still requires the damaged base to be removed by the action of a glycosylase and an AP-endonuclease. At this point, polymerase δ is recruited to synthesise a sequence of 2-10 nucleotides downstream of the DNA damage site (Pascucci et al. 1999). This acts to displace the

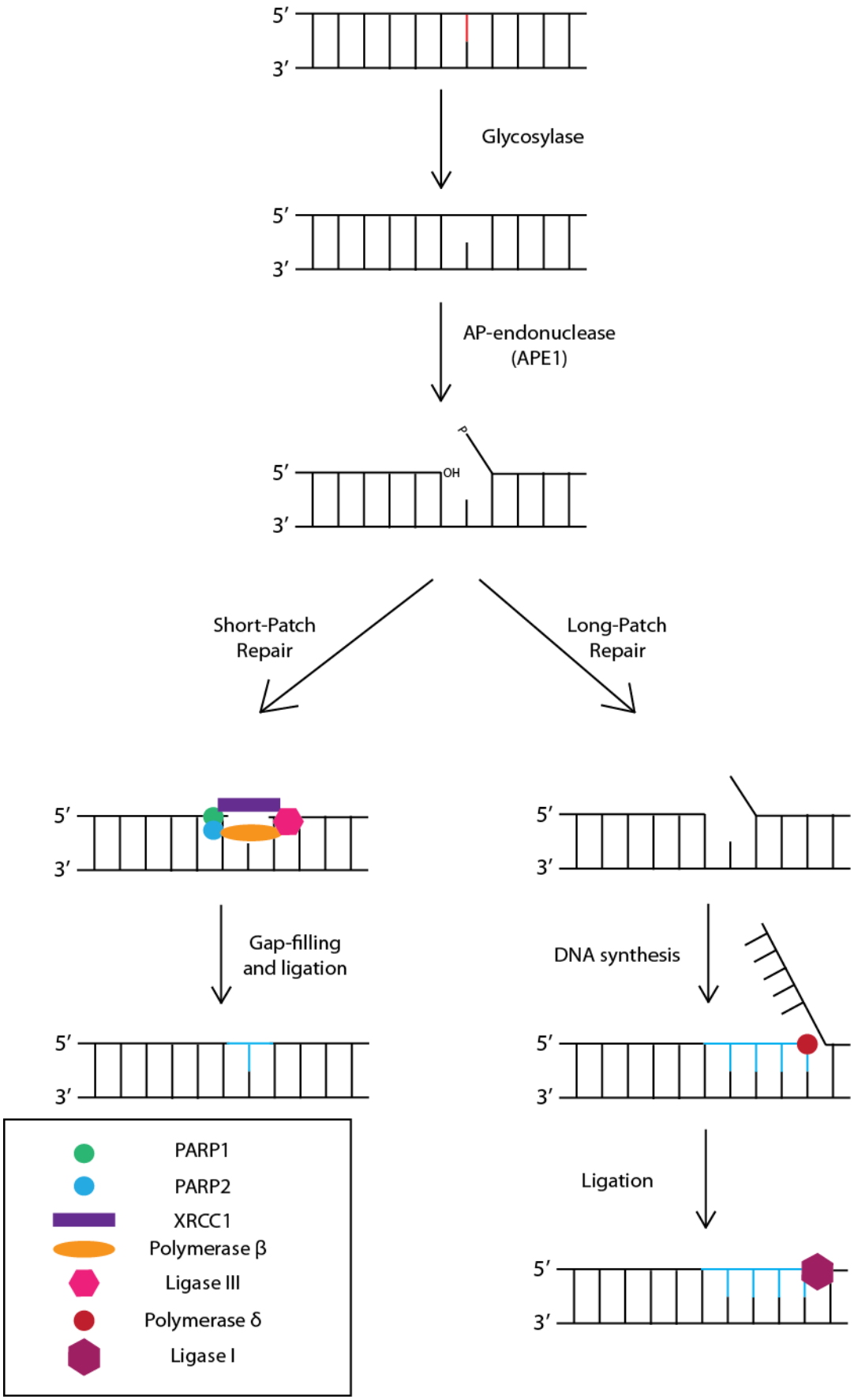

Figure 1.7 - Base Excision Repair
Figure detailing the main steps in base excision repair. This process is mostly used to correct deaminated bases and abasic sites. After the damages base has been removed, repair can proceed either by short- or long-patch repair.

original nucleotide sequence, creating a flap which is then cleaved by flap endonuclease 1 (FEN1). At this point, the nick is sealed by DNA ligase I (Krokan and Bjoras 2013). Mutated forms of FEN1 have been identified in cancer, whereby their presence correlated with a reduction in long-patch repair activity and greater frequencies of genetic damage (Sun et al. 2017).

1.6.1.2 Nucleotide Excision Repair

Nucleotide excision repair (NER) is primarily responsible for correcting base lesions which significantly distort the helical DNA structure. An example of this would be the pyrimidine dimers formed as a result of expose to UV radiation (Fitch et al. 2003). This mechanism can initiate via one of two pathways; global genome repair (GGR) or transcript coupled repair (TCR). Either way, the pathways merge once the transcription factor IIH (TFIIH) complex binds at the site of DNA damage.

During GGR, base lesions are sensed by the UV-damaged DNA-binding (UV-DDB) protein. This stimulates the recruitment of XPC-RAD23B-CENT2, a protein complex which continuously scans the genome. After binding to the site of DNA damage, the RAD23B subunit dissociates and the TFIIH complex is recruited (Kamileri, Karakasilioti, and Garinis 2012). Meanwhile, the TCR pathway is initiated by the stalled translation of an RNA polymerase II molecule. Unable to dissociate, RNA polymerase II instead colocalises with the DNA-dependent ATPase cockayne syndrome B (CSB) protein. This acts to recruit an E3-ubiquitin ligase complex which forces RNA polymerase II to backtrack, allowing TFIIH to access the site of DNA damage (Marteijn et al. 2014).

In the case of either GGR or TCR, a subunit of the TFIIH protein complex then unwinds the double-stranded DNA surrounding the site of damage. Another subunit with endonuclease activity cleaves approximately 27 nucleotides from the single-stranded DNA surrounding the site (Friedberg 2001). DNA polymerase δ and DNA ligase III are

then responsible for filling the resulting nucleotide gap. However, the role that PARP1 and PARP2 play in this mechanism is not well characterised. It has been suggested that PARP1 acts during GGR to modify the XPC-RAD23-CENT2 complex, regulating its ability to bind DNA (Maltseva et al. 2015). Meanwhile, XRCC1 is known to increase the efficiency of DNA polymerase δ and DNA ligase I activity during NER (Moser et al. 2007). Whether PARP1 or PARP2 play a role in the recruitment of XRCC1, as is the case with the BER mechanism, remains to be known.

1.6.1.3 Mismatch Repair

DNA mismatch repair is responsible for correcting the abnormal pairing of nucleotides in a double-stranded DNA sequence. These errors mainly occur during DNA replication, with examples including the alignment of guanine-thymine or adenine-cytosine bases. Defects in the ability of a cell to perform mismatch repair have been associated with a high incidence of cancer, most commonly colorectal and endometrial (Barnetson et al. 2006; Win et al. 2012).

The mechanism is initiated when heterodimers of the DNA mismatch repair (MSH) proteins MSH2, MSH3 or MSH6 bind to the site of damage in an ATP-dependent manner. A second heterodimer, comprised of the MutL homolog 1 (MLH1) and post-meiotic segregation protein-2 (PMS2) proteins, then binds to form a complex. This complex diffuses upstream of the mismatch site, eventually encountering the proliferating cell nuclear antigen (PCNA) protein and the replication factor C (RFC) protein complex. RFC is displaced from the DNA, at which point exonuclease 1 (EXO1) associates. EXO1 then degrades the strand of nucleotides up to and including the site of mismatch repair. RPA is recruited to the remaining single-stranded DNA, stabilising it until polymerase δ and DNA ligase I can synthesis and join a new complementary sequence (Jiricny 2006; Modrich 2006; Hombauer et al. 2011).

1.6.2 Double-Strand DNA Breaks

Although double-strand DNA breaks may be formed by a failure to repair single-strand DNA breaks, they can also result from direct exposure to ionising radiation or ROS. Either way, the cell is required to halt cell cycle progression until the damage is repaired by one of several mechanisms (Shrivastav, De Haro, and Nickoloff 2008). The process of cell cycle arrest is initiated by an ATM-mediated pathway, not to be confused with the ATR-mediated pathway that is triggered in response to single-strand DNA damage. It begins when multiple copies of the MRE11-RAD50-NBS1 (MRN) complex bind to the damaged DNA ends and to each other, acting to bridge the gap and bring the DNA strands closer together (Williams et al. 2008). The complex also recruits inactive ATM homodimers which then dissociate into active monomers (Bakkenist and Kastan 2003).

ATM continues the signalling pathway by interacting with a series of mediator proteins; MDC1, 53BP1, MRN and BRCA1. Their binding, particularly that of MDC1, allows ATM to directly phosphorylate any nearby histone H2AX proteins. This step is crucial for the recruitment of those proteins which are involved in the repair of double-strand DNA breaks (Jazayeri et al. 2006). ATM also phosphorylates CHK-2 and p53, leading to the inhibition of the CDK2-cyclin E complex and preventing the cell from transitioning through the S-phase or G2-M checkpoints (Lobrich and Jeggo 2007; Lee and Paull 2007).

1.6.2.1 Homologous Recombination

Homologous recombination (HR) requires that the ends of each damaged DNA strand undergo resectioning (***see figure 1.8***). This is initiated when exonuclease 1, CtIP and BRCA1 bind to the MRN complex. Together, these remove nucleotides in a 5′ to 3′ direction on each DNA strand to leave behind a single-stranded overhang (Chen et al. 2008; Chen et al. 2017). This overhang is stabilised by the addition of replication protein A (RPA). The breast cancer type 2 susceptibility (BRCA2) protein then mediates the removal of RPA from the single-stranded DNA, as well as the addition of RAD51. RAD51

is necessary for strand invasion, a process whereby each single-stranded overhang binds to its complementary sequence on a homologous chromosome (Krejci et al. 2012). This undamaged chromosome is then used as a template by polymerase δ with which to synthesise the correct nucleotide sequence (Maloisel, Fabre, and Gangloff 2008).

At this point, HR can undertake one of two alternative pathways. The first of these, synthesis-dependent strand annealing (SDSA), ends with the newly synthesised strand of DNA dissociating from the template strand. It then anneals with the other half of the original chromosome, without any DNA being permanently exchanged between the homologous chromosomes (Moynahan and Jasin 2010). This is not the case for the second HR pathway, double-strand break repair (DSBR). Here, each single-stranded DNA overhang from the damaged chromosome binds to its complementary sequence on the homologous template chromosome at the same time. This forms a structure known as a Holliday junction. The BLM/TopoIIIα/RMI1/RMI2 protein complex is then responsible for orchestrating the exchange of single-stranded nucleotide sequences between the homologous chromosomes (Mimitou and Symington 2009). Regardless of which pathway is used, the result is a repaired double-strand DNA break without any loss of nucleotide sequence.

Mutations in either *BRCA1* or *BRCA2* are known to result in a compromised HR pathway, significantly increasing the risk of cancer development (Antoniou et al. 2008). It is thought that *BRCA1* and *BRCA2* mutations confer a 65% and 45% chance of developing breast cancer by age 70 (Antoniou et al. 2003). BRCA-mutated breast and ovarian cancers are commonly treated using the PARP inhibitors Rucaparib or Olaparib (***see section 1.6.3 – PARP Inhibition***). These drugs act to prevent the repair of single-strand DNA breaks, which eventually become double-strand DNA breaks (Knepper, Saller, and Walko 2017; Kim et al. 2015). In the presence of compromised HR pathway, cells must rely on the error-prone non-homologous end joining pathways to repair the increased frequency of DNA damage. The resulting genetic instability can prove catastrophic,

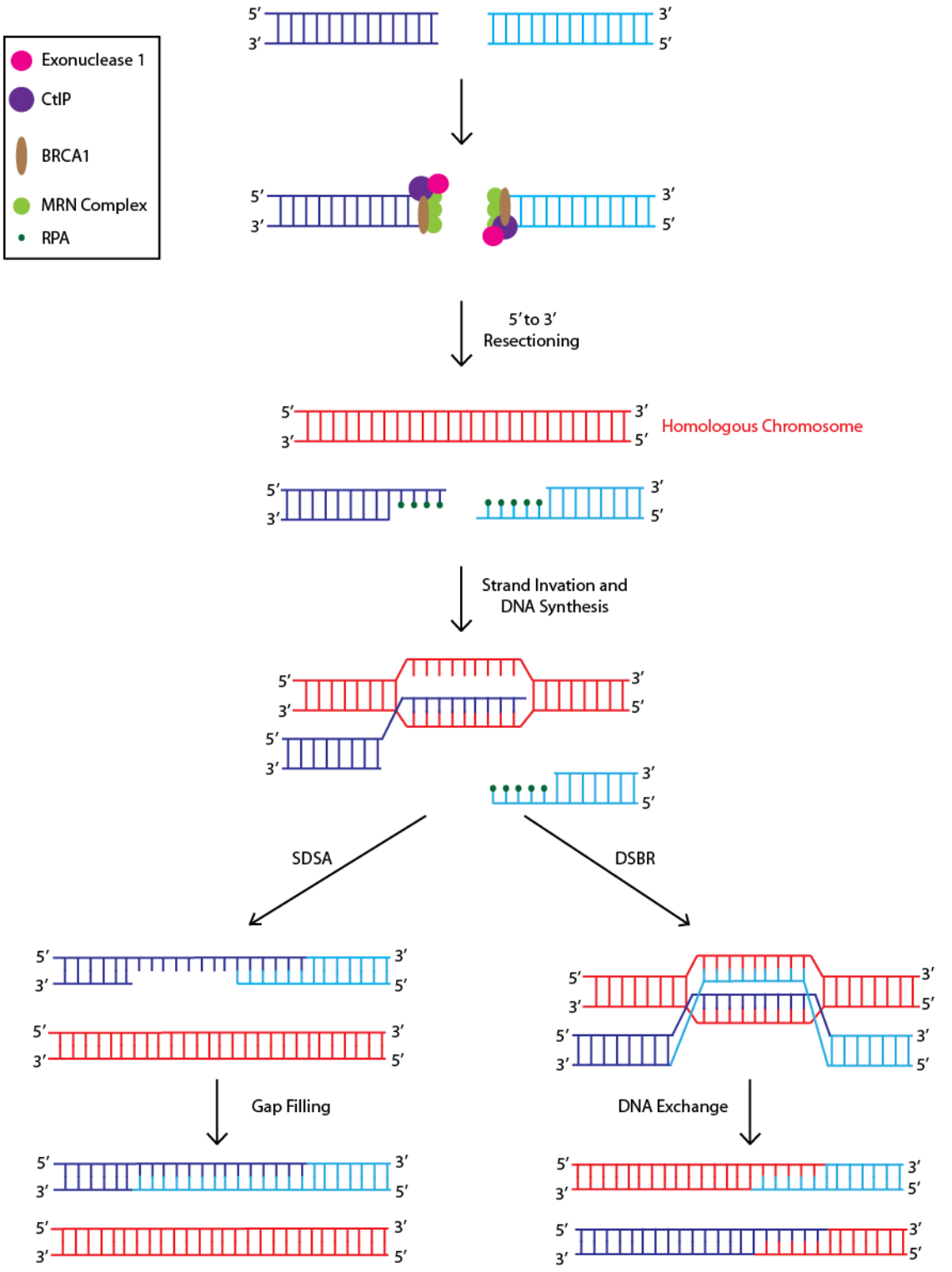

Figure 1.8 - Homologous Recombination
Figure detailing the main steps in homologous recombination. This process begins with the DNA ends undergoing resectioning to produce ssDNA overhangs. A homologous chromosome is then used as a template from which to synthesise the damaged DNA section. One of two pathways can then occur: synthesis-dependent strand annealing (SDSA) whereby the newly synthesised strand anneals with the other half of the original chromosome; or double-strand break repair (DSBR) where DNA is exchanged between each chromosome. *Adapted from 'The resistance of DMC1 D-loops to dissociation may account for the DMC1 requirement in meiosis.' Bugreev et al., Nat Struct Mol Biol, 18: 56-60 (2011)*

triggering apoptosis specifically in the HR-deficient cancer cells (Farmer et al. 2005; Javle and Curtin 2011).

1.6.2.2 Non-Homologous End Joining

Non-homologous end joining (NHEJ) is thought to be the most common mechanism used to repair double-strand DNA breaks in vertebrates (Liang et al. 1998; Rothkamm et al. 2003). Unlike the homology-directed repair observed in HR, NHEJ is simply used to ligate two broken DNA ends together (***see figure 1.9a***). The mechanism is initiated by the Ku70/Ku80 heterodimer. This binds to one of the DNA ends in a double-strand break, acting to recruit the DNA-dependent protein kinase catalytic subunit (DNA-PKcs). The resulting protein complex then binds to an identical complex on the corresponding DNA end, acting to bridge the gaps in the break and bring the DNA ends into proximity with each other (Weterings and Chen 2008). This occurs in conjunction with ligase IV, an enzyme which joins the DNA ends together with the help of the accessory proteins XRCC4 and XLF (Chen et al. 2000). PARP3 also accelerate the repair of double-strand DNA breaks by recruiting the aprataxin-and-PNK-like factor (APLF) protein. This promotes retention of the XRCC4/ligase IV complex at the break site (Rulten et al. 2011). However, a second mechanism is known to take over if the classical NHEJ pathway becomes compromised.

Known as alternative non-homologous end joining (alt-NHEJ), this pathway utilises a short homologous sequence at the broken DNA ends to guide their alignment (Pannunzio et al. 2014). It is from this that the alternative name of microhomology-mediated end joining is derived (***see figure 1.9b***). The switch from the classical pathway to this alt-NHEJ pathway is thought to be driven by the loss of either Ku70/Ku80 or ligase IV (Riballo et al. 2004). Alt-NHEJ is also thought to be promoted by PARP1 which competes with Ku70/80 for binding at the site of double-strand DNA breaks (Wang *et al*., 2006). It has been observed that inhibition of PARP1 function impairs the repair of double-strand DNA breaks (Audebert, Salles, and Calsou 2004). In the case of repair

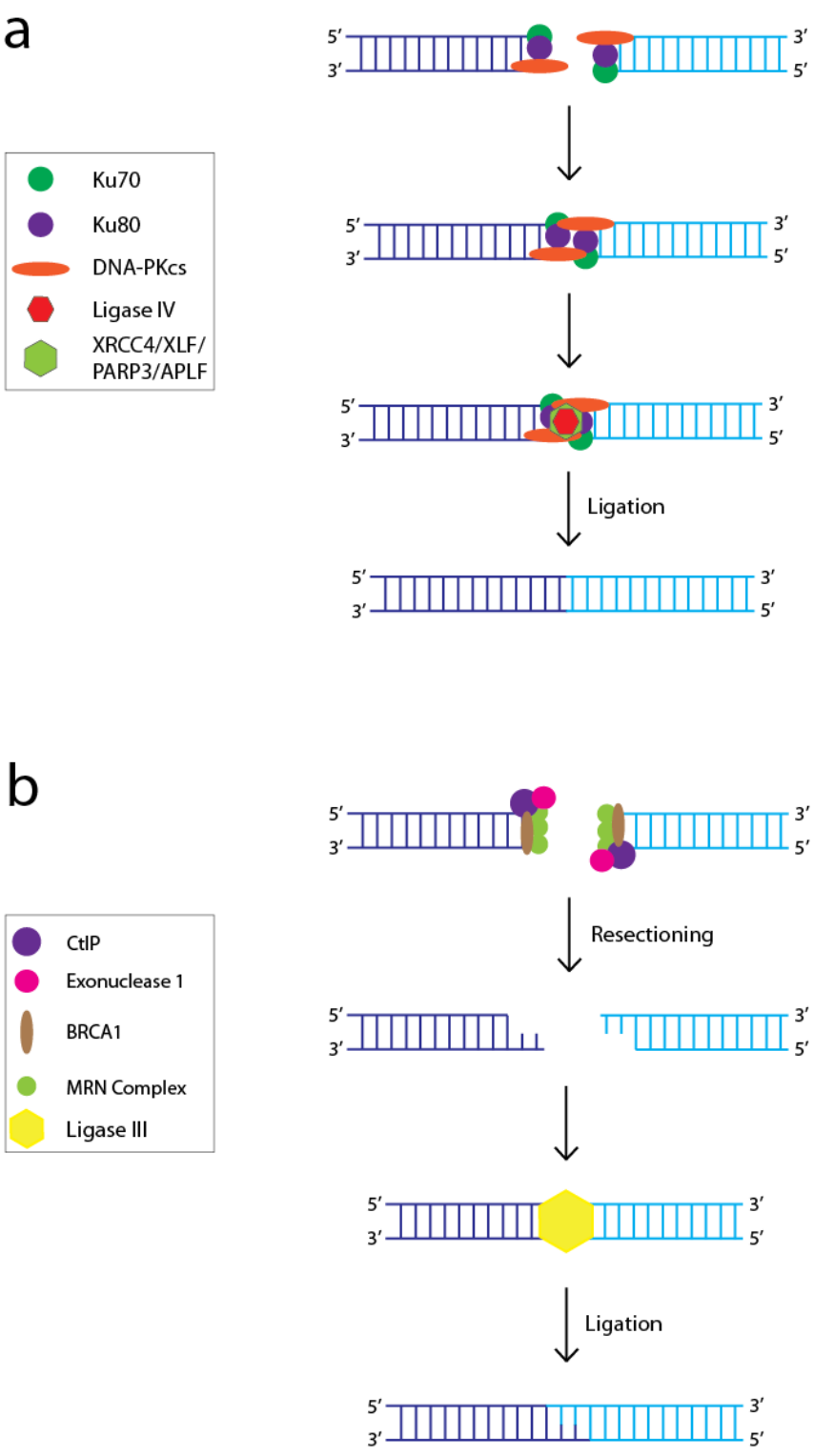

Figure 1.9 - Non-Homologous End Joining and alt-Non-Homologous End Joining
(a) Figure detailing the steps in non-homologous end joining (NHEJ). DNA ends are brought close together by the Ku70/Ku80/DNA-PKcs complex. Ligase IV is then responsible for joining the DNA ends together, a process which is aided by the presence of the accessory proteins XRCC4, XLF, PARP3 and APLF. **(b)** Figure detailing the steps in alternative-non-homologous end joining. The broken ends of DNA are resectioned by exonuclease 1, resulting in microhomology. The two ends are then ligated together by ligase III.

by the alt-NHEJ pathway, damaged DNA ends are trimmed to create the microhomology that facilitates their ligation. Like HR, this is performed by the exonuclease1, CtIP and BRCA1 proteins which bind to the MRN complex at the DNA ends. After aligning the ends based on the newly created homologous sequences, ligation is performed by ligase III (Zhang and Jasin 2011; Truong et al. 2013). However, alt-NHEJ is thought to be more error-prone than either the HR or the classical NHEJ pathways. This is due to the loss of nucleotides that occurs during resectioning of the DNA ends, a process which can result in the disruption of genetic sequences (Rai et al. 2010). It has also been demonstrated that the expression of ligase III is necessary for the escape of cells from a telomere driven crisis, while the expression of ligase IV is not (Jones et al. 2014). This suggests that the alt-NHEJ pathway is responsible for the genetic rearrangements that take place at the ends of critically shortened telomeres, acting to drive cancer progression.

1.6.3 PARP Inhibition

From the descriptions of each repair pathway, it may appear that PARP1 and PARP2 play only minor roles in the repair of single-strand DNA damage. However, PARP inhibitors are now routinely used in the treatment of BRCA-mutated breast and ovarian cancers. This discrepancy comes from the fact that PARP1 and PARP2 directly bind to sites of DNA damage during BER. Their activity not only acts to recruit proteins involved in single-strand DNA repair, but also to promote their own dissociation from DNA. In the presence of a PARP inhibitor, PARP1 and PARP2 are trapped at the site of DNA damage. This blocks any further repair and eventually results in the formation of a double-strand DNA break during S-phase (Murai et al. 2012). In normal cells, this damage would simply be repaired by the HR pathway. However, BRCA-mutations in cancer prevent this pathway from functioning. It therefore becomes necessary for the cell to rely on the more error-prone NHEJ pathways, producing catastrophic DNA damage and rearrangements that inevitably lead to apoptosis (Javle and Curtin 2011).

A sensitivity to PARP inhibition can be induced by co-treating cells with molecules that interfere with HR. In one study, inhibition of RAD51 (a crucial component of the HR pathway) improved the effectiveness of PARP inhibition in cells with no prior defects in the HR pathway (Wang et al. 2012). More commonly, PARP inhibition has been examined in combination with either radiation or DNA damaging agents. It is thought that excessive single-strand DNA breaks are produced in this way, with PARP inhibitors preventing their repair via BER. This results in an overwhelming frequency of double-strand DNA breaks which inevitably leads to apoptosis (Calabrese et al. 2004; Tentori et al. 2006; Donawho et al. 2007).

Although most articles discussing PARP inhibition focus on PARP1 and PARP2, inhibitors rarely target a single member of the PARP family. This is because the catalytic sites of most PARP proteins share a significant homology (Smith 2001). For example, Wahlberg et al. (2012) demonstrated that Veliparib binds to the catalytic sites of PARP1, PARP2, PARP3 and PARP4. Meanwhile, Rucaparib and Olaparib bind to nine and seven different PARP family proteins respectively. A bias in the understanding of PARP protein function exists because PARP1 and PARP2 are some of the most abundant members of this family expressed in cells. They are also the most well-characterised due to their early discovery (Vyas and Chang 2014). Although the inhibition of PARP1 and PARP2 certainly plays an invaluable role during the treatment of BRCA-mutated cancer, the fact that little is known about the effects of PARP inhibition on the remaining PARP family members may be a cause for concern (Rouleau et al. 2010).

Rucaparib and Olaparib are examples of PARP inhibitors which are both promiscuous and only partially understood. Like many inhibitors, their effects on PARP1 and PARP2 are well documented (Murai et al. 2014). However, little has been done to identify their effects on pathways that utilise the other PARP family proteins inhibited by these drugs. Regardless, both Rucaparib and Olaparib have now received accelerated approval for the treatment of BRCA-mutated cancers (Syed 2017; Kim et al. 2015). In both cases,

phase III clinical trials are still ongoing. Phase II clinical trials have shown an improved progression-free survival in the case of both Rucaparib and Olaparib when used to treat BRCA-mutated breast and ovarian cancers (Drew et al. 2016; Swisher et al. 2017; Tutt et al. 2010; Ledermann et al. 2014).

1.7 Aims of the Project

Short dysfunctional telomeres have previously been identified as a driving force in cancer, resulting in chromosomal fusion and rearrangement that acts to facilitate progression of the malignancy. Studies into the telomere dynamics of breast cancer and chronic lymphocytic leukaemia have managed to identify a correlation between telomere length and patient outcome, demonstrating the potential for telomere length measurements to be used as a prognostic indicator. We therefore sought to understand the role that telomeres play in the progression of MM, as well as the use of telomere length measurements in predicting patient outcome. We also sought to use PARP inhibition as a method of combating the ability of MM cell lines to escape from a telomere-driven crisis.

The aims of this project can be discerned from the aims of each individual chapter:

Chapter 3 - Here, we aim to identify the prognostic value of telomere length measurement in patients with MM. We will then attempt to consider whether these measurements can be used to refine existing staging systems, with an emphasis placed on the ISS. Also, we will examine the bone marrow aspirates of MM patients for evidence of chromosomal end-end fusion.

Chapter 4 - It has previously been demonstrated in chronic lymphocytic leukaemia that a relationship exists between telomere length and the frequency of chromosomal end-end fusion. We therefore aim to determine if a similar relationship exists in MM, using

MM cell lines that we will drive into a state of telomere-driven crisis. We will also examine this relationship within the context of the p53 status of each cell line.

Chapter 5 - Little is known about the role that PARP inhibitors might play in treating MM. Even less is known about the effect that these drugs would have on the escape of cells from a telomere-driven crisis. We will therefore seek to explore the use of Rucaparib and Olaparib as novel treatments for MM, analysing their ability to promote apoptosis in combination with critical telomeric erosion.

Chapter 2

Materials and Methods

2.1 Equipment and Reagents

Unless stated otherwise, the following basic equipment was used. Manufacturers and models are listed where possible: ***Biological Safety Cabinet*** – Herasafe ks (Thermo Fisher Scientific); ***Centrifuge (large)*** – Centaur 2 (MSE); ***Centrifuge (small)*** - Fresco 21 Centrifuge (Haraeus) and Biofuge Pico (Heraeus); ***Glassware and Plastics*** – Various types (Ambion, Azlon, Becton Dickenson, Costar, Eppendorf, Fisher, SARSTEDT, Schott Duran, Sigma and Thermo Scientific); ***Hot Block*** – Dri-Block DB2A (Teche) and Grant QBTP (Grant Instruments); ***Hybridisation Oven*** – Hybaid Maxi 14 (Thermo Scientific); ***Incubator*** – Heracell 150 (Heraeus); ***Thermal Cyclers*** – Tetrad 2 (Bio-Rad) and SimpleAmp (Life Technologies); ***Tube Rotor*** - Stuart SB1 Blood Tube Rotator (Stuart Scientific) and Roller Mixer SRT2 (Stuart Scientific); ***UV Transilluminator*** – Flowgen Transilluminator (Flowgen); ***Water Bath*** – Jab 18 (Grant Instruments).

Unless otherwise stated, the following basic chemicals were used. Manufacturers are listed where possible: ***Acetic Acid*** (Fisher); ***bovine serum albumin (BSA)*** (2mg/ml – Thermo Fisher); ***dimethyl sulfoxide (DMSO)*** (Sigma); ***foetal calf serum (FCS)*** (Life Technologies); **Glycene** (Fisher); ***Glycerol*** (Sigma); ***hydrochloric acid (HCl)*** (Fisher); ***sodium chloride (NaCl)*** (Fisher); ***sodium hydroxide (NaOH)*** (Fisher); ***phosphate-buffered saline (PBS)*** (10x – Thermo Fisher Scientific); ***sodium dodecyl sulfate (SDS)*** (Fisher); ***Tris-HCl*** (Fisher); ***Tween20*** (Sigma); **phenylmethylsulfonyl fluoride (PMSF)** (Sigma)**; 4-(2-aminoethyl)benzenesulfonyl fluoride hydrochloride (AEBSF)** (Calbiochem).

2.2 Patient Samples and Tissue Culture

2.2.1 Obtaining Patient Bone Marrow Aspirates and DNA Samples

DNA samples, extracted from the whole bone marrow aspirates of MGUS and MM patients, were provided by Professor James Allen, Newcastle University. Patient samples were collected at diagnosis, prior to treatment, through treating centres within the Heart of England NHS Foundation Trust and the Newcastle upon Tyne NHS Foundation Trust between 1990 and 2005, with ethical approval from the Newcastle Haematology Biobank (07/H0906/109+5) in accordance with the declaration of Helsinki. In total, 202 patient DNA samples were gathered in this manner.

Whole bone marrow aspirates were obtained locally, from patients at the University Hospital of Wales with written informed consent (research ethics committee number: 13/WA/0383). Samples were obtained with help from Professor Chris Fegan, Cardiff University. In total, 19 patient whole bone marrow aspirates were gathered in this manner.

2.2.2 Isolation of Mononuclear Cells from Patient Bone Marrow Samples

Mononuclear cells were first separated from the whole bone marrow aspirate by density gradient centrifugation. 5ml of bone marrow were carefully layered onto 6ml of Histopaque-1077 (Sigma-Aldrich) that had been added to a 15ml Falcon tube. This was centrifuged at 300*g* for 20 minutes with the break off. The mononuclear cell layer was then removed from the tube and added to 10ml of PBS (1x).

2.2.3 Isolation of $CD138^+$ Cells from Patient Mononuclear Cell Samples

After centrifugation at 300*g* for 5 minutes, the supernatant was removed and the cells were suspended in 80µl of autoMACS running buffer (1x PBS, BSA 500mg/ml, EDTA 20mM – Miltenyi Biotech) and 20µl of CD138 MicroBeads (Miltenyi Biotec). This

suspension was mixed thoroughly, before being incubated at 4°C for 15 minutes. 10µl of human CD138-APC antibody (Miltenyi Biotec) was then added and the cells were incubated at 4°C for a further 5 minutes. 2ml of autoMACS running buffer was added and the cells were centrifuged at 300*g* for 5 minutes, with the resulting cell pellet being resuspended in 500µl of autoMACS running buffer. $CD138^+$ selection was achieved using the autoMACS Pro Separator (Miltenyi Biotec) as per the manufacturer's guidelines using the 'Possel' software setting.

The purity of the $CD138^+$ and CD138- fractions was determined using flow cytometry. A sample of the unsorted marrow cells, sorted $CD138^-$ cell fraction and sorted $CD138^+$ cell fraction was centrifuged at 300*g* for 5 minutes. The supernatant was removed and the resulting cell pellet was washed in PBS. Again, the cells were centrifuged at 300*g* for 5 minutes and the supernatant removed. The cell pellet was suspended in 100µl of PBS before being analysed using an Accuri C6 flow cytometer equipped with CFlow software (BD Biosciences). A sample of unsorted marrow cells that had not been exposed to human CD138-APC antibody was used as a control.

In total, 10,000 events were recorded, per sample, using flow cytometry. Cells were first analysed using forward scatter-area (FSC-A) against side scatter-area (SSC-A), with appropriate gating being used to exclude cell debris and dead cells from the analysis. Further analysis was performed on these gated cells to identify the $CD138^-$ and $CD138^+$ fractions, using FL4-A against FL1-A to detect Allophycocyanin (APC)-bound cells with denoted $CD138^+$ plasma cells. Each sample demonstrated >80% purity in the positively selected and negatively selected fractions. An example of this analysis can be seen in ***Supplementary Figure 18***.

2.2.4 Cell Lines and Growth Conditions

The NCI-H929, RPMI-8226 and U266B1 cell lines were purchased from Sigma-Aldrich. Cells were cultured in Roswell Park Memorial Institute (RPMI) 1640 media (Life Technologies) supplemented with Penicillin (100 Units/ml - Sigma), Streptomycin (0.1mg/ml - Sigma), FCS (10% v/v - Thermo Fisher Scientific) and L-glutamine (2mM - Sigma). Cells were incubated at 37^{o}C in 5% CO_2.

The JJN-3 cell line was gifted by Professor Chris Pepper, Cardiff University. Cells were cultured in Dulbecco's Modified Eagle Medium (DMEM - Life Technologies) supplemented with Sodium Pyruvate (1mM - Invitrogen), Penicillin (100 Units/ml - Sigma), Streptomycin (0.1mg/ml - Sigma), non-essential amino acids (1x - Sigma), FCS (20% v/v - Thermo Fisher Scientific) and L-glutamine (2mM - Sigma). Cells were incubated at 37^{o}C in 5% CO_2.

The HEK-293 cell line was gifted by Dr Rhiannon Robinson, Cardiff University. Cells were cultured in Dulbecco's Modified Eagle Medium (DMEM - Life Technologies) supplemented with Penicillin (100 Units/ml - Sigma), Streptomycin (0.1mg/ml - Sigma), FCS (10% v/v - Thermo Fisher Scientific) and L-glutamine (2mM - Sigma). Cells were incubated at 37^{o}C in 5% CO_2.

2.2.5 Trypsinisation and Cell Counting

For the HEK-293 adherent cell line, trypsin was used to detach cells from the culture flasks. Media was removed from the flasks and the adherent cells were washed using PBS (1x). For a 75cm^2 flask, 2ml of trypsin (1x – Thermo Fisher Scientific) was washed over the cells and the flask was incubated at 37^{o}C for 5 minutes. 10ml of fresh Dulbecco's Modified Eagle's Medium (DMEM - Life Technologies) was then added to inactivate the Trypsin and the cells were harvested and centrifuged (175*g* for 5 minutes) prior to resuspension in fresh culture media.

As a method of counting and assessing the viability of each of the cell lines, 2.5µl of solution 13 (Acridine Orange 80µg/ml and DAPI 40µg/ml - Chemometic) was added to a 50µl suspension of cells. Cells were counted using the NucleoCounter NC-250 (Chemometec) as per the manufacturer's guidelines.

2.2.6 Viral Infection of Cell Lines – Reducing Telomerase Activity

$2x10^6$ cells were suspended in 2ml of media (DMEM, 10% v/v FCS, 2mM L-Glutamine, 8µg/ml Hexadimethrine bromide) containing a recombinant retrovirus that was grown using the ΨCRIP cell line (gifted by Richard Mulligan, Whitehead Institute, Cambridge). The retrovirus carried the pBABE-Puro vector (Addgene) which contained the gene encoding a dominant-negative human-TERT protein. Cells were incubated at 37°C with 5% CO_2 for 4 hours, after which 2ml of supplementary media were added.

4-10 days after transfection, cells that had successfully integrated the pBABE-Puro vector into their genome were selected for using puromycin. The addition of puromycin was gradual, with JJN-3 and U266B1 cells initially being exposed to 0.75µg/ml of puromycin for 48 hours; 1.5µg/ml for 48 hours; and then maintained under constant selection (2µg/ml). NCI-H929 cells were initially exposed to 0.25µg/ml puromycin for 48 hours and then maintained under constant selection (0.5µg/ml).

2.2.7 Cell Cloning

Appropriate growth media was used to dilute either the JJN-3 or U266B1 cell lines to a concentration of 20 cells per ml. 100µl of this was then added to each well of a 96-well plate. Cells were incubated at 37°C and 5% CO_2 until a population of cells could be observed in each well (approximately $1.5x10^4$ cells). At this point, the cells were transferred to a 24-well plate containing 500µl of appropriate growth media. Again, the cells were visualised by microscopy and transferred to a 6-well plate containing 2ml of

appropriate growth media once the population was considered to be large enough (approximately $5x10^5$ cells).

2.2.8 Freezing Cells in Liquid Nitrogen and Thawing Procedure

Approximately $1x10^5$ – $1x10^7$ cells were centrifuged at 3421*g* for 5 minutes before being resuspended in 1ml of freezing media (50% appropriate growth media, 25% DMEM, 15% FCS and 10% DMSO). Cells were stored in a freezing ampoule (Thermo Scientific) which was then placed into a freezing container (Mr. Frosty) that was filled with isopropyl alcohol to promote a controlled rate of freezing of the samples. Containers were stored at -80°C for up to a week before being stored in liquid nitrogen.

When needed, cells were removed from liquid nitrogen and thawed at 37°C using a water bath. DMSO-containing freezing media was removed by adding 9ml of the appropriate growth media to cells, dropwise. Cells were then centrifuged (300*g* for 5 minutes) and the supernatant was removed. Cell pellets were suspended in a suitable volume of the appropriate growth media.

2.3 DNA/Protein Extraction and Quantification

2.3.1 DNA Extraction (Phenol – Chloroform)

Genomic DNA was extracted from cell pellets that contained more than $1x10^5$ cells. Cell pellets were re-suspended in 300µl of lysis buffer (100mM NaCl, 10mM Tris.HCl pH 8, 5mM EDTA pH 8 and 0.5% SDS) containing RNase (300ng/µl - Sigma) and Proteinase K (400ng/µl - Sigma). The cell-lysis mixture was incubated at 45°C for around 18 hours. At this point, 300µl of phenol/chloroform (Sigma) were added to the cell lysate. The resulting mixture was placed into a tube rotator and spun for 30 minutes at room temperature. Cell lysates were then centrifuged for 5 minutes at 16,060*g*. The aqueous phase was transferred to a new tube containing 300µl phenol/chloroform. This was spun

for a further 20 minutes using a tube rotator, before being centrifuged for 5 minutes at 16,060g.

The resulting aqueous phase was transferred to a new tube and 30µl of Sodium Acetate (3M, pH 5.2) and 900µl of Ethanol (absolute, -20^{o}C - Fisher) were then added. The resulting mixture was left at -20^{o}C for a minimum of 20 minutes, allowing the DNA to precipitate. Precipitated DNA was then centrifuged for 5 minutes at 16,060g, with the resulting DNA pellet being washed in 70% ethanol (-20^{o}C - Fisher). Residual ethanol was then removed and the DNA was allowed to air dry. DNA was re-suspended in Tris-HCl (10mM, pH 8 - Sigma).

2.3.2 DNA Extraction (QIAamp DNA Micro Kit)

Genomic DNA was extracted from cell pellets that contained less than 1x10^{5} cells. The protocol was performed as outlined in the QIAamp DNA Micro Handbook (*Protocol: Isolation of Genomic DNA from Small Volumes of Blood*). DNA was eluted into a final volume of 50µl using buffer AE.

2.3.3 DNA Quantification

For concentrations of DNA greater than 20ng/µl, Hoechst 33258 fluorometry was used to quantify the DNA with a QuantiFluor-ST Fluorometer (Promega). 2µl of DNA were added to 2ml of TEN buffer (1x, 1µg/ml Hoechst – Bio-Rad) and mixed thoroughly before being quantified according to the manufacturer's instructions.

Where the concentration of DNA in a sample was less than 20ng/µl, an assay was performed using PicoGreen Dye (Life Technologies) and the Nanodrop 3300 Fluorospectrometer (Thermo Scientific). DNA was first diluted 1:100 with Tris-HCl (10mM, pH 8 – Sigma). The 20x stock of PicoGreen Dye was diluted to 1x using TE

buffer (10mM Tris-HCl, 1mM EDTA, pH 7.5). DNA was then further diluted 1:1 with a 1x solution of PicoGreen. The solution was left to incubate at room temperature for 5 minutes before being quantified. Regardless of the method used to quantify DNA, standard curves were developed using calf thymus DNA (Bio-Rad) and all quantification was performed in triplicate.

2.3.4 Protein Extraction (Western Blot)

Cells were washed twice in PBS (4^{o}C), before being centrifuged at 100*g* (4^{o}C) for 5 minutes. The supernatant was removed and the cells were suspended in 2.5x their volume of lysis buffer (150mM NaCl, 50mM Tris-HCl, 5mM EDTA, 1% NP40) that also contained 3% v/v PMSF (100mM - Sigma), 1% v/v Protease Inhibitor Cocktail III (100mM AEBSF Hydrochloride, 80µM Bovine Lung Aprotinin, 5mM Bestatin, 1.5mM E-64 Protease Inhibitor, 2mM Leupeptin Hemisulfate, 1mM Pepstatin A – Calbiochem) and 1% v/v Phosphatase Inhibitor Cocktail II (200mM Imidazole, 100mM Sodium Fluoride, 115mM Sodium Molybdate, 100mM Sodium Orthovanadate, 400mM Sodium Tartrate Dihydrate - Calbiochem). The cells were then left on ice for 5 minutes before being centrifuged at 20,000*g* (4^{o}C) for 30 minutes. The protein-containing supernatant was removed and stored at -80^{o}C until required.

2.3.5 Protein Quantification (Western Blot)

Using lysis buffer, BSA (2mg/ml) was diluted to 0, 100, 200, 300 and 400µg/ml concentrations. The protein samples to be quantified were diluted 1/10 in water. 40µl of either a BSA standard or a protein sample were added to a 1.6ml semi-micro cuvette (Fisher Brand) and mixed thoroughly with 1ml of coomassie blue reagent (Thermo Scientific). An Ultrospec 3100 Pro (Amersham Biosciences) spectrophotometer was used to measure the absorbance at a wavelength of 595nm. A 1/10 dilution of lysis buffer in water was used as a reference. Protein concentration was calculated by

comparing the absorbance recorded for each sample against the absorbance recorded for the BSA standard curve.

2.3.6 Protein Extraction (Telomerase Assay)

Approximately $1x10^6$ cells were suspended in PBS before being centrifuged at 300*g* for 5 minutes. The supernatant was removed and the cell pellet was suspended in 200µl of CHAPS lysis buffer (1x - Millipore) and incubated for 30 minutes on ice. Cell lysates were spun at 12,000*g* (4^oC) for 20 minutes. The protein-containing supernatant was then removed.

2.3.7 Protein Quantification (Telomerase Assay)

Protein quantification was performed using the Coomassie Plus Assay Kit (Thermo Scientific) and BSA (2mg/ml) as a standard. 10µl of each standard or supernatant sample were combined with 300µl of Coomassie Plus Protein Assay Reagent and allowed to incubate at room temperature for 10 minutes. Absorbance at 595nm was then measured using the FLUOstar Optima Microplate Reader (BMG Labtech). Standards were measured in duplicate while supernatant samples were measured in triplicate. Protein concentration was calculated by comparing the absorbance recorded for each sample against the absorbance recorded for the BSA standard curve.

2.4 Oligonucleotides

A list of primers that were used can be found in ***Table 2.1.*** All primers were synthesised by MWG-Biotech.

Application	Primer Name	Primer Sequence (5′ to 3′)
STELA	XpYpE2	TTGTCTCAGGGTCCTAGTG
	17pSeq1rev	GAATCCACGGATTGCTTTGTGTAC
	Teltail	TGCTCCGTGCATCTGGCATC
	Tel2	TGCTCCGTGCATCTGGCATCTAACCCT
Fusion	17p6	GGCTGAACTATAGCCTCTGC
	XpYpM	ACCAGGTTTTCCAGTGTGTT
	16p1	TGGACTTCTCACTTCTAGGGCAG
	21q1	CTTGGTGTCGAGAGAGGTAG
Fusion Reamplification	17p7	CCTGGCATGGTATTGACATG
	XpYpO	CCTGTAACGCT GTTAGGTAC
	16p2	TCACTGCTGTATCTCCCAGTG
	21qSeq1	TGGTCTTATACACTGTGTTCCACTG
Fusion Sequencing	17p2	GCTAGGAATGGAATCATTGACTCA
	17pSeqR1	GAATCCACGGATTGCTTTGTGTAC
	17pSeq1	AAGCAGGTTGAGAGGCTGAGG
	17pFries	CCCTCATCTAAGTCTTGTCGTTTCAT
	17pSeqR3	TTATAAGCTTTACTGTCTCTCCAC
	17pSeqR2	CCATTAGCCTGTGGGGTCTGAT
	17pSeq3	ACTTGTTGAGGACAGGATTCT
	16pSeq4	TGGGTCCTGGCAACACTCTG
	16p2SeqB	GCTCCAGATGACATCACAGGG
	16p6	CTCCACTCCAGTGCTCAGCTTG
	16pRev8	ACACATGAAGAGAAAGAAGAGGTCAAAG
	16pSeq3	TCCAGGGCTTCACCTGCTAG
	16p5	TAGCATGTGTCTCTGCGCCTG
	10q3	AGACACAGGATAGTGGGCTCTG
	21qSeq2	TGCCCCAATCATCATTCACTCTGC
	8p1	TGCACAGGACTCTTAGGCTG
	10q2	TGCAATGTCCCTAGCTGCCAG
	21q3	CTGCAGTTGTCCTAGTCGC
	10q1	AGGTTCCACTCGTCTCTGCG
	21qC	AGAGTTCTTCTCAGGTCAGACCTG

Table 2.1 – A complete list of all primers used during the study

2.5 Polymerase Chain Reaction

2.5.1 STELA PCR

Tris-HCl (10mM, pH 8 - Sigma) was used to dilute genomic DNA to 250pg/µl. Tel2 linker was then added to a final concentration of 250nM. A PCR mixture was produced which contained Taq buffer (75mM Tris-HCl (pH 8.8), 20mM $(NH_4)_2SO_4$, 0.01% Tween 20 – Thermo Scientific); $MgCl_2$ (2mM – Thermo Scientific); NTPs (1.2mM); telomere-adjacent (0.5µM) and teltail (0.5µM) primers; 0.05 Units/µl of a 10:1 mixture of Taq:Pwo Polymerase (Thermo Scientific : Roche); and the DNA/Tel2 mixture (25pg/µl and 25mM respectively). Reactions were made up to 10µl using double distilled water and a total of six repeats were carried out per DNA sample. The reactions were cycled using a Tetrad thermal cycler (Bio-Rad) under the following conditions: 22 cycles of 94°C for 20 seconds, 59°C (17pSeq1rev STELA Primer) or 65°C (XpYpE2 STELA Primer) for 30 seconds and 68°C for 8 minutes.

2.5.2 Fusion PCR

A PCR mixture was produced which contained Taq buffer (75mM Tris-HCl (pH 8.8), 20mM $(NH_4)_2SO_4$, 0.01% Tween 20); $MgCl_2$ (2mM); NTPs (1.2mM); 17p6 (0.5µM), XpYpM (0.5µM), 16p1 (0.5µM) and 21q1 (0.5µM) primers; 0.05 Units/µl of a 10:1 mixture of Taq: Pwo Polymerase; and 10ng/µl of the DNA to be amplified. Reactions were made up to 10µl using double distilled water and a total of nine repeats were carried our per DNA sample. The reactions were cycled using a Tetrad thermal cycler (Bio-Rad) under the following conditions: 25 cycles of 94°C for 20 seconds, 62°C for 30 seconds and 68°C for 8 minutes.

2.5.3 Fusion Reamplification PCR

Successfully amplified Fusion PCR products were diluted 1:40 using double distilled water. A PCR mixture was then produced that contained Taq buffer (75mM Tris-HCl (pH

8.8), 20mM $(NH_4)_2SO_4$, 0.01% Tween 20); $MgCl_2$ (2mM); NTPs (1.2mM); telomere adjacent primers (0.5µM); and 0.05 Units/µl of a 10:1 mixture of Taq: Pwo Polymerase. 3µl of the diluted fusion PCR product were added before the mixture was made up to 30µl using double distilled water. The reactions were cycled using a Tetrad thermal cycler (Bio-Rad) under the following conditions: 33 cycles of 94°C for 20 seconds, 62°C for 30 seconds and 68°C for 8 minutes.

2.5.4 Sanger Sequencing

4.4µl of the purified fusion reamplification PCR product were combined with BigDye Terminator Cycle Sequencing Mix 3.0 or 3.1 (Applied Biosystems) and an appropriate sequencing primer (0.16µM) up to a total reaction volume of 10µl. The reactions were cycled using a Tetrad thermal cycler (Bio-Rad) under the following conditions: 26 cycles of 96°C for 10 seconds, 50°C for 5 seconds and 60°C for 4 minutes.

2.6 Gel Electrophoresis

2.6.1 STELA and Fusion PCR Products

DNA fragments were resolved using a 0.5% agarose (Roche) gel produced using Tris-acetate-EDTA (TAE) buffer (40mM Tris base, 20mM acetic acid, 1mM EDTA) and ethidium bromide (1µg/ml – Fisher Scientific). Gels were submerged in 4°C TAE buffer that was cooled using a refrigerated circulating bath (Grant). 5µl of the STELA or fusion PCR product were mixed with 1µl of a 6x loading dye (5% bromophenol blue, 5% xylene, 15% ficol) before being loaded into the gel. STELA PCR products were run at 120 volts for 17 hours. Fusion PCR products were run at 45 volts for 17 hours. DNA bands were visualised using a UV-transilluminator (Flowgen).

2.6.2 Fusion Reamplification PCR Products

DNA fragments were resolved using a 0.8% agarose (Geneflow) gel produced using Tris-acetate-EDTA buffer (40mM Tris base, 20mM acetic acid, 1mM EDTA) and ethidium bromide (1µg/ml – Fisher Scientific). Gels were submerged at room temperature in TAE buffer and run at 120 volts for 2 hours.

2.6.3 Proteins (Western Blot)

3µl of 3x loading buffer (0.5M Tris-HCl, 30% Glycerol, 10% SDS, 3% 2-mercaptoethanol, 1% bromophenol blue) was added to 10µg of protein in a volume of 12µl. Protein samples and molecular weight markers were then boiled at 100^{o}C for 5 minutes. Proteins were resolved using a 10% Mini-Protean TGX Precast Gel (Bio-Rad), submerged in running buffer (25 mM Tris, 192 mM glycine, 0.1% SDS, pH8.3), and run at 100 volts for 1-2 hours.

2.7 Southern Blot and Radiolabelling

2.7.1 Southern Blot

Agarose gels, containing resolved STELA or fusion products, were washed twice in depurination buffer (0.25M HCl) for 6 minutes per wash. Gels were then washed in denaturation buffer (1.5M NaCl, 0.5M NaOH) for 15 minutes, before the DNA was transferred to a positively charged nylon membrane (GE Healthcare) by southern blotting for 4 hours.

2.7.2 Radiolabelling DNA Probe

A 45µl solution of TE buffer, containing 25ng of a DNA probe (***Table 2.1***), was heated to 96^{o}C for 5 minutes. The solution was then cooled on ice for a further 5 minutes before being added to an Amersham Rediprime II Random Prime Labelling Bead (GE

Healthcare). 4µl of [33P]dCTP (3000Ci/mmol - PerkinElmer) was then added and the reaction mixture was heated at 37°C in a water bath. After 1 hour, 50µl of water and 1µl of a [33P]dCTP-labelled DNA ladder (1:1 of 1Kb and 2.5Kb) were added. Radiolabelled probes were stored at 4°C for up to two weeks.

2.7.3 Hybridisation

Membranes were washed using water and placed into a hybridisation bottle that had been warmed to 56°C. 15ml of church buffer (7% SDS, 0.5M sodium phosphate buffer (1M disodium hydrogen phosphate and 1M sodium dihydrogen phosphate), 1mM EDTA, 1% BSA, pH 7.2), also warmed to 56°C, was added to the bottle. The radiolabelled probe was heated to 96°C for 5 minutes before 25µl was then added to the bottle. Bottles were hybridised at 56°C overnight in a rotating hybridisation oven. Excess probe was then removed by washing the membranes in 56°C washing buffer (0.1% sodium chloride sodium citrate and 0.1% sodium dodecyl sulphate) six times over the course of an hour. Membranes were then dried by placing them at 56°C for 25 minutes.

2.7.4 Visualising Radiolabelled Membranes

Membranes were placed into a cassette (Amersham) with a phosphoimaging screen (Amersham) for 24 hours. The screen was then scanned using a Typhoon FLA 9500 biomolecular imager (GE Healthcare). For STELA, TotalLab TL120 software was used to identify the molecular weights of each telomere in a sample. The distance between the STELA primer binding site and the telomere repeating region was then subtracted: 408bp for the XpYpE2 primer and 311bp for the 17pSeq1rev primer.

2.7.5 Stripping Membranes for Fusion Analysis

Radiolabelled probes were removed by washing the membrane in a boiling solution of 0.2% SDS for one hour, three times. Membranes were then re-probed using the same method outlined previously (**see *2.7.3 Hybridisation***).

2.8 Western Blot

2.8.1 Transfer

A polyvinylidene fluoride transfer membrane (Immobilon-P - Millipore) was submerged in methanol (Fisher), before being washed in water for 2 minutes and then transfer buffer (25 mM Tris, 192 mM glycine, 20% methanol, pH8.3) for 1 minute. Resolved proteins were transferred from the 10% Mini-Protean TGX Precast Gel (Bio-Rad) to the nitrocellulose membrane by western blotting in transfer buffer for 2 hours at 100 volts (4^{o}C).

2.8.2 Immunoprobing

Membranes were blocked in 0.2% Tween/5% milk/PBS for 1 hour. The membranes were then placed into a 15ml falcon tube containing the appropriate antibody solution and the appropriate concentration of primary antibody (***see Table 2.2***). Tubes were left on a roller at 4^{o}C overnight. Membranes were washed using 1% Tween/PBS for 25 minutes (with the 1% Tween/PBS being changed after each 5-minute period). The membranes were added to a second 15ml falcon tube which contained the appropriate antibody solution and the appropriate concentration of secondary antibody (***see Table 2.2***). Tubes were left on a roller at room temperature for 1 hour. Again, membranes were washed using 1% Tween/PBS for 25 minutes (with the 1% Tween/PBS being changed after each 5-minute period).

Primary Antibody (Dilution)	**Primary Antibody (Solution)**	**Secondary Antibody (Dilution)**	**Secondary Antibody (Solution)**
Mouse Polyclonal Anti-PAR (2µl in 2ml)	0.2% Tween/5% Milk/PBS	Anti-Mouse HRP (1µl in 2ml)	0.2% Tween/5% Milk/TBS
Rabbit Polyclonal Anti-Rb (8µl in 2ml)	0.2% Tween/5% Milk/PBS	Anti-Rabbit HRP (1µl in 2ml)	0.2% Tween/5% Milk/TBS
Rabbit Polyclonal Anti-Chk-1 (2µl in 2ml)	0.2% Tween/5% BSA/TBS	Anti-Rabbit HRP (1µl in 2ml)	0.2% Tween/5% Milk/TBS
Rabbit Polyclonal Anti-Actin (2.7µl in 2ml)	0.2% Tween/1% BSA/5% Milk/PBS	Anti-Rabbit HRP (1µl in 2ml)	0.2% Tween/1% BSA/5% Milk/PBS

Table 2.2 – A list of the primary and secondary antibodies used for the immunoprobing procedure, the concentrations used and the appropriate immunoprobing solution. All secondary antibodies were conjugated to horseradish peroxidase (HRP). All antibodies were purchased from Trevigene.

2.8.3 Visualisation with Luminescent Substrates

Visualisation was performed using the ECL Plus kit (Thermo Scientific). 50µl of reagent A were added to 2ml of reagent B. This solution was then poured over the membrane and left at room temperature for 5 minutes. Excess ECL reagent was poured off and the membrane was wrapped in Saran wrap. In a dark room, Chemiluminescence Hyperfilm ECK (Amersham) was exposed to the membrane before being developed and fixed using the SRX-101A Medical Film Processor (Konica Minolta Medical and Graphic Inc.). Proteins were identified by their molecular weight, using molecular weight markers of known size for comparison.

2.8.4 Stripping Antibody from Membrane

Membranes were washed for 5 minutes in water, 5 minutes with NaOH (0.2M) and 5 minutes with water. The membranes were then ready to undergo immunoprobing with a different antibody (***see 2.8.2 Immunoprobing***).

2.9 Telomerase Assay

The telomerase activity of each supernatant sample was measured using the TRAPeze XL Telomerase Detection Kit (Millipore). 50µl reaction volumes were produced by combining sterile water, TRAPeze XL Reaction Mixture (1x), Taq Polymerase (5 Units) and 2µl of each sample. The reactions were cycled using a Tetrad thermal cycler (Bio-Rad) under the following conditions: 30^{o}C for 30 minutes; 36 cycles of 94^{o}C for 30 seconds, 59^{o}C for 30 seconds and 72^{o}C for 60 seconds; and 72^{o}C for 3 minutes.

The 50µl reaction mixture was then combined with 150µl of TRAPeze buffer (10mM Tris-HCl pH 7.4, 0.15M NaCl and 2mM $MgCl_2$) in a black 96-well microplate (ThermoFisher Scientific). The fluorescence of fluorescein and sulforhodamine were measured using

the FLUOstar Omega Microplate Reader (BMG Labtech): fluorescein using an excitation wavelength of 485nm and emission was detected at 584nm, sulforhodamine using an excitation at 585nm and an emission at 612nm. Telomerase activity was then calculated as per the manufacturers guideline's.

Chapter 3

Using the Mean XpYp Telomere Length of Whole Bone Marrow Aspirates as a Prognostic Indicator in Multiple Myeloma

3.1 Abstract

Short dysfunctional telomeres have previously been identified as a driving force in cancer, resulting in chromosomal fusion and rearrangement that acts to facilitate progression of the malignancy. As it has recently been demonstrated that telomere length is an accurate predictor of clinical outcome in patients with chronic lymphocytic leukaemia (CLL), we aimed to determine whether a similar relationship existed in monoclonal gammopathy of undetermined significance (MGUS) and Multiple Myeloma (MM). We used single telomere length analysis (STELA) to measure XpYp telomeres in the whole bone marrow aspirates of 61 MGUS and 141 MM patients. From this, we identified a mean XpYp telomere length threshold of 3.92kb which could be used to stratify MM patients as either low- or high-risk. Multivariate analysis was then employed to establish the most significant factors enabling prognostication of the MM cohort. This concluded that the international staging system (ISS) for MM was the most important, followed by age at diagnosis and then mean XpYp telomere length. We therefore sought to incorporate this threshold into the ISS for MM, allowing each prognostic subset to be further risk-stratified. Consequently, we argue for the inclusion of telomere length data in the ISS, with the aim of increasing the prognostic resolution of this staging system.

The inferior prognosis that often accompanies patients with critically shortened telomeres has previously been attributed to chromosomal end-end fusion that drives the genomic rearrangement underpinning cancer progression. We therefore sought to determine whether these fusion events were present within the whole bone marrow aspirates of MM patients. Of the 16 samples analysed, each showed evidence of

chromosomal end-end fusion. However, we were unable to demonstrate that the presence of these fusion events was directly linked to mean XpYp telomere length. Instead, we identified a significant relationship between the standard deviation of each STELA profile and the frequency of fusion, suggesting that a subset of critically shortened telomeres may be responsible for the genomic instability and chromosomal rearrangements that define MM.

3.2 Introduction

Multiple myeloma (MM) is a plasma cell disorder, characterised by osteolytic bone lesions, renal failure and anaemia (International Myeloma Working 2003). It is caused by an uncontrolled growth of abnormal plasma cells within the bone marrow, resulting in the release of large quantities of paraprotein into the blood (Rajkumar et al. 2014). MM is often preceded by monoclonal gammopathy of undetermined significance (MGUS), an asymptomatic disorder from which the risk of developing symptomatic MM is 1% per year for each patient (Kyle et al. 2002). Rates of survival for MM patients can range from months to years, resulting in a disease which is characterised by its heterogeneous clinical course (Jimenez-Zepeda et al. 2016). Reliable prognostic markers are therefore necessary to provide accurate risk stratification and aid in clinical decision making.

Developed in 1975, the Durie-Salmon staging system was one of the earliest methods used to stratify MM patients. Its intention was to estimate the risk of disease progression based upon some of the most common clinical features of MM (Durie and Salmon 1975). One such feature is an increased concentration of serum calcium, a product of the bone resorption that occurs when abnormal plasma cells activate osteoclasts within the bone marrow. The resulting loss of bone density also produces lesions, manifesting as weakened bones or painful fractures (Tanaka et al. 2007; Terpos, Moulopoulos, and Dimopoulos 2011). A further feature of MM is the presence of circulating paraprotein, with increasing concentrations in the blood pointing towards a greater number of abnormal plasma cells within the bone marrow. These cells cause a loss of bone marrow homeostasis resulting in, for example, impaired red blood cell production and anaemia (Maes et al. 2010). Together, these four features (reduced serum calcium, evidence of bone lesions, increased paraprotein concentration and reduced haemoglobin concentration) are used by the Durie-Salmon staging system to gauge the clinical stage of each MM patient.

However, a new staging system was developed in 2005 by the International Myeloma Working Group. This is known as the international staging system (ISS) and primarily utilises the concentration of serum β2 microglobulin to stratify patients (Greipp et al. 2005). As a component of the MHC class I molecule, β2 microglobulin is present on the surface of all nucleated cells. Free β2 microglobulin is normally filtered from the blood by the kidneys, but the impaired renal function that often accompanies MM can result in its accumulation (Rossi et al. 2010). For this reason, β2 microglobulin concentrations are thought to act as an indirect measurement of both tumour mass and renal function. Serum albumin, the main component of blood plasma, is also used to stratify low- and intermediate-risk MM patients when β2 microglobulin concentrations are below 3.5mg/L. It is thought that reduced concentrations of serum albumin are the result of increased IL-6 production by the myeloma microenvironment (Jacobson et al. 2003).

In 2015, the ISS was revised to incorporate chromosomal abnormalities and serum lactate dehydrogenase (LDH) concentrations (Palumbo et al. 2015). The presence of del(17p), t(4;14) or t(14;16) was now enough to classify a patient as high-risk. This was due to the loss of TP53 conferred by del(17p), resulting in disruption to apoptotic and senescent pathways (Avet-Loiseau et al. 2007). Meanwhile, t(4;14) and t(14;16) are known to enhance the survival of malignant plasma cells by upregulating cyclin D2 and c-MAF expression (Bergsagel and Kuehl 2005; Zhan et al. 2006). Increased concentrations of LDH also indicate higher tumour burden, with intermediate- and high-risk patients being identified based on abnormal serum LDH levels (Terpos et al. 2010).

However, performing four separate tests in line with the revised ISS guidelines increases both the cost and time required for prognostication. Meanwhile, the original ISS relies too heavily on the concentration of serum β2 microglobulin to accurately stratify intermediate- and high-risk patients. For these reasons, a new cost-effective prognostic indicator is necessary which can increase the prognostic resolution of the ISS for MM.

It has recently been demonstrated that telomere length holds significant prognostic value in chronic lymphocytic leukaemia (CLL), breast cancer and myelodysplasia (Lin et al. 2014; Simpson et al. 2015; Williams et al. 2017). In the case of CLL, the mean XpYp telomere length threshold of 3.81kb was identified, below which chromosomal end-end fusion events were detected. Of those patients in which fusion events were detected, the mean XpYp telomere length was 2.26kb. Using both 3.81kb and 2.26kb to stratify CLL patients proved to be highly prognostic, although 2.26kb was shown to hold the greatest prognostic significance (Lin et al. 2014). This 2.26kb threshold also held the greatest prognostic significance when used to stratify breast cancer patients (Simpson et al. 2015).

However, these are not the only studies linking telomere length to prognosis. Shorter mean telomere length has also been shown to correlate with poor survival in bladder, prostate and lung cancer (Russo et al. 2014; Heaphy et al. 2013; Jeon et al. 2014). A meta-analysis by Zhang et al. (2015) concluded that shorter mean telomere length was significantly associated with poor cancer survival across forty-five independent studies. The reason for this prognostic significance is likely to be the relationship between critically shortened telomeres and genomic instability. If the DNA damage signalling pathways in a cell are compromised, then cell division may continue beyond the Hayflick limit. Once the protective function of the telomere is lost, chromosomal ends can be recognised as double-strand DNA breaks and may be subject to fusion with other unprotected ends. The resulting genomic instability is known as a telomere-driven crisis and is thought to drive cancer progression (Lin et al. 2010; Roger et al. 2013; Gisselsson et al. 2001).

A small-scale study has already established that the bone marrow aspirates of MM patients demonstrate a shorter mean telomere length than the aspirates of healthy individuals (Cottliar et al. 2003). The mean telomere length of plasma cells from MM

patients are also known to be shorter than those of leukocytes isolated from the same patient (Wu et al. 2003). However, little is known about the prognostic value of these telomere length measurements. We therefore sought to assess whether a relationship existed between mean XpYp telomere length and overall survival in cohorts of MGUS (n = 61) and MM (n = 141) patients. This involved measuring mean telomere length in the whole bone marrow aspirates of these patients using STELA.

We used a mean XpYp telomere length threshold of 3.92kb to stratify low- and high-risk MM patients. Multivariate analysis was then employed to establish the most significant factors enabling prognostication of the MM cohort. This concluded that the international staging system (ISS) for MM was the most important, followed by age at diagnosis and then mean XpYp telomere length (Hyatt et al. 2017). Inclusion of this telomere length threshold within the ISS criteria increased prognostic resolution, resulting in the further stratification of stage I/II and stage III patients. We then attempted to identify the underlying mechanism for the prognostic significance of telomere length measurements in MM, seeking to explore the relationship between telomere shortening and genomic instability. Utilising a small cohort of 16 MM patients, we observed that the frequency of chromosomal end-end fusion events was not directly linked to mean XpYp telomere length in this study, but was significantly linked to the standard deviation of the STELA profile.

3.3 Aims of the Chapter

We hypothesised that telomere length measurements held prognostic value within the context of MM. The aim of this chapter was therefore to identify whether STELA could be used to isolate low- and high-risk patients within a MM cohort. We then considered whether telomere length measurements could be used to refine the prognostic resolution of the ISS. We also aimed to determine whether chromosomal end-end fusion events could be detected in the bone marrow aspirates of MM patients, as well as whether a relationship existed between telomere length and the frequency of these fusion events.

3.4 Results

3.4.1 Characteristics of the MGUS and MM Cohorts

Bone marrow aspirates were obtained from 61 MGUS and 141 MM patients. Clinical data was also available for the majority of patients in each cohort. This included the patient's serum β2 microglobulin, haemoglobin, albumin and calcium levels ***(Table 3.1)***. When compared to the cohort of patients used to outline the original ISS guidelines (Greipp et al. 2005), our MM cohort had almost identical mean β2 microglobulin (3.8mg/L versus 4.0mg/L) and albumin (3.6g/dL versus 3.6g/dL) levels. The gender composition of the Greipp et al. (2005) cohort was 57% male and 43% female; our MM cohort was 54% male and 46% female. Average age at diagnosis for the Greipp et al. (2005) cohort was 66 years, against our MM cohort which was 72 years. From this, we concluded that our patient cohort was directly comparable to that of the original ISS cohort. It is important to note that mean and median values for the serum haemoglobin and calcium concentrations of our cohort could not be established due to the presence of non-numerical values. Calcium concentrations were defined as being either 'normal' or 'high', preventing a comparison with other studies from being made.

By combining this data with the outcomes for each patient, we could plot Kaplan-Meier survival curves for our MM cohort ***(Figure 3.1)***. In each case, the thresholds used to stratify patients were the same as those used in the ISS (β2 microglobulin </>5.5mg/L and albumin </>3.5g/dL) or Durie-Salmon staging system (haemoglobin </>10g/dL). From this, it was observed that β2 microglobulin levels held the greatest prognostic value (HR = 3.6), followed by haemoglobin (HR = 3.1), age at diagnosis (HR = 2.5) and serum albumin concentration (HR = 2.0). Meanwhile, stratification of patients based on serum calcium concentration (HR = 1.3) and gender (HR = 0.83) proved to hold little prognostic value. Again, this observation closely mirrored the results of the original ISS cohort (Greipp et al. 2005). In this case, β2 microglobulin was shown to have the greatest prognostic value, followed by age at diagnosis, haemoglobin, serum albumin, serum

MGUS

	Patient Data Available for…	Mean	Median	Range
Age at Diagnosis (Years)	49	66.31	69	33 - 90
Survival (Months)	41	31.78	19	1 - 200
β2 microglobulin (mg/L)	50	5.16	4.85	1.3 - 22
Albumin (g/dL)	45	4.18	4.2	3.5 – 4.7
Haemoglobin (g/dL)	48	-	-	-
Calcium (Normal vs High)	46 (46 vs 0)	-	-	-
Gender (Male vs Female)	52 (22 vs 30)	-	-	-
XpYp Telomere Length (kb)	61	5.33	5.41	1.00 - 7.61
Telomere Length Standard deviation (kb)	61	2.23	2.23	0.82 – 3.77

Multiple Myeloma

	Patient Data Available for…	Mean	Median	Range
Age at Diagnosis (Years)	129	64.31	66	34 - 87
Survival (Months)	131	50.89	48	1 - 192
β2 microglobulin (mg/L)	95	7.26	4	1.6 – 53.2
Albumin (g/dL)	73	3.55	3.6	2.2-4.8
Haemoglobin (g/dL)	111	-	-	-
Calcium (Normal vs High)	115 (74 vs 41)	-	-	-
Gender (Male vs Female)	137 (74 vs 63)	-	-	-
XpYp Telomere Length (kb)	141	4.84	4.96	1.26-7.51
Telomere Length Standard Deviation (kb)	141	2.12	2.08	0.60 – 4.20

Table 3.1 – Characteristics of the MGUS and MM Cohorts
Mean XpYp telomere length was measured in the whole bone marrow aspirates of 202 MGUS and MM patients. This table lists the characteristics of each cohort.

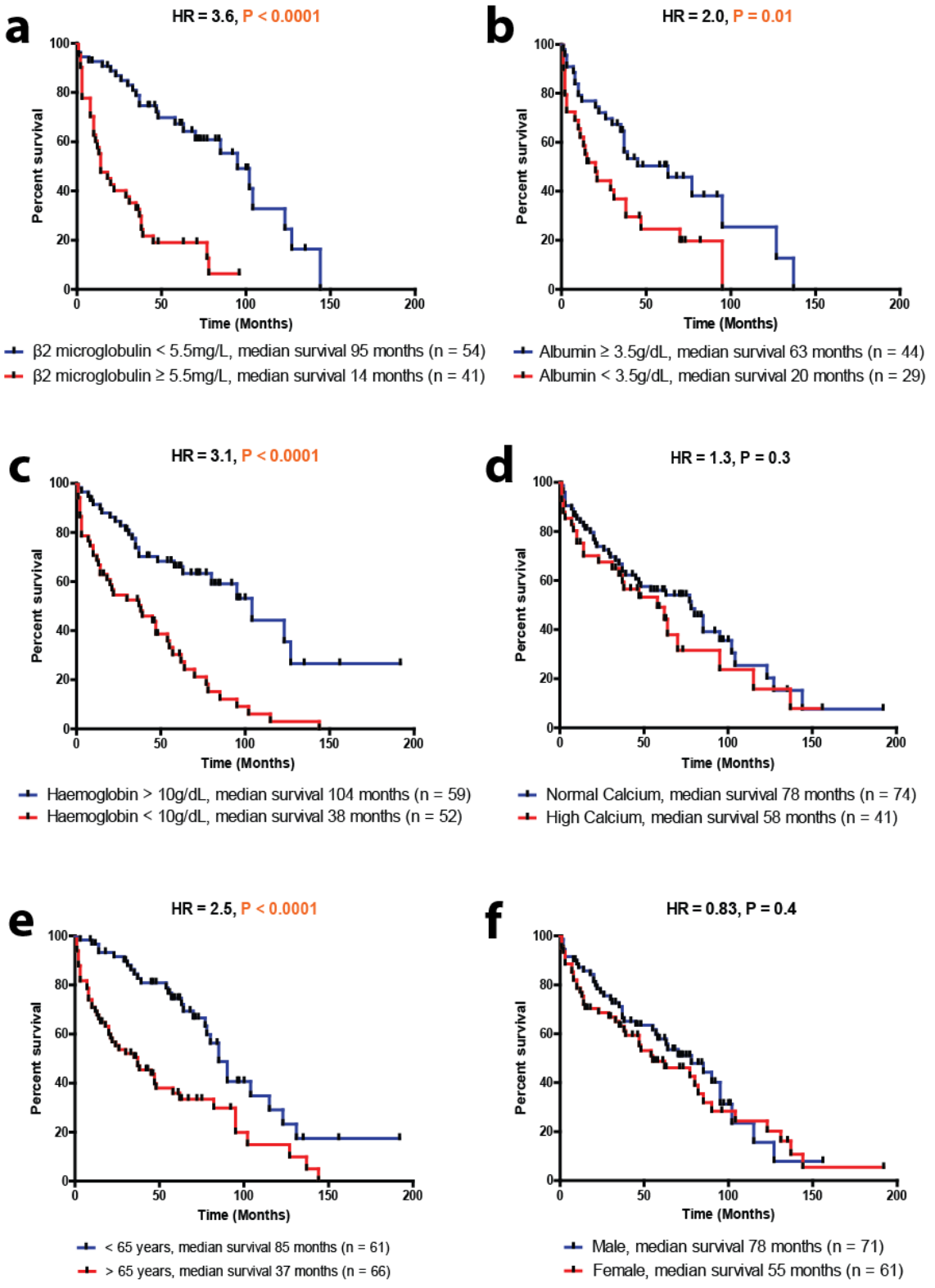

Figure 3.1 - Stratification of the MM Cohort based on Available Data
(a) Kaplan Meier curve which stratifies the MM patient cohort based on their β2 microglobulin levels (as outlined in the ISS). **(b)** Kaplain Meier curve which stratifies the MM patient cohort based on their albumin levels (as outlined in the ISS). **(c)** Kaplain Meier curve which stratifies the MM patient cohort based on their haemoglobin levels (as outlined in the Durie-Salmon staging system). **(d)** Kaplain Meier curve which stratifies the MM patients cohort based on their serum calcium levels. **(e)** Kaplain Meier curve which stratifies the MM patient cohort based on the age at diagnosis **(f)** Kaplain Meier curve which stratifies the MM patient cohort based on their sex. Significance was defined as $P<0.05$

calcium and patient gender. The major difference was that Greipp et al. (2005) still found serum calcium concentrations to hold significant prognostic value, whereas we did not. This was likely due to the limited size of our MM cohort (n = 141) against the larger cohort size used to define the ISS (n = 10,750).

3.4.2 MGUS and MM Exhibit Heterogeneous Telomere Length Distributions

Single telomere length analysis (STELA) is a single-molecule PCR-based technique which allows individual telomeres from specific chromosomal ends to be measured (Baird et al. 2003). We used STELA to measure the mean XpYp telomere length in 61 MGUS and 141 MM patients. ***Figure 3.2a*** is an example of the STELA profiles that were produced for each of these patients. Every band represents a single XpYp telomere, with the mean telomere length of a patient being calculated from this profile. The mean XpYp telomere length across the MGUS and MM cohorts were 5.33kb and 4.84kb respectively. Comparisons with Cottliar et al. (2003) suggested that these values were shorter than the average telomere length of healthy control bone marrow aspirates (8.50kb), but similar to those of MM bone marrow aspirates (5.20kb) calculated using TRF analysis.

Standard deviation was used as a measurement of telomere length heterogeneity within an individual STELA profile. The mean of the standard deviations across the MGUS and MM cohorts were 2.23kb and 2.12kb respectively. These values were much greater than that of the clonal fibroblast populations (~0.85kb) or purified B cell populations (~1.00kb) identified by Lin et al. (2010). Although MM is characterised by the growth of clonal plasma cell populations, the DNA samples analysed here were isolated from unsorted bone marrow aspirates. This means that the XpYp telomeres of multiple cell types were being measured, unlike that of a clonal population whereby a single cell type is being measured. Therefore, the heterogeneous telomere length profiles observed may have

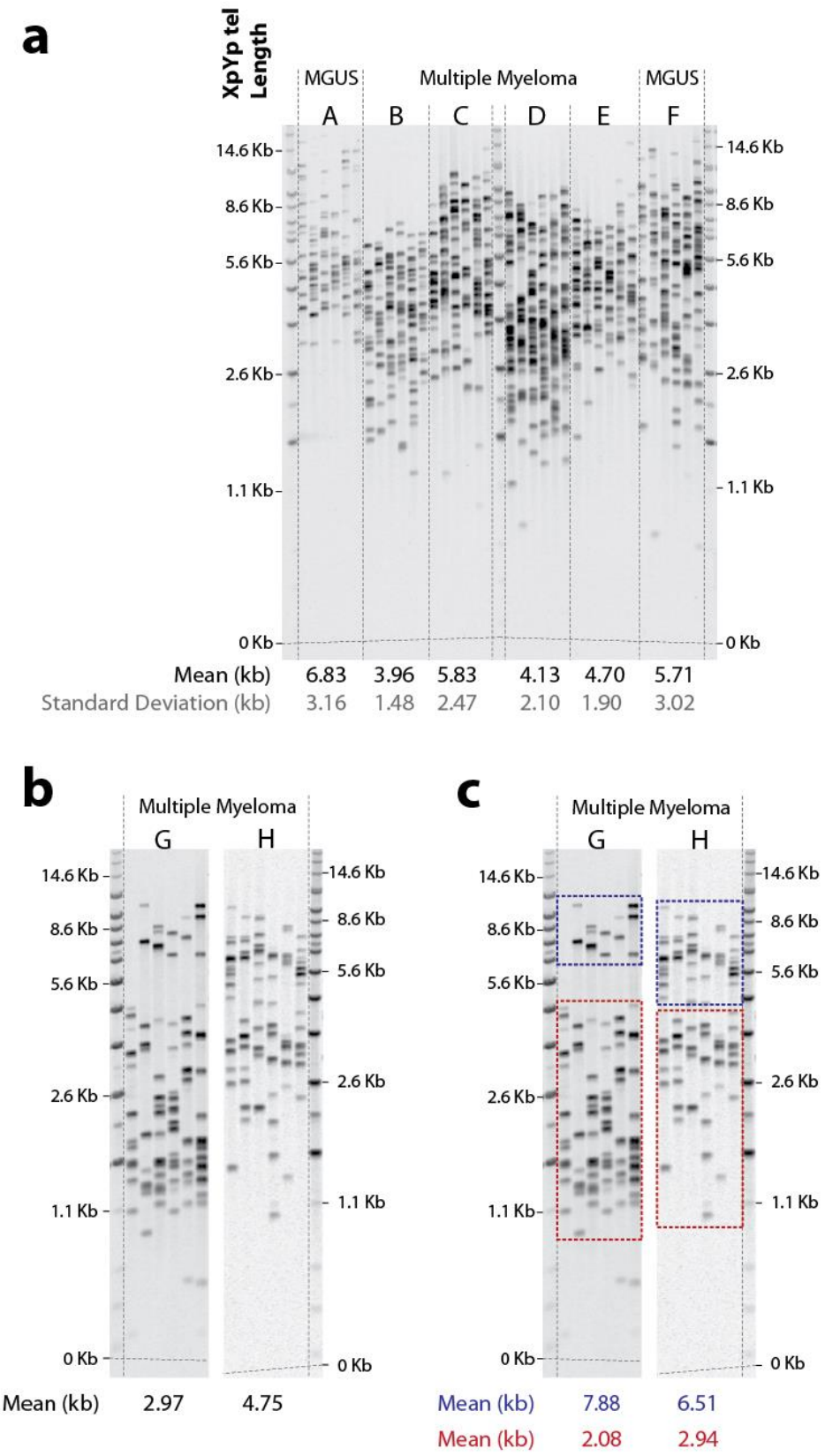

Figure 3.2 - MM and MGUS Exhibit Heterogeneous Telomere Length Distributions
(a) An example of the XpYp STELA profiles obtained for two MGUS and four MM patients (labelled A-F). The mean XpYp telomere length has been listed under each patient's profile, along with the standard deviation. In total, the XpYp telomere lengths of 61 MGUS and 141 MM patients were analysed using this method. Patient D is an example of a STELA profile with a multimodal distribution. **(b) and (c)** An example of two MM patient XpYp STELA profiles which have multimodal distributions. Mean values for the **upper** and **lower** distributions have been calculated, demonstrating that a patients mean telomere length can vary significantly from that of the longest and shortest telomeres.

been caused by the diverse cellular composition of each DNA sample and/or the replicative history of each cell type.

A number of STELA profiles also displayed multimodal distributions ***(Figure 3.2b and 3.2c)***. These are distinct distributions of telomere lengths within a single STELA profile, with each distribution having a unique mean telomere length. Again, their presence reflects the different replicative histories of the various cell types that compose the bone marrow microenvironment. Given that the mean telomere lengths of plasma cells isolated from MM patients are known to be significantly shorter than those of healthy controls (Wu et al. 2003), we next sought to determine whether plasma cells were responsible for the presence of these shortened telomere length distributions within the STELA profiles of MM patients.

Isolation of $CD138^+$ cells from the whole bone marrow aspirates of three MM patients, followed by STELA of both the $CD138^-$ and $CD138^+$ fractions, revealed that $CD138^+$ cells often had significantly shortened telomeres when compared to the rest of the aspirate ***(Figure 3.3)***. In the case of each patient, mean XpYp telomere length of the whole aspirate lay above the 3.81kb fusogenic threshold identified in CLL. However, mean XpYp telomere length of the $CD138^+$ fraction fell below this threshold in each case, with the $CD138^+$ cells of patient J also falling below the CLL fusogenic mean threshold of 2.26kb (Lin et al. 2014). The mean XpYp telomere length of the $CD138^+$ fractions from these three patients was 2.40kb.

Plotting the mean XpYp telomere lengths of MGUS and MM patients revealed that a significant difference existed ($p = 0.01$) between the two cohorts ***(Figure 3.4a).*** MGUS patients often had longer telomeres (mean = 5.33kb) than MM patients (mean = 4.84kb). Also, a much greater proportion of MM patients had a mean XpYp telomere length that fell below the CLL fusogenic threshold of 3.81kb (5 MGUS against 26 MM). A significant

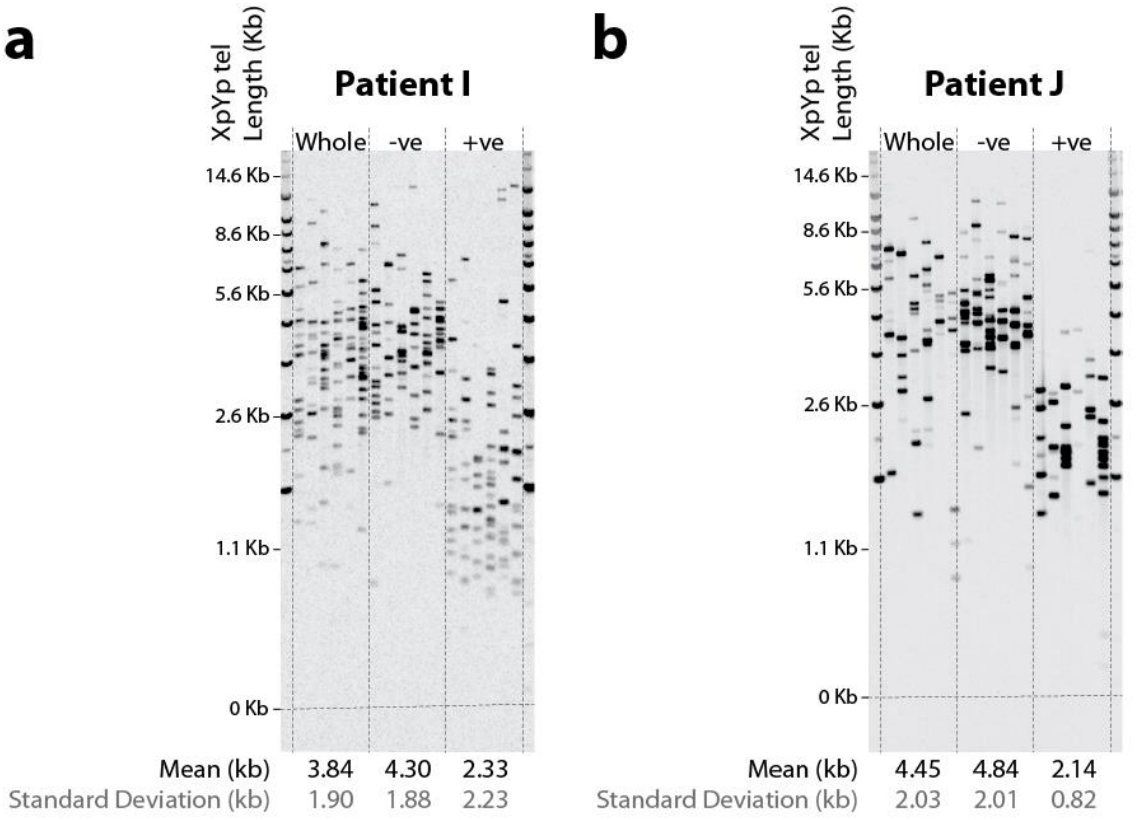

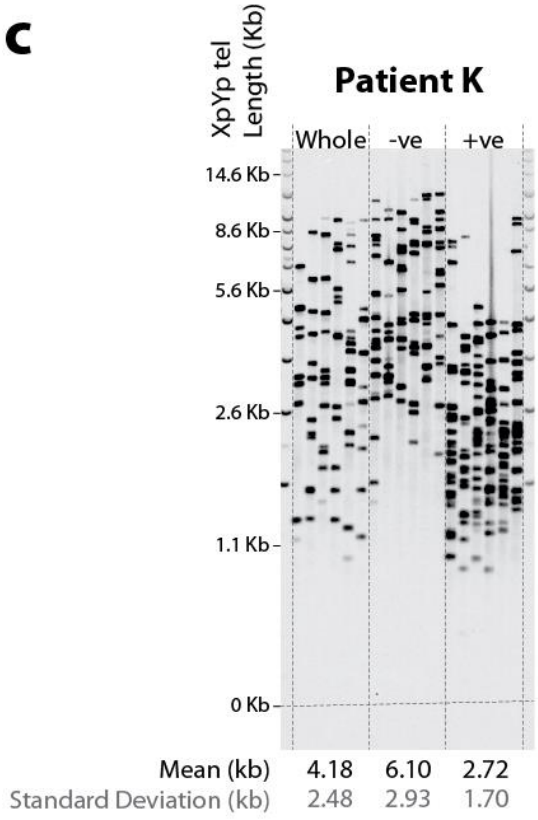

Figure 3.3 - CD138+ Cells Show a Significantly Reduced Telomere Length When Compared to CD138- Cells from the Same Patient

(a) to (c) STELA profiles showing the XpYp telomere lengths of cells, obtained from the whole bone marrow aspirates of three MM patients (I-K), that had been sorted for CD138 expression.

Whole: bone marrow aspirates that had not undergone a selection procedure.

-ve: the fraction of cells which were not positively selected for and did not express CD138.

+ve: the fraction of cells which were positively selected for and did express CD138.

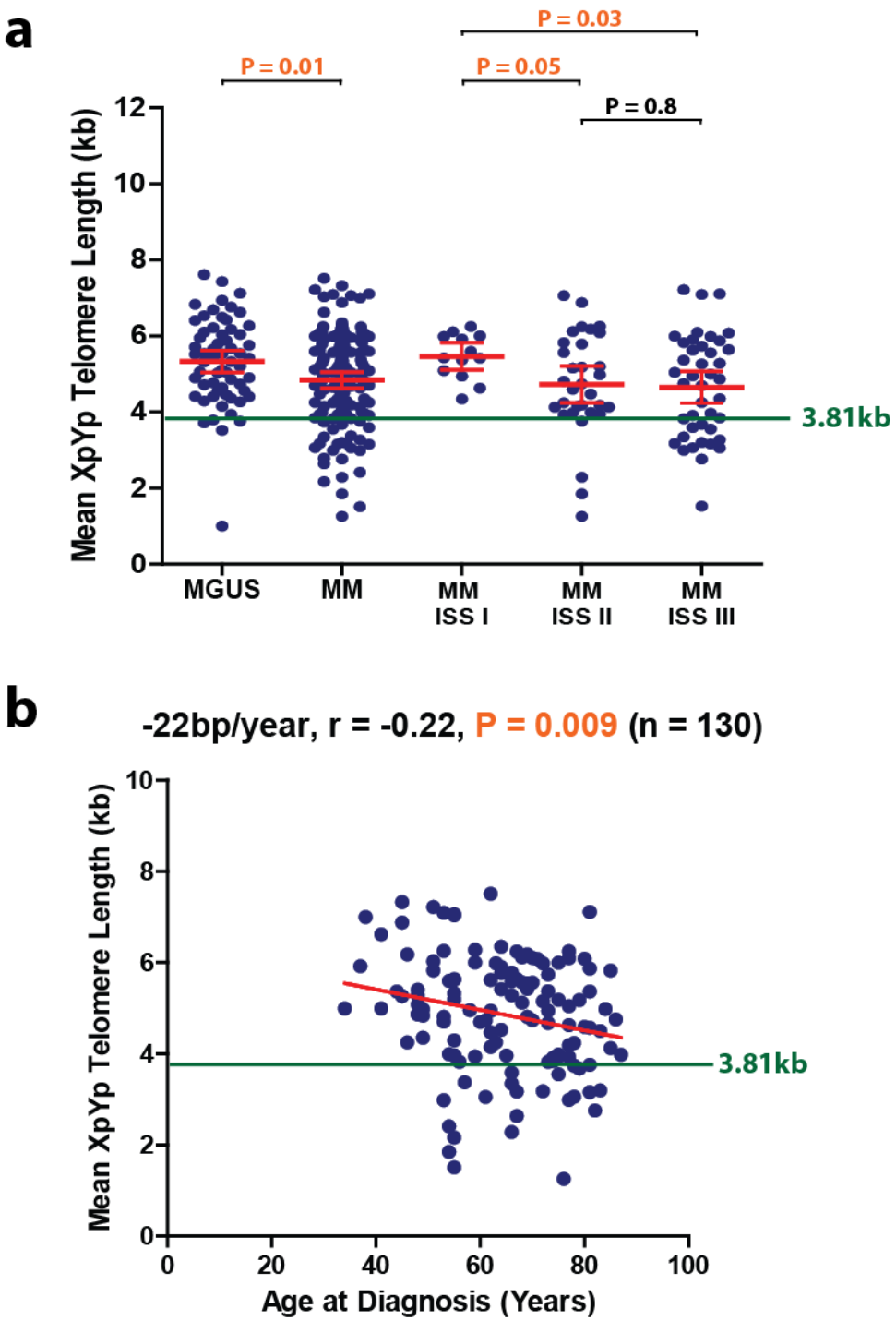

Figure 3.4 - Mean Telomere Length is Shorter in MM when Compared to MGUS
(a) Scatter plot comparing the mean XpYp telomere lengths of MGUS patients (n = 61) and MM patients (n = 141). Where β2 microglobulin and albumin levels were available, the MM cohort was then split between the stage I (n = 13), stage II patient (n = 42) and stage III patient (n = 42) sub-groups. The previously-defined upper limit of telomere dysfunction in CLL (3.81kb) is shown as a green horizontal line. Non-parametric Mann-Whitney tests were used for statistical comparisons. **(b)** Plot showing the mean XpYp telomere lengths of MM patients (n = 130) against the age at which each patient was diagnosed. Linear regression was plotted as a red line. The previously-defined upper limit of telomere dysfunction in CLL (3.81kb) is shown as a green horizontal line. Spearman correlation was used for statistical analysis. Significance was defined as $P<0.05$

difference was also observed between the mean XpYp telomere lengths of ISS I and ISS II MM patients (*p = 0.05*), as well as ISS I and ISS III MM patients (*p = 0.03*). However, a significant difference did not appear to exist between the mean XpYp telomere lengths of ISS II and ISS III MM patients (*p = 0.8*).

Plotting the mean XpYp telomere length of whole bone marrow aspirates against the patient's age at diagnosis ***(Figure 3.4b)*** demonstrated that a statistically significant relationship existed (*p = 0.009*). Mean XpYp telomere length of the cohort was shown to decrease by an average of 22 base pairs per year, consistent with the average telomeric erosion rates observed in the leukocytes (-26bp per year), muscle (-24bp per year) and skin (-23bp per year) of healthy adults (Daniali et al. 2013).

3.4.3 Telomere Length is Highly Prognostic in MM

To determine whether the mean telomere length of whole bone marrow aspirates held prognostic significance in MM, we attempted to stratify patients as either low- or high-risk based on an XpYp telomere length threshold. It is important to note that data regarding overall survival was only available for 131 of the 141 MM patients. Recursive partitioning was used to test a range of telomere-length thresholds between 2kb and 6kb ***(Figure 3.5a)***. The optimum threshold in the 131-patient cohort that provided the most prognostic significance (HR = 3.6; P < 0.0001) was found to be 3.93kb. A Kaplan-Meier survival curve was then plotted using this threshold ***(Figure 3.5b)***, showing that patients with a mean XpYp telomere length greater than 3.92kb had a significantly increased median survival (85 months) when compared to patients with a mean XpYp telomere length less than 3.92kb (16 months). For comparison, a second threshold of 4.96kb was plotted as this was the median value of the 131 mean XpYp telomere lengths ***(Figure 3.5c)***. This threshold was shown to hold prognostic significance (HR = 1.7; P = 0.02), but did not confer the same level of significance as the 3.92kb threshold.

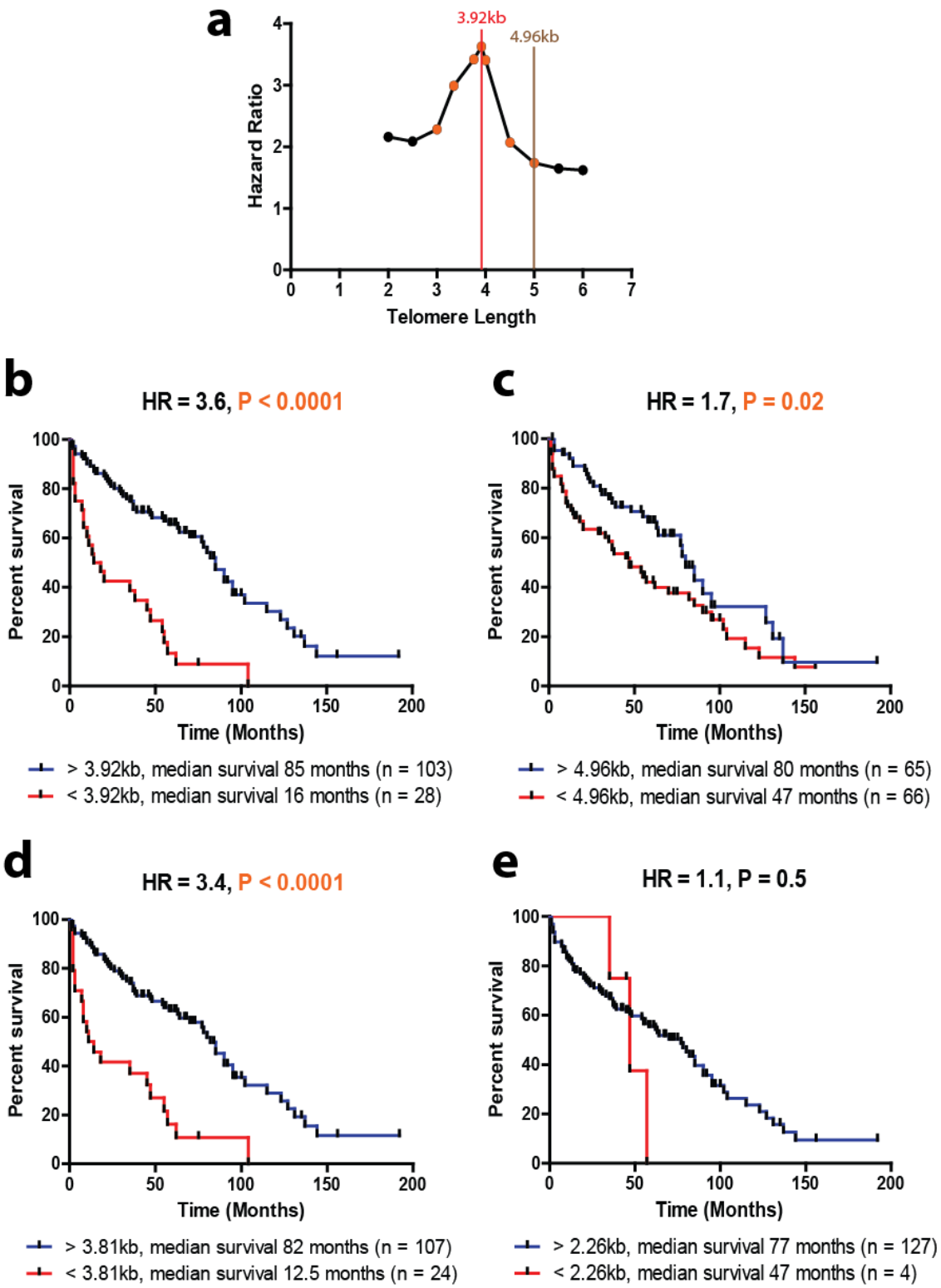

Figure 3.5 - Telomere Length is Highly Prognostic in MM
(a) Recursive partitioning of the 131-patient cohort, identifying the 3.92kb threshold which was used to stratify patients. Median telomere length has also been labelled as a blue vertical line. **(b)** Kaplan Meier curve which used the 3.92kb threshold to identify subsets of patients with superior and inferior survival. **(c)** Kaplan Meier curve which stratified patients based on a median telomere length of 4.96kb. **(d)** Kaplan Meier curve which stratified patients using a 3.81kb threshold. This value was previously identified as an upper threshold of telomere dysfunction in a cohort of CLL patients. **(e)** Kaplan Meier curve which stratified patients using a 2.26kb threshold. This value was previously identified as a fusogenic-mean threshold in a cohort of CLL patients. Significance was defined as P<0.05

A survival curve was then plotted using the 3.81kb fusogenic threshold identified in CLL ***(Figure 3.5d)***. Due to the proximity of this threshold to our 3.92kb threshold, only four patients were recategorised. Unsurprisingly, this also held prognostic significance and had an almost identical hazard ratio (HR = 3.4; P < 0.0001) to that of the 3.92kb threshold. Although the 2.26kb fusogenic mean threshold identified in CLL was also plotted for our 131-patient MM cohort, the small number of patients (n = 5) whose mean XpYp telomere length fell below 2.26kb rendered this result insignificant ***(Figure 3.5e)***. An insufficient number of patients was also the reason why this analysis was not conducted in the MGUS cohort. Data regarding overall survival was only available for 41 MGUS patients, with each having a mean XpYp telomere length greater than 3.92kb. There was therefore limited merit in undertaking univariate analysis in this cohort.

3.4.4 Incorporating Telomere Length Measurements into the ISS

Although mean XpYp telomere length measurements held significant prognostic value in our MM cohort, they did not provide the same level of stratification as the ISS. Even as an isolated marker, serum β2 microglobulin concentrations held greater prognostic significance than the 3.92kb telomere length threshold. Multivariate analysis, carried out by Professor Robert Hills of Cardiff University, was employed to establish the most significant factors enabling prognostication of the MM cohort. This concluded that the international staging system (ISS) for MM was the most important, followed by age at diagnosis and then a mean XpYp telomere length below 3.81kb. Even after adjusting for ISS and age, patients with a telomere length below 3.81kb had a significantly shorter survival (Hyatt et al. 2017). We therefore sought to combine ISS grouping and telomere length measurements, with a view to increasing the prognostic resolution of the ISS.

Of the 131 MM patients for which survival data was available, serum β2 microglobulin concentrations were known for 95 of these. However, data regarding serum albumin concentration was only available for 66 patients. For this reason, as well as the fact that

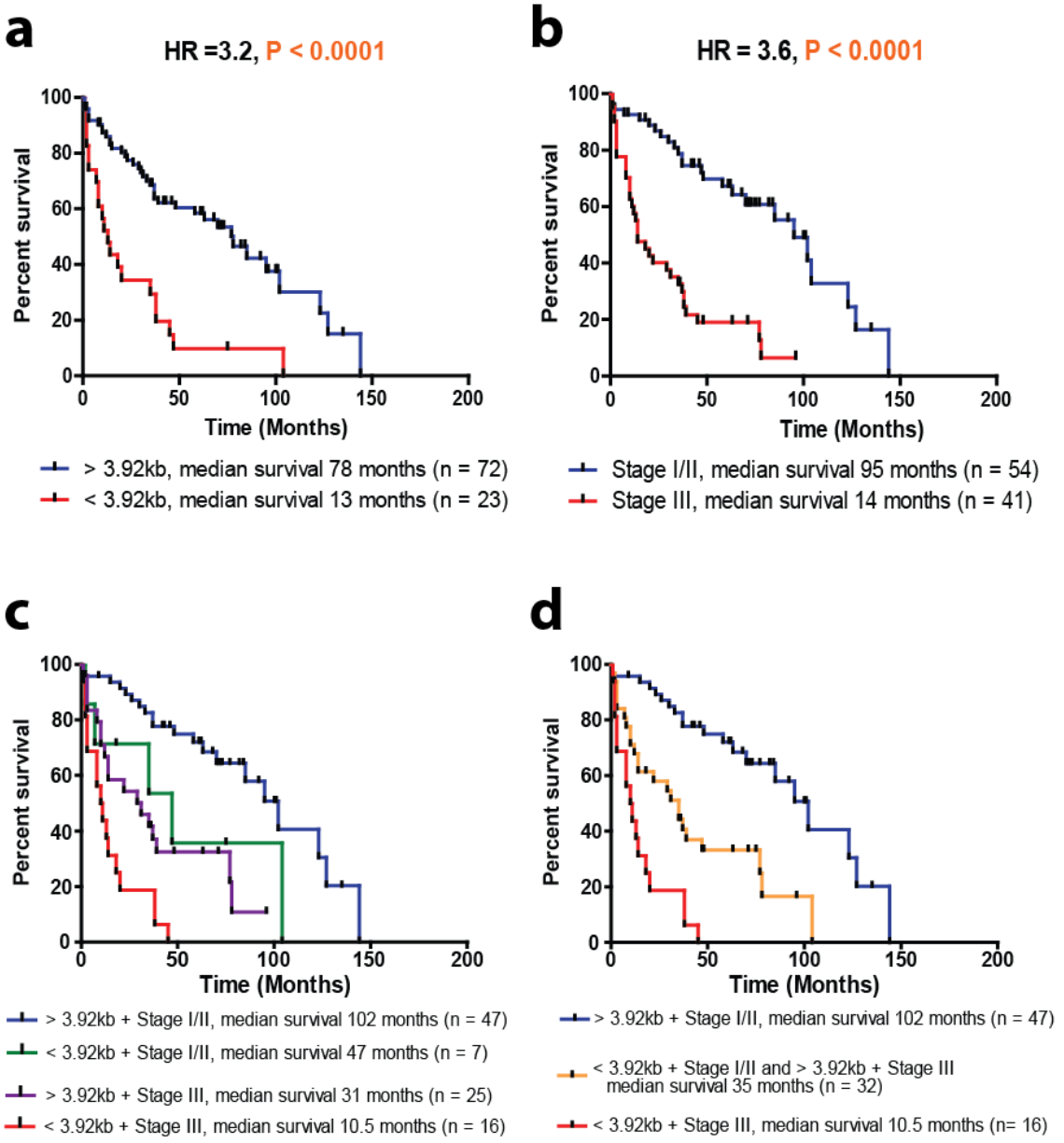

Figure 3.6 - Prognostic Resolution can be Increased by Incorporating Mean Telomere Length into the ISS

Of the 131-patient cohort, ISS staging was also available for 95 of these patients. **(a)** Kaplan Meier curve which stratifies patients using a 3.92kb threshold. **(b)** Kaplan Meier curve which stratifies patients based on their ISS staging. **(c)** Kaplan Meier curve which used a combination of the 3.92kb threshold and ISS staging to stratify patients. This resulted in both the ISS I/II and ISS III cohorts splitting into two further sub-groups. **(d)** Kaplan Meier curve which also uses a combination of the 3.92kb threshold and ISS staging, but combines the **< 3.92kb + Stage I/II** and **> 3.92kb + Stage III** patient groups. Significance was defined as $P<0.05$

serum albumin only plays a minor role in stratifying low- and intermediate-risk patients, we sought to combine stage I and stage II patients into a single cohort. Using this data, we aimed to use mean XpYp telomere length measurements as a way to improve the prognostic resolution of the ISS with regard to intermediate- (stage I/II, <5.5mg/L β2 microglobulin) and high-risk (stage III, >5.5mg/L β2 microglobulin) patients.

Kaplan-Meier survival curves were plotted based on either the mean XpYp telomere length of the 95-patient cohort ***(Figure 3.6a)***, or their staging within the ISS ***(Figure 3.6b)***. Strikingly, the two curves appeared to plot a similar result for median survival, with <3.92kb mean XpYp telomere length patients and stage III patients having a median overall survival of 13 months and 14 months respectively. Combining the mean XpYp telomere length threshold of 3.92kb with the ISS scoring for each patient resulted in further stratification of the stage I/II and stage III patients ***(Figure 3.6c)***. ISS I/II patients with a mean XpYp telomere length below the 3.92kb threshold had a significantly reduced survival, while ISS III patients with a mean telomere length above the 3.92kb threshold had a significantly increased survival. Combining these two new subgroups resulted in the formation of an intermediate subgroup, increasing prognostic resolution when compared to serum β2 microglobulin concentrations alone ***(Figure 3.6d)***. For comparison, this analysis was repeated using the 3.81kb CLL fusogenic threshold (***Supplementary Figure 1***). However, little difference was observed between this threshold and the 3.92kb threshold.

3.4.5 Identifying Chromosomal Fusion Events in the Bone Marrow Aspirates of MM Patients

Although we had demonstrated that mean XpYp telomere length measurements held significant prognostic value within the context of MM, an explanation for this observation had yet to be established. Previous studies in CLL and colorectal cancer had identified a relationship between critically shortened telomeres and genomic instability

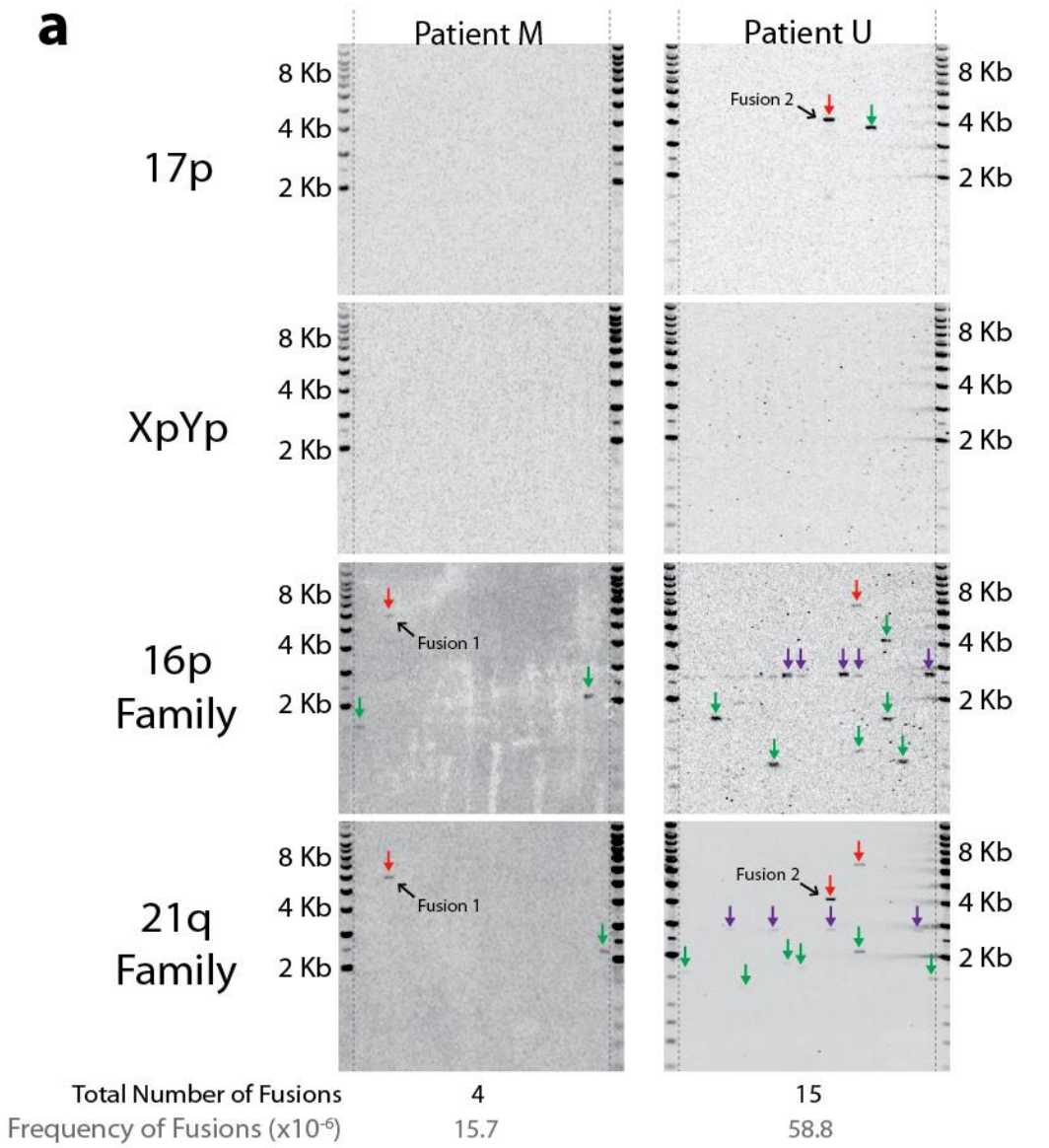

Figure 3.7 - Bone Marrow Cells of MM Patients Show Evidence of Chromosomal Fusion Events
(a) Examples of two MM patients whose DNA was examined for the presence of chromosomal fusion events. In total, 1530ng of DNA was analysed per patient. The frequency of chromosomal fusion was estimated by dividing the number of observable fusion bands by the number of input molecules (around 255,000 cells). Bands representing possible intrachromosomal fusion events were highlighted in green, while interchromosomal fusion events were highlighted in red. Purple arrows were used to highlight bands that were located in areas known for backgrounds bands (these were not included in the final analysis). **(b)** Examples of three MM patient chromosomal fusion events that have been sequenced. The number of bases that have been erroded from the end of each chromosome (or the number of telomere repeats remaining) has been listed. Any microhomology between the chromosome ends has been highlighted in blue.

(Lin et al. 2010; Roger et al. 2013). It was thought that chromosomal end-end fusion events, which can occur after significant telomeric erosion, drove genomic rearrangement and cancer progression. We therefore set out to determine whether these fusion events could be detected within the bone marrow aspirates of MM patients, as well as if the frequency of fusion was in some way linked to the mean XpYp telomere length of the whole bone marrow aspirate.

Aspirates were obtained from 16 MM patients attending the haematology outpatient clinic at the University Hospital of Wales. Patients were analysed for chromosomal end-end fusion events involving the 17p, XpYp, 16p family and 21q family of chromosomal ends (***Figure 3.7a***). In each case, multiple fusion events were identified (***Figure 3.7a; Supplementary Figures 2, 3, 4, 5, 6 and 7***). Of these, we were able to sequence three fusion events as a way of observing the extent of genomic erosion and the different types of events that can present (***Figure 3.7b***). At five of these chromosomal ends, between 1096 and 2770 base pairs of genomic DNA had been lost. Only a single 17p chromosomal end showed any evidence of telomeric repeats, with fifty-seven TTAGGG repeats or variant repeats identified. It could also be seen that fusion 3 contained extensive microhomology at the fusion site, with both chromosomes sharing an overlapping sequence of eight base pairs.

Subsequent STELA of the 16 whole bone marrow aspirates identified a heterogeneous range of mean XpYp telomere lengths (***Figure 3.8***). Simply plotting the frequency of chromosomal fusion observed for each patient against their respective mean XpYp telomere length (***Figure 3.9a***) was shown to hold little significance ($p = 0.3$). However, plotting fusion frequency against the standard deviation for each STELA profile (***Figure 3.9b***) resulted in the identification of a significant relationship ($p = 0.04$).

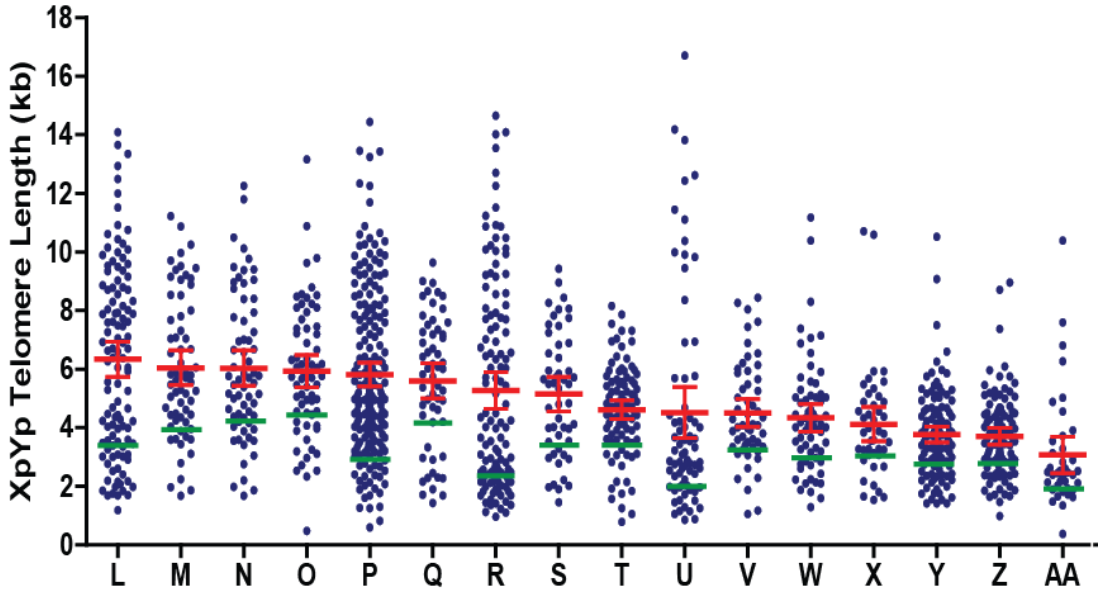

	L	M	N	O	P	Q	R	S	T	U	V	W	X	Y	Z	AA
Mean (kb)	6.33	6.21	6.03	5.92	5.81	5.59	5.27	5.14	4.61	4.51	4.50	4.34	4.12	3.76	3.71	3.07
Standard Deviation (kb)	3.20	3.49	2.46	2.25	2.84	2.24	3.53	2.10	1.55	3.69	1.73	1.91	1.89	1.48	1.42	1.93
25% Percentile (kb)	3.48	3.95	4.27	4.49	3.69	4.19	2.31	3.46	3.61	2.02	3.35	3.01	3.08	2.75	2.72	1.92
Number of Fusions	22	4	16	13	15	5	20	3	3	15	12	12	13	9	11	11
Frequency of Fusions ($x10^{-6}$)	86.3	15.7	62.7	51.0	58.8	19.6	78.4	11.8	11.8	58.8	47.1	47.1	51.0	35.3	43.1	43.1

Figure 3.8 - Mean XpYp Telomere Length Measurments and Frequency of Chromosomal End-End Fusion in 16 MM Patients

(a) Graphical representation of the XpYp STELA profiles for 16 MM patients (**labelled L to AA**). DNA was extracted from their whole bone marrow aspirates. Patients were arranged from the longest mean telomere length (**L**) to the shortest mean telomere length (**AA**). The mean telomere length for each patient is shown in red alongside the uper and lower 95% confidance intervals. The mean value for the lowest 25th quartile is shown in green. The number of chromosomal fusion events and the frequency of chromosomal fusion has been listed in purple under each patient.

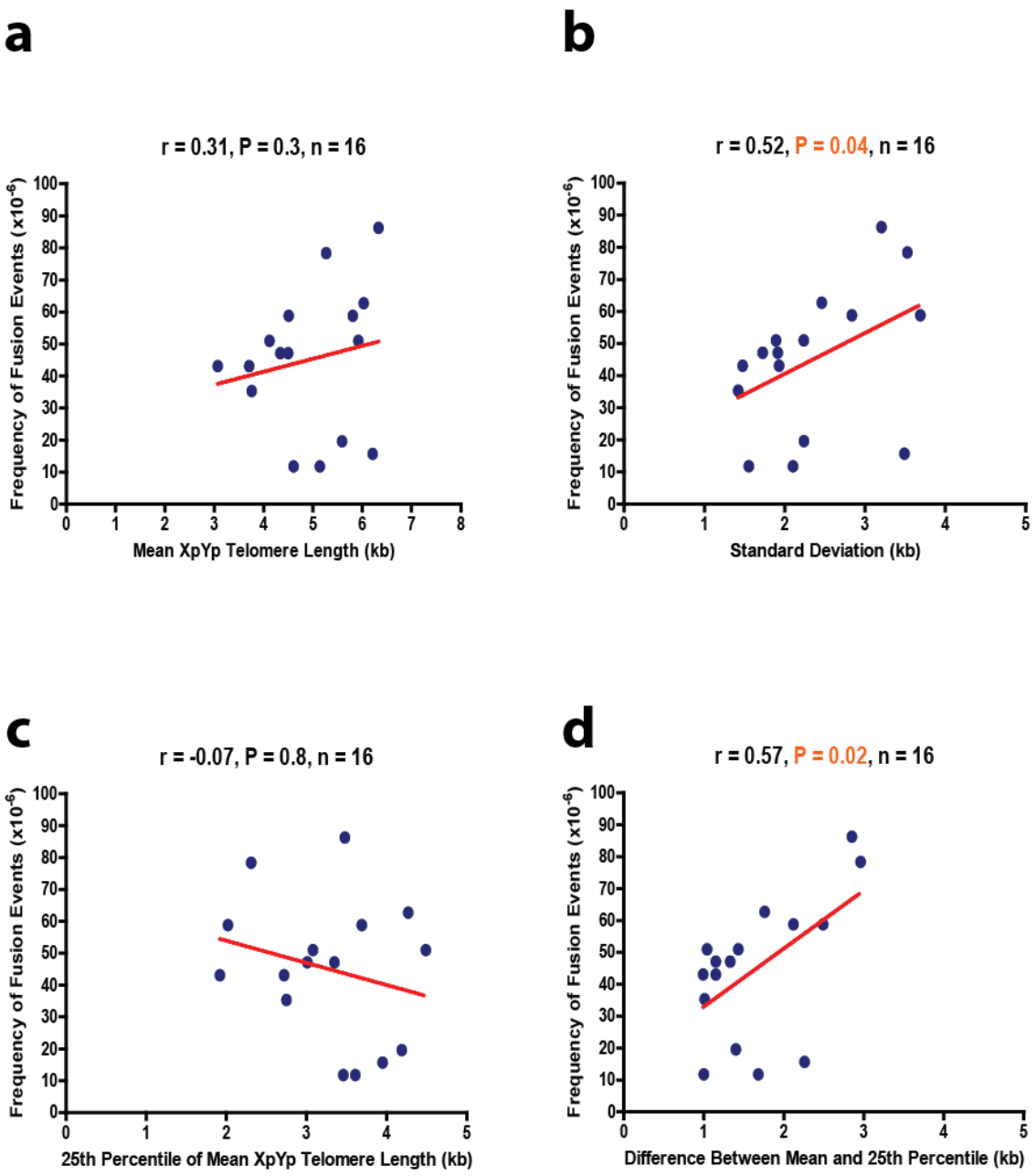

Figure 3.9 - Examining the Relationship Between Telomere Length and Fusion Frequency in 16 MM Patients

Graphs showing the frequency of chromosomal end-end fusion events in 16 MM patients against either **(a)** the mean XpYp telomere length of each patient, **(b)** the standard deviation of each STELA profile, **(c)** the 25th percentile of each STELA profile, or **(d)** the difference between the mean telomere length and the 25th percentile of each STELA profile. Spearman correlation was used for statistical analysis. Significance was defined as $P<0.05$

As we had previously demonstrated that the $CD138^+$ plasma cells of MM patient bone marrow aspirates had significantly shorter telomeres than the $CD138^-$ cells, we used the mean of the 25th percentile of XpYp telomere lengths as an estimation of plasma cell telomere length in this 16-patient cohort. Unfortunately, plotting the frequency of chromosomal fusion events against the telomere length of the 25th percentile (***Figure 3.9c***) failed to demonstrate any significant correlation ($p = 0.8$). However, plotting the frequency of chromosomal fusion events against the difference between the mean of the whole STELA profile and the 25th percentile (***Figure 3.9d***) resulted in significance ($p = 0.02$). It was thought that the different between the mean XpYp telomere length and the 25th percentile was similar to that of the standard deviation of the STELA profiles, estimating the extent to which the telomere length of the plasma cell population differed from that of the remaining bone marrow stromal cells.

3.5 Discussion

3.5.1 Telomeric Shortening in MM

It has been well documented that a shorter mean telomere length is associated with a poorer outcome in specific cancers (Zhang et al. 2015). With regard to CLL and breast cancer, telomere length measurements are known to hold significant prognostic value (Lin et al. 2014; Simpson et al. 2015). We therefore hypothesised that this relationship may extend to MM, whereby telomere length measurements could be used to stratify patients based on their risk of disease progression. Using a high-resolution telomere length analysis technique (STELA) on the whole bone marrow aspirates of 61 MGUS and 141 MM patients, we sought to identify whether mean XpYp telomere length measurements held prognostic value within the context of these disorders.

Comparing the mean XpYp telomere length of the cohorts demonstrated that MGUS patients had a significantly longer telomere length than that of MM patients. The mean XpYp telomere length of ISS I patients was also significantly longer than that of ISS II and ISS III patients. This result is supported by Cottliar et al. (2003), a small-scale study which demonstrated that the whole bone marrow aspirates of MM patients had a shorter mean telomere length than those of healthy controls. This relationship is mirrored in CLL, whereby a shorter mean XpYp telomere length is associated with an increased Binet staging classification (Lin et al. 2010). But although malignant B-cells were identified as the cause of this telomeric shortening in CLL, we had yet to establish a similar cause in MM (Lin et al. 2010).

As it is unlikely that telomere length is dynamically regulated throughout the course of the disease, due in part to the observation that telomerase activity also increases during the progression of MM (Xu, Zheng, et al. 2001; Shiratsuchi et al. 2002), it could be argued that the telomeric erosion originates from a single cell which will eventually give rise to a clonal population. This idea was explored by Roger et al. (2013) using polyps and

carcinoma samples from patients with colorectal cancer. It was demonstrated that telomere length was extremely variable between different colorectal polyps obtained from the same individual. Also, mean telomere length did not significantly differ between a patient's polyp and carcinoma samples, suggesting that telomere length was established before the progression of the cancer. It was therefore thought that cells with shorter telomeres gave rise to tumours with shorter telomeres which were genetically unstable, rather than the mean telomere length of an individual cell decreasing as the disease progressed.

As a way of identifying the source of the telomeric shortening observed in MM patients, we next isolated $CD138^+$ plasma cells from the whole bone marrow aspirates of three MM patients. Mean XpYp telomere length was then calculated for both the $CD138^+$ and $CD138^-$ cell fractions, demonstrating that plasma cells had a significantly reduced telomere length when compared to other non-malignant marrow cells. This was consistent with the idea that these plasma cells exhibited an extensive replicative history when compared to the $CD138^-$ cells of the bone marrow. These results were corroborated by Wu et al. (2003), whereby the $CD138^+$ cells of MM patients were shown to have significantly shorter mean telomere lengths than those of leukocytes extracted from the same patient. Given these findings, it could be argued that mean XpYp telomere length measurements in MGUS and MM patients reflect the tumour mass within the bone marrow. As the disease progresses and the plasma cell population increases, mean XpYp telomere length of the whole bone marrow aspirate would decrease. This would appear to concur with Cottliar et al. (2003), who demonstrated that the mean telomere length of MM patient whole bone marrow aspirates decreased as plasma cell infiltration increased.

Although an estimation of the percentage of plasma cells within the bone marrow is used during the diagnosis of MGUS and MM, it is not used to stage the disease (Rajkumar et

al. 2014; Palumbo et al. 2015). This is partially because quantifying plasma cell infiltration can be open to interpretation, reducing the accuracy of risk stratification (Al-Quran et al. 2007). Instead, clinical features such as serum β2 microglobulin concentration are used as a precise and consistent reflection of tumour mass (Greipp et al. 2005). However, the original ISS relies heavily on serum β2 microglobulin concentrations to stratify patients. Serum albumin concentrations are only considered when β2 microglobulin is <3.5g/dL, differentiating between ISS I and certain ISS II patients. The remaining intermediate- and high-risk patients are stratified based solely on whether β2 microglobulin is >3.5g/dL or >5.5g/dL. The next step was therefore to identify whether telomere length measurements held significant prognostic value with regard to MM, as well as to explore whether mean telomere length measurements might refine the staging criteria of the ISS.

3.5.2 Telomere Length as a Prognostic Indicator in MM

Taken as isolated prognostic factors, the mean XpYp telomere length threshold of 3.92kb was found to be one of the most significant methods used to stratify our MM cohort. Only serum β2 microglobulin concentrations held greater prognostic value. Although not as significant as measuring mean XpYp telomere length, serum albumin (</>3.5g/dL) and haemoglobin (</>10g/dL) concentrations also held prognostic value. In line with the current literature, age (</>65 years) was shown to be a significant prognostic indicator, while gender was not (Kim et al. 2010; Palumbo et al. 2015).

However, calcium concentration was found to hold little significance when used to stratify our MM cohort. This is not a view shared by other studies, whereby a serum calcium concentration >10mg/dL led to a poorer patient outcome (Kim et al. 2010; Greipp et al. 2005). Although we also demonstrated that a higher serum calcium concentration resulted in a poorer patient outcome, this was not shown to be a significant result. One possible explanation for this discrepancy could be that the patient numbers used in our

study were too low. While we had access to the serum calcium concentrations and survival data of 115 MM patients, Kim et al. (2010) and Greipp et al. (2005) had access to 372 and 10,750 patients respectively.

Regardless, including the 3.92kb mean XpYp telomere length threshold within the ISS significantly increased prognostic resolution when compared to serum β2 microglobulin concentrations alone. It could be argued that a limitation of this study was the lack of data regarding patient serum albumin concentrations, thus requiring ISS I and ISS II patients to be combined. However, albumin is only necessary to stratify low- and intermediate-risk MM patients. There is little need to develop a new staging criteria for these patients when albumin concentrations already suffice. Our focus was therefore on increasing the prognostic resolution of those intermediate- and high-risk patients for which β2 microglobulin concentrations are the only staging criteria.

In this sense, we were successful in further risk-stratifying the ISS III patient cohort. We therefore suggest that the stratification of patients based on tumour burden alone, as measured by serum β2 microglobulin concentration, is insufficient as it fails to account for highly aggressive and genetically unstable tumour subtypes. Telomere length measurements may not only reflect the tumour mass within the bone marrow, but might also account for those plasma cell populations that have short dysfunctional telomeres and may be more prone to fusion and genomic rearrangement (Capper et al. 2007). Furthermore, the ability of telomere length measurements to sub-stratify ISS I/II patients calls into question the value of measuring serum albumin concentrations. Further work needs to focus on identifying whether telomere length measurements could replace albumin in the ISS, or whether telomere length measurements should be used alongside serum β2 microglobulin and albumin concentrations to develop a four-stage ISS.

However, it is also worth noting that the ISS has recently been updated to include the presence of genetic abnormalities and serum lactate dehydrogenase (LDH) concentrations. Known as the revised ISS, patients can be classified as high-risk if del(17p), t(4;14) or t(14;16) abnormalities are detected within the plasma cells. Unfortunately, this data was not available for our cohort and so we were unable to incorporate telomere length measurements into this updated staging system. Future work may therefore require a new MM cohort to be establish for which genetic information is known. This would allow the prognostic value of telomere length measurements to be examined within the context of the revised ISS.

In any case, the identification of a 3.92kb prognostic threshold in MM was striking due to its proximity to the 3.81kb fusogenic threshold identified in CLL. Hazard ratios for the 3.92kb and 3.81kb telomere length thresholds in MM were 3.6 and 3.4 respectively, with this similarity likely caused by a difference of only four patients. Lin et al. (2014) observed that chromosomal end-end fusion could only be detected in the isolated B-cells cells of CLL patients when mean XpYp telomere length fell below 3.81kb. This genomic instability was thought to be driven by critically shortened telomeres, leading to a reduction in patient overall survival and accounting for the prognostic value of this 3.81kb threshold. It could therefore be suggested that the prognostic value of the 3.92kb threshold in MM may have also been due to genomic instability. This would most likely be driven by the shorter mean XpYp telomere lengths of the $CD138^{+}$ plasma cell populations within the bone marrow.

However, 3.81kb was not the most significant prognostic threshold identified in CLL. This was 2.26kb, defined as the median XpYp telomere length of those patients whose isolated B-cells showed evidence of chromosomal end-end fusion. Again, critically shortened telomeres were thought to be the cause of this genomic instability, resulting in the prognostic significance of the threshold (Lin et al. 2014). Unfortunately, this 2.26kb

threshold could not be used to stratify our MM cohort as only four patients had a mean XpYp telomere length below 2.26kb. This difference was thought to be due to cell types used in each study, with Lin et al. (2014) analysing the mean telomere length of CD19-sorted B-cells and our study analysing the mean telomere length of unsorted bone marrow. For this reason, we next sought to examine the mean XpYp telomere lengths of isolated $CD138^+$ plasma cells in relation to a 2.26kb threshold.

As described earlier, $CD138^+$ plasma cells were shown to be the source of telomeric shortening in the whole bone marrow aspirates of three MM patients. The average XpYp telomere length in the case of these three patients was 2.40kb, only marginally longer than the 2.26kb median fusogenic threshold identified in CLL (Lin et al. 2014). This begs the question of whether the prognostic significance of XpYp telomere length measurements in MM could be improved by first isolating $CD138^+$ cells from the whole bone marrow aspirate. This method could potentially be used to recognise high-risk patients whose $CD138^+$ cells contain shorter fusion-prone telomeres, even when plasma cell infiltration within the bone marrow is low.

3.5.3 Chromosomal Fusion in MM

Lin et al. (2014) observed that chromosomal end-end fusion events could only be detected in the isolated B-cells of CLL patients when mean XpYp telomere length fell below 3.81kb. Not only did a significant number of MM patients within our cohort have a mean XpYp telomere length below this threshold, but these patients were also shown to have a poorer outcome. We therefore attempted to detect chromosomal end-end fusion events in the whole bone marrow aspirates of sixteen MM patients, before trying to establish whether the extent of genomic instability correlated with telomere length. It was expected that, as genomic instability was closely linked to mean telomere length and patient outcome in CLL, a similar relationship may exist in MM.

Of the sixteen MM patients analysed, each showed evidence of chromosomal end-end fusion. We then sequenced three of these fusions to demonstrate that they were legitimate events. Telomeres at five of the chromosomal ends involved had been completely lost, either due to erosion during cell division or deletion during breakage-fusion-bridge cycles. This was consistent with the results of Capper et al. (2007) who had attempted to define the critical telomere length at which fusion occurred in MRC5 cells. After sequencing seventy-nine chromosomal end-end fusion events, they determined that 47% contained no TTAGGG repeats immediately adjacent to the fusion site. It was also observed that each fusion event analysed involved the deletion of one or both telomeres from the chromosomal ends involved, again consistent with our results.

Although one of the fusion events isolated from our 16-patient MM cohort had fifty-seven telomeric repeats at the fusion site, those repeats immediately adjacent to the fusion site were telomere variant repeats. It is known that these non-TTAGGG sequences do not confer telomeric function, offering an explanation as to why telomeric sequence was present within the fusion (Baumann and Cech 2001; Conomos et al. 2012). However, the telomere does not need to have been completely eroded at both chromosomal ends for fusion to occur. Capper et al. (2007) detected fusion events that contained up to 12.8 TTAGGG repeats immediately adjacent to the fusion site, concluding that fusion events involving >13 TTAGGG repeats were rare and offering a definition of the critical telomere length necessary for fusion in human cells.

A microhomology of 8 nucleotides was also recorded at the fusion site in one of the MM fusion events that we had managed to sequence. This was much larger than the average microhomology (1.9 nucleotides) present within the fusion events of HCT116 cells (Jones et al. 2014). It was also larger than the maximum microhomology identified in HCT116 cells where the alt-NHEJ pathway had been disrupted (5 nucleotides), but not larger than the maximum microhomology identified when the c-NHEJ pathway had been disrupted

instead (10 nucleotides). This may suggest that the processing and repair of the telomere-deficient chromosomal ends involved in this MM fusion event was orchestrated by the alt-NHEJ pathway.

Although further work would be necessary to conclusively prove that this was the case, it would still be an important discovery as the alt-NHEJ pathway is known to be necessary for the escape of cells from a telomere-driven crisis (Jones et al. 2014). Not only would we be able to conclude that the bone marrow cells of MM patients show evidence of chromosomal end-end fusion, but we would also be able to state that this genetic instability was driven by the same pathway that enable cells to escape crisis. However, without sequencing a greater number of fusion events, it becomes impossible to make any convincing predictions about the nature of chromosomal fusion in MM.

3.5.4 The Relationship Between Telomere Length and Fusion Frequency

Having identified chromosomal end-end fusion events in each of the 16 whole bone marrow aspirates of MM patients, we next sought to compare the frequency of fusion observed to the mean XpYp telomere length of each patient. From this, we failed to demonstrate that any significant relationship existed. This was unsurprising given the relatively small size of the cohort, with this result likely being due to an insufficient number of patients studied. It was also possible that, because we were using whole bone marrow aspirates rather than isolated plasma cells, the presence of healthy marrow cells with longer telomeres was obscuring any potential relationship between the shortened telomeres of $CD138^+$ cells and genomic instability. As we had previously demonstrated that $CD138^+$ cells had a significantly shortened mean XpYp telomere length, relative to the remaining marrow cells, we used the mean of the 25^{th} percentile of telomere lengths as an estimation of plasma cell telomere length. However, comparing the 25^{th} percentile to the frequency of fusion observed also failed to expose any significant relationship.

However, comparing the standard deviation of each STELA profile to the frequency of chromosomal end-end fusion resulted in the identification of a significant relationship. It was thought that the standard deviation offered an estimation of the extent to which the telomere length of the plasma cell population differed from that of the remaining marrow cells. As the population of abnormal plasma cells within the bone marrow increases, the frequency of critically shortened telomeres within the STELA profile would also increase. This would increase the standard deviation of the profile and would also lead to a greater frequency of chromosomal end-end fusion events. Although a significant relationship was identified, this result carried a number of caveats that need to be carefully considered.

As we had attempted to identify chromosomal end-end fusion events from the whole bone marrow aspirates of MM patients, we had no way of knowing if these events were observed in malignant plasma cells or normal marrow cells. All we could conclude was that the whole bone marrow aspirates of these 16 MM patients showed evidence of genomic instability, manifesting as chromosomal end-end fusion. Also, the standard deviation and 25th percentiles of each STELA profile may not accurately represent the difference between the telomere lengths of the plasma cell population and the remaining marrow cells. It was simply an estimation based on fact that the CD138^{+} cells of three MM patients were previously shown to have a significantly shorter mean telomere length than that of the remaining marrow cells.

This work should therefore form the basis for further experiments examining the relationship between telomere length and genomic instability in MM. Although we have demonstrated that chromosomal end-end fusion can be observed in the whole bone marrow aspirates of MM patients, future work should focus on repeating these experiments using isolated CD138^{+} cells. In this way, it would not only be possible to conclude that any fusion events recorded were from plasma cells only, but it would also

allow a direct comparison between plasma cells telomere length and the levels of genomic instability.

3.5.5 Conclusions

The aim of this chapter was to determine whether telomere length measurements held prognostic value within the context of MM. Using a cohort of 61 MGUS and 141 MM patients, we demonstrated that a shorter mean XpYp telomere length was associated with a more advanced disease stage. We then identified a 3.92kb telomere length threshold which held the greatest prognostic significance when used to stratify our cohort of MM patients, almost identical to the 3.81kb fusogenic threshold identified in CLL. Inclusion of this 3.92kb threshold within the ISS criteria allowed each prognostic subset to be further risk-stratified. Further work should now focus on determining whether telomere length measurements could be used in place of serum albumin concentrations, or whether they could be used in conjunction with albumin data to develop a four-stage ISS. Work should also be carried out to determine whether first isolating $CD138^+$ plasma cells from the whole bone marrow aspirate would further improve the prognostic value of telomere length measurements in MM.

We also aimed to determine whether chromosomal end-end fusion could be detected within the whole bone marrow aspirates of MM patients, and whether a relationship existed between this genomic instability and telomere length. Although fusion events were recorded in each of the 16 MM patients analysed, we could not conclude that the frequency of fusion correlated with mean XpYp telomere length. However, we could demonstrate that a significant relationship existed between the standard deviation of the STELA profile and the frequency of fusion. Future work should focus on the detection of chromosomal end-end fusion events from isolated $CD138^+$ plasma cells. The relationship between mean telomere length and the frequency of fusion should then be

examined. This would determine whether the shortened telomeres of $CD138^+$ plasma cells are the source of genomic instability in MM.

Chapter 4

The Role of a Telomere-Driven Crisis in Generating Chromosomal Instability in Multiple Myeloma

4.1 Abstract

Chromosomal abnormalities are a common feature of multiple myeloma (MM), with the presence of del(17p), t(4;14) or t(14;16) now being used as prognostic indicators (Palumbo et al. 2015). Although the cause of this genetic instability has yet to be fully elucidated, previous studies of another B-cell neoplasm, chronic lymphocytic leukaemia, have demonstrated that a shorter mean XpYp telomere length is closely linked to a greater frequency of chromosomal end-end fusion (Lin et al. 2010). Here, we have used DN-hTERT expression to significantly reduce the telomerase activity in three MM cell lines as a method of examining the telomere dynamics of these cells as they enter a telomere-driven crisis. As each cell line had a different p53 expression profile (Hurt et al. 2006; Surget et al. 2014; Landau et al. 2012), it was also possible to analyse their response to critical telomere shortening in the context of a compromised tumour suppressive pathway.

Each cell line behaved differently when faced with a significant reduction in telomerase activity. The JJN-3 cell line ($p53^{neg}$) exhibited telomere erosion and entered a telomere-driven crisis, but was capable of escaping crisis. This escape was marked by the recovery of growth and viability within the JJN-3 population, as well as an increased mean XpYp telomere length. The NCI-H929 cell line ($p53^{wt}$) also underwent crisis after mean XpYp telomere length fell from 1.32kb to 1.00kb, but this cell line was not capable of escaping. While a reduced telomerase activity had little effect on either the mean XpYp telomere length or viability of the U266B1 cell line ($p53^{mut}$).

The ability of the JJN-3 cells to avoid senescence was probed further, with three clonal populations of DN-hTERT cells being monitored during a telomere-driven crisis. Before crisis, it was observed that a reduction in telomerase activity caused mean XpYp telomere length to fall as low as 0.76kb. During this period, the frequency of observable chromosomal fusion events increased in line with telomere shortening. After crisis, telomerase activity was shown to be significantly increased. This was followed by a gradual increase in mean XpYp telomere length, as well as a decrease in the frequency of fusion events recorded. We therefore argue that critical telomere shortening, especially in cells with damaged tumour suppressive pathways, increases the risk of chromosomal end-end fusion. This may result in genomic instability which is thought to drive the progression of multiple myeloma.

4.2 Introduction

Replicative senescence is a process by which cells lose the ability to divide, but remain viable and metabolically active. This phenomenon is primarily regulated by telomeres, with telomere length acting to limit the replicative capacity of normal cells (Munoz-Espin and Serrano 2014). Telomere erosion is considered to act as a tumour suppressive mechanism, limiting the growth capacity of cells which have acquired genetic abnormalities (Campisi 2001). When a telomere becomes critically shortened in a normal cell, a DNA damage response is initiated. This results in a G1/S cell-cycle arrest which is established primarily via the TP53 tumour suppressive pathway (Campisi and d'Adda di Fagagna 2007). However, TP53 abnormalities are common in haematological malignancies, occurring in approximately 14% of acute myeloid leukaemia (AML), 13% of chronic lymphocytic leukaemia (CLL) and 13% of multiple myeloma (MM) patients (Haferlach et al. 2008; Dicker et al. 2009; Chng et al. 2007). Without functional TP53, cells may continue to divide beyond their Hayflick limit (Chin et al. 1999).

As well as limiting the replicative potential of a cell, telomeres also act to prevent the ends of chromosomes from being recognised as a double-strand DNA break (Doksani and de Lange 2014). If a telomere erodes completely, and the cell is unable to trigger senescence due to abnormalities within the DNA damage signalling pathways, then this chromosomal end may be subject to fusion with other unprotected chromosomal ends. The result is a dicentric chromosome, an inherently unstable structure which may undergo breakage-fusion-bridge cycles. Aneuploidy, loss of heterozygosity, chromosomal translocation and gene amplification can follow, acting as drivers of cancer progression. This state of widespread genomic instability and rearrangement is known as a telomere-driven crisis (Maciejowski and de Lange 2017).

It is possible for a cell to escape from crisis by reactivating telomerase, leading to the survival and proliferation of a clonal cancer cell with a significantly rearranged genome.

This ability is dependent on intrachromosomal fusion events which are products of the alternative nonhomologous end-joining (alt-NHEJ) pathway (Jones et al. 2014). Sister chromatid fusion is thought to be responsible for the amplification or deletion of specific chromosomal arms that typifies almost every type of cancer. Interchromosomal fusion events, products of the classical nonhomologous end-joining (C-NHEJ) pathway, are also frequent but are not sufficient to trigger an escape from a telomere driven crisis (Jones et al. 2014). Chromosomal abnormalities and rearrangements are a common feature of MM, with specific types now being used as prognostic indicators. The revised international staging system for MM lists the presence of del(17p), t(4;14) or t(14;16) abnormalities as indicators of high risk disease (Palumbo et al. 2015). The deletion of the 17p chromosomal end is particularly striking given the presence of the TP53 gene on this arm, the loss of which could prevent the activation of a DNA damage response after critical telomere shortening (Lode et al. 2010).

However, a mechanistic link between telomere dysfunction and genomic instability has yet to be established in MM. Evidence for this relationship already exists in CLL (Lin et al. 2010) and colorectal cancer (Roger et al. 2013), with shorter mean telomere length being associated with an increased frequency of chromosomal end-end fusion and large-scale genetic rearrangement. As the previous chapter demonstrated that high-risk MM patients are more likely to have a mean XpYp telomere length below 3.92kb, we next examined the hypothesis that critical telomere shortening in MM may result in the genomic instability which drives cancer progression.

To do this, we used a dominant-negative form of the human TERT subunit (DN-hTERT) that effectively abrogates telomerase activity, resulting in telomeric erosion, as a consequence of cell division, and the eventual onset of a telomere-driven crisis. The influence of TP53 on this process was examined by utilising MM cell lines that varied in their p53 expression, allowing the response of the JJN-3 cell line ($p53^{neg}$) to be assessed

alongside the NCI-H929 ($p53^{wt}$) and U266B1 ($p53^{mut}$) cell lines. From this, we demonstrated that critical telomeric shortening resulted in the initiation of a telomere-driven crisis, with only the JJN-3 cell line showing evidence of being able to escape. It was also observed, using clonal populations of JJN-3 cells, that the frequency of inter- and intrachromosomal fusion events directly correlated with telomere length.

4.3 Aims of the Chapter

We hypothesised that a causal relationship existed in MM between telomere length, the frequency of chromosomal fusion events and the onset of crisis. In this chapter, we aimed to determine whether p53 expression was necessary for the escape of cells from a telomere-driven crisis in MM. We then examined the idea that critically shortened telomeres in a $p53^{neg}$ MM cell line can result in an increased frequency of chromosomal end-end fusion and the escape of cells from crisis.

4.4 Results

4.4.1 Characteristics of the Four Myeloma Cell Lines

The MM cell lines JJN-3, NCI-H929, RPMI-8226 and U266B1 were chosen due to their varying TP53 status. While JJN-3 cells do not express p53, NCI-H929 cells express a functional p53 protein that elicits a corresponding p21 response following DNA damage (Hurt et al. 2006; Surget et al. 2014). Having been exposed to radiation, both RPMI-8226 and U266B1 cells produce a mutated p53 protein. However, U266B1 cells remain capable of generating a p21 response (Landau et al. 2012). ***Table 4.1*** lists the characteristics of each cell line, along with information regarding their p53 status and cell surface marker expression.

4.4.2 Mean XpYp and 17p Telomere Length in Four Myeloma Cell Lines

As a method of observing any potential relationship between telomere length and the frequency of chromosomal end-end fusion events in MM, the mean length of the XpYp and 17p telomeres were calculated using STELA. Of the four MM cell lines, NCI-H929 and RPMI-8226 were identified as having the shortest mean XpYp telomere lengths at 1.66kb and 1.62kb respectively (***Figure 4.1a***). The mean XpYp telomere length of the JJN-3 cell line was shown to be longer at 3.05kb, but still shorter than that of the U266B1 cell line whose mean XpYp telomere length was calculated as 4.38kb. Standard deviation was used as a measurement of telomere length heterogeneity within each STELA profile, with smaller values indicating a more clonal population of cells. Standard deviation for the four cell lines varied greatly, with NCI-H929 and RPMI-8226 having homogeneous telomere length distributions (0.52kb and 0.42kb respectively) relative to the more heterogeneous telomere length distributions of JJN-3 and U266B1 (1.31kb and 2.83kb respectively).

	JJN-3	NCI-H929	RPMI-8226	U266B1
ORIGIN OF CELL LINE	Female 52 Years	Female 62 Years	Male 61 Years	Male 53 Years
DISEASE TYPE	Plasma Cell Leukaemia (evolved from MM)	Multiple Myeloma	Multiple Myeloma	Multiple Myeloma
ISOTYPE	IgA *k*	IgA *k*	IgG λ	IgE λ
CELL SURFACE MARKERS	CD138+ CD38+ CD19- CD56+ CD20-	CD138+ CD38+ CD19- CD56+ CD20-	CD138+ CD38+ CD19- CD56+ CD20-	CD138+ CD38+ CD19- CD56- CD20-
KARYOTYPE	Hypotriploid with 9% Polyploidy	Near-Tetraploid (8q+)	Hypotriploid with 7.5% Polyploidy	Unknown
TP53	Homozygous Deletion (Not Functional)	Wild Type (Functional)	Homozygous Mutation (Not Functional)	Homozygous Mutation (Functional)
POPULATION DOUBLING TIME	20-35 hours	~70 hours	~60-70 hours	~55 hours

Table 4.1: The Characteristics of the four MM cell lines (Gooding et al. 1999)

Measuring the mean 17p telomere length for the same four cell lines allowed comparisons to be drawn between the two telomere ends (***Figure 4.1b***). At 2.99kb, the mean 17p telomere length of the JJN-3 cell line was almost identical to that of the mean XpYp telomere length of 3.05kb. Standard deviation at the 17p telomere end, calculated as 1.51kb, was similar to that observed at the XpYp telomere (1.31kb).

However, mean XpYp and 17p telomere length measurements varied greatly within the NCI-H929 cell line. Compared to the mean length of the XpYp telomere end (1.66kb) and homogeneous telomere length distribution (standard deviation 0.52kb), the mean length of the 17p telomere end was much longer (2.84kb) and showed greater heterogeneity (standard deviation 1.66kb). A multimodal distribution within the 17p telomere profile was also identified and may go towards explaining this difference. Multimodal distributions can reflect the presence of allelic variation in telomere length, clonal heterogeneity or the presence of additional copies of the telomere analysed. In this case, gain of 17p has not been identified in the NCI-H929 cell line. However, populations of these cells are known to be comprised of two subpopulations; $CD138^{++}$ (95%) and $CD138^{low}$ (5%) (Paino et al. 2014). While this might suggest that the multimodal distribution observed is due to clonal heterogeneity, rather than the presence of an additional 17p telomere, it is also impossible to rule out allelic variation as a cause without knowing the exact subtelomeric sequence of each individual chromosome.

Like the JJN-3 cell line, the RPMI-8226 cell line also showed little difference between the mean telomere length at the XpYp and 17p telomere ends (1.62kb and 1.63kb respectively). However, standard deviation at the 17p telomere end (1.59kb) was significantly increased when compared to the XpYp telomere end (0.42kb). This is likely due to the presence of a small number of 17p telomere ends in the region of 8.7kb – 14.7kb whose presence acted to skew the standard deviation.

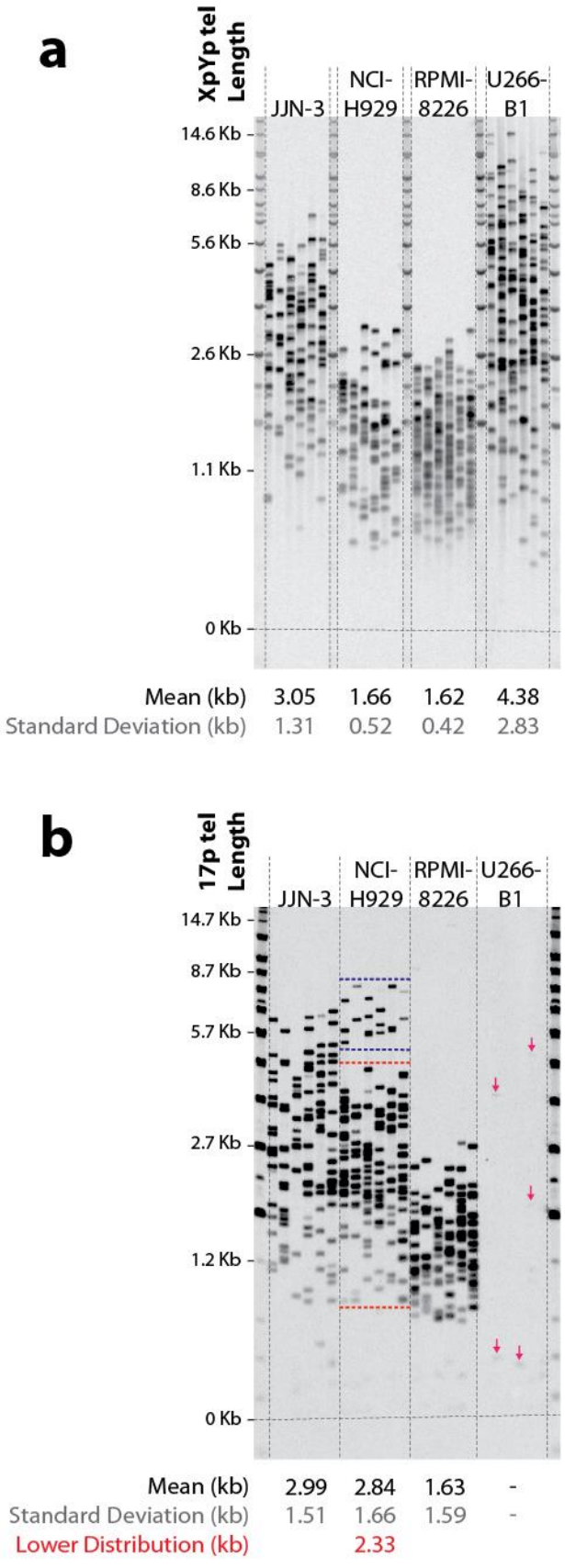

Figure 4.1 - XpYp and 17p Telomere Lengths in Four Myeloma Cell Lines.
(a) STELA profile showing the XpYp telomere lengths for the myeloma cell lines JJN-3, NCI-H929, RPMI-8226 and U266B1. **(b)** STELA profile showing the 17p telomere lengths for the myeloma cell lines JJN-3, NCI-H929, RPMI-8226 and U266B1. The two distinct telomere length distributions within the NCI-H929 cell line have been highlighted in red (lower distribution) and blue (upper distribution). The small number of bands within the U266B1 profile have been highlighted.

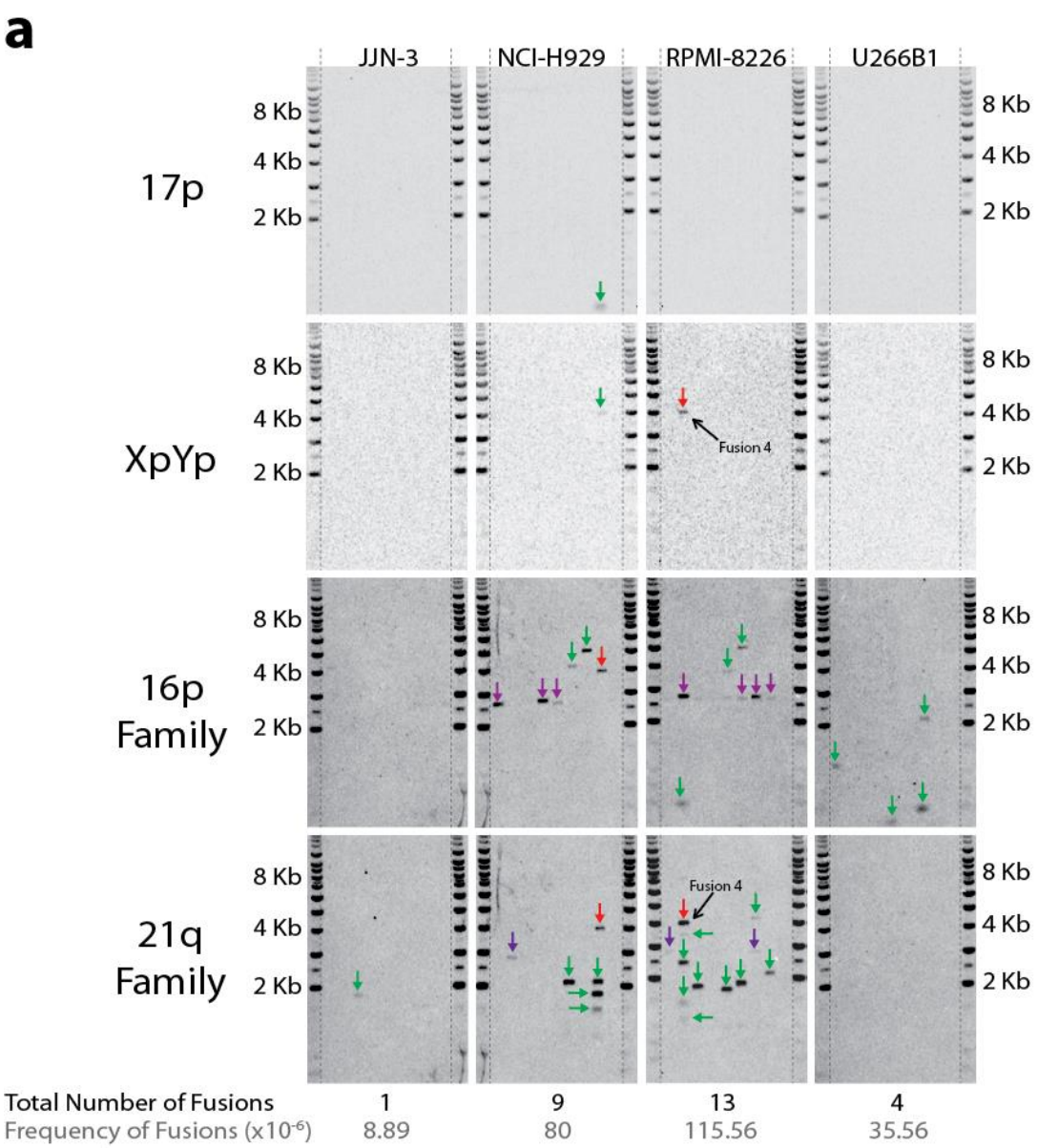

Figure 4.2 - The Frequency of Telomeric Fusion in Four Myeloma Cell Lines.
(a) The JJN-3, NCI-H929, RPMI-8226 and U266B1 myeloma cell lines were examined for the presence of chromosomal fusion events. In total, 675ng of DNA was examined per cell line (75ng per reaction). The frequency of chromosomal fusion was estimated by dividing the number of observable fusion bands by the number of input molecules (around 112,500 cells). Bands representing possible intrachromosomal fusion events were highlighted in green, while interchromosomal fusion events were highlighted in red. Interchromosomal bands were identifed by the presence of two corresponding bands at the same position on two different membranes. Purple arrows were used to highlight bands that were located in areas known for backgrounds bands (these are of a constant size and were not included in the final analysis). **(b)** An example of a 21q-XpYp chromosomal fusion event, identified from the RPMI-8226 cell line. The number of bases that have been deleted from the start of the telomere repeat array (or the number of telomere repeats remaining) has been listed. Any microhomology between the chromosome ends has been highlighted in blue.

It was not possible to calculate a mean 17p telomere length for the U266B1 cell line due to the limited number of bands present within the STELA profile. This could either be due to the loss of the 17p chromosomal arm, or complete erosion of the 17p telomere. Either case would inhibit STELA by preventing the telorette primer from binding at the end of the 17p chromosomal arm. However, it should be noted that the U266B1 17p STELA profile was not completely blank. It contained a small number of bands which were each of varying size.

4.4.3 The Frequency of Chromosomal Fusion in Four Myeloma Cell Lines

Chromosomal fusion events were identified in the four MM cell lines using a single-molecule telomere fusion assay with primers 17p6, XpYpM, 16p1 and 21q1. It is important to note that, while the 17p6 and XpYpM primers were specific to their respective chromosomal ends, the 16p1 and 21q1 primers recognise several chromosomal ends; the 16p1 family primer binds at 16p, 1p, 9p, 12p, 15q, XqYq and the 2q14 interstitial locus, while the 21q1 family primer binds at 21q, 1q, 2q, 5q, 6q, 6p, 8p, 10q, 13q, 17q, 19p, 19q, 22q and the 2q13 interstitial telomeric locus.

Although chromosomal fusion events were identified in each of the four myeloma cell lines (***Figure 4.2a***), the greatest frequency of fusion events were found within the RPMI-8226 cell line (frequency of fusion = 115.56×10^{-6} events per cell). A significant number of fusion events were also isolated from the NCI-H929 cell line (frequency of fusion = 80×10^{-6}/cell). However, the U266B1 (frequency of fusion = 35.56×10^{-6}/cell) and JJN-3 (frequency of fusion = 8.89×10^{-6}/cell) cell lines showed relatively few chromosomal fusion events.

The true significance of this finding does not become apparent until the frequency of chromosomal fusion is viewed within the context of mean telomere length (***Figure 4.3a and 4.3b***). The cell lines with the shortest mean XpYp telomere lengths, NCI-H929 and

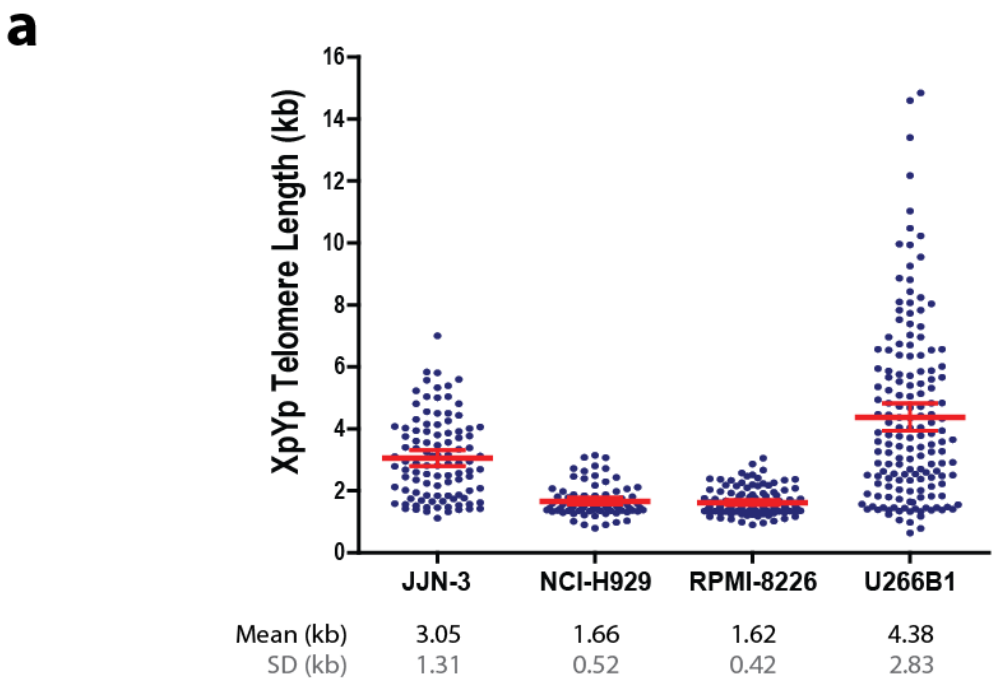

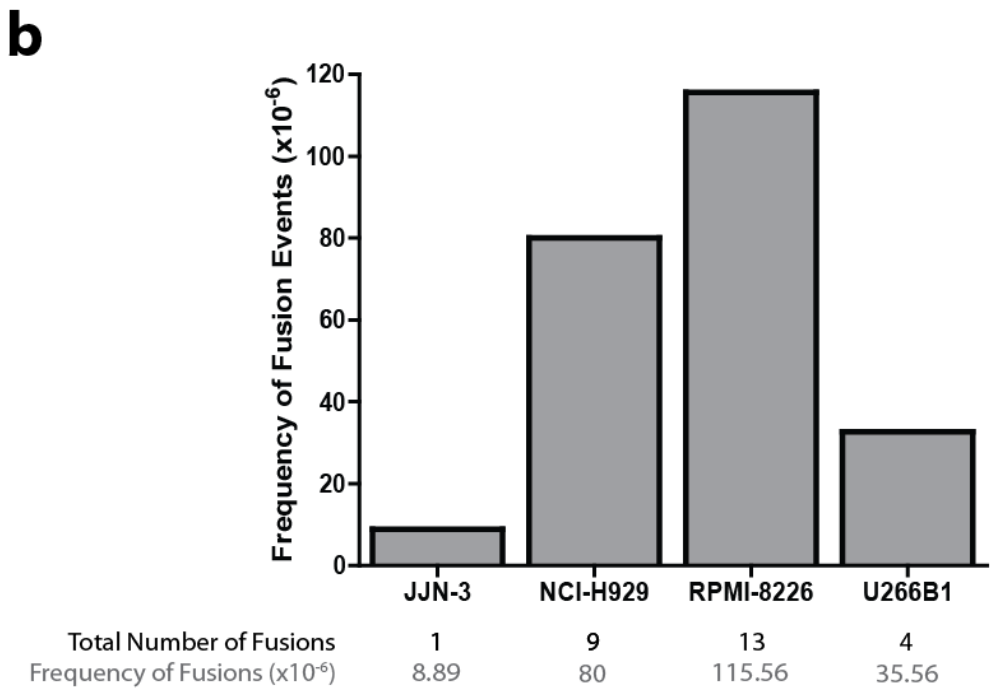

Figure 4.3 - The Relationship Between Telomere Length and the Frequency of Chromosomal Fusion Events in Four Myeloma Cell Lines.
(a) Graphical representation of the XpYp STELA profiles for the myeloma cell lines JJN-3, NCI-H929, RPMI-8226 and U266B1. The mean telomere length for each cell line is shown in red alongside the upper and lower 95% confidence intervals. **(b)** Graph showing the total number of fusions and the total frequency of fusions for each of the four myeloma cell lines. The frequency of chromosomal fusion was estimated by dividing the number of observable fusion bands by the number of input molecules (around 112,500 cells).

RPMI-8226, also had the greatest number of identified chromosomal fusion events. JJN-3 and U266B1, each with a considerably longer mean XpYp telomere length, exhibited fewer detectable chromosomal fusion events.

4.4.4 A Telomere-Driven Crisis in the JJN-3 Cell Line

As the telomere length of the JJN-3, NCI-H929 and U266B1 cell lines are maintained by telomerase activity, we aimed to force these cells into a state of telomere-driven crisis by disrupting this enzyme via the incorporation of a dominant-negative (DN) TERT subunit. DN-hTERT competitively inhibits the binding of wild-type TERT to the TERC subunit (Rahman, Mo, and Cui 2006). It also forms dimers with wild-type TERT which are then actively degraded in the cytoplasm (Nguyen, Elmore, and Holt 2009). The gene encoding the DN-hTERT subunit was packaged within a pBABE-puro retroviral vector and was delivered into the cells using viral transduction. The control cells were generated expressing only the pBABE-puro vector, thus conferring a level of resistance to the antibiotic puromycin without the associated disruption to telomerase activity.

After transfecting a population of JJN-3 cells (day 0) with either the DN-hTERT construct or the empty pBABE-puro vector as a control, puromycin was used to select for those cells (day 10) which had successfully incorporated the vector. During the 51 days following transduction, cell growth was monitored in each population, as well as in an additional un-transfected control population of JJN-3 cells. After the addition of puromycin, the growth of each population initially stalled for a period between day 5 and day 15 (***Figure 4.4a***). However, by day 20 the growth of the DN-hTERT and puromycin-resistant control cells had returned to normal. Only the un-transfected JJN-3 control cells failed to continue growing once puromycin was introduced.

Cell viability was also monitored during this period using the Vi-Cell XR (Beckman Coulter) automated trypan blue dye-exclusion assay (F***igure 4.4b***). Initially the viability

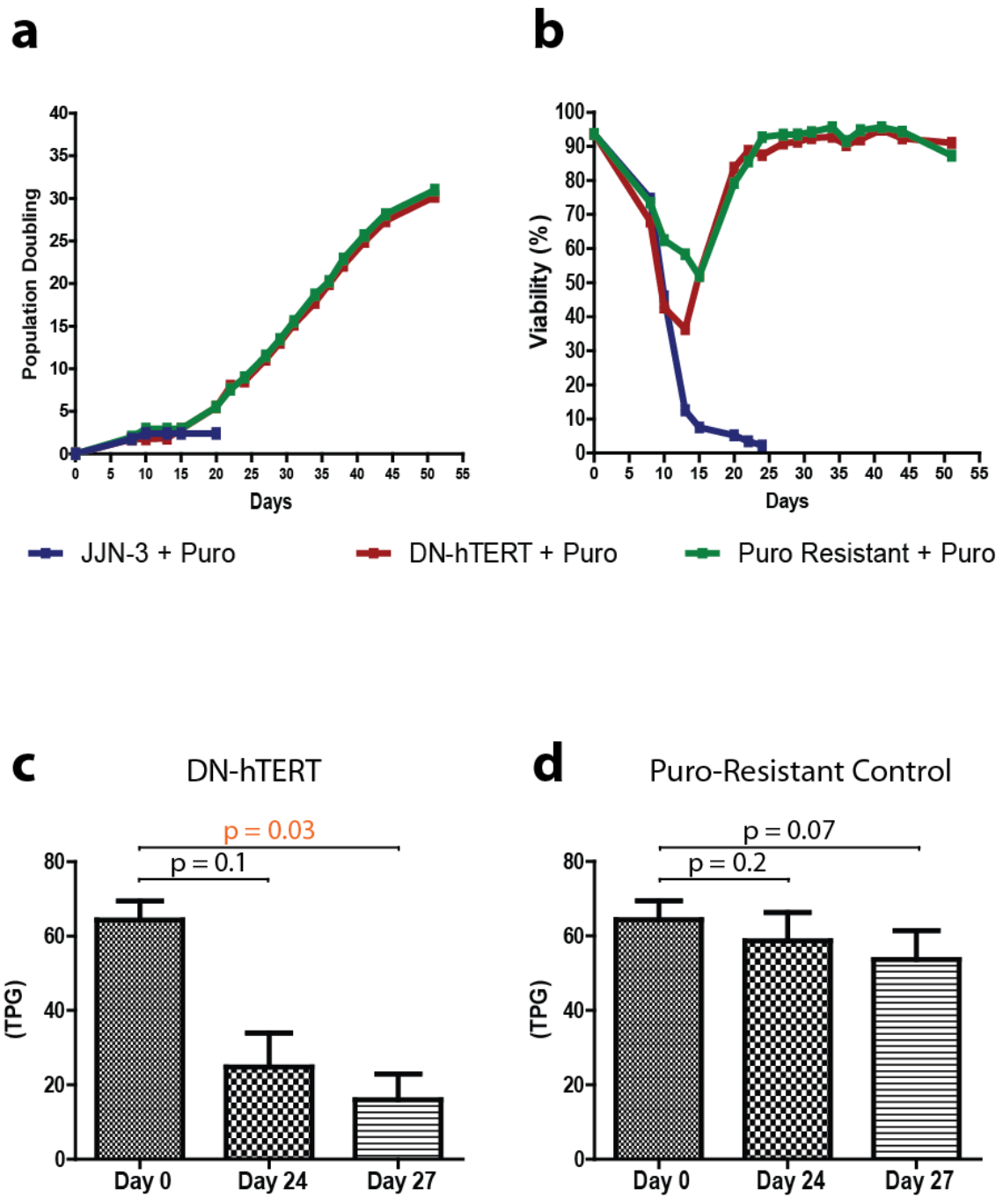

Figure 4.4 - Positive Selection of JJN-3 Cells Expressing DN-hTERT and the Resutling Telomerase Activity.

(a) Graph showing the number of population doublings undergone by each **DN-hTERT**, **puromycin-resistant control**, and **untransduced control** population of cells after transduction (day 0) and puromycin selection (**2µg/ml** - began on day 10). **(b)** Graph showing the viability of each population of cells during the period of transduction and puromycin selection. **(c) and (d)** Telomerase activity was measured at two different time points in both the JJN-3 DN-hTERT and JJN-3 Empty Vector populations. Total Product Generated (**TPG**) is a unit specific to the TRAPeze detection kit used to measure telomerase activity. Significance was determined using a paired t-test and defined as <0.05

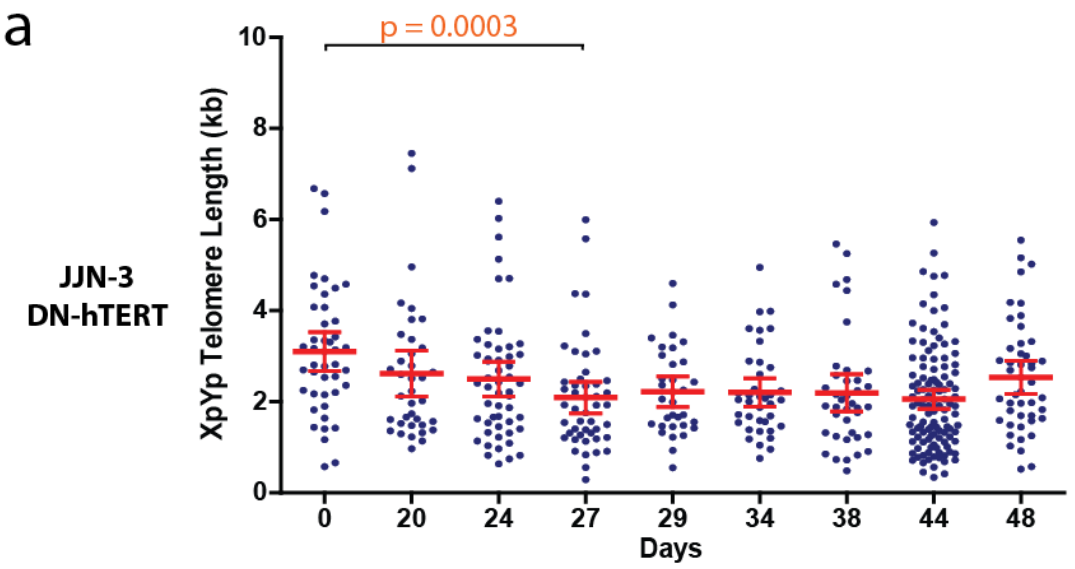

	0	20	24	27	29	34	38	44	48
Mean (kb)	3.10	2.61	2.49	2.09	2.22	2.19	2.19	2.05	2.53
Standard Deviation (kb)	1.41	1.50	1.36	1.19	0.95	0.96	1.25	1.14	1.22

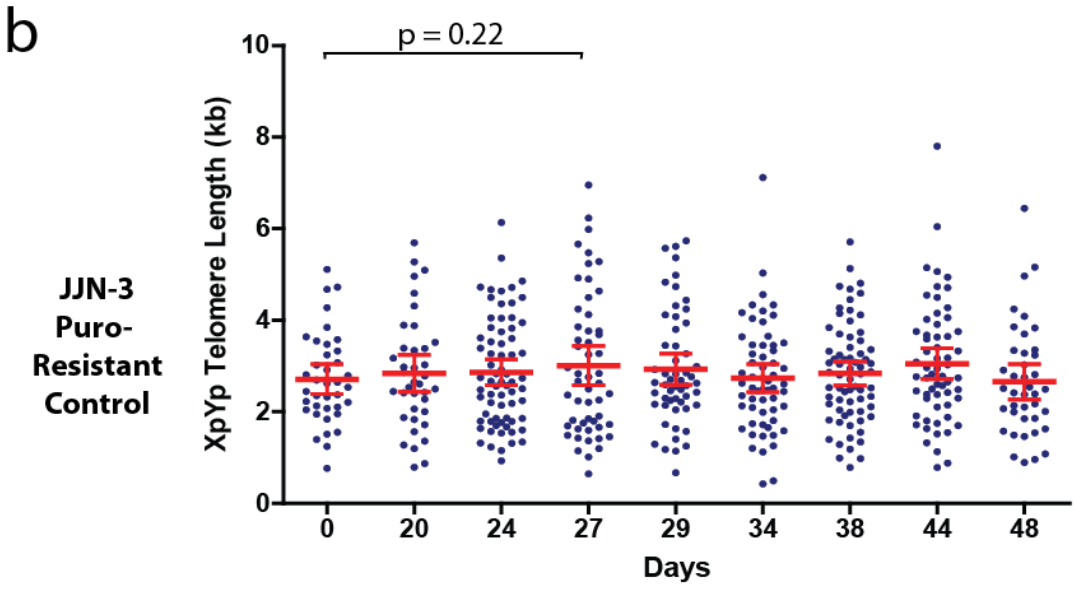

	0	20	24	27	29	34	38	44	48
Mean (kb)	2.71	2.84	2.87	3.01	2.93	2.74	2.84	3.05	2.66
Standard Deviation (kb)	0.99	1.22	1.18	1.55	1.24	1.17	1.08	1.30	1.21

Figure 4.5 - Telomere Length Measurments in a JJN-3 Cell Line which is Expressing a DN-hTERT Construct

JJN-3 cells which expressed a DN-hTERT protein were grown over a period of 51 days. During this period, samples of cells were taken and the DNA was extracted. STELA was used to measure the mean XpYp telomere length at each time point. **(a)** Graphical representation of the STELA profiles produced for JJN-3 cells which expressed DN-hTERT. **(b)** Graphical representation of the STELA profiles produced for JJN-3 cells which did not express DN-hTERT. The mean telomere length for each patient is shown in red alongside the upper and lower 95% confidance intervals. Significant was determined using a paired t-test and defined as being <0.05

of each population decreased, with the normal JJN-3 control cells finally reaching 2.2% viability by day 24. DN-hTERT cells reached a low of 36.4% viability by day 13, before recovering to 83.7% viability by day 20 and finishing with a viability of 91% by day 51. The viability of puromycin-resistant control cells also decreased, reaching a low of 51.9% at day 15 before recovering to 83.7% by day 20 and finishing with a viability of 87.3%.

Telomerase activity was measured in DN-hTERT and puromycin-resistant control JJN-3 populations to determine whether the DN-hTERT construct was successfully reducing the activity of the telomerase enzyme (***Figures 4.4c and 4.4d***). On day 27, the total product generated (TPG) by telomerase enzymes isolated from DN-hTERT cells was significantly reduced when compared to day 0 ($p = 0.03$). This was in contrast to the puromycin-resistant control cells, where telomerase activity was not significantly reduced ($p = 0.07$) when compared to day 0.

To directly observe the effect of a reduced telomerase activity, telomere length was monitored using STELA of the XpYp telomere at 9 time points during the growth of the JJN-3 cells. Over a period of 27 days, mean XpYp telomere length was reduced from an initial 3.10kb to a low of 2.09kb in DN-hTERT JJN-3 cells ($p = 0.0003$; ***Figure 4.5a***). Although a lower mean telomere length of between 2.22kb and 2.19kb was maintained after this period, mean telomere length had eventually risen back to 2.53kb by day 48. In the puromycin-resistant control cells, mean XpYp telomere length initially rose from 2.71kb at day 0 to 3.01kb at day 27 ($p = 0.22$; ***Figure 4.5b***). A mean XpYp telomere length of between 3.05kb and 2.66kb was then maintained up until day 48.

In summary, forcing the expression of DN-hTERT in a population of JJN-3 cells significantly reduced telomerase activity. This resulted in telomeric erosion which eventually stabilised at around 2.20kb. The viability of the DN-hTERT population also decreased by a greater extent than the puromycin-resistant control population, which

may be indicative that the cells were forced into a telomere-driven crisis following the DN-hTERT-mediated reduction in telomerase activity. Eventually, viability recovered to around 90% and mean XpYp telomere length began to increase suggesting that the cells had escaped crisis.

4.4.5 A Telomere-Driven Crisis in the NCI-H929 Cell Line

Using the same technique as for JJN-3 cells, DN-hTERT was introduced into the NCI-H929 cell line (day 0) to disrupt telomerase activity and force the cells into a state of telomere-driven crisis. Until the addition of puromycin at day 4, the DN-hTERT and un-transfected control NCI-H929 populations continued to experience growth (***Figure 4.6a***). The control cells which expressed only the puromycin-resistance gene continued to grow until day 6. Between day 4 and day 8 in the DN-hTERT and un-transfected control NCI-H929 populations (day 6 and day 8 in the puromycin-resistant control population) cell growth appeared to stop and the number of population doublings recorded did not increase. Between day 8 and day 20, growth of the puromycin-resistant control cells returned to normal. However, neither the DN-hTERT or the un-transfected control NCI-H929 cells recovered and remained at 0.70 and 0.62 population doublings respectively until the experiment was ended.

Cell viability followed a similar pattern, with the puromycin-resistant control cells falling from 73.8% viability on day 0 to 37.7% viability by day 10 (***Figure 4.6b***). Between day 8 and day 20, cells recovered to 59.9% viability. Un-transfected NCI-H929 cells experienced a reduction in viability immediately after the addition of puromycin, falling to 11.7% viability between day 4 and day 8. This did not recover and the cells remained at around 9% viability up to day 20. DN-hTERT cells also experienced a loss of viability, although this occurred at day 6, slightly after the normal NCI-H929 cells. However, viability then continued to drop and did not recover. DN-hTERT cells reached a final viability of 7.8% by day 20. The telomerase activity assay for NCI-H929 cells at day 0

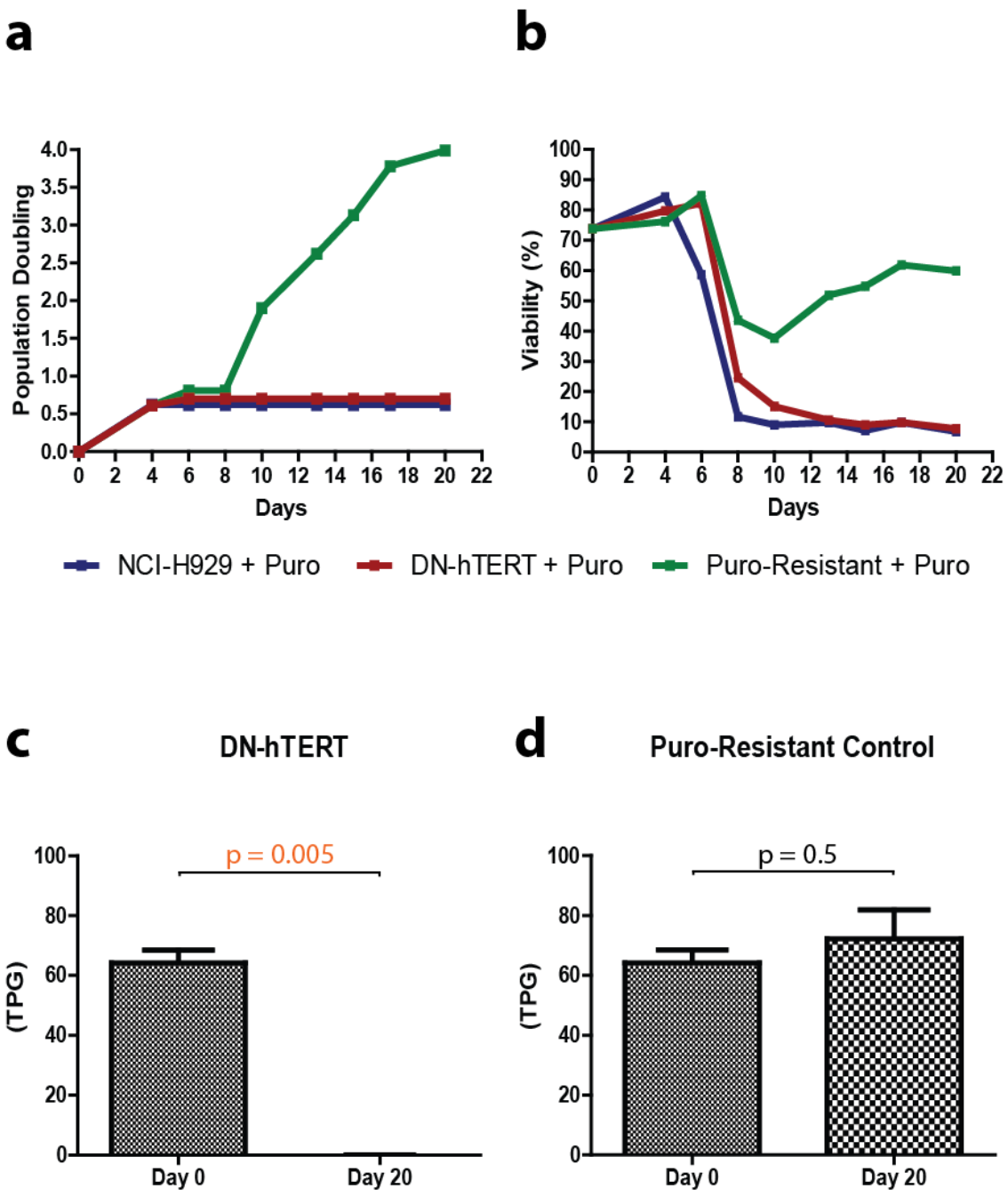

Figure 4.6 - Positive Selection of NCI-H929 Cells Expressing DN-hTERT and the Resutling Telomerase Activity.

(a) Graph showing the number of population doublings undergone by each **DN-hTERT**, **puromycin-resistant control**, and **untransduced control** population of cells after transduction (day 0) and puromycin selection (**0.5µg/ml** - began on day 4). **(b)** Graph showing the viability of each population of cells during the period of transduction and puromycin selection. **(c) and (d)** Telomerase activity was measured at two different time points in both the NCI-H929 DN-hTERT and NCI-H929 Empty Vector populations. Total Product Generated (**TPG**) is a unit specific to the TRAPeze detection kit used to measure telomerase activity. Significance was determined using a paired t-test and defined as <0.05

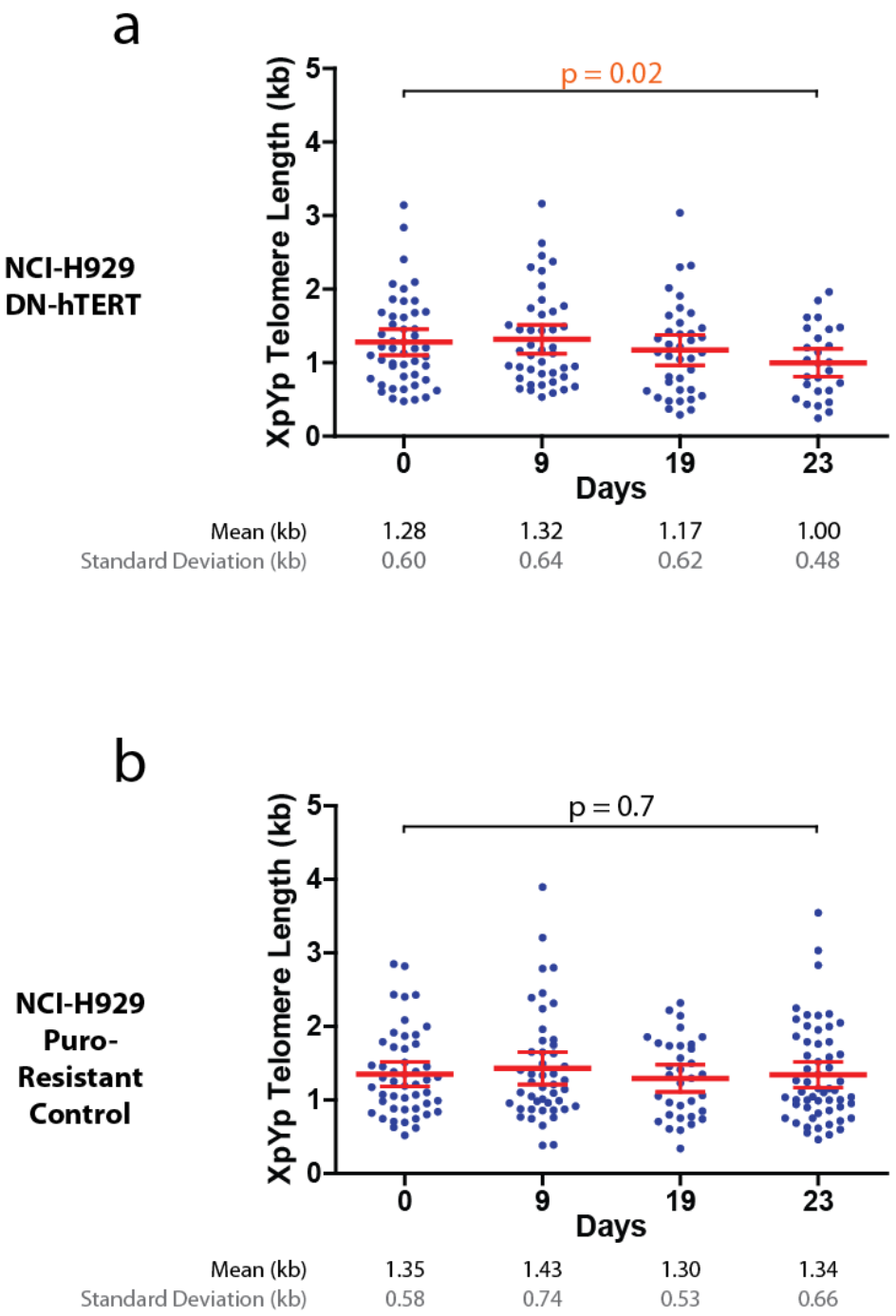

Figure 4.7 - Telomere Length Measurments in an NCI-H929 Cell Line which is Expressing a DN-hTERT Construct

NCI-H929 cells which expressed a DN-hTERT protein were grown over a period of 23 days. During this period, samples of cells were taken and the DNA was extracted. STELA was used to measure the mean XpYp telomere length at each time point. **(a)** Graphical representation of the STELA profiles produced for NCI-H929 cells which expressed DN-hTERT. **(b)** Graphical representation of the STELA profiles produced for NCI-H929 cells which did not express DN-hTERT. The mean telomere length for each patient is shown in red alongside the upper and lower 95% confidance interval. Significant was determined using a paired t-test and defined as being <0.05

showed that telomerase activity could be recorded as 64.23 TPG. In the DN-hTERT cells, this value dropped significantly (p = *0.005*) to almost 0 TPG at day 20 (***Figure 4.6c***) but increased to 72.31 TPG (p = *0.5*) in the puromycin-resistant control cells (***Figure 4.6d***).

STELA was performed to measure mean XpYp telomere length during the telomere-driven crisis in the populations of NCI-H929 cells. In the DN-hTERT cells, mean XpYp telomere length increased marginally between days 0 and 9 (***figure 4.7a***). By day 19, mean XpYp telomere length had decreased to 1.17kb and then again to 1.00kb by day 23 (*p = 0.02*). At this point, cell viability fell below 10% and the experiment was ended. In the puromycin-resistant control cells, mean XpYp telomere length remained constant and never fell below 1.30kb (*p = 0.7*; ***figure 4.7b***).

In summary, forcing the expression of DN-hTERT in a population of NCI-H929 cells significantly reduced telomerase activity. This resulted in telomeric erosion which caused the mean XpYp telomere length to fall to 1.00kb. Unlike the puromycin-resistant control population, the viability of the DN-hTERT population quickly fell below 10% and did not recover.

4.4.6 A Telomere-Driven Crisis in the U266B1 Cell Line

Cell growth in the un-transfected control U266B1, DN-hTERT and puromycin-resistant control populations continued at a steady rate until puromycin was added on day 5 (***Figure 4.8a***). At this point, the un-transfected control U266B1 cells failed to demonstrate any further growth. The puromycin-resistant control cells grew almost uninterrupted by the presence of puromycin until day 17. At this point, and again at day 24, cells experienced a period of stalled growth that was immediately corrected by the following time point. However, the overall trend between day 0 and day 54 was that of growth.

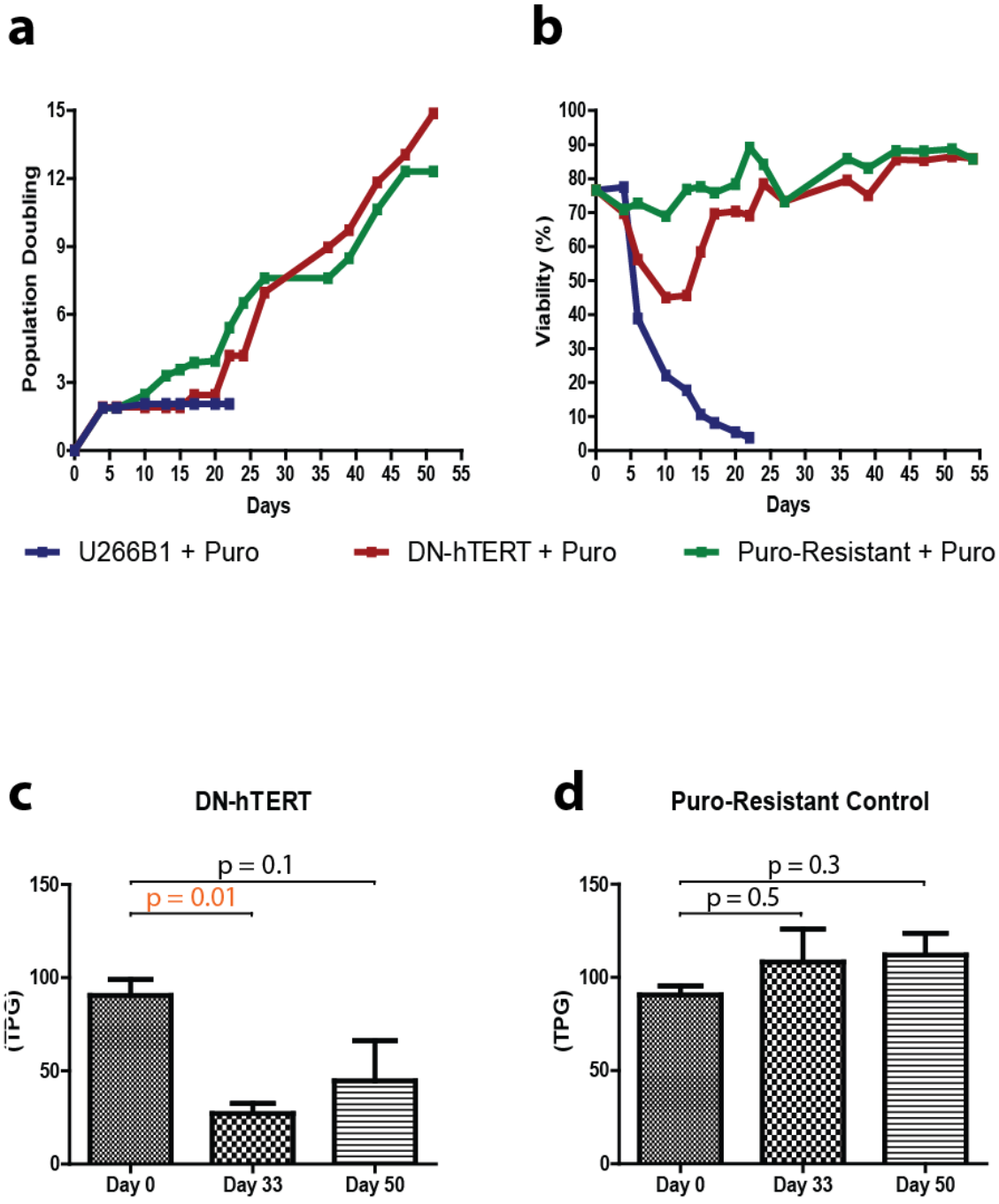

Figure 4.8 - Positive Selection of U266B1 Cells Expressing DN-hTERT and the Resutling Telomerase Activity

(a) Graph showing the number of population doublings undergone by each **DN-hTERT**, **puromycin-resistant control**, and **untransduced control** population of cells after transduction (day 0) and puromycin selection (**2µg/ml** - began on day 5). **(b)** Graph showing the viability of each population of cells during the period of transduction and puromycin selection. **(c) and (d)** Telomerase activity was measured at two different time points in both the U266B1 DN-hTERT and U266B1 Empty Vector populations. Total Product Generated (**TPG**) is a unit specific to the TRAPeze detection kit used to measure telomerase activity. Significance was determined using a paired t-test and defined as <0.05

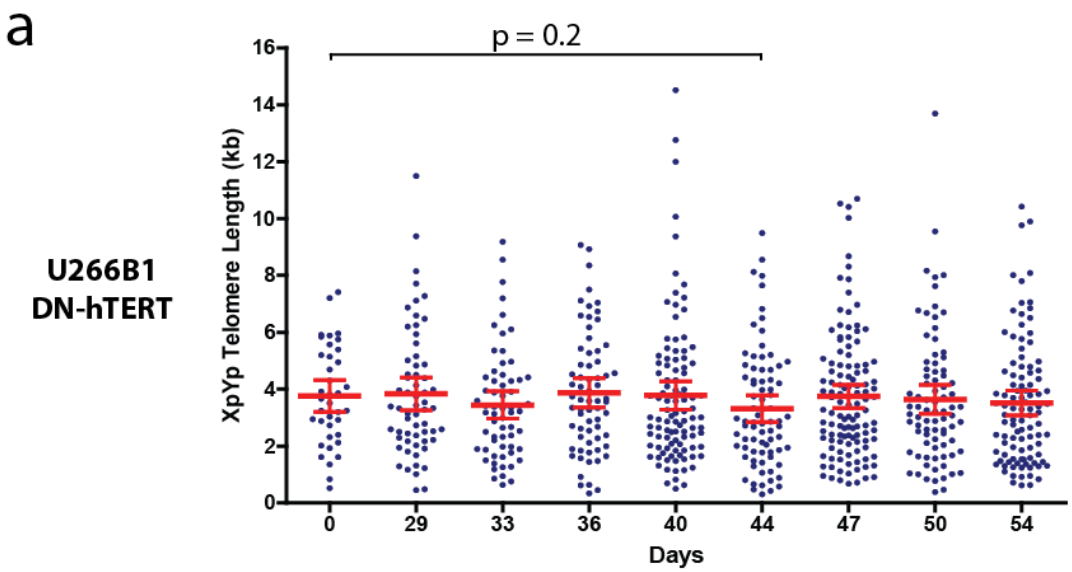

	0	29	33	36	40	44	47	50	54
Mean (kb)	3.76	3.84	3.44	3.87	3.78	3.32	3.75	3.64	3.51
Standard Deviation (kb)	1.72	2.24	1.92	2.10	2.54	2.07	2.22	2.31	2.19

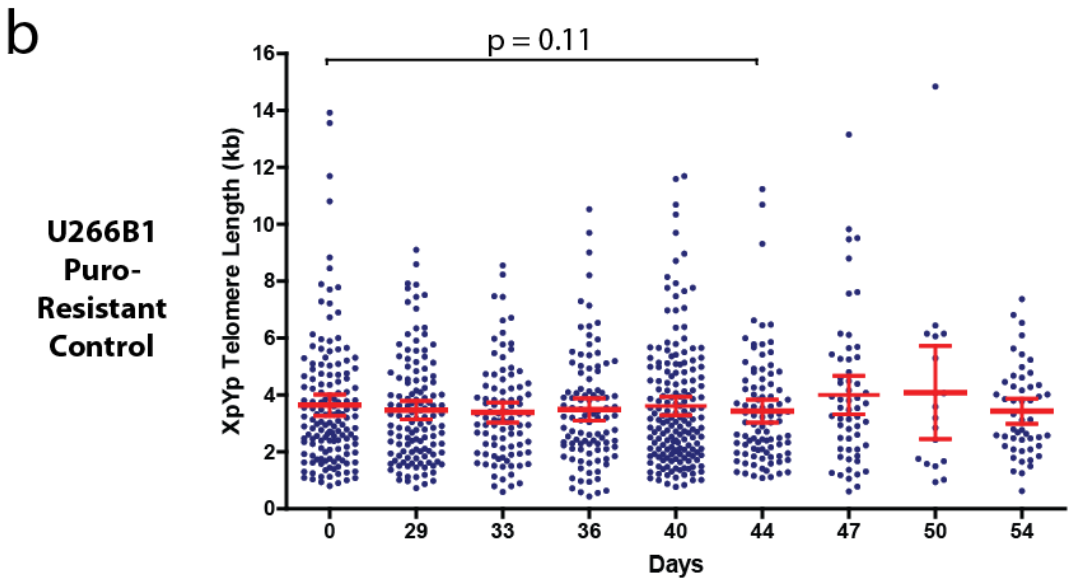

	0	29	33	36	40	44	47	50	54
Mean (kb)	3.65	3.47	3.39	3.49	3.61	3.43	4.00	4.09	3.43
Standard Deviation (kb)	2.29	1.85	1.71	1.97	2.18	1.94	2.56	3.29	1.55

Figure 4.9 - Telomere Length Measurments in a U266B1 Cell Line which is Expressing a DN-hTERT Construct

U266B1 cells which expressed a DN-hTERT protein were grown over a period of 54 days. During this period, samples of cells were taken and the DNA was extracted. STELA was used to measure the mean XpYp telomere length at each time point. **(a)** Graphical representation of the STELA profiles produced for U266B1 cells which expressed DN-hTERT. **(b)** Graphical representation of the STELA profiles produced for U266B1 cells which did not express DN-hTERT. These cells were used as a control due to their unaltered telomerase activity. The mean telomere length for each patient is shown in red alongside the upper and lower 95% confidance intervals. Significance was determined using a t-test and defined as being <0.05

The DN-hTERT cells experienced a period of stalled growth between day 4 and day 15, eventually returning to normal growth between day 17 and day 54.

The viability of un-transfected control U266B1 cells during this period decreased from 77.5% at day 4 to 10.6% by day 15 and did not recover (***Figure 4.8b***). The viability of the puromycin-resistant control cells fell from 76.6% to 68.9% between day 0 and day 10, but increased rapidly to 89.2% by day 22. Between day 24 and day 54, viability remained between 73.2% and 88.7%. The viability of the DN-hTERT population decreased from 76.6% at day 0 to 45.0% by day 10. At this point, the viability increased rapidly between days 13 and 17. Between days 20 and 54, viability remained between 70.4% to 85.9%.

Telomerase activity was measured at three time points in both the DN-hTERT and puromycin-resistant control populations. In the DN-hTERT cells, telomerase activity decreased from 90.53 TPG at day 0 to 27.18 TPG at day 33 ($p = 0.01$) but this increased to 44.65 TPG by day 50 and was no longer significantly different from day 0 ($p = 0.1$). In the puromycin-resistant control population, telomerase activity increased between day 0 (90.53 TPG) and day 33 (108.32 TPG) and again by day 50 (112.12 TPG). However, neither of these changes in telomerase activity were significant ($p = 0.5$ and $p = 0.3$).

Using STELA, the mean XpYp telomere length was analysed during the 54 days immediately following viral transduction. The mean XpYp telomere length showed no significant change between day 0 and day 29 in the DN-hTERT population ($p = 0.743$), increasing from 3.75kb to 3.84kb (***Figure 4.9a***). Between day 29 and day 33, the mean XpYp telomere length decreased to 3.44kb ($p = 0.299$). This contrasted with the puromycin-resistant control cells whose mean XpYp telomere length decreased from 3.65kb to 3.39kb between day 0 and day 33 (***Figure 4.9b***). The mean XpYp telomere length in the DN-hTERT population alternated between a high of 3.87kb and a low of

3.32kb (*p = 0.1554*). While the mean XpYp telomere length of the puromycin-resistant control population never rose above 4.00kb or fell below 3.43kb (*p = 0.3526*).

In summary, forcing the expression of DN-hTERT in a population of U266B1 cells significantly reduced telomerase activity. However, the effect on telomere length was minimal. The mean XpYp telomere length of the DN-hTERT population remained stable at between 3.84kb and 3.32kb. Immediately after transfection, the viability of the DN-hTERT population decreased by a greater extent than the puromycin-resistant control population, but this alone was not enough to indicate that the cells had been driven into a telomere-driven crisis. Eventually, viability recovered to around 80% and telomerase activity showed a small but insignificant increase.

4.4.7 The Extent of Chromosomal Fusion in Three Myeloma Cell Lines During a Period of Telomere-Driven Crisis

The JJN-3, NCI-H929 and U266B1 cell lines were examined for changes in the frequency of chromosomal fusion events during the period of telomere-driven crisis induced following the expression of DN-hTERT. Each measurement was performed at the same time points at which STELA was performed. The frequency of chromosomal fusion was examined in both the DN-hTERT and puromycin-resistant control populations to allow for comparison. However, no significant difference (*p = 0.2334*; *p = 0.8501*; *p = 0.4258*) was observed between the frequency of fusion in the DN-hTERT and puromycin-resistant control populations for each of the three cell lines (***Figure 4.10***).

In the JJN-3 DN-hTERT population, the frequency of chromosomal fusion events increased between day 0 and day 20 from $40x10^{-6}$/cell to $80x10^{-6}$/cell. However, this was also true for the JJN-3 puromycin-resistant control population whereby the frequency of fusion events was calculated as $47x10^{-6}$/cell on day 0 and $80x10^{-6}$/cell by day 20 (***Figure 4.10a***). Overall, the number of fusion events totalled 78 for the DN-

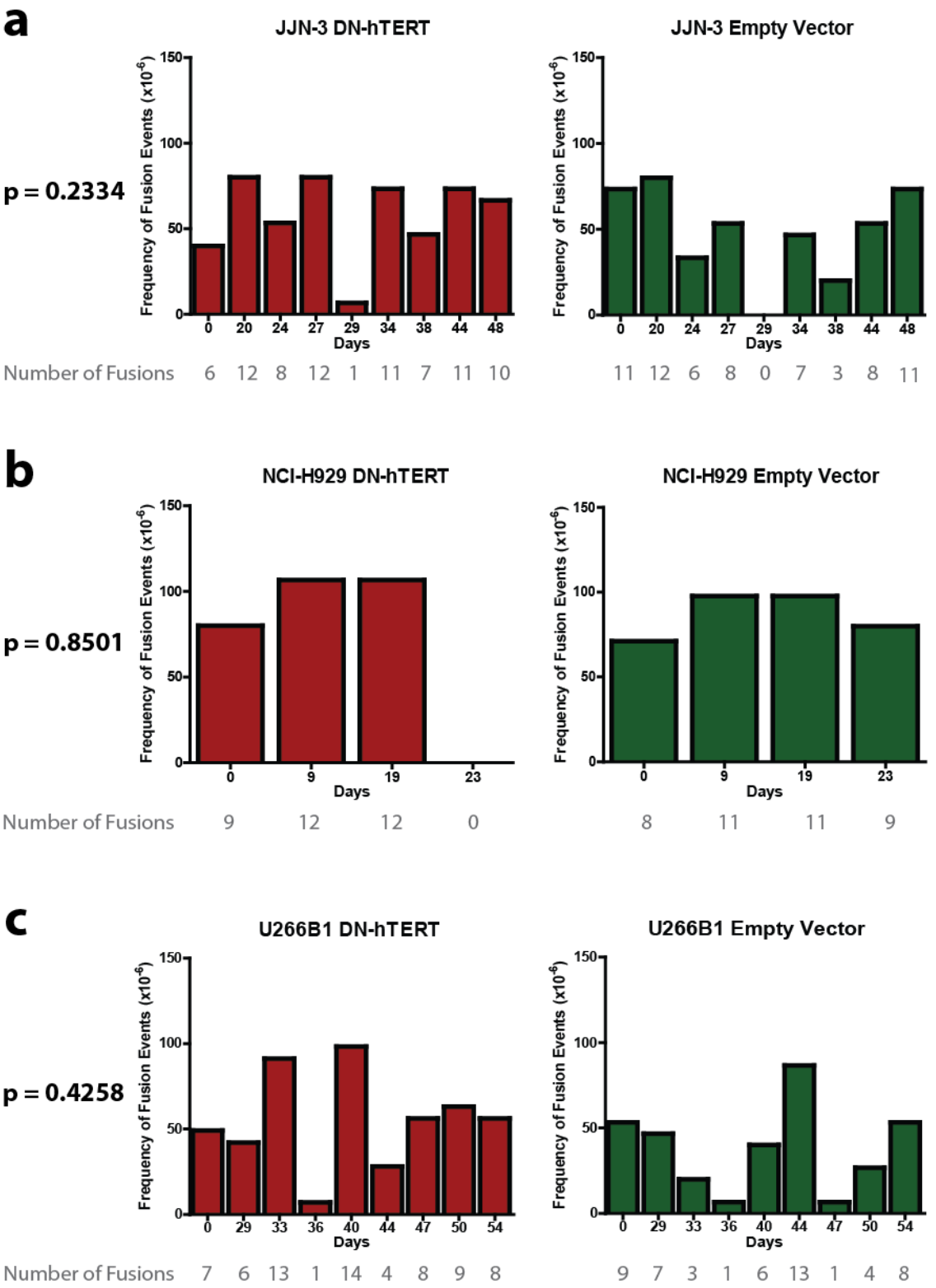

Figure 4.10 - The Frequency of Chromosomal Fusion Events, During a Period of Telomere-Driven Crisis, in Three MM Cell Lines

The JJN-3, NCI-H929 and U266B1 DN-hTERT cell lines were examined for chromosomal fusion events during a period a telomere-driven crisis. The empty vector colonies were also examined for chromosomal fusion events during this same period. In total, 900ng of DNA was examined per cell line. The frequency of chromosomal fusion was estimated by dividing the number of observable fusion bands by the number of input molecules (around 150,000 cells). **(a)** JJN-3 DN-hTERT and Empty Vector. **(b)** NCI-H929 DN-hTERT and Empty Vector. **(c)** U266B1 DN-hTERT and Empty Vector. A Wilcoxon matched pairs test was used to determine significance between the number of chromsomal fusion events at each time point between the DN-hTERT and empty vector cultures. Significance was defined as <0.05

hTERT population and 66 for the puromycin-resistant control population. Using a Wilcoxon matched pairs test, treating identical days in the DN-hTERT and puromycin-resistant control populations as pairs, the overall difference between the change in the frequency of fusion events for each population was found not to be significant ($p = 0.2334$).

For the NCI-H929 cells, the number of chromosomal fusion events identified increased marginally between day 0 and day 19 for both the DN-hTERT and puromycin-resistant control populations (***Figure 4.10b***). However, fusion events were undetectable in the DN-hTERT population at day 23. This is in contrast to the puromycin-resistant control population whereby the frequency of fusion events was calculated as $60x10^{-6}$/cell at the same time point. However, this change was not significant when assessed using a Wilcoxon matched pairs test ($p = 0.8501$).

The number of chromosomal fusion events identified in the U266B1 DN-hTERT population did not change significantly when compared with the puromycin-resistant counterpart ($p = 0.4258$; ***Figure 4.10c***). The largest number of fusion events identified occurred at day 40 (frequency of fusion = $93x10^{-6}$/cell) for the DN-hTERT population and day 44 for the puromycin-resistant control population (frequency of fusion = $87x10^{-6}$/cell). Overall, 70 events were recorded for the DN-hTERT population and 52 for the puromycin-resistant control population. Again, these values were shown not to be significant using a Wilcoxon matched pairs test ($p = 0.4258$).

In summary, chromosomal end-end fusion events were identified in the JJN-3, NCI-H929 and U266B1 cell lines. However, no significant change in the frequency of fusion was detected, relative to the puromycin-resistant controls, when DN-hTERT was expressed. This was perhaps unsurprising for the U266B1 cell line, as the insignificant change in fusion frequency was consistent with the insignificant change to mean XpYp telomere

length recorded previously. However, an insignificant change to fusion frequency in the JJN-3 and NCI-H929 cell lines was unexpected as the viability and telomeric erosion recorded previously in DN-hTERT populations was consistent with a telomere-driven crisis. One possible explanation for the lack of change in NCI-H929 fusion frequency was that the cells had been unable to undergo significant genomic rearrangement due to the expression of a functional p53 protein. Having the capacity to successfully trigger apoptosis in this way may also explain why the cells were unable to escape from a telomere-driven crisis, with viability of the DN-hTERT population eventually falling below 10% and never recovering.

As for the JJN-3 cell line, true fusion frequency might have been masked by the heterogeneity of the telomere lengths within the population of cells. JJN-3 cells that had a shorter telomere length would enter into a telomere-driven crisis at an earlier time point to those cells with longer telomeres, with any resulting change in fusion frequency being obscured by the bulk of pre-crisis cells. To test this hypothesis, clonal populations of cells would need to be driven into a telomere-driven crisis through the expression of DN-hTERT. Populations of cells derived from a single clone commonly express a significantly homogeneous range of telomere lengths, thus allowing the entire population to be driven into crisis together.

4.4.8 Clonal Growth and Telomerase Activity During Crisis in Three JJN-3 Clonal Populations

Telomere length distributions within a cell line are commonly heterogeneous, with DN-hTERT expression driving each cell into a state of telomere-driven crisis at different time points. This can result in a population of cells being in a state of crisis for days or weeks, with any change in the frequency of fusion within an individual cell being masked by the range of pre- and post-crisis cells within the population. As the JJN-3 and U266B1 cell lines contained heterogeneous telomere length distributions, attempts were made to create clonal colonies of these cell lines which expressed the DN-hTERT construct and

contained a more homogeneous telomere length distribution. Several attempts were also made using dilution cloning to isolate single cell clones from the NCI-H929 cell line, but no viable clones could be established. It was considered that this may be attributable to the relatively short telomere lengths observed in NCI-H929 cells which provide insufficient replicative capacity for the clones to establish prior to the onset of crisis. Instead, a method of dilution cloning was carried out on both the JJN-3 and U266B1 cell lines, resulting in the successful formation of clonal colonies of JJN-3 cells. Although multiple attempts were made to clone the U266B1 cell line, it was not possible using the method of dilution cloning employed.

Three clonal populations of JJN-3 cells, each expressing DN-hTERT, were monitored over a period of months for signs of a telomere-induced crisis (***highlighted in red - Figure 4.11a***). During the initial 30 to 40 days, each clone grew normally before entering a period of slowed or stalled growth which was thought to represent crisis. This period occurred between day 37 and day 52 in clone A, between day 42 and day 59 in clone B, and between day 44 and day 62 in clone C. After this, each clone returned to a steady rate of growth similar to that observed before the onset of crisis. The same pattern was not observed in the control cells, a clonal population of JJN-3 cells which expressed only the empty pBABE-puro vector.

Telomerase activity was measured before the onset of crisis and after crisis in the three clonal populations of JJN-3 DN-hTERT cells (***Figure 4.11b***). The telomerase activity before crisis in each clonal DN-hTERT population was greatly reduced when compared to the control clone at a similar time point. However, telomerase activity in each DN-hTERT clone following a period of crisis had increased (***Figure 4.11b***). Instead of returning to the normal levels seen in the control clone (43.45 TPG) or remaining at pre-crisis levels, each DN-hTERT clone had significantly increased telomerase expression. This included clone A whose telomerase activity was 2.26x greater ($p = 0.007$), clone B

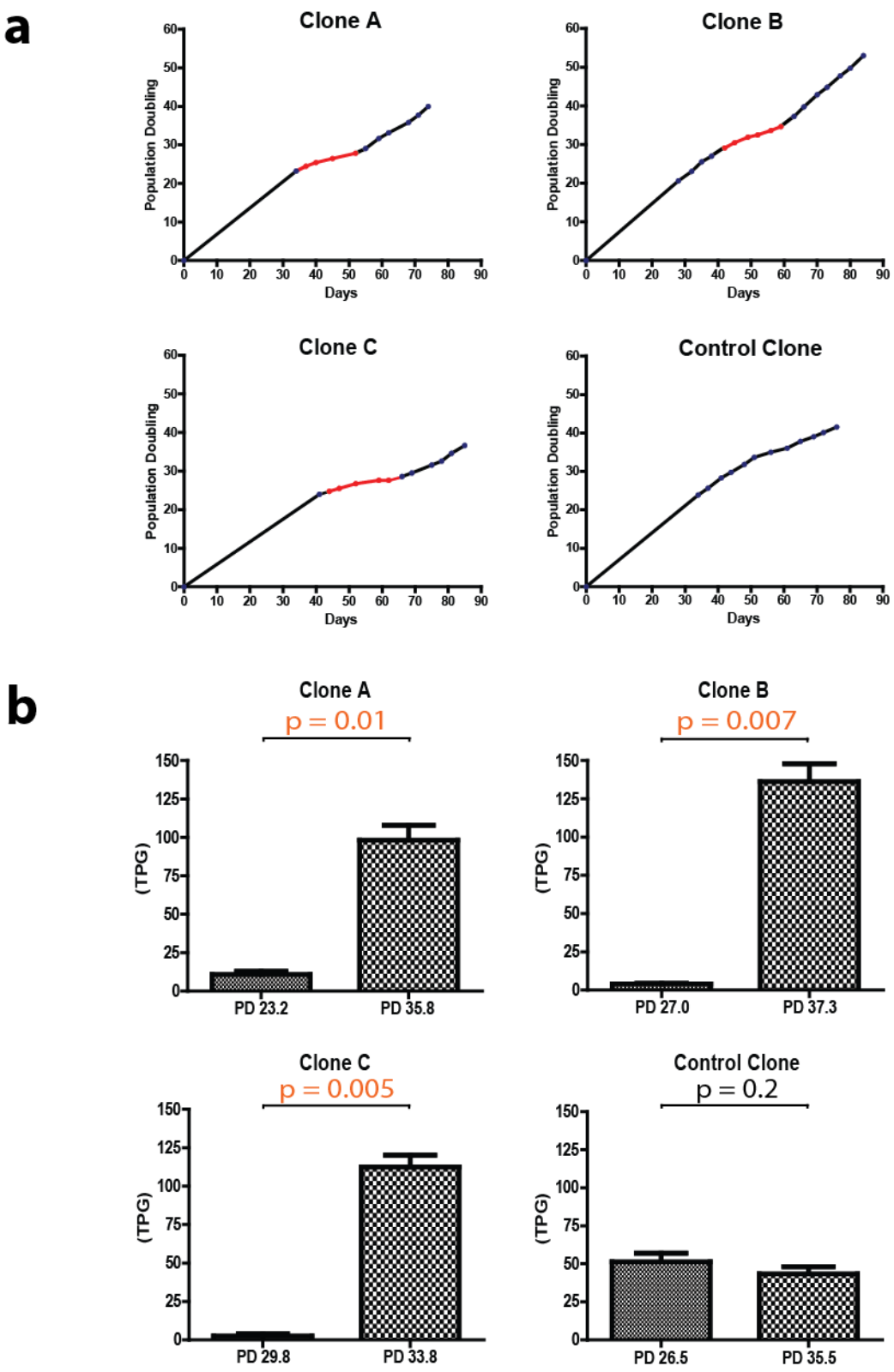

Figure 4.11 - Telomerase Activity in JJN-3 DNhTERT Clonal Populations Before and After Crisis. **(a)** Clonal populations of the JJN-3 cell line, each expressing the DN-hTERT protein, had their growth monitored over a perid of weeks. During this time, each clone experienced a period of stalled growth which was thought to be caused by a telomere-induced crisis (highlighted in red). Eventually, each clonal population managed to escape from this period of crisis and resume the level of growth seen pre-crisis. A JJN-3 clonal population containing an empty pBABE-puro vector was also monitored as a control. **(b)** The telomerase activity of each JJN-3 clonal population was monitored before and after crisis. Total Product Generated (**TPG**) is a until specific to the TRAPeze detection kit used to measure telomerase activity. Significance was determined using a paired t-test and defined as <0.05

whose telomerase activity was 3.14x greater (p = *0.002*), and clone C whose telomerase activity was 2.59x greater (p = *0.002*) than that of the control clone at a similar timepoint.

4.4.9 The Change in the Frequency of Chromosomal Fusion Events During a Telomere-Driven Crisis in JJN-3 DN-hTERT Clone A

STELA was used to measure the mean telomere length, at both the XpYp and 17p telomere ends, in three clonal JJN-3 DN-hTERT populations during a period of telomere-driven crisis. Clonal populations of cells are commonly identified by their homogeneous telomere length distributions, measured by the standard deviation within a STELA profile (Baird et al. 2003). An example of this can be seen in the STELA profile of clone A which was recoded at population doubling (PD) 23.2 (***Figure 4.12***). With a standard deviation of 0.27kb at the XpYp telomere, this is a significant decrease from the standard deviation of 1.31kb originally identified in the parental JJN-3 population (p = *<0.0001*; ***Figure 4.1a***).

Between PD 23.23 and PD 26.49, before the onset of a telomere-driven crisis, the standard deviation (clonality) of each STELA profile remained relatively small at between 0.27 – 0.34kb. It can also be clearly seen that mean telomere length decreased by around 115 base pairs per PD during this period, falling from 1.82kb at PD 23.2 to 1.44kb by PD 26.5. This is consistent with the telomeric erosion rates of MRC5 fibroblast clonal populations (~112bp/PD) and WI-38 fibroblast bulk populations (~132bp/PD), but greater than that of HCA-2 fibroblast bulk populations (65bp/PD) and HCT116 colorectal carcinoma clonal populations (45bp/PD) which were monitored using STELA at the XpYp telomere (Britt-Compton et al. 2006; Jones et al. 2014). Between PD 27.9 and PD 37.8, during and after the period of crisis, the standard deviation within the STELA profile increased from 0.89kb to 1.18kb. This occurred alongside an increase in the mean XpYp telomere length from 1.87kb at PD 27.9 to 2.47kb at PD 37.8.

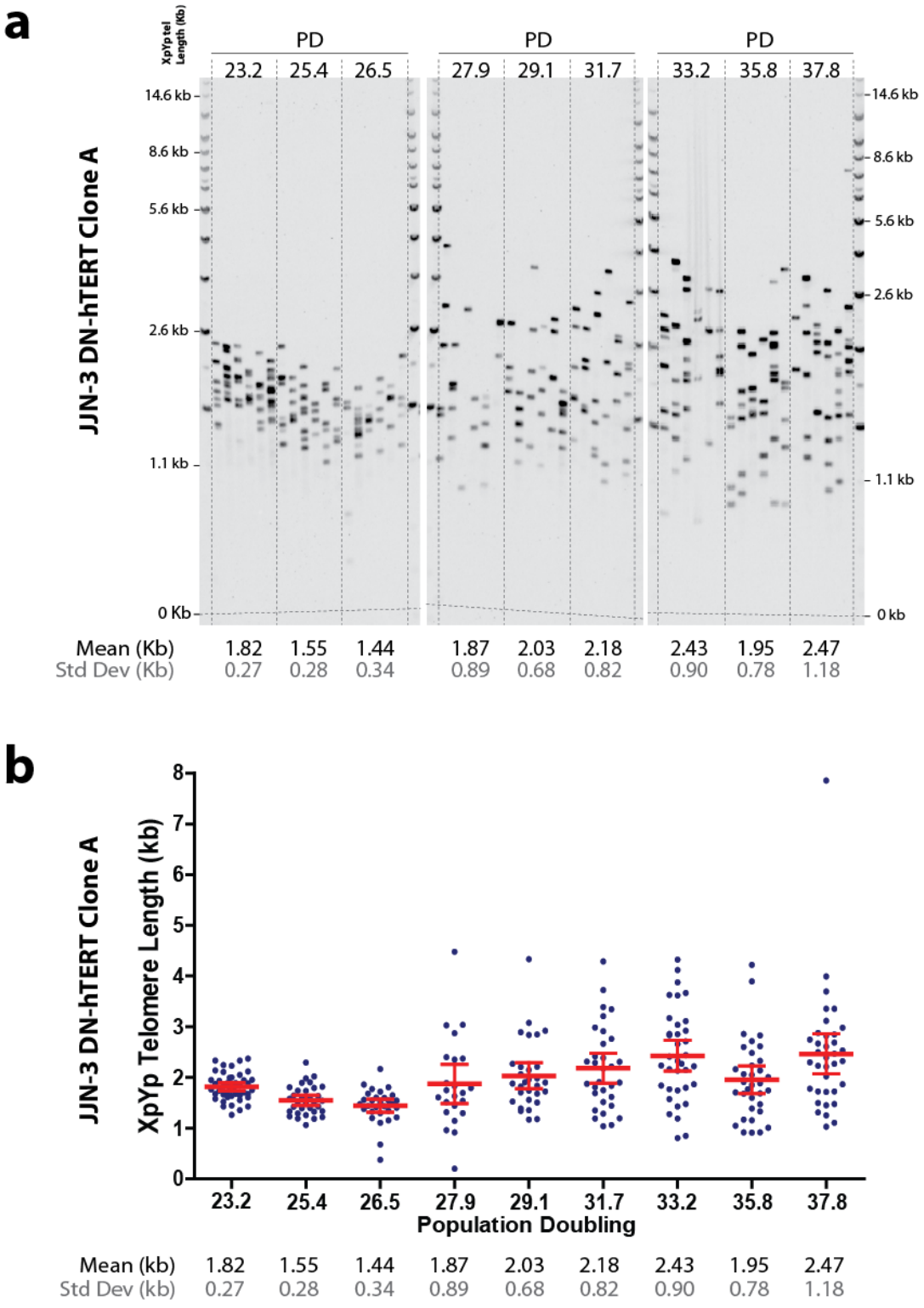

Figure 4.12 - The Change in the XpYp Telomere Length of JJN-3 Clone A During a Period of Telomere-Driven Crisis

A clonal population of JJN-3 cells expressing DN-hTERT was grown over a period of 37.8 population doublings. Samples of cells were taken at 9 time points during this period, with STELA being performed as a way to measure the resulting XpYp telomere length. **(a)** STELA profiles showing the XpYp telomere lengths, during a period of telomere-driven crisis, in a clonal population of JJN-3 cells expressing DN-hTERT. **(b)** Graphical representation of the STELA profiles. The mean telomere length for each time point is shown in red alongside the upper and lower 95% confidence intervals.

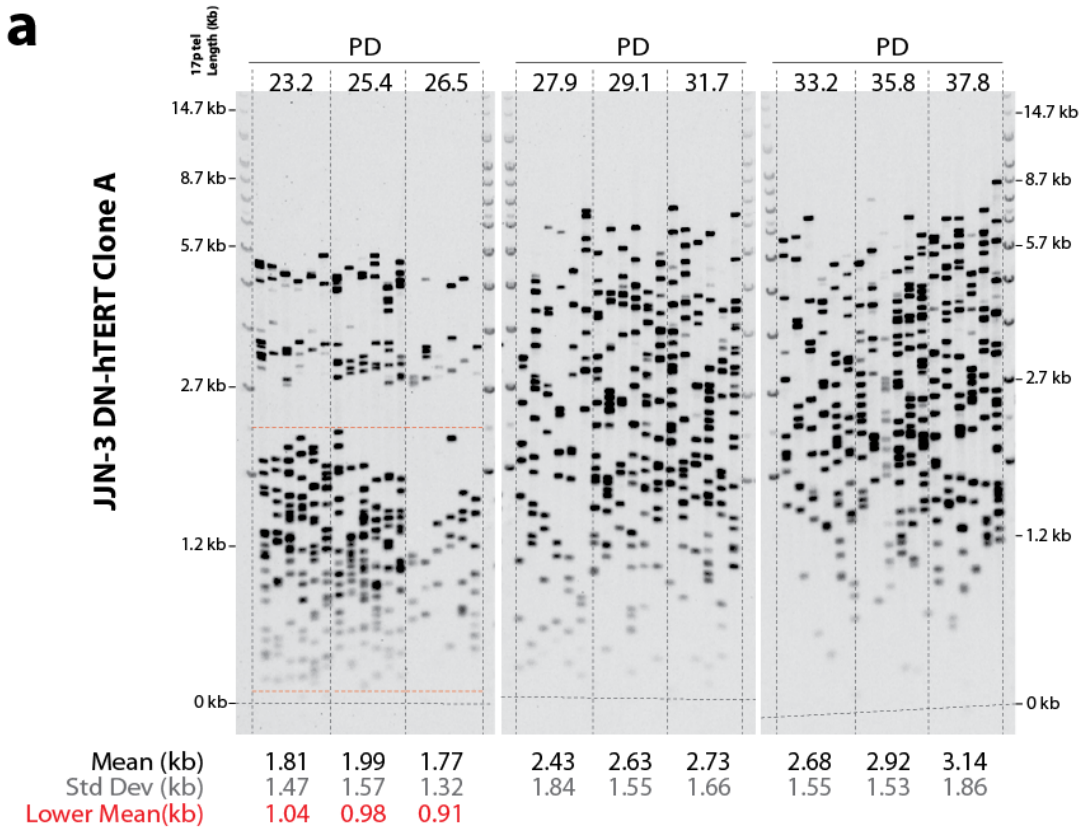

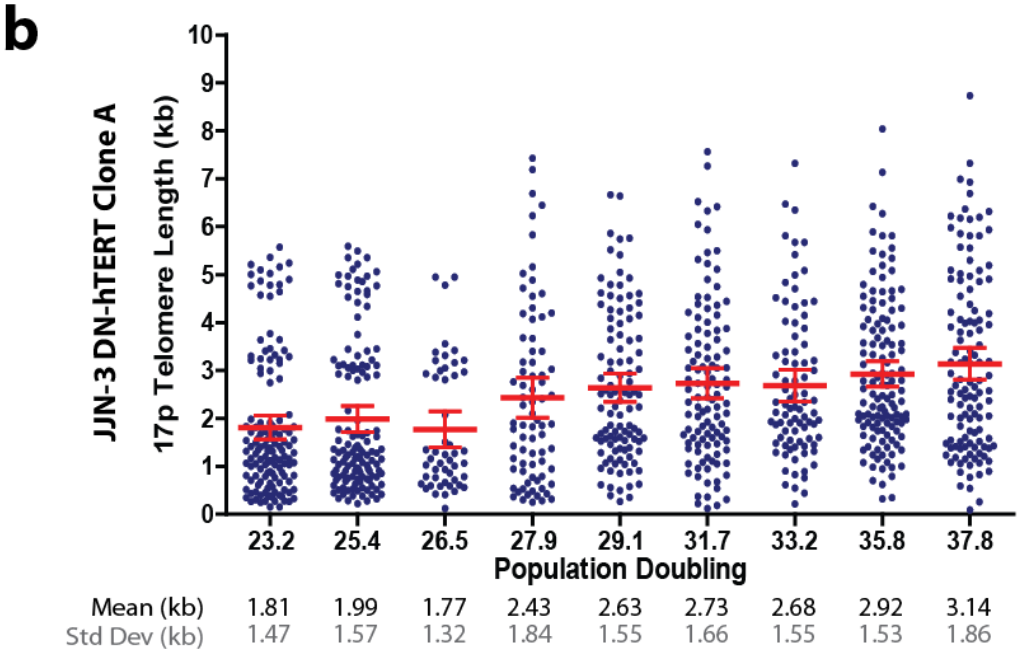

Figure 4.13 - The Change in the 17p Telomere Length of JJN-3 Clone A During a Period of Telomere-Driven Crisis

A clonal population of JJN-3 cells expressing DN-hTERT were grown over a period of 37.8 population doublings. Samples of cells were taken at 9 time points during this period, with STELA being performed as a way to measure the resulting XpYp telomere length. **(a)** STELA profiles showing the 17p telomere lengths, during a period of telomere-driven crisis, in a clonal population of JJN-3 cells expressing DN-hTERT. **(b)** Graphical representation of the STELA profiles. The mean telomere length for each time point is shown in red alongside the upper and lower 95% confidance intervals.

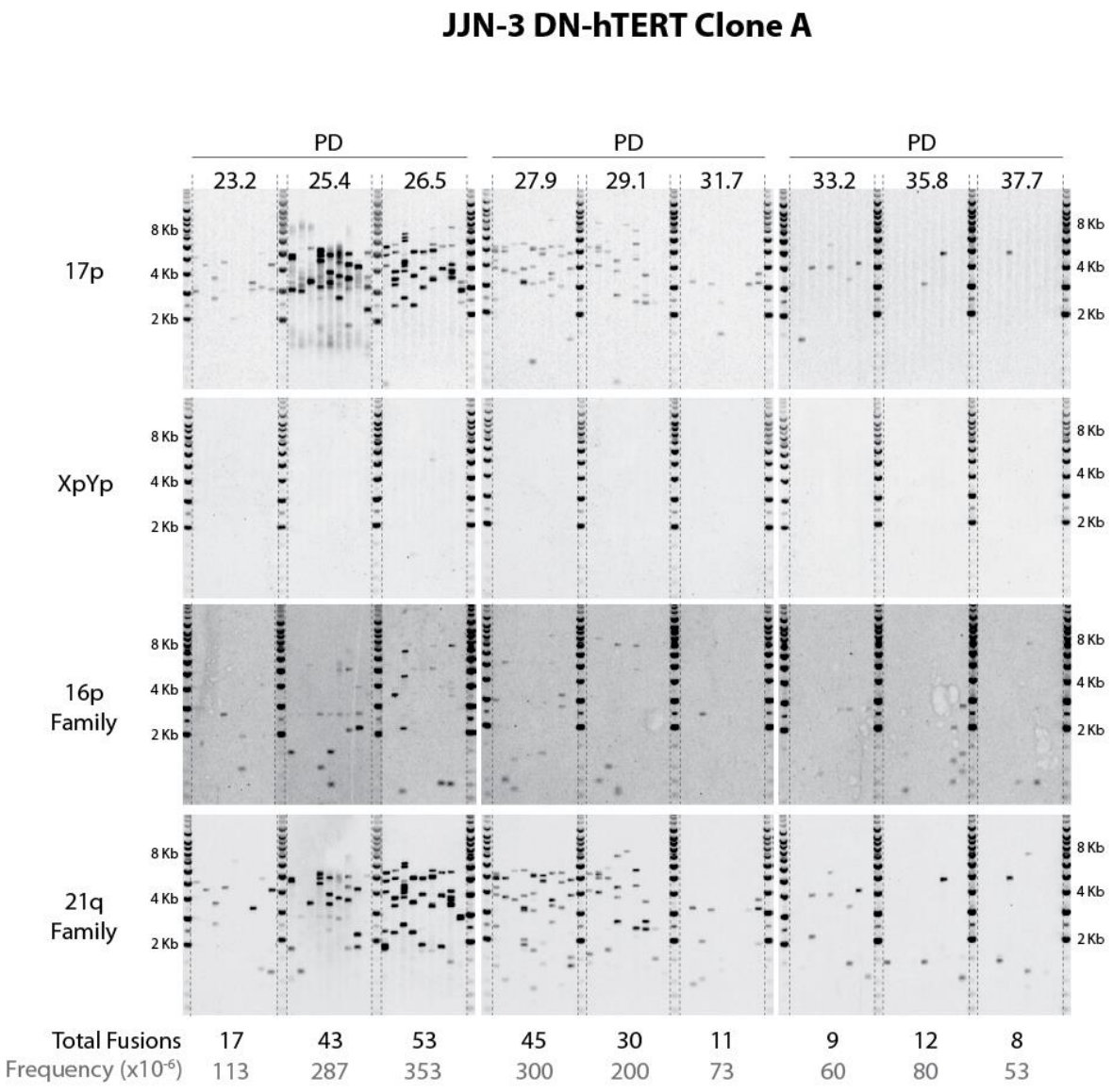

Figure 4.14 - The Change in the Frequency of Chromosomal Fusion Events for JJN-3 Clone A During a Period of Telomere-Driven Crisis

The frequency of chromosomal fusion events in clone A was monitored during a period of telomere-driven crisis. In total, 900ng of DNA were examined per time point. The frequency of chromosomal fusion was estimated by dividing the number of observable fusion bands by the number of input molecules (around 150,000 cells). Visualisation of these events was performed using the oligonucleotide probes 17p6, XpYpO-G, 16p1 and 21q1.

The 17p telomere length was also measured at the same time points, but the STELA profile was much more complex than that of the XpYp profile (***Figure 4.13***). This was due to the presence of a multimodal distribution, with three distinct populations of 17p telomere lengths being identified. One explanation for this may be that multiple independent clones exist within the population, with each clone having a significantly different 17p telomere length. However, as a multimodal distribution could not be identified from the XpYp STELA profile of clone A, it became less likely that this was the case. Instead, each copy of chromosome 17 within the cells (of which there could be more than two per cell) may have a significantly different telomere length. This allelic variation, combined with gain of 17p, may explain the multimodal distribution. For this reason, the standard deviation of the 17p profile (1.47kb at PD 23.2) was not as homogeneous as the XpYp profile (0.27kb at PD 23.2). Regardless, mean 17p telomere length decreased from 1.81kb at PD 23.2 to 1.77kb at PD 26.5. This was followed by a sudden increase in both mean 17p telomere length (2.73kb by PD 31.7) and standard deviation (1.66kb by PD 31.7) immediately after the onset of crisis.

The mean value of the lowest 17p distribution was also recorded so that the extent of telomere erosion could be monitored. Again, mean 17p telomere length decreased from 1.04kb at PD 23.2 to 0.91kb at PD26.5. This was followed by a change in the distribution of telomere lengths throughout the 17p profile such that the individual telomere length distributions that were apparent prior to crisis could no longer be distinguished.

The extent of chromosomal fusion in clone A, during the period of telomere-driven crisis, was also identified (***Figure 4.14***). As mean telomere length shortened between PD 23.2 and PD 26.5, the number of chromosomal fusion events identified increased. After reaching a peak frequency of fusion at $353x10^{-6}$ events per cell, the frequency of fusion decreased between PD 28.0 and PD 37.8. Most fusion events involved either the 17p chromosomal end or the 21q-family of chromosomal ends, while the 16p-family of

chromosomal ends showed relatively little change in fusion frequency throughout crisis. However, only two fusion events involving the XpYp chromosomal end were identified. This is likely explained by the longer mean XpYp telomere length, relative to the mean telomere length of the lower distribution in the 17p STELA profile. This may have resulted in a smaller number of critically shortened XpYp telomeres, when compared to the 17p telomere, that were able to undergo fusion before a telomere-driven crisis was triggered.

In summary, this clonal population of JJN-3 cells exhibited a period of stalled growth that was consistent with the onset of crisis. STELA was used to identify the homogeneous telomere length profile that is characteristic of a clonal population, as well as track the extent of telomeric erosion in response to DN-hTERT expression. As the cells entered a state of telomere-driven crisis, the frequency of chromosomal end-end fusion increased in line with mean telomere length. The clonal population was then able to escape from crisis, resulting from an increased telomerase activity. During this time, mean telomere length and standard deviation increased and the frequency of fusion decreased.

4.4.10 The Change in the Frequency of Chromosomal Fusion Events During a Telomere-Driven Crisis in JJN-3 DN-hTERT Clone B

The clonality of JJN-3 DN-hTERT clone B was demonstrated by its standard deviation of 0.45kb at PD 25.5 (***Figure 4.15***). In a similar pattern to that observed in clone A before crisis, mean XpYp telomere length decreased at a rate of 97bp/PD from 2.02kb at PD 25.5 to 1.40kb at PD 31.9. During this period, standard deviation remained almost constant and never increased beyond 0.48kb. After escaping from a state of crisis, mean telomere length increased to 2.44kb and the telomere length profile became more heterogeneous with the standard deviation increasing to 1.07kb by PD 49.7.

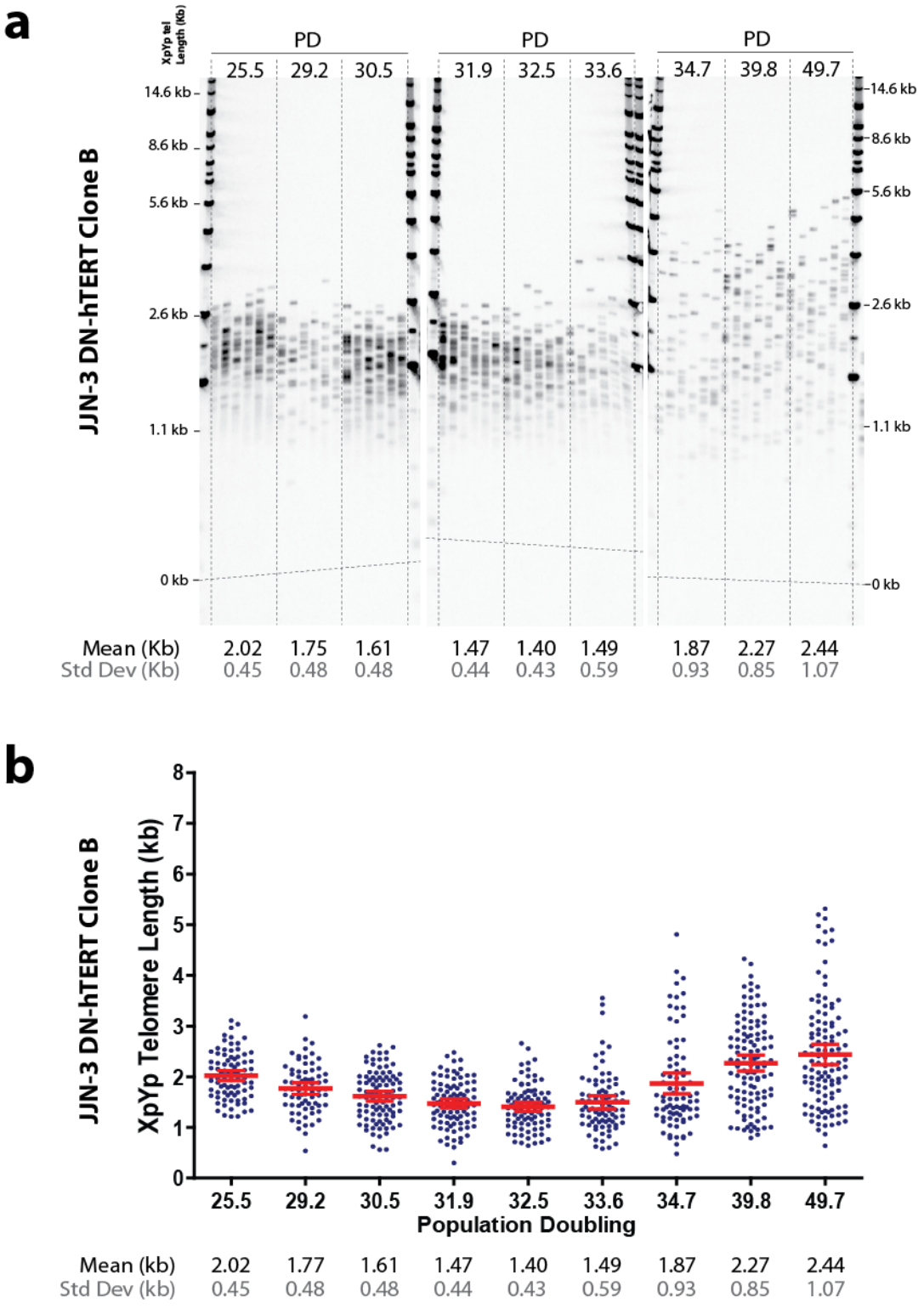

Figure 4.15 - The Change in the XpYp Telomere Length of JJN-3 Clone B During a Period of Telomere-Driven Crisis

A clonal population of JJN-3 cells expressing DN-hTERT were grown over a period of 49.7 population doublings. Samples of cells were taken at 9 time points during this period, with STELA being performed as a way to measure the resulting XpYp telomere length. **(a)** STELA profile showing the XpYp telomere lengths, during a period of telomere-driven crisis, in a clonal population of JJN-3 cells expressing DN-hTERT. **(b)** Graphical representation of the STELA profiles. The mean telomere length for each time point is shown in red alongside the upper and lower 95% confidence intervals.

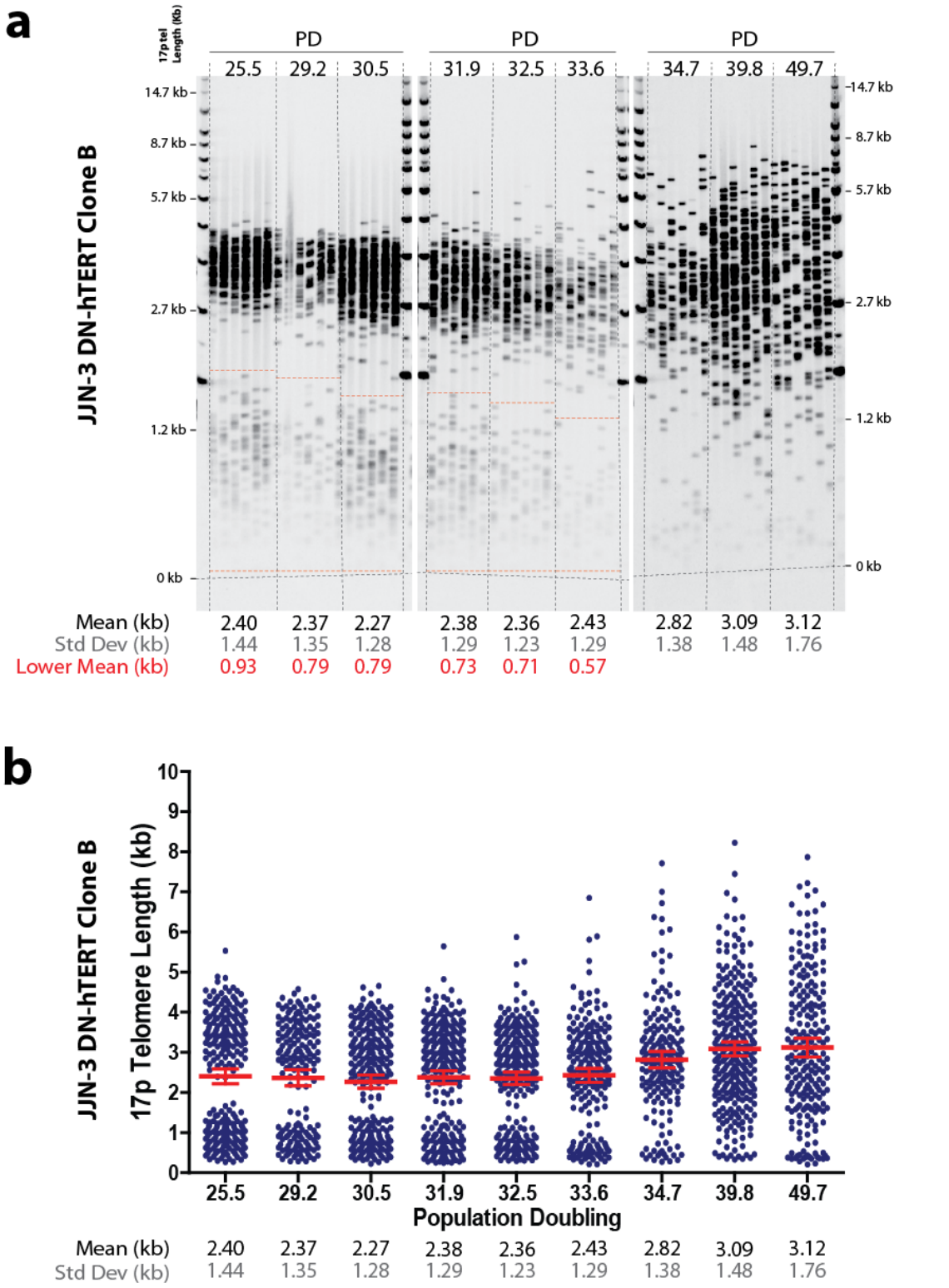

Figure 4.16 - The Change in the 17p Telomere Length of JJN-3 Clone B During a Period of Telomere-Driven Crisis

A clonal population of JJN-3 cells expressing DN-hTERT were grown over a period of 49.7 population doublings. Samples of cells were taken at 9 time points during this period, with STELA being performed as a way to measure the resulting 17p telomere length. **(a)** STELA profiles showing the 17p telomere lengths, during a period of telomere-driven crisis, in a clonal population of JJN-3 cells expressing DN-hTERT. **(b)** Graphical representation of the STELA profiles. The mean telomere length for each time point is shown in red alongside the upper and lower 95% confidance intervals.

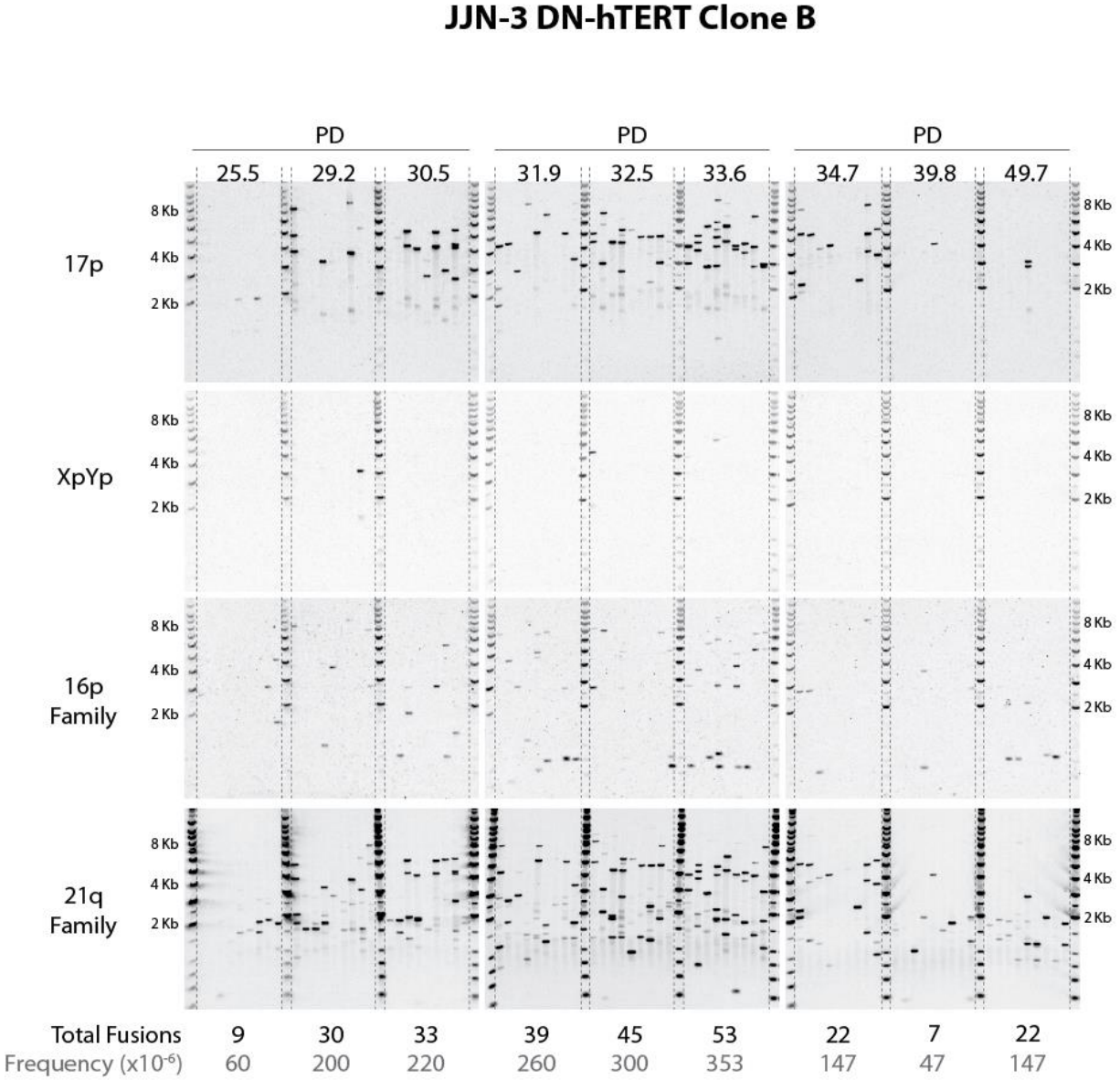

Figure 4.17 - The Change in the Frequency of Chromosomal Fusion Events for JJN-3 Clone B During a Period of Telomere-Driven Crisis

The frequency of chromosomal fusion events in clone B was monitored during a period of telomere-driven crisis. In total, 900ng of DNA were examined per time point. The frequency of chromosomal fusion was estimated by dividing the number of observable fusion bands by the number of input molecules (around 150,000 cells). Visualisation of these events was performed using the oligonucleotide probes 17p6, XpYpO-G, 16p1 and 21q1.

The 17p STELA profile of this clone also exhibited a multimodal distribution which increased the standard deviation of the profile to 1.44kb at PD 25.5 (***Figure 4.16***). This is again consistent with the presence of multiple copies of the 17p subtelomeric sequence. However, the overall mean of the 17p telomere length decreased from 2.40kb at PD 25.5 to 2.27kb at PD 30.5. The mean of the lower distribution also decreased from 0.93kb at PD 25.5 to 0.57kb at PD 33.6, at which point this distribution could no longer be identified as the telomere may have been completely eroded. This coincided with a significant increase in both the mean 17p telomere length and standard deviation between PD 34.7 and PD 49.7. Again, this is consistent with the increase in telomere length and standard deviation observed at the XpYp telomere at the same time points.

During this time, the frequency of chromosomal fusion events was also monitored for the 17p, XpYp, 16p-family and 21q family of chromosomal ends (***Figure 4.17***). Again, the frequency of chromosomal fusion events increased as mean telomere length decreased. This resulted in an increase from $60x10^{-6}$ fusion events per cell at PD 25.53 to $353x10^{-6}$ fusion events per cell by PD 33.64. As the cells began their escape from a telomere driven crisis, the frequency of chromosomal fusion events began to decrease which culminated in a reduction in fusion frequency ($47x10^{-6}$/cell) at PD 39.77. The fusion profile was again dominated by 17p and 21q-family chromosomal fusion events, with only a modest increase in 16p-family fusion events being seen during the period of crisis. However, fusion events involving the XpYp telomere end continued to remain elusive.

In summary, JJN-3 clone B cells that expressed DN-hTERT exhibited a period of stalled growth that was consistent with the onset of a telomere-driven crisis. As the telomeres were eroded during each PD, the frequency of chromosomal end-end fusion increased in line with telomeric shortening. In an identical manor to clone A, the population was then able to escape from crisis, as evidenced by a return to a pre-crisis growth rate and increased telomerase activity. During this time, mean telomere length and standard

deviation increased and a corresponding decrease in the frequency of fusion was observed.

4.4.11 The Change in the Frequency of Chromosomal Fusion Events During a Telomere-Driven Crisis in JJN-3 DN-hTERT Clone C

The mean XpYp telomere length of JJN-3 DN-hTERT clone C decreased by 128bp/PD from PD 24.0 (1.12kb) to PD 26.8 (0.76kb), at which point the cells had already begun to enter a state of telomere-driven crisis (***Figure 4.18***). After this, mean XpYp telomere length began to increase and reached a maximum of 2.02kb by PD 35.9. The homogeneous telomere length distribution of 0.25kb, a mark of the clonality of a population of cells, was also lost as the standard deviation increased after crisis to 0.97kb.

A similar effect was recorded at the 17p telomere end, with mean telomere length falling from 2.83kb at PD 24.0 to 1.86kb by PD 26.8 (***Figure 4.19***). As with clone A and clone B, multimodal distributions were present within the 17p STELA profile, increasing each measurement of the standard deviation relative to the XpYp profile. The mean of the lower distribution fell by 142bp/PD between PD 24.0 (1.21kb) and PD 27.8 (0.67kb), after which the ability to detect specific telomere length distributions within the profile was lost. Again, this was likely the result of complete telomeric erosion. At both the XpYp and 17p telomere ends, mean telomere length decreased between PD 24.0 and PD 26.8 and then increased until PD 35.9.

The overall number of fusions in clone C, as well as the peak number of fusions as the cells entered crisis, were much smaller than in clone A or clone B (***Figure 4.20***). Between PD 24.0 and PD 27.8, the number of observable fusions increased from $67x10^{-6}$/cell to $120x10^{-6}$/cell. This eventually fell to a low of $40x10^{-6}$ fusion events per cell by PD 33.8. However, fusion events involving the XpYp and 16p-family of chromosome ends

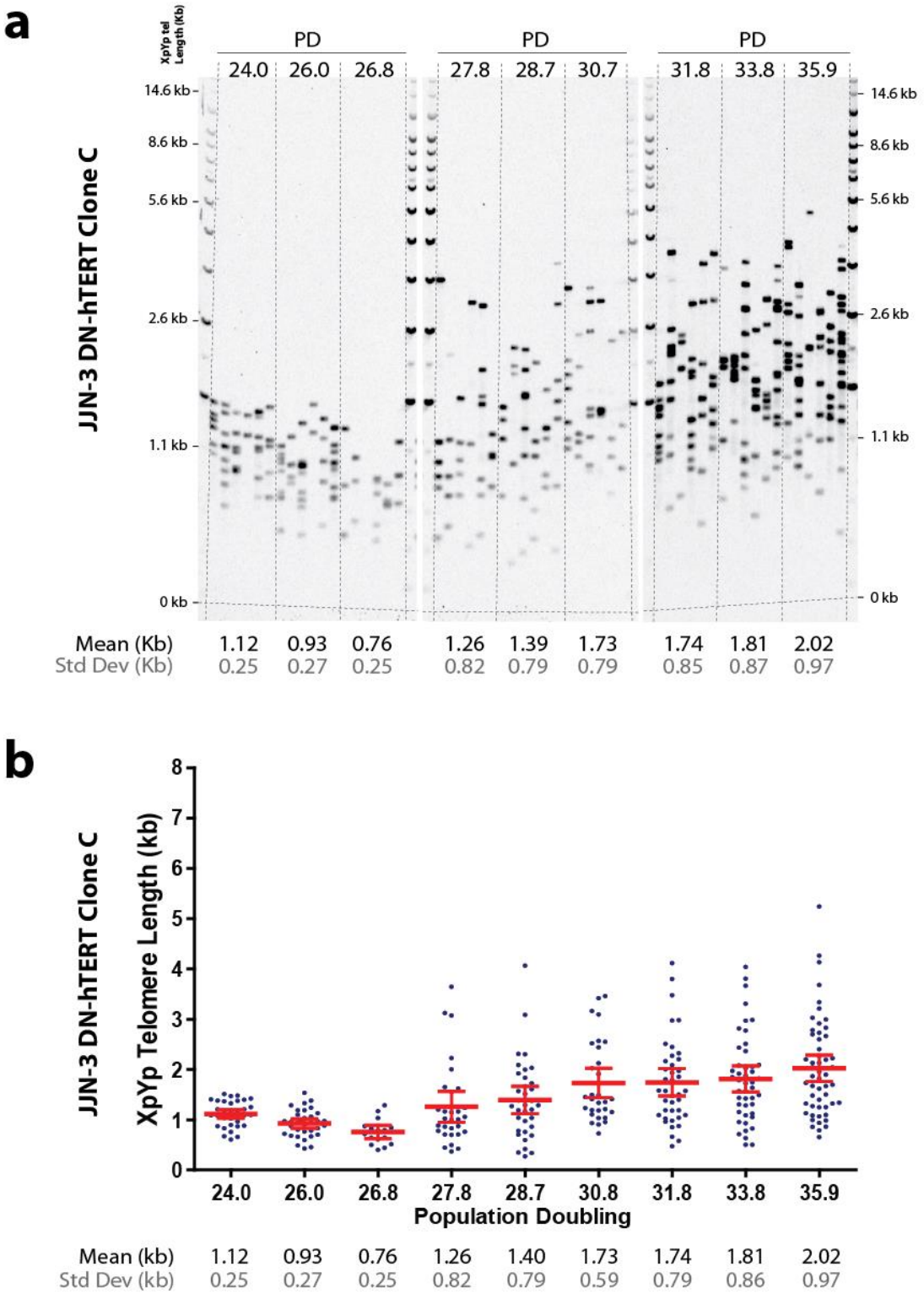

Figure 4.18 - The Change in the XpYp Telomere Length of JJN-3 Clone C During a Period of Telomere-Driven Crisis

A clonal population of JJN-3 cells expressing DN-hTERT were grown over a period of 35.9 population doublings. Samples of cells were taken at 9 time points during this period, with STELA being performed as a way to measure the resulting XpYp telomere length. **(a)** STELA profiles showing the XpYp telomere lengths, during a period of telomere-driven crisis, in a clonal population of JJN-3 cells expressing DN-hTERT. **(b)** Graphical representation of the STELA profiles. The mean telomere length for each time point is shown in red alongside the upper and lower 95% confidance intervals.

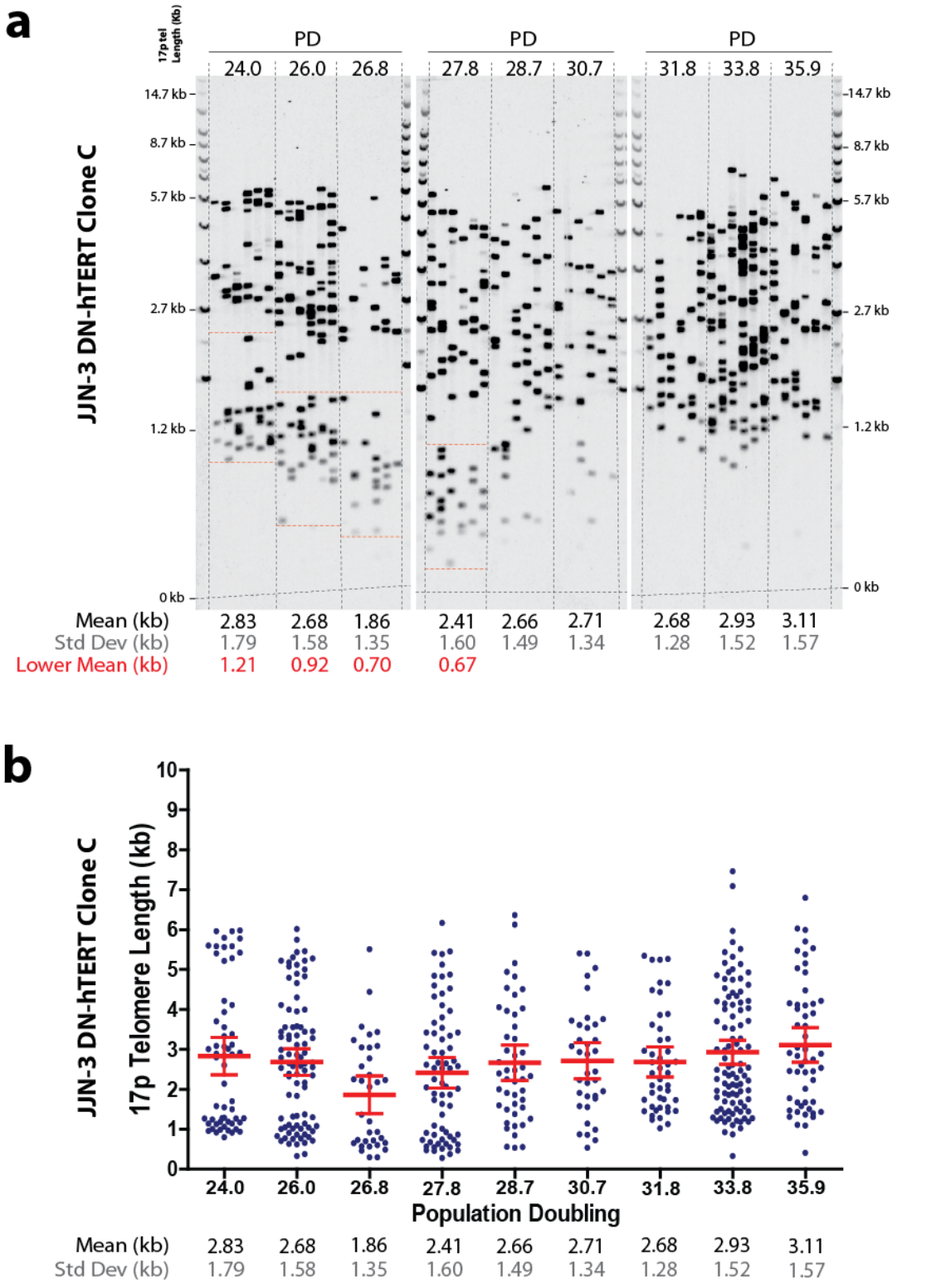

Figure 4.19 - The Change in the 17p Telomere Length of JJN-3 Clone C During a Period of Telomere-Driven Crisis

A clonal population of JJN-3 cells expressing DN-hTERT were grown over a period of 35.9 population doublings. Samples of cells were taken at 9 time points during this period, with STELA being performed as a way to measure the resulting 17p telomere length. **(a)** STELA profiles showing the 17p telomere lengths, during a period of telomere-driven crisis, in a clonal population of JJN-3 cells expressing DN-hTERT. **(b)** Graphical representation of the STELA profiles. The mean telomere length for each time point is shown in red alongside the upper and lower 95% confidence intervals.

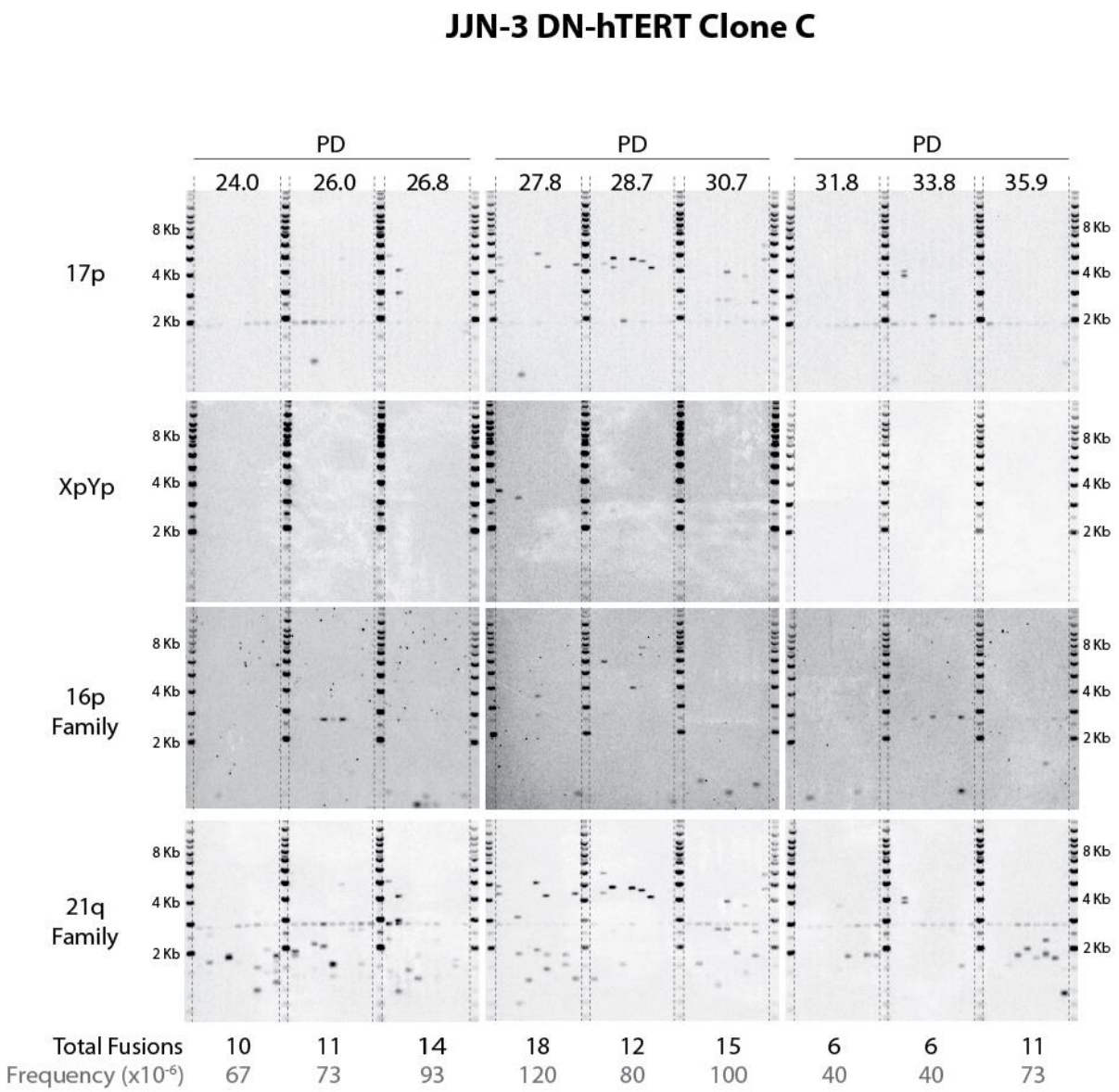

Figure 4.20 - The Change in the Frequency of Chromosomal Fusion Events for JJN-3 Clone C During a Period of Telomere-Driven Crisis

The frequency of chromosomal fusion events in clone C was monitored during a period of telomere-driven crisis. In total, 900ng of DNA were examined per time point. The frequency of chromosomal fusion was estimated by dividing the number of observable fusion bands by the number of input molecules (around 150,000 cells). Visualisation of these events was performed using the oligonucleotide probes 17p6, XpYpO-G, 16p1 and 21q1.

were rarely detected. Most fusion events involved either the 17p or 21q-family of chromosome ends.

In summary, the telomere dynamics of JJN-3 clone C closely mirrored that of clones A and B. The expression of DN-hTERT caused a period of stalled growth throughout the clonal population that was consistent with the onset of a telomere-driven crisis. The homogeneous XpYp telomere length distribution was eroded at a rate of 142bp/PD, as opposed to the 115bp/PD and 97bp/PD for clone A and clone B respectively. The frequency of chromosomal end-end fusion increased in line with telomeric shortening, although the peak fusion frequency ($120x10^{-6}$/cell) was lower than that of either clone A ($353x10^{-6}$/cell) or clone B ($353x10^{-6}$/cell). Eventually, clone C escaped from a telomere-driven crisis, possibly driven by the corresponding increase in telomerase activity. At this point, telomere length and standard deviation increased and a corresponding decrease in the frequency of fusion was observed.

4.4.12 Chromosomal Fusion Events within the JJN-3 DN-hTERT Clonal Populations Predominantly Involve the 17p or 21q-Family of Chromosome Ends

Although several chromosomal ends were analysed during this study, the 17p and 21q-family of chromosome ends showed the greatest change in the frequency of fusion as a direct result of changes in mean telomere length. This was analysed graphically (***Figure 4.12***), with 17p and 21q-family interchromosomal fusion events being plotted separately. In each case, the frequency of fusion events detected increased as telomere length decreased.

In summary, this work demonstrated that DN-hTERT expression significantly reduced the activity of telomerase in three clonal populations of the JJN-3 cell line. The resulting telomeric erosion (XpYp - 115bp/PD, 97bp/PD and 142bp/PD; 17p lower distribution – 39bp/PD, 44bp/PD and 142bp/PD for clones A, B and C respectively) forced the cells

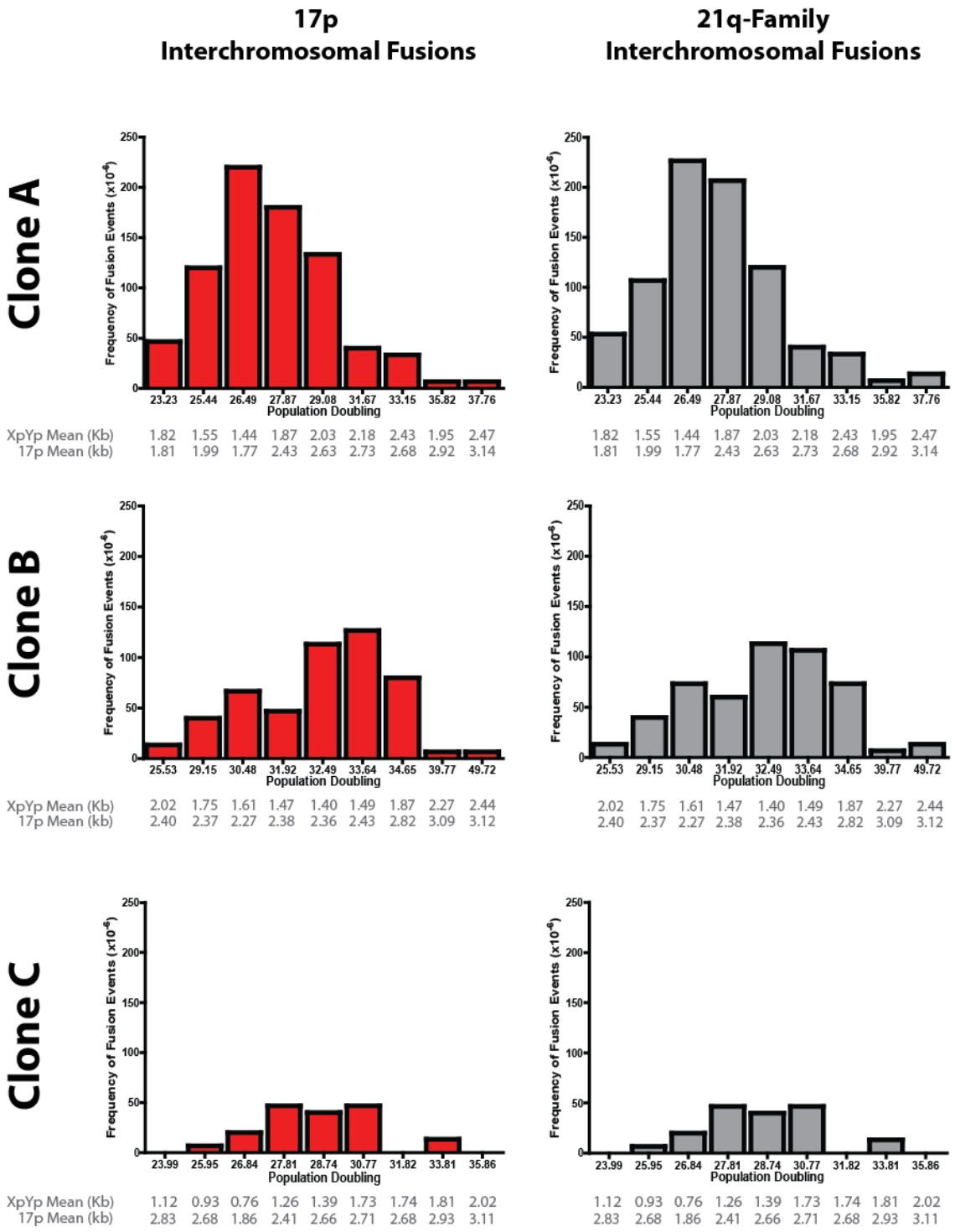

Figure 4.21 - The Change in the Frequency of 17p and 21q-Family Interchromosomal Fusion Events During a Period of Telomere-Induced Crsis in Three Clonal Populations of JJN-3 DN-hTERT Cells

Graphs showing the frequency of interchromosomal fusion events involving either the 17p or 21q-family of chromosome ends. In total, 900ng of DNA were examined per time point. The frequency of chromosomal fusion was estimated by dividing the number of observable fusion bands by the number of input molecules (around 150,000 cells). Visualisation of these events was performed using the oligonucleotide probes 17p6, XpYpO-G, 16p1 and 21q1. The mean XpYp and 17p telomere lengths have been listed for each time point, underneath each graph.

into a state of telomere-driven crisis, with the frequency of chromosomal end-end fusion increasing in line with telomeric shortening. Eventually, each clonal population managed to escape from crisis, an event which was marked by the reactivation of telomerase and increasing mean XpYp and 17p telomere lengths. Standard deviations also increased immediately after crisis, with telomere length profiles becoming significantly more heterogeneous. As mean telomere length increased, a corresponding decrease in the frequency of fusion events was observed.

4.5 Discussion

4.5.1 Telomere Length and Chromosomal Fusion in Four MM Cell Lines

In the previous chapter, we demonstrated that mean XpYp telomere length measurements held prognostic value within the context of MM. Having measured the mean XpYp telomere length of 141 MM patient whole bone marrow aspirates, we demonstrated that shorter XpYp telomere length (< 3.92kb) correlated with a decrease in overall survival. However, we were unable to identify a cause for this relationship from the patient data alone. Here, we hypothesised that shorter mean telomere length led to an increase in the frequency of chromosomal fusion events in MM. This was based on our findings in the previous chapter, combined with the extensive literature regarding shortened telomeres and genomic instability in other haematological neoplasms (O'Sullivan and Karlseder 2010; Lin et al. 2010). We expected that the presence of fusion events would drive the genomic rearrangements that are a characteristic of MM (Rajkumar et al. 2013).

We attempted to address our hypothesis using the JJN-3, NCI-H929, RPMI-8226 and U266B1 cell lines. This was necessary due to the difficulty in culturing primary $CD138^+$ MM cells derived from patient bone marrow. Most primary plasma cells have a lifespan of only a few days (Oracki et al. 2010) making them unsuitable for the long-term experiments performed here. While long-lived memory plasma cells have been successfully cultured, their presence in bone marrow can be as low as 0.25% (Jourdan et al. 2014). This makes them an unsuitable model due to the quantities of bone marrow required and the time needed for sufficient $CD138^+$ isolation. Using well-characterised cells lines, rather than primary cells, also meant that the p53 expression profiles were known. This allowed the response to critical telomere shortening to be examined within the context of a damaged tumour suppressive pathway.

Telomere Length: Characterisation of the XpYp chromosome ends within the four cell lines revealed that the mean telomere lengths of NCI-H929 and RPMI-8226 were relatively short. This is in comparison to the longer XpYp telomere lengths of the JJN-3 and U266B1 cell lines. The difference in mean telomere length between the four cell lines is simply a result of their origin, with each cell line being derived from a separate individual. As we demonstrated in the previous chapter, mean telomere length can depend on several factors. This includes the age of the individual, the type of cell being examined, and whether the cells under examination are healthy or diseased (Friedrich et al. 2000; Svenson et al. 2011).

However, the mean telomere length at the XpYp chromosome end did not always correlate with the mean 17p telomere length. Within the NCI-H929 cell line, this difference was caused by the presence of a multimodal distribution. These distributions can occur because a cell may have multiple copies of the sub-telomeric sequence used for STELA, with each copy located at a different chromosomal end (Baird et al. 2003). If the telomere length of these chromosomes is significantly different, then a gap can form between the two distributions which allows each of the multimodal distributions to be analysed separately. However, this difference between telomere lengths may not always be enough for individual distributions to be identified.

This was not the cause of the differences between the mean XpYp and 17p telomere lengths in the U266B1 cell line. While a heterogeneous telomere length distribution could be identified at the XpYp chromosomal end, the 17p telomere was not detectable using STELA. One explanation for this could be the deletion of the 17p arm of the chromosome in this cell line. Del(17p) is thought to be present in around 11% of MM patients (Avet-Loiseau et al. 2007), however there is nothing in the current literature to suggest that the U266B1 cell line has a del(17p) abnormality. Alternatively, the 17p telomere and/or the subtelomeric region containing the telomere-specific primer binding site could have been

completely eroded in this cell line due to cell division beyond the Hayflick limit. A chromosomal fusion event or de novo telomere seeding by telomerase would then stabilise the unprotected chromosomal end. Either way, the result would be loss of one or both primer binding sites and the inhibition of STELA at 17p telomere.

One further possibility is that a mutation exists at the 17pSeq1Rev primer binding site in U266B1 which reduces the efficiency of the PCR. To test these theories, Quantitative Fluorescent in situ hybridization (Q-FISH) could be used to show whether a telomere exists at the 17p chromosome end in U266B1 cells. If it does, then simply changing the subtelomeric telomere-specific primer that is used in the PCR could yield a STELA profile at the 17p chromosomal end. If it does not, then it may be possible that U266B1 cells have either an eroded 17p telomere or subtelomeric primer binding site.

Chromosomal Fusion: Having examined mean XpYp and 17p telomere length, chromosomal fusion events were then quantified for each cell line. We observed that the two cell lines with the shortest mean XpYp telomere length, NCI-H929 and RPMI-8226, also had the greatest number of detectable chromosomal fusion events. This result was the first evidence that a shorter mean telomere length may correlate with an increase in the frequency of fusion events in MM.

Although we could not produce a 17p STELA profile for the U266B1 cell line, comparing mean 17p telomere length against the frequency of chromosomal fusion in the remaining cell lines did not change our result. RPMI-8226 had the shortest mean 17p telomere length and the greatest frequency of chromosomal fusion events, while JJN-3 had the longest mean 17p telomere length and the lowest frequency of chromosomal fusion events.

However, it is important to note that mean telomere length was measured using STELA at only 2 of the potential 46 chromosomal ends. Because of this, it became impossible to know how the mean telomere length at other chromosomal ends impacted on genomic instability and the frequency of fusion events. Unfortunately, calculating every mean telomere length would not have been possible due to the requirement for a unique telomere-adjacent primer at each chromosomal end. Designing these telomere-specific primers would necessitate generating sequence information for the subtelomeric regions of every chromosome. For this reason, as well as the presence of a multimodal distribution within some of the 17p STELA profiles, we used mean XpYp telomere length as a standard throughout the chapter.

Problems also arise when comparing different cell lines, with the possibility that each cell line may have an inherent genomic instability that is independent of telomere length. To truly demonstrate that telomere length was the direct cause of the frequency of chromosomal fusion in MM, it became necessary to artificially reduce mean telomere length in each cell line and measure any change in the frequency of chromosomal fusion events.

4.5.2 Expression of DN-hTERT in Three MM Cell lines

Immortalised cell lines commonly express the enzyme telomerase as a method of maintaining telomere length and avoiding senescence. We have attempted to disrupt this mechanism by using DN-hTERT expression to reduce telomerase activity within three MM cell lines; JJN3, NCI-H929 and U266B1. We expected that mean telomere length would then decrease, forcing the cells into a state of telomere-driven crisis. Due to the differing p53 expression profiles of the three cell lines, it was also possible to examine the role that p53 expression played in telomere fusion and the escape from a telomere-driven crisis; JJN-3 ($p53^{neg}$), NCI-H929 ($p53^{wt}$) and U266B1 ($p53^{mut}$).

JJN-3: In the 15 days immediately following retroviral transduction of the JJN-3 cell line, the number of viable cells in the DN-hTERT population was much lower than that of the puromycin-resistant control. This may suggest that the resulting telomere shortening had a deleterious effect on cell viability, one that is not simply a result of the transduction procedure or puromycin selection. It could be the case that a lack of telomerase resulted in critical telomere shortening, causing additional cell death that is not experienced by the puromycin-resistant population.

However, it should also be noted that the retroviral titre was unknown before conducting the transduction procedure. This could also explain the difference if the DN-hTERT retroviral titre was lower than that of the puromycin-resistant control retroviral titre. If this were the case, fewer cells within the DN-hTERT population would contain the pBABE-puro vector which would then lead to greater cell death during the puromycin selection stage. Incorporating a fluorescent reporter gene within the viral vector may allow the relative expression of the puromycin resistance gene to be estimated in both the DN-hTERT and puromycin-resistant control JJN-3 populations (Soboleski, Oaks, and Halford 2005). If the expression of the fluorescent reporter, and by extension the puromycin-resistance gene, was equal in both the DN-hTERT and control cells, then it could be argued that any difference in cell viability after the addition of puromycin might be caused by the expression of DN-hTERT.

After transduction, telomerase activity was shown to be significantly decreased within the DN-hTERT population. This coincided with a decrease in mean XpYp telomere length from 3.10kb to 2.09kb by day 27. Surprisingly, mean XpYp telomere length did not fall further and was instead maintained at around 2.20kb for several weeks. Mean XpYp telomere length had even increased by the time the final sample was taken at day 48.

One possible explanation for this was that reactivation of telomerase had occurred, with the cells finding a way to bypass or outcompete DN-hTERT expression. Had telomerase activity been recorded again closer to day 48, it may have been possible to identify whether this mechanism was responsible for preventing further telomeric erosion. However, evidence to support this hypothesis was uncovered by Delhommeau et al. (2002) who managed to transduce the UT-7 and U937 leukaemia cell lines with a Mig-R vector which contained the DN-hTERT gene. Clonal populations were then grown, with 50% of these populations later being shown to have reactivated telomerase.

The authors identified two distinct mechanisms by which telomerase reactivation took place. In most of the clonal populations, the cause was identified as the loss of DN-hTERT expression following genomic instability. However, one clonal population had an increased hTERT expression which resulted in telomerase activity being maintained, despite continued DN-hTERT expression. In our experiments, performing a further telomerase assay at day 48 may have answered the question of whether telomerase had been reactivated, but it would have failed to answer by which (if either) mechanism this occurred.

Another possibility for overcoming a reduction in telomerase activation is that the cells are undergoing alternative lengthening of telomeres (ALT). This is a process by which cells lengthen telomeres in the absence of telomerase (Bryan et al. 1997). During ALT, telomeres are elongated using either a second telomere or extra-chromosomal telomeric DNA as a template for telomere synthesis. This process is known to occur in approximately 10% of cancers (Henson et al. 2009) and is thought to be implicated in at least one type of haematological malignancy (Samassekou 2013). Again, a measurement of telomerase activity towards the end of the experiment may have gone towards explaining whether this observed telomere elongation was telomerase-independent. However, ALT is an unlikely explanation for the telomere length

maintenance observed here. This mechanism has never been shown to occur in MM and the JJN-3 STELA profile does not fit with the heterogeneous telomere length profile described in ALT-dependent cells (Bryan et al. 1995).

NCI-H929: Unlike the JJN-3 cell line, NCI-H929 cells expressing the DN-hTERT construct appeared to die immediately after puromycin selection. This was preceded by a reduction in telomere length during the three weeks immediately after transduction. Although it may be argued that the cells could be sensitive to the effects of puromycin selection, the puromycin-resistant control cells appeared to recover quickly and did not experience the associated reduction in mean XpYp telomere length. There are also examples of other researchers successfully growing NCI-H929 cells in the presence of up to 2 µg/ml of puromycin following a transduction procedure (Amodio et al. 2012; Ling et al. 2012). It is therefore likely that cell death was the result of a decrease in telomere length brought on by a reduction in telomerase activity.

This result also shares similarities with a previous study involving the use of a drug which inhibits telomerase activity. Brennan et al. (2010) sorted $CD138^{neg}$ cells from the NCI-H929 cell line ($CD138^{neg}$ cells were thought to more closely resemble memory B cells) and grew them in the presence of Imetelstat. This is a 13-mer oligonucleotide which binds to the TERC subunit and inhibits the reverse transcriptase activity of telomerase. The growth of colonies treated with Imetelstat remained suppressed after 5 weeks. When we inhibited telomerase activity in the NCI-H929 cell line using a DN-hTERT construct, we also observed suppressed growth for the 3 weeks until the experiment was ended.

This is not the only example of crisis being triggered in a MM cell line using Imetelstat. Akiyama et al. (2003) managed to shorten telomere length and inhibit growth in the MM.1S myeloma cell line (also $p53^{wt}$). Shammas et al. (2008) used this same compound

to inhibit growth and induce cell death in the INA-6, ARP-1 and OPM-1 myeloma cell lines. This suggests that telomerase-inhibiting drugs offer a novel approach to treating MM, triggering a telomere-driven crisis by critically shortening telomere length.

U266B1: However, not all myeloma cell lines are affected by the activity of telomerase-inhibiting drugs. When treated with Imetelstat (Akiyama et al. 2003) the growth of U266B1 cells remained constant and the level of cell death was almost unchanged. This remained true even after 56 days of treatment, a confirmed reduction in telomerase activity and a >1kb reduction in telomere length. This result mirrored our own study, whereby U266B1 cells expressing the DN-hTERT construct did not experience inhibited growth. Cells showed a reduction in telomerase activity and a minor reduction in telomere length, but no change in growth that could not be attributed to the puromycin selection procedure.

By the end of our experiment, cell viability and growth had returned to pre-crisis levels and telomere length stabilised. Telomerase activity in the U266B1 cell line also remained lower than before transduction. This suggests that telomere length is being maintained, even with a significantly reduced telomerase activity. However, this could simply mean that low levels of telomerase activity are sufficient to maintain telomere length in U266B1 cells. This cell line is slow-growing, relative to the JJN-3 cell line, which may allow the small number of active telomerase enzymes to elongate telomeres at a faster rate than cell division occurs. One way to overcome this is to reduce telomerase activity further, possibly by combining DN-hTERT expression with a telomerase-inhibiting drug (e.g. Imetelstat). In this way, it would be possible to identify whether telomere length is maintained by the action of telomerase, or by an alternative mechanism.

ALT could also explain telomere length maintenance in the absence of telomerase activity. One of the phenotypic hallmarks of ALT is a significantly heterogeneous

telomere length profile (Bryan et al. 1995). The XpYp STELA profile of the U266B1 cell line appeared to meet this criterion, having a standard deviation that was much greater than that of the other MM cell lines examined here. The findings of (Shammas et al. 2003), whereby treatment with the drug Telomestatin reduced U266B1 telomere length and cell viability, could also be used to suggest an ALT mechanism. Telomestatin has previously been shown to inhibit the growth of fibroblast and osteosarcoma cell lines which were known to maintain telomere length using the ALT pathway (Kim et al. 2003; Fujimori et al. 2011).

However, it is important to note that Telomestatin works via several different mechanisms. Although the drug is thought to organise the 3′ overhang in such a way as to block reverse transcription and inhibit lengthening via ALT, is it also known to be responsible for downregulating c-MYC expression which leads to decreasing hTERT expression and thus lower telomerase activity (Mergny and Helene 1998; Grand et al. 2002). As well as showing that Telomestatin reduced the viability of U266B1 populations, Shammas et al. (2003) also demonstrated that the drug caused a ~98% reduction in telomerase activity.

Given these findings, it is more likely that the mean XpYp telomere length of our U266B1 population is being maintained by low level telomerase activity. Future work should therefore focus on further reducing telomerase activity, possible by combining DN-hTERT expression with telomerase inhibiting drugs. It is in this way that we would hope to force the cells into a state of telomere-driven crisis and examine both the effect of telomeric erosion on the frequency of chromosomal end-end fusion, as well as the ability of U266B1 cells to escape from crisis.

The Role of p53: JJN-3 cells do not express a functioning p53 protein ($p53^{neg}$) and the population was able to escape from a telomere-driven crisis. Meanwhile, NCI-H929 cells

express a functioning p53 protein ($p53^{wt}$) and the population was unable to escape from a telomere-driven crisis. From this data alone, it may seem that p53 has a prominent role in dictating whether cells can escape crisis. This is an important line of enquiry as around 13% of newly diagnosed MM cases are thought to involve TP53 abnormalities (Chng et al. 2007).

However, it is also important to consider the response of the U266B1 cell line. While these cells carry a mutation within the TP53 gene, U266B1 has been shown to express a functional p53 protein which can elicit a p21 response following genotoxic stress (Landau et al. 2012). As significant telomeric erosion did not take place following DN-hTERT expression, and so the cells did not experience a telomere-driven crisis, it was difficult to comment on the role that p53 expression may play in triggering U266B1 senescence.

While we may have been unable to cause a reduction in telomerase activity which triggered crisis in the U266B1 cell line, the use of Telomestatin by Shammas et al. (2003) managed to reduce telomerase activity by 98%. This telomerase inhibition caused telomeric shortening followed by cell death. In a similar manner to the NCI-H929 cell line, it may appear that the a functional p53 response prevented U266B1 cells from escaping a telomere-driven crisis. It is also worth remembering that (Akiyama et al. 2003)used Imetelstat to reduce telomerase activity in the $p53^{wt}$ MM.1S myeloma cell line, causing cell death.

While both examples within the literature backup our hypothesis, there are also examples that do not. (Shammas et al. 2008) demonstrated that telomerase inhibition caused the death of the ARP-1 and OPM-1 myeloma cell lines, both of which were shown elsewhere to be $p53^{neg}$ and $p53^{mut}/p21^{neg}$ respectively (Nardiello et al. 2011; Chauhan et al. 2007;

Gorgun et al. 2010). This may rule out the idea that p53 alone is necessary to induce senescence.

Chromosomal Fusion: Although we have described three different responses to the expression of DN-hTERT in three MM cell lines, the effect on the frequency of chromosomal fusion events was almost identical. Chromosomal fusion events were present in the JJN-3, NCI-H929 and U266B1 cells lines, but their frequency was relatively unchanged when compared to a puromycin-resistant control. Any minor changes between timepoints can be attributed to errors in the quantification of DNA samples or pipetting. Only the DN-hTERT-expressing NCI-H929 population showed any real change, with chromosomal fusion events being undetectable by day 23. However, this can simply be explained by the extent of cell death as viability decreased to 7.8%.

In the U266B1 cell line, a lack of change in the frequency of fusion events could be attributed to the fact that the mean XpYp telomere length does not alter significantly. However, the JJN-3 cell line does experience a significant decrease in the mean XpYp telomere length, but without the corresponding change in the frequency of chromosomal fusion events. One explanation for this is that the chromosomal ends under examination were simply not the ends undergoing fusion. The fusion assay performed here only examined 21 of the potential 46 chromosomal ends. It is therefore possible that the chromosomal ends which were not under examination have undergone a significantly greater level of erosion and fusion. However, it is unlikely that we would not have observed some form of existing change in the frequency of chromosomal fusion events after examining 46% of all chromosomal ends.

Another possible cause for this observation might have been the heterogeneity of the telomere length profiles in these cell lines. The cells with the shortest telomere lengths would enter a state of crisis much sooner than those with longer telomeres (Allsopp et

al. 1992; Capper et al. 2007). Although these cells then experience greater level of chromosomal fusion, this could be overshadowed by the bulk of the pre-crisis population. By the time the cells with the longest telomeres enter a state of telomere-driven crisis, those with shorter telomeres would have already escaped from crisis or undergone apoptosis. It is in this way that a heterogeneous telomere length profile may disguise the change in the frequency of chromosomal fusion events, by constantly having a stream of cells that are entering and escaping crisis. The easiest way to overcome this is to use a clonal population of cells. Clonal populations typically exhibit more homogeneous telomere length profiles, as each cell is derived from the same parental cell. In this way, all cells within a population will enter crisis at roughly the same time.

4.5.3 Expression of DN-hTERT in Three Clonal Populations of JJN-3 Cells

Telomerase Reactivation: Clonal populations of the JJN-3 cell line, each expressing DN-hTERT, were monitored during a telomere-driven crisis. Telomerase assays, performed before this period of crisis, show that telomerase activity was significantly decreased in each population. After crisis, telomerase activity had increased. This suggests that reactivation of telomerase had occurred, but does not explain the mechanism by which it had been triggered. Most surprising was the observation that telomerase activity had increased well beyond the base levels recorded in the clonal population of control JJN-3 cells.

One possible explanation for the reactivation of telomerase is that genomic instability and rearrangement, brought about by critical telomeric shortening, caused the gene encoding the DN-hTERT construct to be damaged and rendered inactive. Retroviral transduction works by integrating DNA into the host's genome. As telomere shortening led to chromosomal instability, it is possible that double-stranded DNA breaks caused the DN-hTERT gene to be interrupted and inactivated. Only a single cell would need to undergo this process, which would then express functional telomerase, allowing it to

outgrow the remaining cells. This mechanism was shown to occur preferentially in the Delhommeau et al. (2002) study mentioned previously. However, this mechanism fails to explain why telomerase activity was increased beyond the levels recorded in the control population. DN-hTERT inactivation should simply lead to telomerase activity returning to normal levels.

An alternative explanation is that hTERT expression was significantly increased, allowing functional hTERT to outcompete the inactivation caused by DN-hTERT expression. Although the signalling pathways connecting telomere length and telomerase activity are not fully understood, it is possible that critical telomere shortening results in an upregulation of the transcription factors responsible for synthesis of the telomerase subunits (De Boeck et al. 2009). Amplification of the hTERT locus could also occur via genomic rearrangements which place the gene under the control of a strong promotor. Both mechanisms would go towards explaining the significantly increased telomerase activity, relative to the control JJN-3 population, which was observed post-crisis.

Discerning which of these mechanisms are responsible for telomerase reactivation would first require identifying whether DN-hTERT expression had decreased or whether hTERT expression has increased. Delhommeau et al. (2002) achieved this by utilising a Mig-R1 plasmid that contained a green fluorescent protein (GFP) reporter gene alongside the DN-hTERT gene. It was concluded that loss of DN-hTERT expression also resulted in the loss of GFP expression. By repeating our experiment under these conditions, we could identify whether DN-hTERT expression has been lost (loss of GFP expression) or hTERT expression was simply outcompeting DN-hTERT expression (continued expression of GFP).

Demonstrating that telomerase activity increased significantly after crisis in clonal JJN-3 populations may go some way towards explaining the behaviour of the JJN-3 bulk

population described earlier (***see 4.5.2 – Expression of DN-hTERT in Three MM Cell Lines***). We previously recorded a decrease in telomerase activity immediately after DN-hTERT expression, but then failed to measure telomerase activity again as telomere length began to stabilise and then increase. Here, in a clonal JJN-3 population expressing DN-hTERT, we have demonstrated that telomerase activity eventually increased after a period of telomere-driven crisis. This adds weight to the argument that telomerase reactivation is responsible for the increase in mean XpYp telomere length that was observed in the non-clonal JJN-3 population.

Telomere Length: The effect on telomere length in the three clonal JJN-3 populations, caused by this increase in telomerase activity, was examined by measuring mean telomere length during a period of telomere-driven crisis. We observed that an escape from crisis was marked by an increase in mean XpYp and 17p telomere length, as well as increased heterogeneity within the STELA profile of each clonal population. These telomere dynamics closely mirrored the results observed when clonal populations of a colorectal carcinoma cell line were monitored though a telomere-driven crisis (Jones et al. 2014). This increasing telomere length and heterogeneity could simply have been caused by the cells within each clonal population entering crisis at slightly different times, resulting in each JJN-3 cell being at a different stage of telomere elongation. Continuing to monitor mean telomere length in the clonal population would have been the simplest way of proving this hypothesis, with the expectation that a homogeneous telomere length distribution would eventually reform (albeit with a longer mean telomere length) once each cell has undergone telomerase-dependent telomere elongation.

However, it is also possible that the STELA profile would remain heterogeneous. This could be caused by differing levels of telomerase activity within each post-crisis cell of the population, with greater telomerase activity in a cell leading to a longer telomere length. The idea that greater telomerase activity leads to greater mean telomere length

was explored in Cristofari and Lingner (2006), whereby the telomerase activity of HeLa cells was increased artificially by transduction with a vector encoding hTERT. This resulted in the transduced cells having a longer telomere length than control cells with a lower telomerase activity. Although we could record the average telomerase activity across each of the JJN-3 clonal populations, we do not know the levels of telomerase activity in the individual cells. As it is not possible to measure and compare the expression of telomerase between single cells, it would be necessary to sub-clone cells from the post-crisis JJN-3 DN-hTERT population and compare the relative telomerase activities of each new sub-clonal population. This is the only way that we would be able to determine whether the heterogeneous telomere length distribution is caused by a significant difference in telomerase activity between the individual post-crisis cells.

When comparing the three clonal populations, mean telomere length could not be used to predict when the cells would enter a state of telomere-driven crisis. As clone A entered crisis, it had a mean XpYp telomere length of 1.44kb. This is in comparison to clone C which had a shorter mean XpYp telomere length of 0.76kb. When 17p telomere length was measured instead, this order was reversed. Clone C began crisis with a longer mean 17p telomere length of 2.41kb, while clone A had a shorter mean 17p telomere length of 1.77kb. This suggests that measuring the mean telomere length of a single chromosomal end is not enough to accurately predict when crisis will occur. The telomere lengths of each chromosome within a cell will differ, as will the telomere lengths between identical chromosomes in different cells. This leads to each clonal population having distinct telomere length profile, with different critically-shortened telomeres initiating crisis in each clone. Predicting crisis therefore requires all chromosomal ends to measured, as well as each STELA profile to be considered as a whole. This includes the presence of multimodal distributions and the number of critically shortened telomeres.

Frequency of Fusion: However, we could demonstrate that mean telomere length directly correlated with the frequency of chromosomal fusion events observed throughout the genome. While we were unable to measure mean telomere length at any of the chromosomal ends targeted by the 16p-family or 21q-family of fusion primers, we were still able to compare the mean telomere length at the 17p and XpYp chromosomal ends with their respective frequency of fusion events.

From this, it became clear that the XpYp chromosome was involved in relatively few fusion events throughout each of the three JJN-3 clonal populations. This may be explained in clone A and clone B by the longer pre-crisis mean XpYp telomere length, relative to the mean of the 17p lower distribution at the same timepoint. Lin et al. (2010) demonstrated that chromosomal fusion events, identified and sequenced from the peripheral blood mononuclear cells of CLL patients, contained an average of 5.8 TTAGGG repeats. More than 30% of the fusions identified in CLL patients did not contain a single TTAGGG repeat between the two chromosomal ends. It is therefore unlikely that the mean XpYp telomere lengths recorded here, which in clone A and clone B never fell below 1.40kb, would be short enough for a detectable number of XpYp fusion events to occur. The homogeneous XpYp STELA profiles recorded in all three JJN-3 clonal populations further explain the lack of fusion events, with no individual XpYp telomere falling below 350bp in length (about 58 TTAGGG repeats).

By contrast, the mean of the lowest distribution of 17p telomere ends in each clone almost always fell below 1.00kb. Also, due to the heterogeneous distribution of telomere lengths within the 17p STELA profiles, a significant proportion of individual telomere ends fell towards the bottom of the profile. This suggest that a greater number of critically shortened 17p telomeres are present. It is therefore more likely in these cells for a 17p chromosome to exist where the telomere has been eroded completely, when compared to an XpYp chromosome with >58 telomeric repeats.

When the total number of chromosomal fusion events were examined in each clonal population, it became clear that the 17p and 21q-family of chromosomal ends experienced the greatest frequency of fusion. For the 21q-family primer, this may be explained by the large number of chromosomal targets (21q, 1q, 2q, 5q, 6q, 6p, 8p, 10q, 13q, 17q, 19p, 19q, 22q and the 2q13 interstitial telomeric locus). The greater the number of primer binding sites, the greater the chance of observing a fusion event. However, this does not remain true for the 16p-family primer which also has many chromosomal targets (16p, 1p, 9p, 12p, 15q, XqYq and the 2q14 interstitial locus). Also, the 17p primer only binds at one chromosomal end, but the number of chromosomal fusion events are almost equal to the 21q-family primer. In fact, most chromosomal fusion events observed were interchromosomal between the 17p and the 21q-family.

This high frequency of fusion involving either the 17p or 21q-family of chromosomal ends may go some way towards explaining the incidence of certain chromosomal abnormalities in MM. Walker et al. (2010) analysed 372 MM patient DNA samples and showed that several common abnormalities involve the 21q-family of chromosomal ends. Del(13q) was shown to occur in 59% of MM patients, resulting in the loss of the retinoblastoma protein (RB1). Del(6p) was shown to occur in 33% of cases, resulting in a deregulation of cyclin D3. And del(8p) was shown to occur in 25% of MM cases. The frequency of del(17p) in MM is so significant that it is now listed by the revised ISS as a potential indicator of high-risk disease (Palumbo et al. 2015). This is particularly relevant for the JJN-3 cell line, as these cells are known lack p53 expression (Hurt et al. 2006).

This protein, which is necessary for triggering senescence after telomeric erosion, is located close to the end of the 17p chromosomal arm (Deng, Chan, and Chang 2008). Loss of p53 may explain why this cell line, unlike the NCI-H929 cell line which has normal p53 expression, can avoid the senescence that should be triggered by critical telomere shortening. As around 11% of MM cases are thought to involve del(17p) (Avet-Loiseau

et al. 2007), disruption of p53 and the ability of MM cells to escape from a telomere-driven crisis may be a significant event that requires further exploration.

4.5.4 Conclusions

The aim of this chapter was to determine whether myeloma cell lines had the capacity to avoid senescence after undergoing a telomere-induced crisis. This was achieved through the expression of DN-hTERT which reduced the activity of telomerase, the enzyme responsible for adding telomeric repeats to the ends of chromosomes. Although DN-hTERT expression had little effect on the viability and mean XpYp telomere length of the U266B1 cell line, reducing telomerase activity in the NCI-H929 cell line caused a reduction in both viability and mean XpYp telomere length. It was concluded that NCI-H929 cells were unable to escape from a telomere-driven crisis and underwent apoptosis after critical telomere shortening. However, the JJN-3 cell line did not undergo apoptosis, even after a significant reduction in mean XpYp telomere length. Instead, JJN-3 cells managed to escape from a telomere-driven crisis by reactivation of the telomerase enzyme. Although the p53 expression profiles of each cell line may explain their different responses to critical telomere shortening, more works needs to be done in this area before a definitive conclusion can be established.

We also used clonal populations of JJN-3 cells, each expressing DN-hTERT, to demonstrate that critically shortening telomeres results in an increased frequency of chromosomal end-end fusion. We therefore conclude that, in the JJN-3 myeloma cell line, a causal relationship exists between mean XpYp or 17p telomere length and the frequency of chromosomal end-end fusion. Our results also point towards a significant number of these events involving the 17p and 21q-family of chromosome ends. Due to the high incidence of del(17p) and 21-family abnormalities in MM, we believe that critical telomere shortening may play a significant role in driving genomic instability and the progression of MM.

Chapter 5

Using the PARP Inhibitors Rucaparib and Olaparib to Prevent Escape from a Telomere-Driven Crisis

5.1 Abstract

PARP inhibition is primarily used in the treatment of BRCA-deficient ovarian cancer, with preliminary results suggesting that it may also prove effective in treating other homologous recombination-deficient cancers. PARP inhibitors are thought to work by interfering with the cells ability to repair DNA damage, specifically by preventing PARP family proteins from targeting single- and double-strand DNA breaks for repair. Due to the increased frequency of chromosomal end-end fusion during a telomere-driven crisis, we attempted to use the PARP inhibitors Rucaparib and Olaparib as a method of restricting the erroneous repair of telomere-deficient chromosomal ends. We hypothesised that PARP inhibition would interfere with the alt-NHEJ pathway, limiting the formation intrachromosomal fusion events which have previously been identified as necessary for facilitating an escape from a telomere-driven crisis.

Clonal populations of JJN-3 cells were transfected with a DN-hTERT construct and grown in culture until they entered a state of telomere-driven crisis. The cells were then exposed to varying concentrations of either Rucaparib or Olaparib indefinitely. We observed that treating this MM cell line with either 7.50μM Rucaparib or 3.75μM Olaparib prevented an escape from crisis, whilst having little effect on the growth of a control population of JJN-3 cells. XpYp telomere length measurements, recorded immediately before the onset of crisis, showed that treating these cells with 3.75μM Olaparib resulted in a significantly longer mean XpYp telomere length when compared to untreated controls. However, no significant difference in mean XpYp telomere length was recorded when cells were instead treated with 7.50μM Rucaparib. Measuring the frequency of

chromosomal end-end fusion in Rucaparib- and Olaparib-treated JJN-3 subpopulations also failed to identify a significant change, relative to control subpopulations. We therefore concluded that PARP inhibitors show promise as a novel treatment for MM, although attempts to identify the mechanism by which Rucaparib and Olaparib prevented an escape from crisis proved inconclusive. We argue that PARP inhibition may hold particular therapeutic value when used to treat high-risk MM patients, previously identified as having a shorter mean XpYp telomere length, due to the increased genetic instability that might otherwise drive cancer progression.

5.2 Introduction

DNA repair pathways play an important role in maintaining genomic stability by preventing single- and double-strand DNA breaks from inducing harmful mutations and rearrangements which may potentially result in the formation of cancer. DNA damage can often prevent a cell from passing through the various cell cycle checkpoints that regulate eukaryotic cell division. These checkpoints offer an opportunity to repair DNA damage, with failure to do so resulting in cell cycle arrest (Otto and Sicinski 2017). Single-strand DNA breaks are often identified for repair by PARP1 and PARP2, members of the poly (ADP-ribose) polymerase (PARP) family which use NAD^+ as a substrate to modify target proteins (Caldecott 2014). Depending on the PARP family member, these modifications can either result in the addition of individual ADP-ribose units called MAR (mono (ADP-ribose)) or branched chains of ADP-ribose units called PAR (poly (ADP-ribose)). In the case of PARP1 and PARP2, PAR modification is used to recruit several scaffold proteins to the site of a single-strand DNA break, most notably XRCC1 which is required for enlisting the enzymatic components of the base excision repair (BER) pathway (Hanzlikova et al. 2017).

PARP1 has also been implicated in several double-strand DNA break repair pathways, although its roles within these pathways are not fully understood. PARP1 is known to be active at stalled and collapsed replication forks, recruiting MRE11 which is necessary for initiating the homologous recombination (HR) pathway and restarting DNA replication (Yang et al. 2004; Bryant et al. 2009). PARP1 is also thought to compete with Ku70/Ku80 for binding at double-strand DNA breaks, shifting repair away from the classical non-homologous end joining (NHEJ) pathway and towards a PARP1-driven alternative-NHEJ pathway (Mansour et al. 2013). This is important as the alt-NHEJ pathway has been implicated in the escape of cells from a telomere-driven crisis (Jones et al. 2014). Meanwhile PARP3, another PARP family member which modifies target proteins through

the addition of PAR, is thought to recruit Ku80 to double-strand DNA breaks which then accelerates repair via the classical-NHEJ pathway (Rulten et al. 2011).

However, only 3 of the 17 PARP family proteins have been shown to regulate DNA damage repair pathways. The remaining members play a diverse array of roles, ranging from stress granule assembly to promotors of cell migration (Vyas and Chang 2014). PARP5a and PARP5b (also known as Tankyrase-1 and Tankyrase-2) are even known to positively regulate telomere length by modifying TRF1, a key member of the shelterin complex. This activity inhibits the binding of TRF1 at the telomere, allowing telomere-elongation by the enzyme telomerase (Smith and de Lange 2000; Cook et al. 2002). The importance of each PARP protein also varies, with knockdown studies concluding that some PARP family members are more necessary than others for survival. For example, Vyas et al. (2013) demonstrated that PARP4 and PARP6 knockdown barely impacted HeLa cell viability, while PARP8 knockdown almost completely inhibited cell growth.

Due to the numerous functions carried out by the PARP family proteins, PARP inhibition continues to be investigated as a method of treating cancers. However, PARP inhibition is currently used exclusively to treat those cancers which are BRCA1/BRCA2 deficient (Fong et al. 2009). Breast cancer susceptibility (BRCA) proteins are an integral part of the HR pathway, recruiting RAD51 to sites of double-strand DNA breaks (Powell and Kachnic 2003). This protein then forms a complex with MRE11 and NBS1, triggering cell cycle arrest and enabling the damaged DNA ends to be processed (Uziel et al. 2003). In the case of BRCA-deficiency, cells must rely on the more error-prone NHEJ pathways for repair of double-strand DNA breaks (Patel, Sarkaria, and Kaufmann 2011). It is thought that inhibition of PARP prevents the modification and recruitment of target proteins to a single-strand DNA break, whilst still allowing PARP to bind DNA. In this way, PARP becomes trapped at sites of DNA damage and prevents the repair of single-strand DNA breaks. An overwhelming number of double-strand DNA breaks then form which the cell, unable to undergo HR due to BRCA-deficiency, then incorrectly repairs

via NHEJ pathways. The resulting genetic damage is overwhelming and is thought to promote apoptosis (Konecny and Kristeleit 2016; Patel, Sarkaria, and Kaufmann 2011).

Attempts are now being made to treat HR-normal cancers by inhibiting both PARP family proteins and the HR pathway. It has been demonstrated *in vitro* that supressing phosphoinositide 3-kinase (PI3K) expression induces BRCA1/BRCA2 downregulation, thus sensitising breast cancer cell lines to PARP inhibition (Ibrahim et al. 2012). The use of bortezomib in multiple myeloma (MM) cell lines was also shown to suppress the HR pathway indirectly, resulting in apoptosis when these cells were exposed to the PARP inhibitor Veliparib (Neri et al. 2011). However, *in vivo* studies which combine inhibitors of HR and PARP have never been attempted. Instead, most clinical trials involving PARP inhibitors have focused on the treatment of those breast and ovarian cancers which are already HR-deficient (Tutt et al. 2010; Ledermann et al. 2014).

The first PARP inhibitor to be approved for use in the treatment of cancer was Olaparib. Marketed as Lynparza, this PARP inhibitor is used to treat BRCA-deficient ovarian cancer (Kim et al. 2015). However, several other PARP-inhibiting drugs are currently undergoing clinical trials. One of these is Rucaparib which is currently undergoing phase III trials, as well as also having been granted accelerated approval by the USA FDA for use in BRCA-deficient ovarian cancer (Knepper, Saller, and Walko 2017). Due to the homologous nature of the catalytic domains within the PARP family, PARP inhibitors such as Rucaparib and Olaparib very rarely bind to a single PARP protein (Ame, Spenlehauer, and de Murcia 2004). As well as binding to PARP1, PARP2, PARP3, PARP4, PARP15 and PARP16 *in vitro*, Rucaparib and Olaparib also have their own individual targets. Rucaparib has been shown to bind at the catalytic sites of PARP5a, PARP5b and PARP10. While Olaparib also binds to PARP12 (Wahlberg et al. 2012).

In the previous chapter, we demonstrated that a telomere-driven crisis in the JJN-3 MM cell line caused a significant increase in the frequency of chromosomal end-end fusion events. This eventually resulted in the reactivation of telomerase and the escape of these cells from crisis. Here, we have attempted to reduce the frequency of fusion by employing the PARP inhibitors Rucaparib and Olaparib. We hypothesised that the inhibition of PARP1, PARP2 and PARP3 would not only result in catastrophic genomic damage as single-strand DNA breaks went unrepaired, but also that the frequency of chromosomal end-end fusion would decrease as the efficiency of double-strand DNA break repair was reduced. It was considered that this might change the types genomic rearrangements that occur in the context of telomere dysfunction, which in turn may modulate the ability of cells to escape from a telomere-driven crisis.

We observed that clonal JJN-3 populations, each expressing DN-hTERT, were unable to escape from crisis when treated with either 7.50μM Rucaparib or 3.75μM Olaparib. A change in the pre-crisis mean telomere length was also recorded, whereby those subpopulations treated with 3.75μM Olaparib had a longer mean XpYp telomere length than control subpopulations. However, Rucaparib treatment had little effect on mean XpYp telomere length, and no significant change in the frequency of chromosomal end-end fusion was observed for either PARP inhibitor. We therefore concluded that Rucaparib and Olaparib could prevent the escape of JJN-3 cells from a telomere-driven crisis, possibly by impeding their progression through the cell cycle and by selectively killing those cells with critically shortened telomeres. However, further work would be required to explain these results, especially given the wide range of PARP family proteins targeted by Rucaparib and Olaparib.

5.3 Aims of the Chapter

We hypothesised that PARP inhibition may interfere with the ability of MM cells to identify and repair DNA damage, including those pathways which recognise telomere-deficient chromosomal ends as double-strand DNA breaks. We anticipated that there might be a change in the types of telomere fusion detected, with the frequency of intrachromosomal fusion reduced as the alt-NHEJ pathway was disrupted. It was thought that this would impact on the ability of MM cells to escape from a telomere-driven crisis. In this chapter, clonal populations of JJN-3 DN-hTERT cells were exposed to the PARP inhibitors Rucaparib and Olaparib. In this way, we aimed to drive the cells into a telomere-driven crisis, whilst simultaneously limiting their capacity to repair telomere-deficient chromosomal ends. We expected that treatment with either Rucaparib or Olaparib would reduce the frequency of chromosomal end-end fusion and modulate the ability of cells to escape from a telomere-driven crisis.

5.4 Results

5.4.1 Exposure of PARP Inhibitors to Clonal Populations of JJN-3 DN-hTERT Cells During a Telomere-Driven Crisis

Three clonal populations of JJN-3 cells, each expressing DN-hTERT, were exposed to the PARP inhibitors Rucaparib or Olaparib during a telomere-driven crisis. Although clone B and clone C were used in the previous chapter, clone A could not be used here due to an insufficient number of cells. We therefore utilised a fourth clonal population of JJN-3 DN-hTERT cells (clone D), the characteristics of which matched those of the other DN-hTERT clonal populations used in these experiments (see ***Supplementary Figures 8, 9, 10 and 11***). A clonal JJN-3 population expressing only the pBABE-puro vector (control clone) was also exposed to the same concentrations of Rucaparib and Olaparib. This control enabled the effects of the PARP inhibitors to be evaluated in a JJN-3 clonal population with longer, functional telomeres than those undergoing a telomere-driven crisis.

Each clonal JJN-3 population was split into twelve subpopulations before the onset of crisis, allowing different concentrations of Rucaparib or Olaparib to be added. Cells were grown in 1.00μM - 7.50μM of Rucaparib or 0.50μM - 3.75μM of Olaparib. Controls for each DN-hTERT clone included an untreated subpopulation and a subpopulation which was exposed to 0.1% (v/v) DMSO. The DMSO control was necessary as both Rucaparib and Olaparib were dissolved in DMSO, thereby allowing the effects of the PARP inhibitors to be distinguished from that of the solvent. The growth of each subpopulation was statistically compared to that of the untreated control using one-way ANOVA with Dunnett's post-hoc test. This allowed the effects of Rucaparib and Olaparib on cell growth to be examined, comparing the growth of each treated subpopulation to that of the untreated controls. Significance was defined as $p < 0.05$.

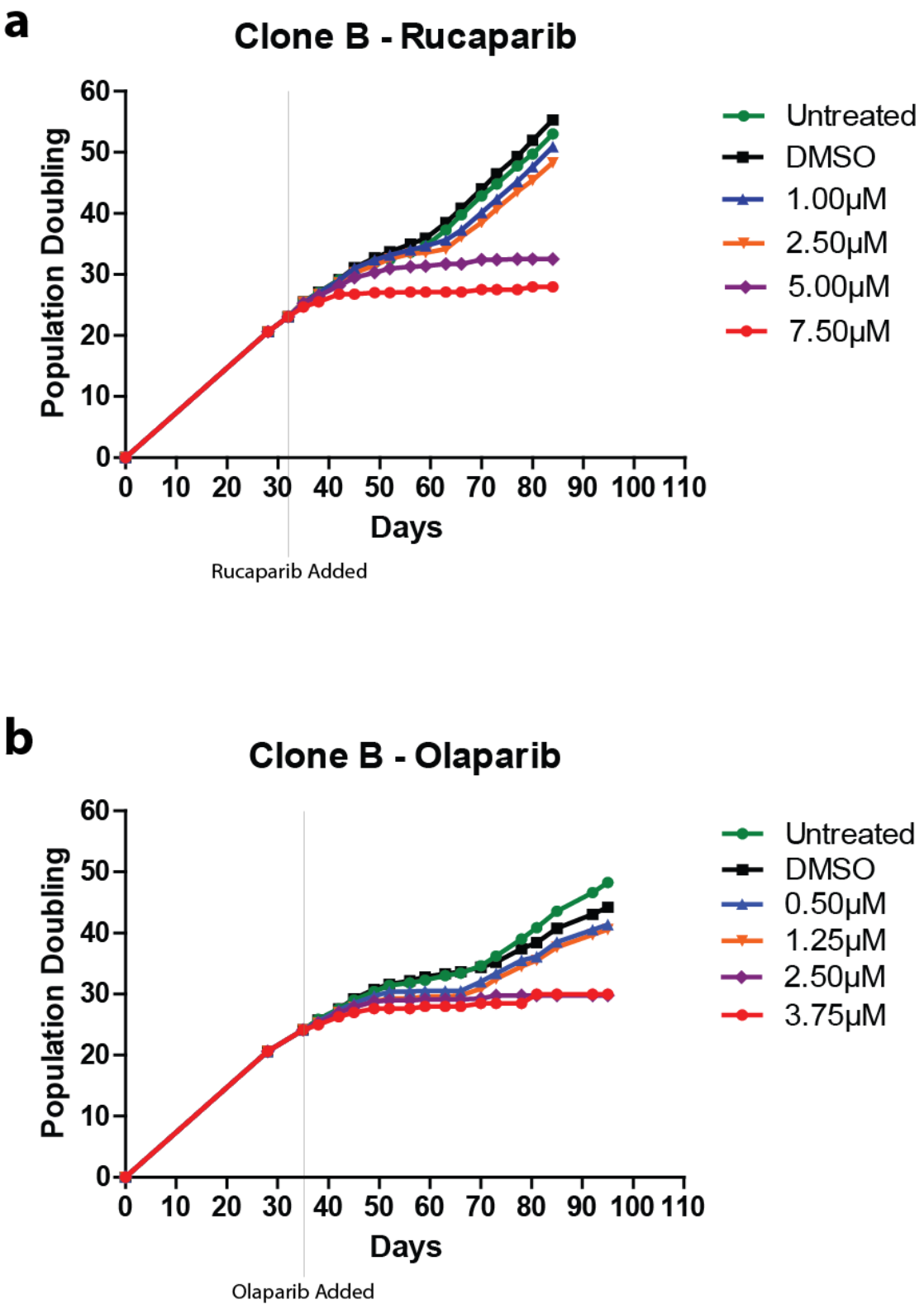

Figure 5.1 - The Effect of Rucaparib and Olaparib Treatment on the Growth of JJN-3 DN-hTERT Clone B Subpopulations During a Telomere-Driven Crisis

The growth of JJN-3 DN-hTERT clone B subpopulations were monitored during a telomere-driven crisis. During this time, each subpopulation underwent treatment with either Rucaparib or Olaparib at the stated concentrations. Each PARP inhibitor was added at the time indicated on the graph, with media/PARP inhibitor replaced every 2-3 days. Each subpopulation was exposed to the approprite PARP inhibitor for the remainder of the experiment. As DMSO was the solvent used to prepare each solution of PARP inhibitor, a control population was exposed to the appropriate growth media containing 0.1% DMSO (v/v).

After following the clone B cells for a period of 84 days (***Figure 5.1a***), the untreated subpopulation escaped from a telomere-driven crisis and underwent a total of 53.0 population doublings (PD) before being terminated. Culturing the cells in either 1.00μM or 2.50μM Rucaparib did not prevent an escape from crisis, but did have a negative impact on the growth of the subpopulations. Clone B cells which were grown in the presence of 1.00μM Rucaparib underwent a total of 50.9 PDs ($p = 0.06$), whereas those grown in 2.50μM Rucaparib underwent only 48.3 PD ($p = 0.007$) before being terminated. The subpopulations which were grown in either 5.00μM or 7.50μM Rucaparib failed to escape from a telomere-driven crisis. Those grown in 5.00μM Rucaparib experienced 32.5 PDs by day 84 ($p = 0.01$), while those grown in 7.50μM Rucaparib experienced only 28.0 PDs ($p = 0.002$).

Treating clone B subpopulations with Olaparib had a similar effect to that of Rucaparib, although Olaparib was used at half the concentration of Rucaparib (***Figure 5.1b***). The untreated subpopulation managed to escape from crisis and was recorded as having undergone 48.3 PDs by day 95. Culturing the cells in concentrations of either 0.50μM or 1.25μM Olaparib did not impact on their ability to escape from a telomere-driven crisis, but higher concentrations of Olaparib did have a negative impact on the growth of each subpopulation. By day 95, cells treated with 0.50μM Olaparib had undergone 41.4 PDs ($p = 0.001$) while the 1.25μM Olaparib subpopulation had undergone 40.6 PDs ($p = 0.0002$). Those subpopulations which were grown in either 2.50μM or 3.75μM Olaparib did not manage to escape from a telomere-induced crisis. The 2.50μM subpopulation underwent a total 29.78 PDs ($p = 0.004$), while the 3.75μM subpopulation underwent a total of 30.0 PDs ($p = 0.0009$).

Clone C differed from clone B in the sense that 5.00μM Rucaparib did not prevent the cells escaping from a telomere-driven crisis, although it did delay the escape (***Figure 5.2a***). The final PD attained by the untreated clone C subpopulation was 38.4 by day 99. Again, higher concentrations of Rucaparib had greater impacts on cell growth. The

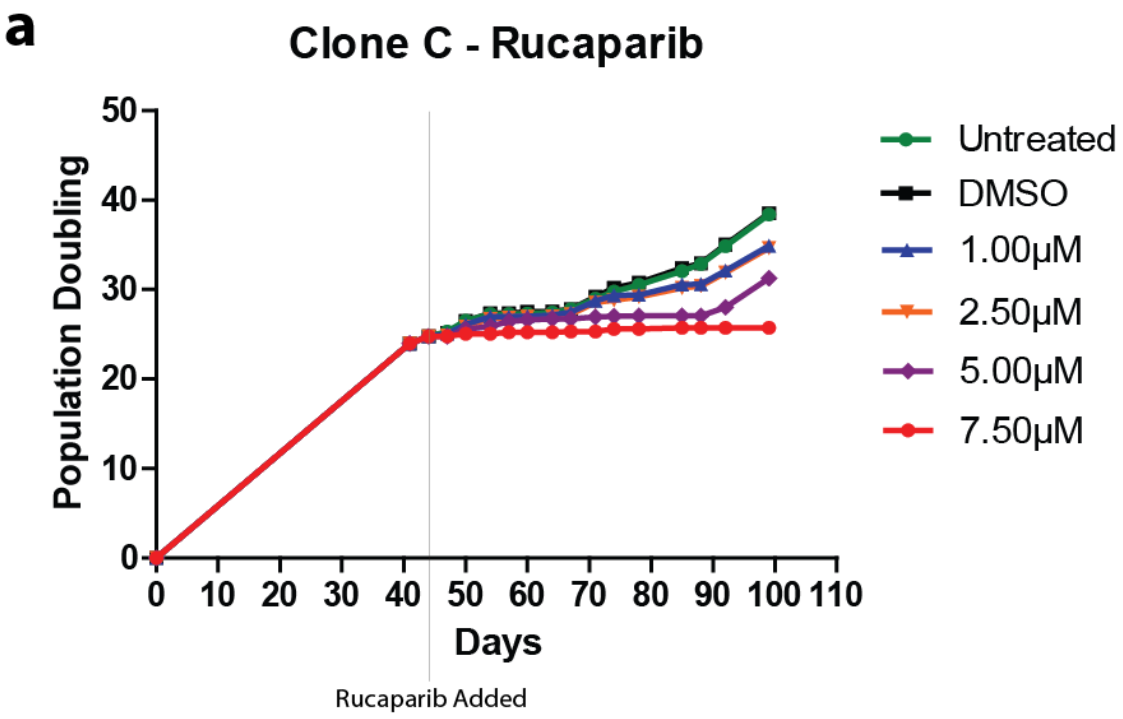

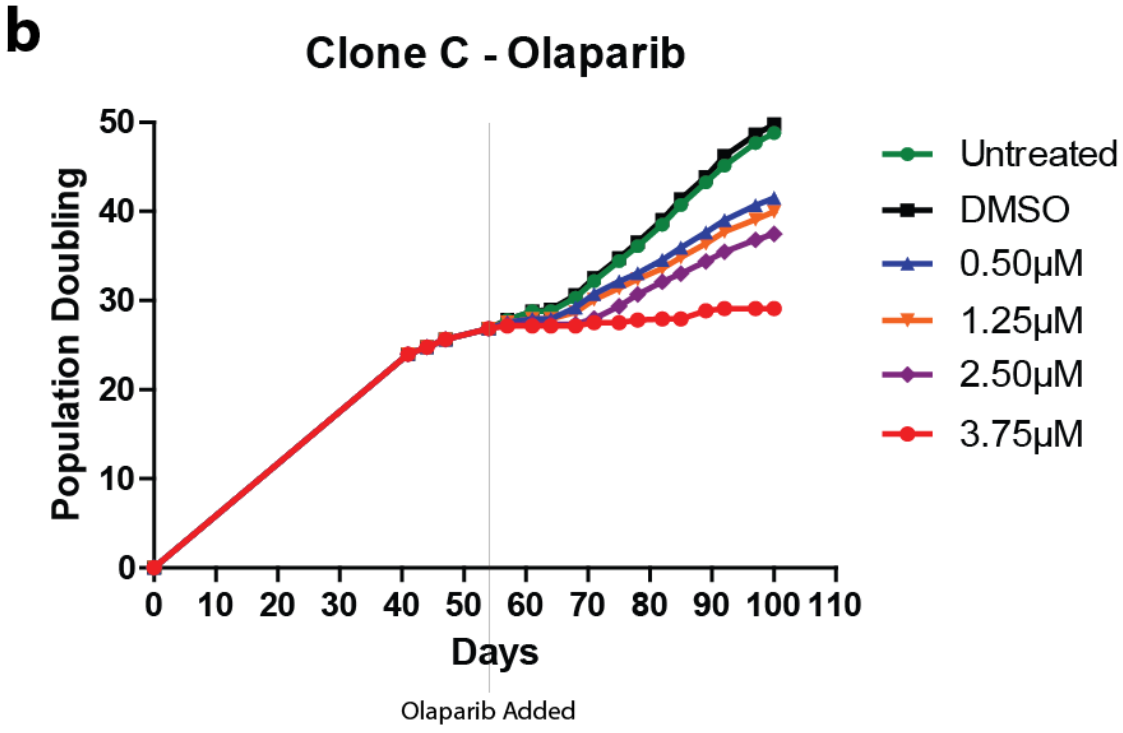

Figure 5.2 - The Effect of Rucaparib and Olaparib Treatment on the Growth of JJN-3 DN-hTERT Clone C Subpopulations During a Telomere-Driven Crisis

The growth of JJN-3 DN-hTERT clone C subpopulations were monitored during a telomere-driven crisis. During this time, each subpopulation underwent treatment with either Rucaparib or Olaparib at the stated concentrations. Each PARP inhibitor was added at the time indicated on the graph, with media/PARP inhibitor replaced every 2-3 days. Each subpopulation was exposed to the approprite PARP inhibitor for the remainder of the experiment. As DMSO was the solvent used to prepare each solution of PARP inhibitor, a control population was exposed to the appropriate growth media containing 0.1% DMSO (v/v).

1.00μM Rucaparib subpopulation managed just 34.9 PDs by day 99 ($p = 0.02$), while the 2.5μM and 5.00μM Rucaparib subpopulations managed just 34.6 PDs and 31.3 PDs respectively ($p = 0.008$; $p = 0.005$). Regardless, all but the 7.50μM Rucaparib-treated subpopulation escaped from a telomere-driven crisis ($p = 0.003$). However, the various subpopulations did not all escape from crisis at the same time. The untreated, DMSO, 1.00μM and 2.50μM-treated subpopulations all appeared to escape from crisis by day 71. While the 5.00μM subpopulation did not escape from crisis until day 92.

Treating clone C cells using Olaparib had a similar effect to treatment with Rucaparib, in that all but the 3.75μM Olaparib subpopulation escaped from a telomere-driven crisis (***Figure 5.2b***). By day 100, the untreated subpopulation had reached a final PD of 48.8. Meanwhile, the growth of the 0.50μM, 1.25μM and 2.50μM Olaparib subpopulations was marginally but significantly inhibited ($p = 0.004$; $p = 0.004$; $p = 0.002$), with higher concentrations of Olaparib leading to greater growth inhibition. However, the cells treated with these concentrations of Olaparib were still able to escape from a telomere-driven crisis. Growth of those cells treated with 3.75μM Olaparib was not completely absent during crisis. Between the onset of crisis at day 54 and the final measurement on day 100, the total PD of the 3.75μM subpopulation increased by 2.3. However, the growth of this population was significantly reduced when compared to the untreated subpopulation ($p = 0.004$) and had stopped completely between day 92 and 100.

When clone D was treated with Rucaparib, only the 7.50μM subpopulation failed to escape from a telomere-driven crisis (***Figure 5.3a***). As with the previous two clones, Rucaparib had a slight but significant impact on population growth and marginally increased the time it took for each subpopulation to escape from a telomere-driven crisis. The untreated subpopulation underwent 47.7 PD by day 90, while the 1.25μM, 2.50μM and 5.00μM subpopulations underwent only 44.7, 44.1 and 41.7 PD respectively ($p = 0.005$; $p = 0.006$; $p = 0.02$). The untreated,1.00μM and 2.50μM Rucaparib

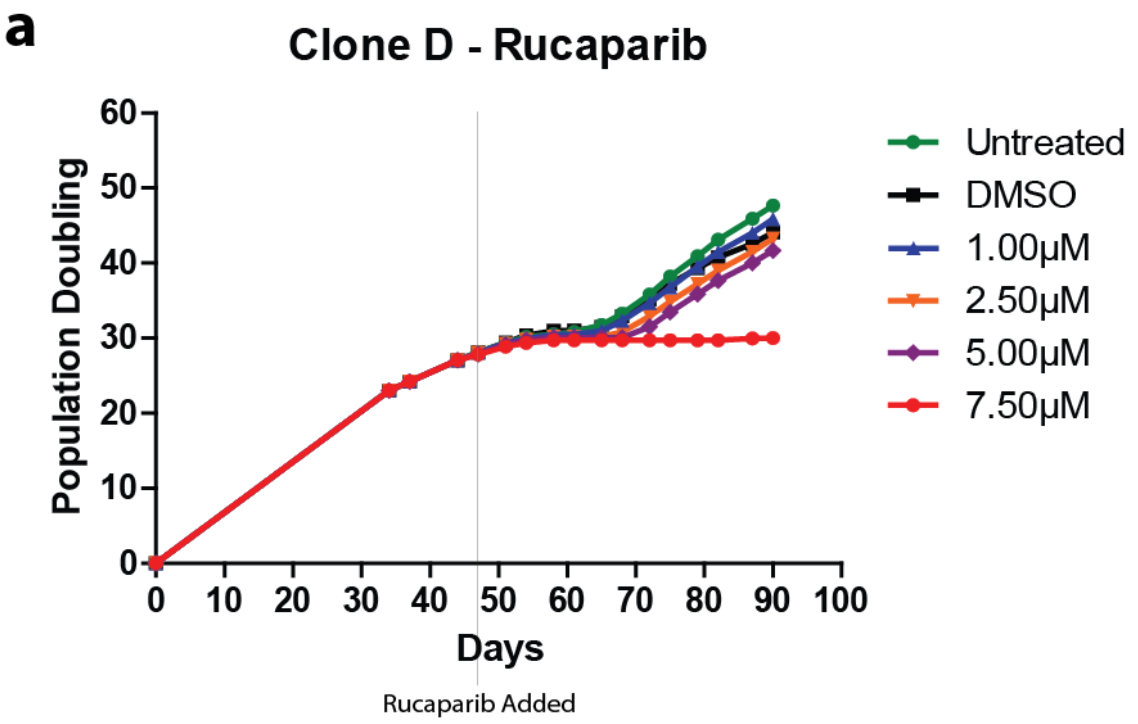

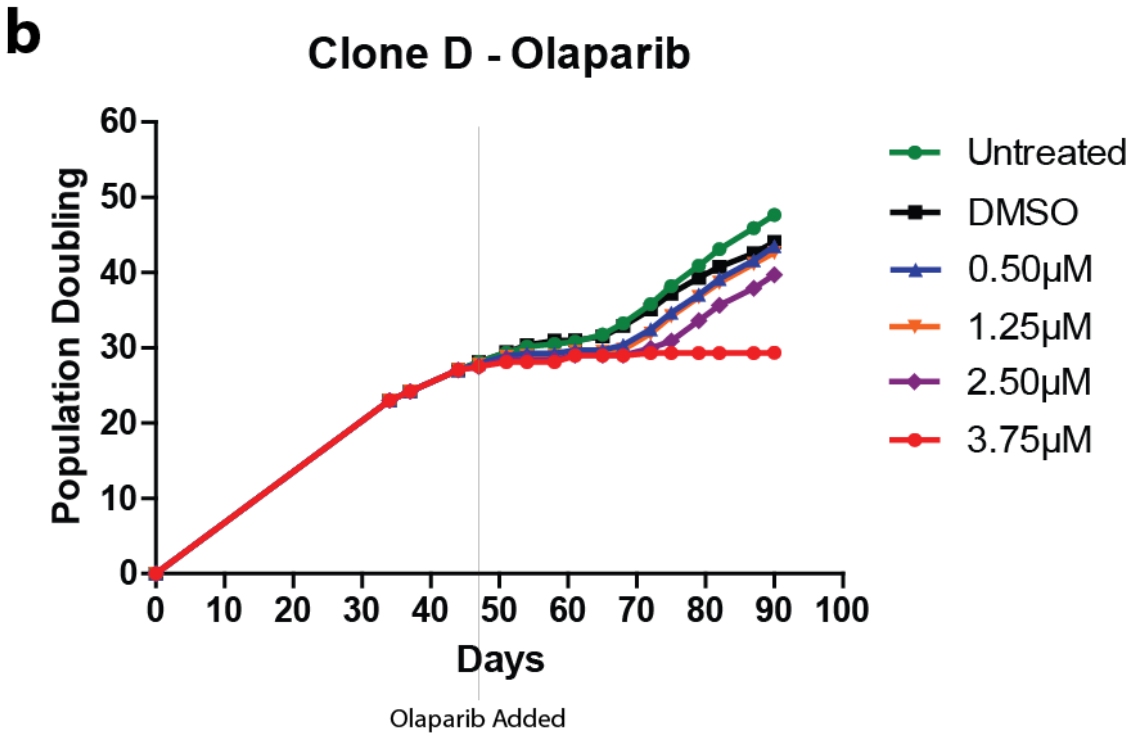

Figure 5.3 - The Effect of Rucaparib and Olaparib Treatment on the Growth of JJN-3 DN-hTERT Clone D Subpopulations During a Telomere-Driven Crisis

The growth of JJN-3 DN-hTERT clone D subpopulations were monitored during a telomere-driven crisis. During this time, each subpopulation underwent treatment with either Rucaparib or Olaparib at the stated concentrations. Each PARP inhibitor was added at the time indicated on the graph, with media/PARP inhibitor replaced every 2-3 days. Each subpopulation was exposed to the approprite PARP inhibitor for the remainder of the experiment. As DMSO was the solvent used to prepare each solution of PARP inhibitor, a control population was exposed to the appropriate growth media containing 0.1% DMSO (v/v).

subpopulations appeared to escape from crisis by day 65, while the 5.00μM subpopulation did not escape until day 72.

This result was mirrored upon treatment with Olaparib, whereby the 3.75μM subpopulation failed to escape from a telomere-driven crisis (***Figure 5.3b***). Higher concentrations of Olaparib resulted in significantly reduced growth. The final PD on day 90 for the untreated subpopulation was 47.7, while the final PDs for the 0.50μM, 1.25μM and 2.50μM subpopulations were 43.5, 42.7 and 39.7 respectively (*p = 0.001; p = 0.001; p = 0.002*). The 3.75μM-treated subpopulation failed to escape crisis, undergoing no more than 29.4 PDs (*p = 0.01*).

Treatment of a JJN-3 control population (transfected with an empty vector) with Rucaparib or Olaparib allowed the effects of the drugs to be evaluated. This control clone did not express DN-hTERT and so maintained its telomere length above that which could lead to a telomere-driven crisis. When the control clone was exposed to Rucaparib, growth was never completely inhibited (***Figure 5.4a***). Even at 7.50μM Rucaparib, growth continued at a steady rate. This contrasted with the DN-hTERT clones, whereby treatment with 7.50μM Rucaparib during a telomere-driven crisis prevented any further growth of the subpopulation. As with the previous DN-hTERT clones, increasing concentrations of Rucaparib significantly decreased the overall growth of the subpopulation. The final PD of the untreated subpopulation was 58.5, while the final PDs of the 1.25μM, 2.50μM, 5.00μM and 7.50μM Rucaparib subpopulation were 54.6, 52.5, 49.5 and 45.8 respectively (*p = 0.001; p = 0.001; p = 0.001; p = 0.001*). Treatment with Olaparib also failed to completely inhibit growth, but caused a significant decrease in the growth of each subpopulation (***Figure 5.4b***). The final PD of the untreated subpopulation was 58.5, while the 1.00μM, 2.50μM, 5.00μM, and 7.50μM subpopulations reached final PDs of 52.4, 50.6, 46.3 and 42.3 respectively (*p = 0.0008; p = 0.0008; p = 0.0007; p = 0.0008*).

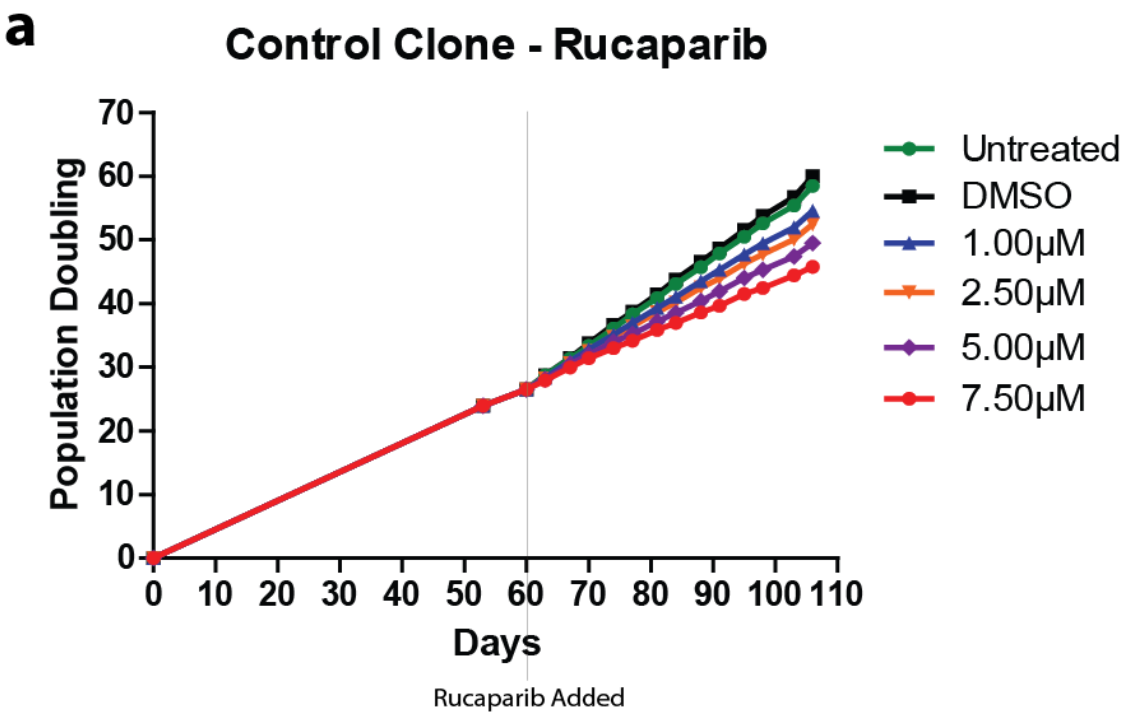

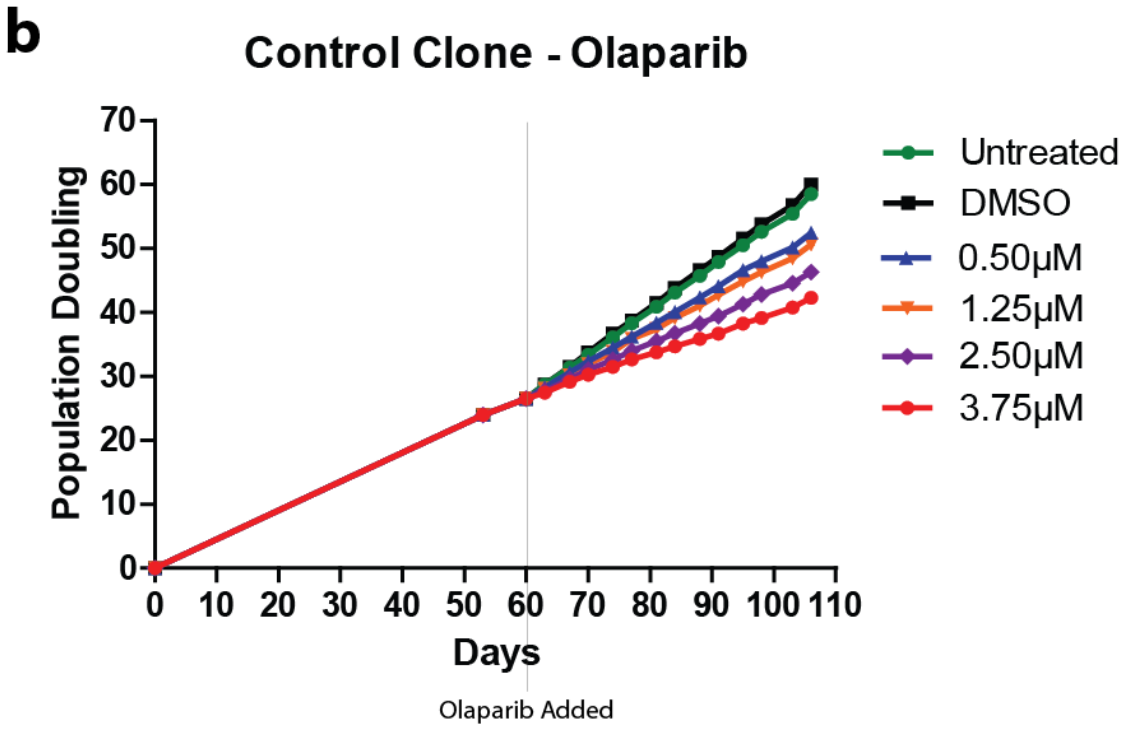

Figure 5.4 - The Effect of Rucaparib and Olaparib Treatment on the Growth of JJN-3 Control Clone Subpopulations

The growth of JJN-3 clonal subpopulations, which did not express DN-hTERT, were monitored during exposure to the PARP inhibitors Rucaparib or Olaparib at the stated concentrations. Each PARP inhibitor was added at the time indicated on the graph, with media/PARP inhibitor replaced every 2-3 days. Each subpopulation was exposed to the appropriate PARP inhibitor for the remainder of the experiment. As DMSO was the solvent used to prepare each solution of PARP inhibitor, a control population was exposed to the appropriate growth media containing 0.1% DMSO (v/v).

5.4.2 Identifying the Efficiency of PARP Inhibition by Rucaparib and Olaparib in Clonal Populations of JJN-3 Cells

Western blotting was used to try and identify the extent of PARP inhibition caused by the different concentrations of Rucaparib and Olaparib. PARP is activated in response to DNA damage, resulting in the production of PAR. We therefore used hydrogen peroxide (H_2O_2) to induce DNA damage in our clonal subpopulations and then measured the quantities of PAR produced by the cells. It was in this way that we expected to show whether PARP inhibition would influence the quantities of PAR produced. We also quantified the retinoblastoma protein and Chk-1 protein levels in each subpopulation as these are also involved in coordinating a DNA damage response. We first began by using the control JJN-3 clone to identify the necessary concentration of H_2O_2 required to cause a DNA damage response (***Figure 5.5a***). Surprisingly, PAR could not be detected even when the cells were exposed to 10nM H_2O_2 for 30 minutes. Regardless of the quantity of H_2O_2 added, no change in the levels of retinoblastoma protein was detected. However, when compared to the -H_2O_2 control, Chk-1 levels increased dramatically when H_2O_2 was added.

Although PAR could not be detected in the control cells, western blotting was still performed on each clonal subpopulation using 2.5nM of H_2O_2. However, it was again demonstrated that PAR could not be detected in the remaining JJN-3 DN-hTERT clonal populations. In clone B, the quantities of Retinoblastoma protein appeared to increase as Rucaparib and Olaparib were added (***Figure 5.5b***). As the concentration of Rucaparib was increased from 1.00μM to 7.50μM, the intensity of the retinoblastoma band increased relative to that of the untreated subpopulation. Regardless of the concentration of Olaparib used, the intensity of the bands was always greater than that of the untreated subpopulation. Although treatment with Rucaparib and Olaparib had little effect on the quantities of Chk-1 measured, not treating the cells with H_2O_2 resulted in no Chk-1 being detected.

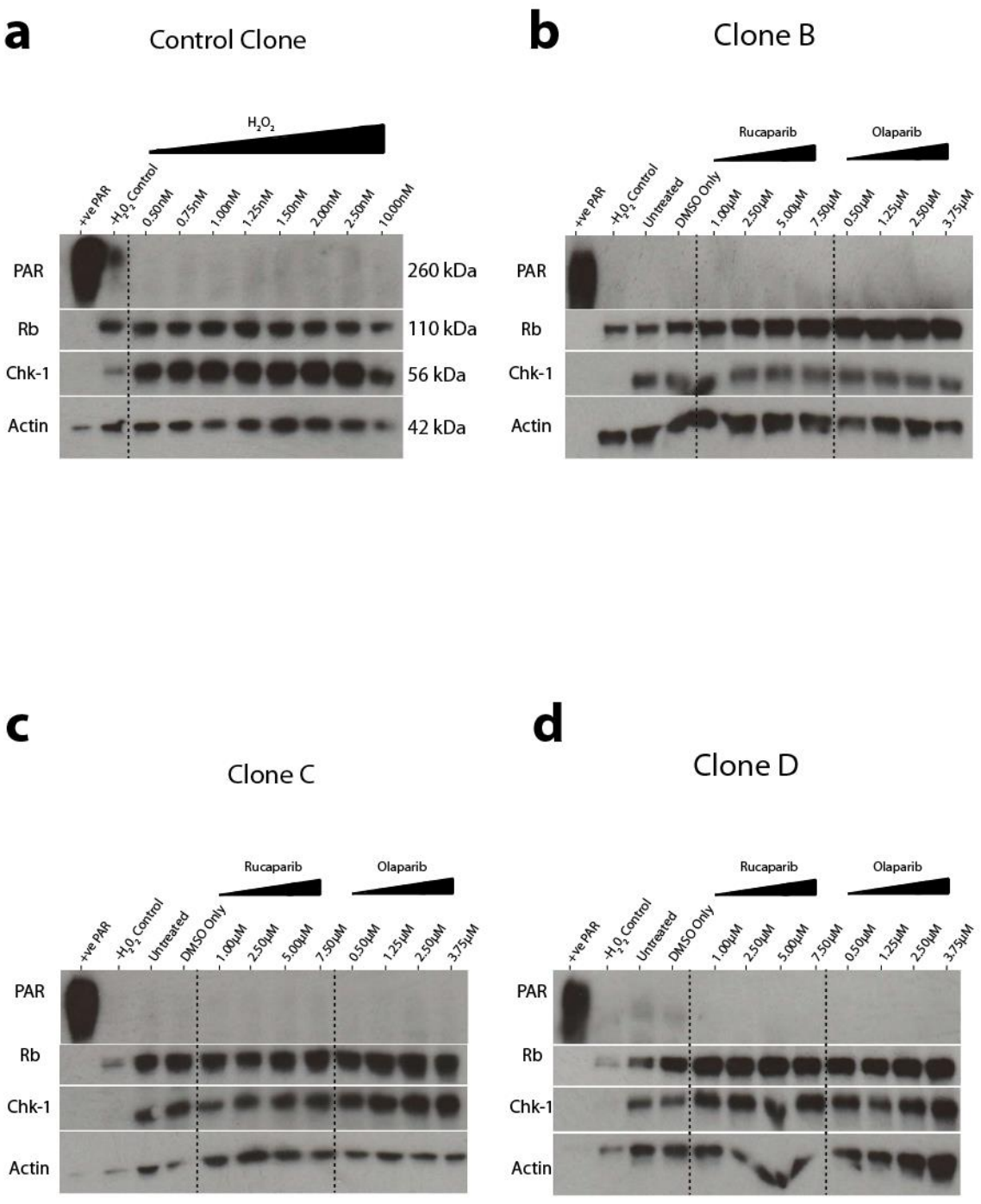

Figure 5.5 - Identifying the Extent of DNA Damage During H_2O_2 Treatment, as well as the Efficiency of PARP Inhibition by Rucaparib and Olaparib

(a) Subpopulations of the JJN-3 control clone were exposed to the stated concentrations of H_2O_2 for 30 minutes before being harvested. Western blotting was performed to try and identify the optimal concentration of H_2O_2 which would elicit PAR expression by PARP family proteins. In total, 10μg of protein were loaded per lane **(b)**, **(c)** and **(d)** Subpopulations of the stated JJN-3 DN-hTERT clone were exposed to either Rucaparib or Olaparib for 48 hours. Cells were then resuspended in fresh media/PARP inhibitor. H_2O_2 was added at a concentration of 2.50nM and the cells were left for 30 minutes before harvesting. Western blotting was performed to try and identify and change in the expression of PAR protein, retinoblastoma protein or Chk-1 protein in response to PARP inhibition. In total, 10μg of protein were loaded per lane.

When clone C subpopulations were treated with either Rucaparib or Olaparib, the intensity of the retinoblastoma protein band did not appear to change from that of the untreated control subpopulation (***Figure 5.5c***). The same could be said for Chk-1 which did not change when either Rucaparib or Olaparib were added. Although the quantities of retinoblastoma protein and Chk-1 protein were reduced in the -H_2O_2 control, the actin band was also reduced in comparison to the Rucaparib- and Olaparib-treated bands. This suggests that a technical artefact may have been the cause of this difference, as opposed to action of hydrogen peroxide. This problem was also observed when treating clone D, whereby the intensity of the retinoblastoma and Chk-1 bands in the -H_2O_2 control were reduced, but the actin band was also reduced (***Figure 5.5d***).

5.4.3 The Effect of PARP Inhibition on Mean XpYp Telomere Length

After the growth of each clonal JJN-3 population had arrested (***Figure 5.1, Figure 5.2 and Figure 5.3***), a period that was thought to indicate that the cells had entered a state of telomere-driven crisis, samples of cells were taken for DNA extraction. STELA was performed to measure the mean XpYp telomere length of each clonal subpopulation at a specific timepoint, while the cells were under the effects of either Rucaparib or Olaparib. One-way ANOVA with Dunnett's post-hoc test was used to determine if the differences in mean XpYp telomere length were statistically significant (***Figure 5.9***)

After performing STELA on samples of the Rucaparib- and Olaparib-treated clone B cells, mean XpYp telomere length was calculated for each subpopulation. It appeared that the presence of Rucaparib had no significant effect on the mean XpYp telomere lengths of cells, relative to the control subpopulations (***Figures 5.6a and 5.9a***). Meanwhile, treating clone B cells with either 1.25μM Olaparib or 3.75μM Olaparib resulted in a significant increase in mean XpYp telomere length when compared to the untreated subpopulation (***Figures 5.6b and 5.9a***).

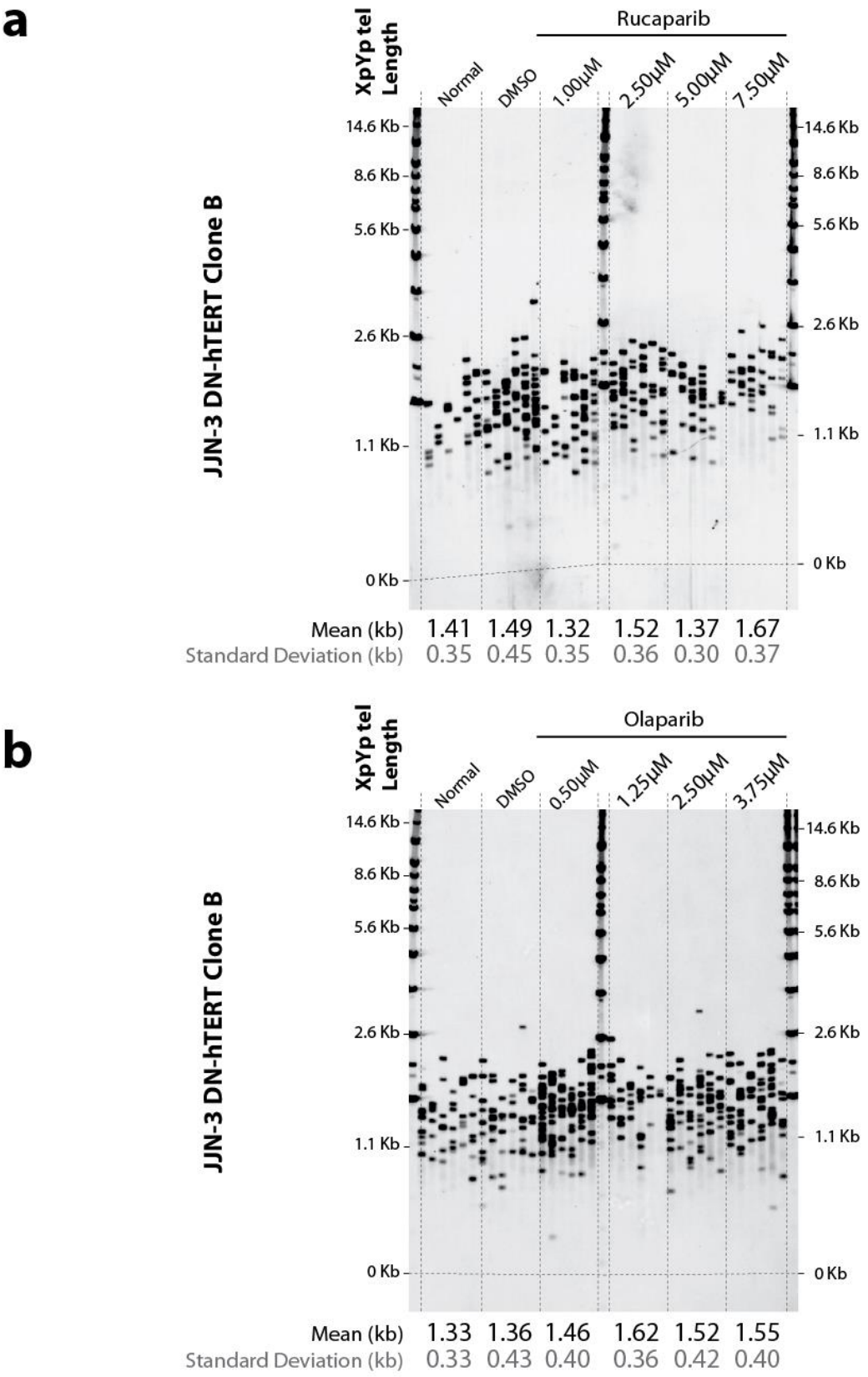

Figure 5.6 - Mean XpYp Telomere Length After Treatment with the PARP Inhibitors Rucaparib or Olaparib

JJN-3 DN-hTERT clone B was grown in the presence of either Rucaparib or Olaparib. On day 52 (Rucaparib - see ***figure 5.1a***) or day 56 (Olaparib - see ***figure 5.1b***), samples of cells were taken for DNA extraction. Mean XpYp telomere length was then calculated using STELA. Images show the raw STELA profiles for cells grown in the presence of either **(a)** Rucaparib or **(b)** Olaparib.

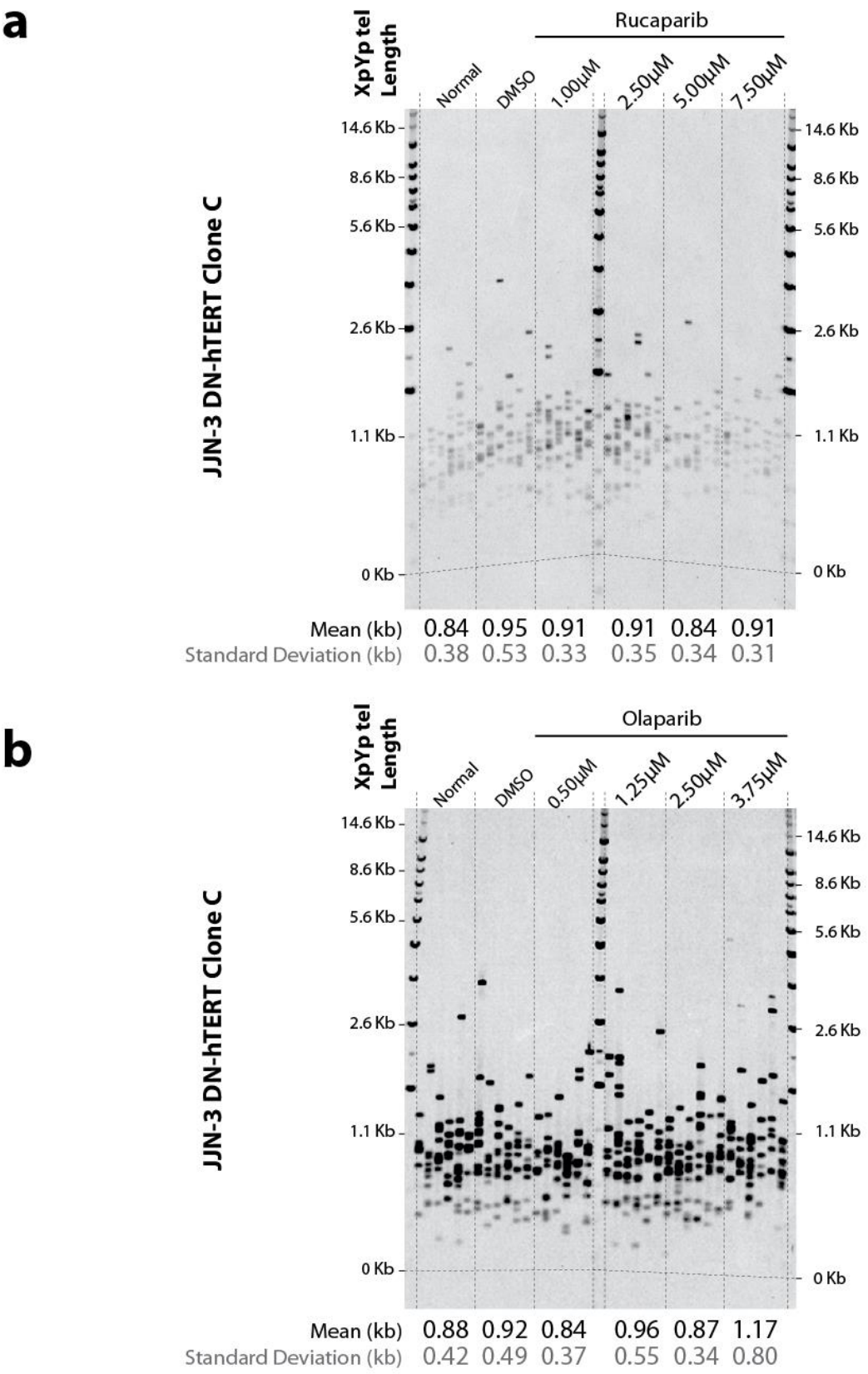

Figure 5.7 - Mean XpYp Telomere Length After Treatment with the PARP Inhibitors Rucaparib or Olaparib

JJN-3 DN-hTERT clone C was grown in the presence of either Rucaparib or Olaparib. On day 67 (Rucaparib - see ***figure 5.2a***) or day 61 (Olaparib - see ***figure 5.2b***), samples of cells were taken for DNA extraction. Mean XpYp telomere length was then calculated using STELA. Images show the raw STELA profiles for cells grown in the presence of either **(a)** Rucaparib or **(b)** Olaparib.

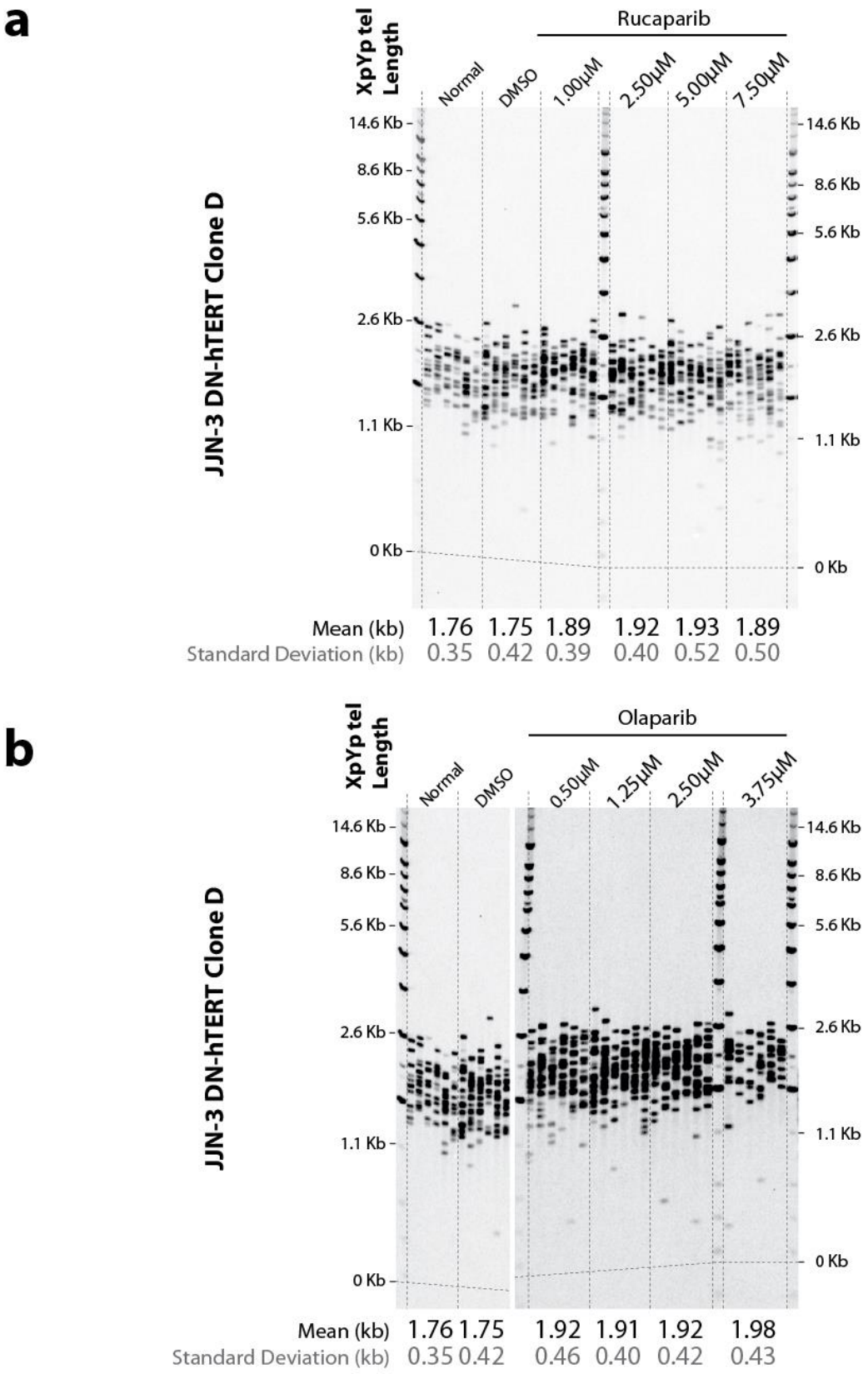

Figure 5.8 - Mean XpYp Telomere Length After Treatment with the PARP Inhibitors Rucaparib or Olaparib

JJN-3 DN-hTERT clone D was grown in the presence of either Rucaparib or Olaparib. On day 58 (Rucaparib - see ***figure 5.3a***) or day 58 (Olaparib - see ***figure 5.3b***), samples of cells were taken for DNA extraction. Mean XpYp telomere length was then calculated using STELA. Images show the raw STELA profiles for cells grown in the presence of either **(a)** Rucaparib or **(b)** Olaparib.

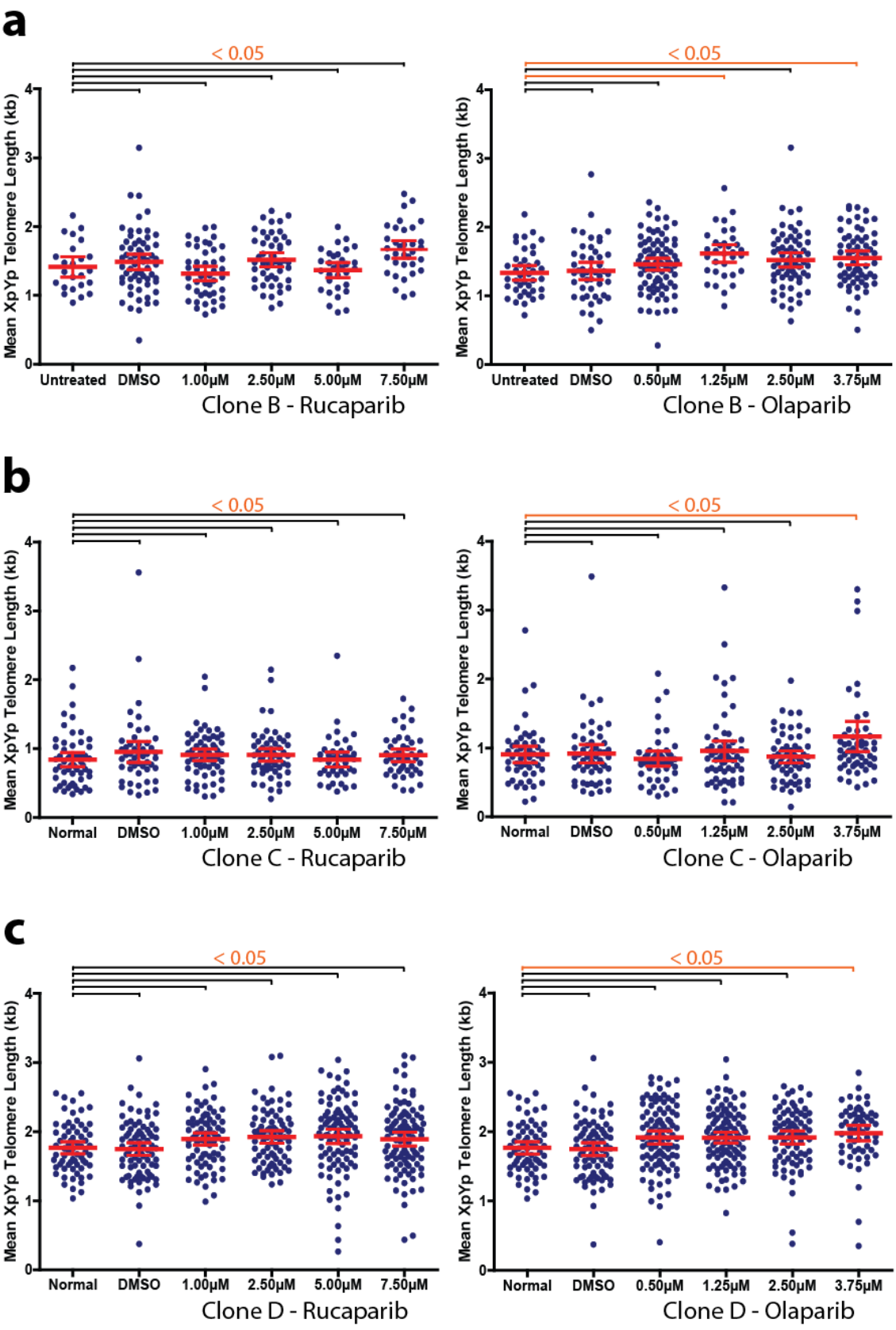

Figure 5.9 - The Mean XpYp Telomere Length of JJN-3 DN-hTERT Clones After Treatment with the PARP Inhibitors Rucaparib or Olaparib

Graphical representations of the STELA profiles depicted in *Figure 5.5*, *Figure 5.6* and *Figure 5.7* **(a)** Clone B **(b)** Clone C **(c)** Clone D grown in the presence of either Rucaparib or Olaparib. The mean telomere length for each patient is shown in red alongside the uper and lower 95% confidance intervals. Significance was determined using one-way ANOVA with Dunnett's post-hoc test. Significance >0.05 was signified with black lines, while significance <0.05 was signified with orange lines.

Samples of clone C cells which were exposed to Rucaparib were taken on day 67, while samples of cells cultured with Olaparib were taken on day 61. In the Rucaparib-treated subpopulations, no significant difference in mean XpYp telomere length was observed (***Figures 5.7a and 5.9b***). Clone C subpopulations varied in their response to Olaparib treatment, with only the 3.75μM Olaparib-treated subpopulation having a significantly greater mean XpYp telomere length than both the untreated and DMSO-treated subpopulations (***Figures 5.7b and 5.9b***).

Finally, samples of each Rucaparib- and Olaparib-treated clone D subpopulation were collected on day 58. As with clone B and clone C, Rucaparib had little effect on mean XpYp telomere length, relative to the control subpopulation (***Figures 5.8a and 5.9c***). Only 3.75μM Olaparib had an effect, resulting in a significantly increased mean XpYp telomere length relative to the control subpopulation (***Figures 5.8b and 5.9c***).

5.4.4 The Effect of PARP Inhibition on the Frequency of Chromosomal Fusion Events

After measuring mean XpYp telomere length in the Rucaparib- and Olaparib-treated subpopulations of three JJN-3 DN-hTERT clones, chromosomal fusions were quantified to determine the effect that PARP inhibition had on the frequency of fusion events. As in chapter 4, this analysis focused on the fusion events involving the 17p, XpYp, 16p-family and 21q-family of chromosomal ends. However, due to the large quantities of data collected and the low frequency of XpYp and 16p-family fusion events, this chapter emphasised the presence of 17p-21q-family fusion events and their change in frequency after treatment with Rucaparib or Olaparib. A complete listing of all the fusion events recorded is shown in ***Supplementary Figure 12*** (clone B – Rucaparib), ***Supplementary Figure 13*** (clone B – Olaparib), ***Supplementary Figure 14*** (clone C – Rucaparib), ***Supplementary Figure 15*** (clone C – Olaparib), ***Supplementary Figure 16*** (clone D – Rucaparib) and ***Supplementary Figure 17*** (clone D – Olaparib).

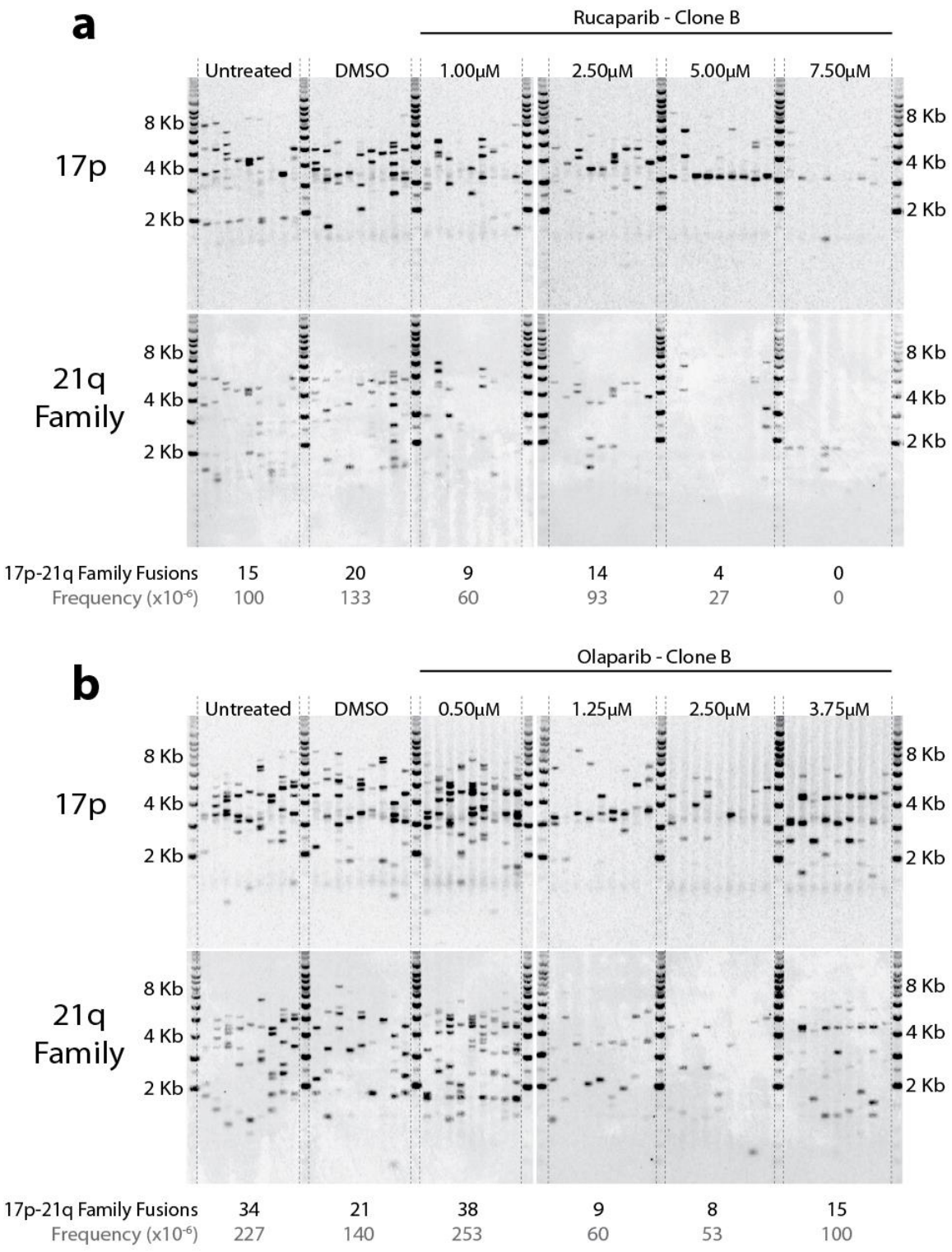

Figure 5.10 - The Change in the Frequency of Chromosomal Fusion Events for JJN-3 DN-hTERT Clone B, Grown in the Presence of Either Rucaparib or Olaparib

JJN-3 DN-hTERT clone B was grown in the presence of either **(a)** Rucaparib or **(b)** Olaparib. On day 52 (Rucaparib - see ***figure 5.1a***) or day 56 (Olaparib - see ***figure 5.1b***), samples of cells were taken for DNA extraction. In total, 900ng of DNA were examined per time point. The frequency of chromosomal fusion was estimated by dividing the number of observable fusion bands by the number of input molecules (around 150,000 cells). Visualisation of these events was performed using the oligonucleotide probes 17p6, XpYpO-G, 16p1 and 21q1. Only the 17p and 21q-Family of chromosomal fusion events are shown.

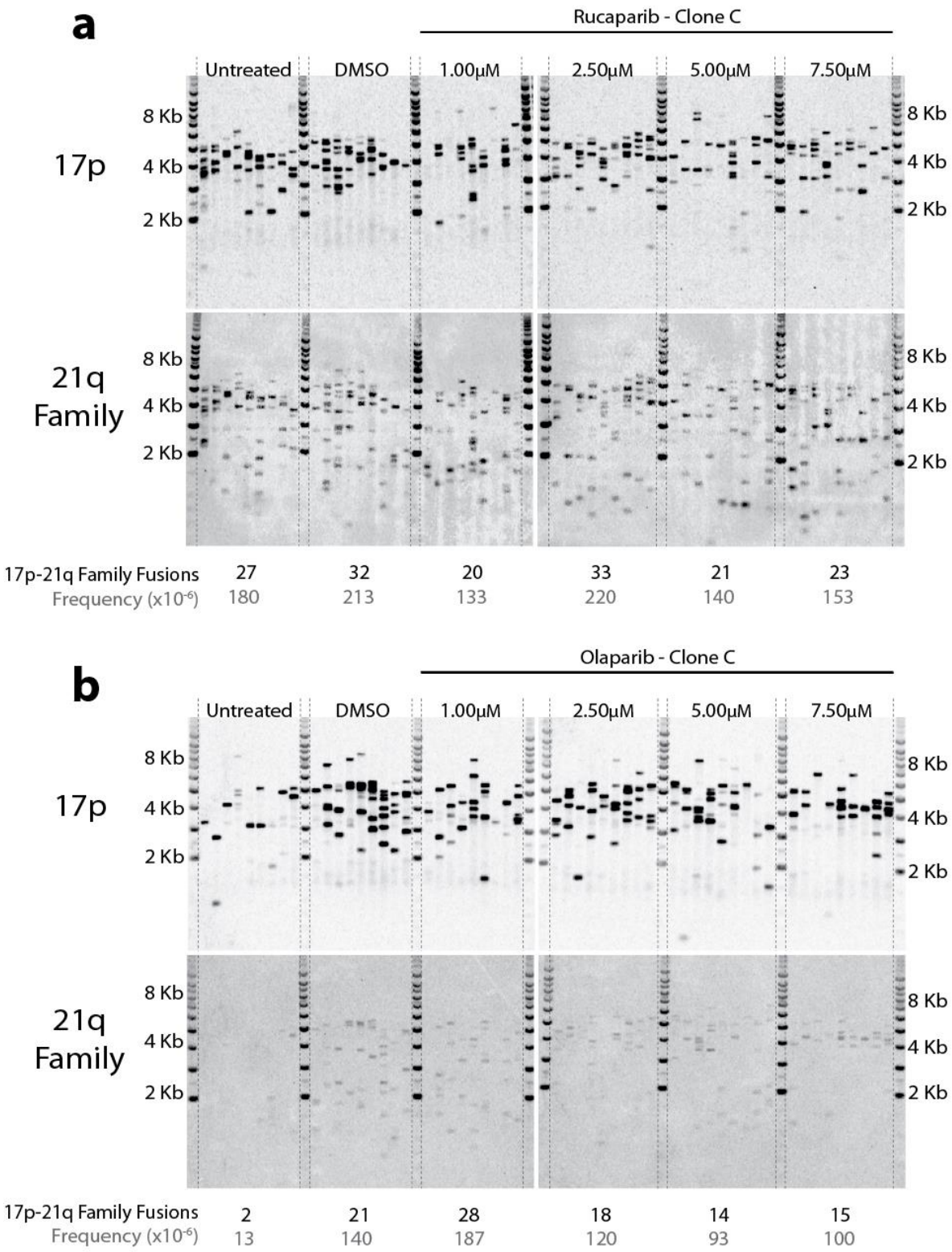

Figure 5.11 - The Change in the Frequency of Chromosomal Fusion Events for JJN-3 DN-hTERT Clone C, Grown in the Presence of Either Rucaparib or Olaparib

JJN-3 DN-hTERT clone C was grown in the presence of either **(a)** Rucaparib or **(b)** Olaparib. On day 67 (Rucaparib - see ***figure 5.2a***) or day 61 (Olaparib - see ***figure 5.2b***), samples of cells were taken for DNA extraction. In total, 900ng of DNA were examined per time point. The frequency of chromosomal fusion was estimated by dividing the number of observable fusion bands by the number of input molecules (around 150,000 cells). Visualisation of these events was performed using the oligonucleotide probes 17p6, XpYpO-G, 16p1 and 21q1. Only the 17p and 21q-Family of chromosomal fusion events are shown.

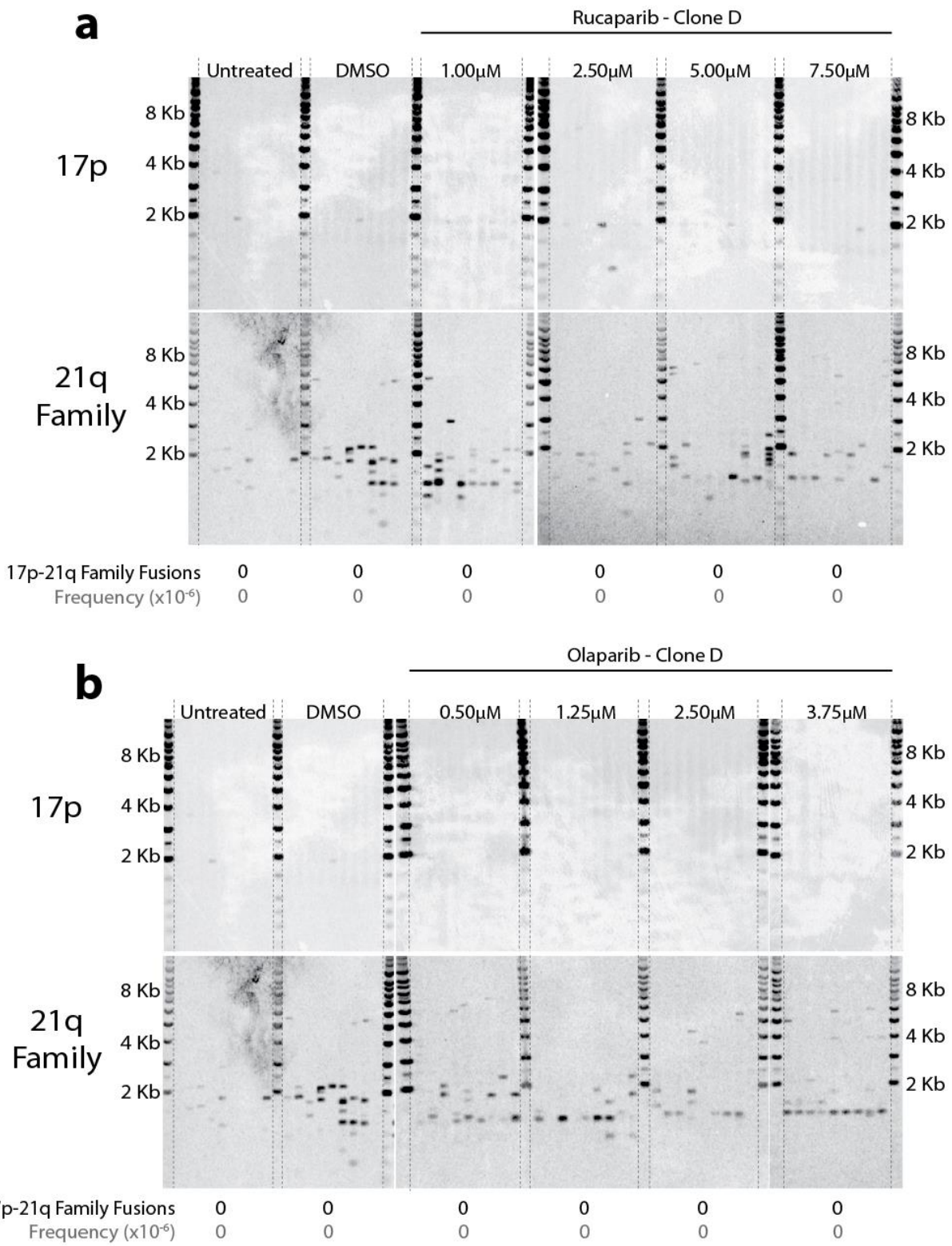

Figure 5.12 - The Change in the Frequency of Chromosomal Fusion Events for JJN-3 DN-hTERT Clone D, Grown in the Presence of Either Rucaparib or Olaparib

JJN-3 DN-hTERT clone B was grown in the presence of either **(a)** Rucaparib or **(b)** Olaparib. On day 58 (Rucaparib - see ***figure 5.3a***) or day 58 (Olaparib - see ***figure 5.3b***), samples of cells were taken for DNA extraction. In total, 900ng of DNA were examined per time point. The frequency of chromosomal fusion was estimated by dividing the number of observable fusion bands by the number of input molecules (around 150,000 cells). Visualisation of these events was performed using the oligonucleotide probes 17p6, XpYpO-G, 16p1 and 21q1. Only the 17p and 21q-Family of chromosomal fusion events are shown.

In clone B, the frequency of 17p-21q-family fusions in the untreated and DMSO-treated subpopulations were $100x10^{-6}$/cell and $133x10^{-6}$/cell respectively (***Figure 5.10a***). A slight decrease in the frequency of 17p-21q-family fusions was observed when Rucaparib was added, with the frequency of fusion events in 5.00μM Rucaparib-treated cells being $27x10^{-6}$/cell and $0x10^{-6}$/cell in those treated with 7.50μM Rucaparib. When clone B cells were treated using Olaparib, a similar decrease in the frequency of chromosomal fusion events was observed (***Figure 5.10b***). The frequency of 17p-21q-family fusion events in the untreated and DMSO-treated subpopulations was $227x10^{-6}$/cell and $140x10^{-6}$/cell respectively. Although a slight increase in fusion frequency was observed in the 0.50μM Olaparib subpopulation ($253x10^{-6}$/cell), the 1.25μM, 2.50μM and 3,75μM Olaparib subpopulations all had a frequency of 17p-21q-family fusion events that was between $100x10^{-6}$/cell and $53x10^{-6}$/cell.

For clone C, the frequency of 17p-21q-family fusion events in the untreated and DMSO-treated subpopulations was $180x10^{-6}$/cell and $213x10^{-6}$/cell respectively (***Figure 5.11a***). When treated with Rucaparib, the 1.00μM, 5.00μM and 7.50μM subpopulations all had a frequency of fusion below $153x10^{-6}$/cell. However, the 2.50μM Rucaparib-treated subpopulation saw a slight increase in fusion frequency to $220x10^{-6}$/cell. This contrasts with Olaparib treatment, whereby only the 1.00μM Olaparib-treated subpopulation had a fusion frequency below that of the DMSO-treated control (***Figure 5.11b***). Unexpectedly, only two 17p-21q-family fusion events were identified from the untreated subpopulation of clone C cells. This resulted in every other subpopulation having a larger frequency of fusion than the $13x10^{-6}$/cell recorded for the untreated control.

Surprisingly, no 17p-21q-family fusion events were recorded in any of the clone D subpopulations (***Figure 5.12***). For this reason, it became necessary to plot both the total frequency of 17p-21q-family fusions observed for each clonal subpopulation (***Figure 5.13***), as well as the total frequency of fusions recorded. By comparing the subpopulations based on the total number of 17p, XpYp, 16p-family and 21q-family

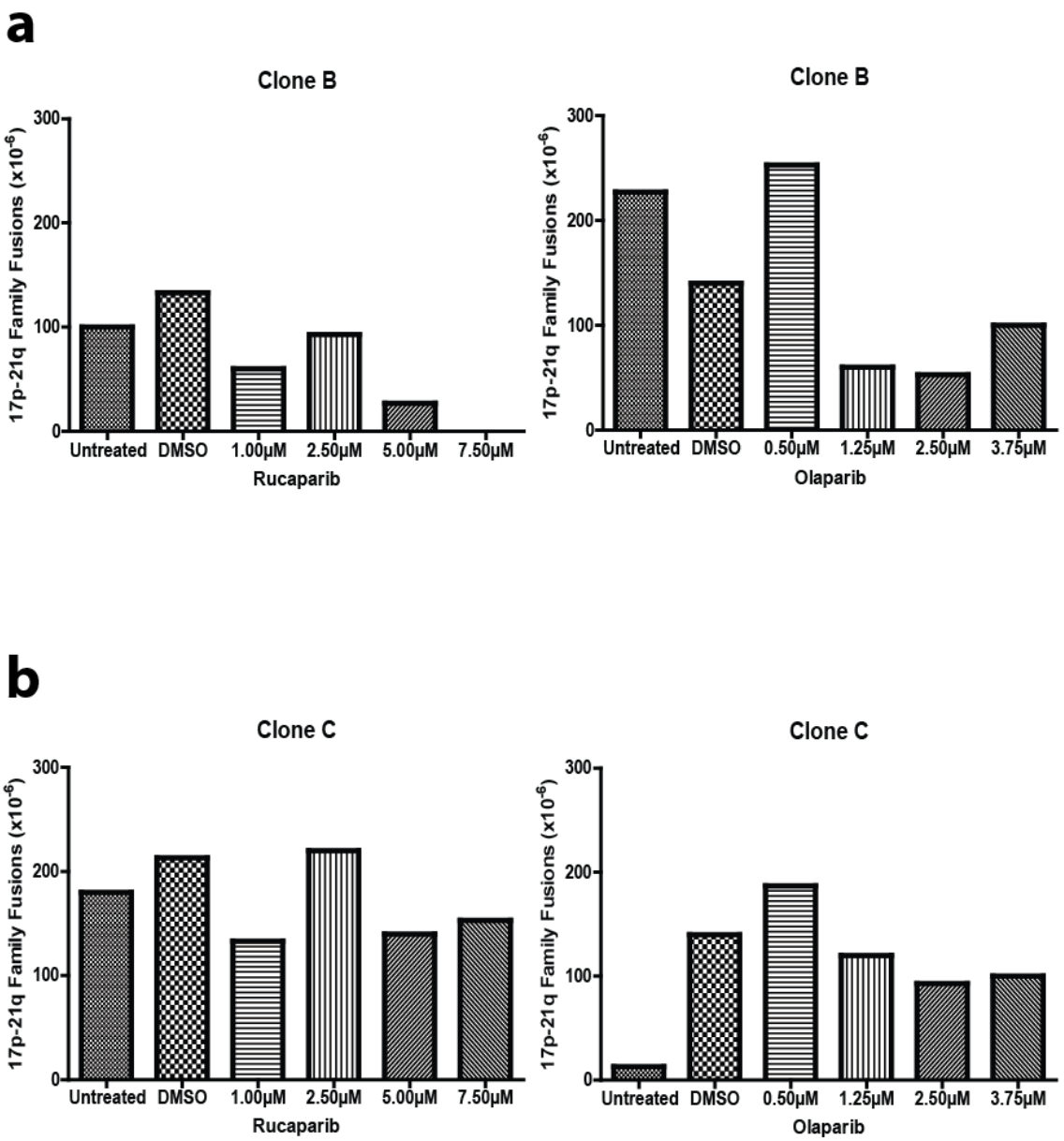

Figure 5.13 - The Change in the Frequency of Chromosomal Fusion Events for JJN-3 DN-hTERT Clones, Grown in the Presence of Either Rucaparib or Olaparib

Graphical representations of the fusion profiles depicted in *Figure 5.10* and *Figure 5.11* . Graphs depict the total frequency of 17-21q family fusion events recorded for JJN-3 DN-hTERT clone B and clone C, treated with either Rucaparib or Olaparib. No 17p-21q family fusion events were detected in clone D.

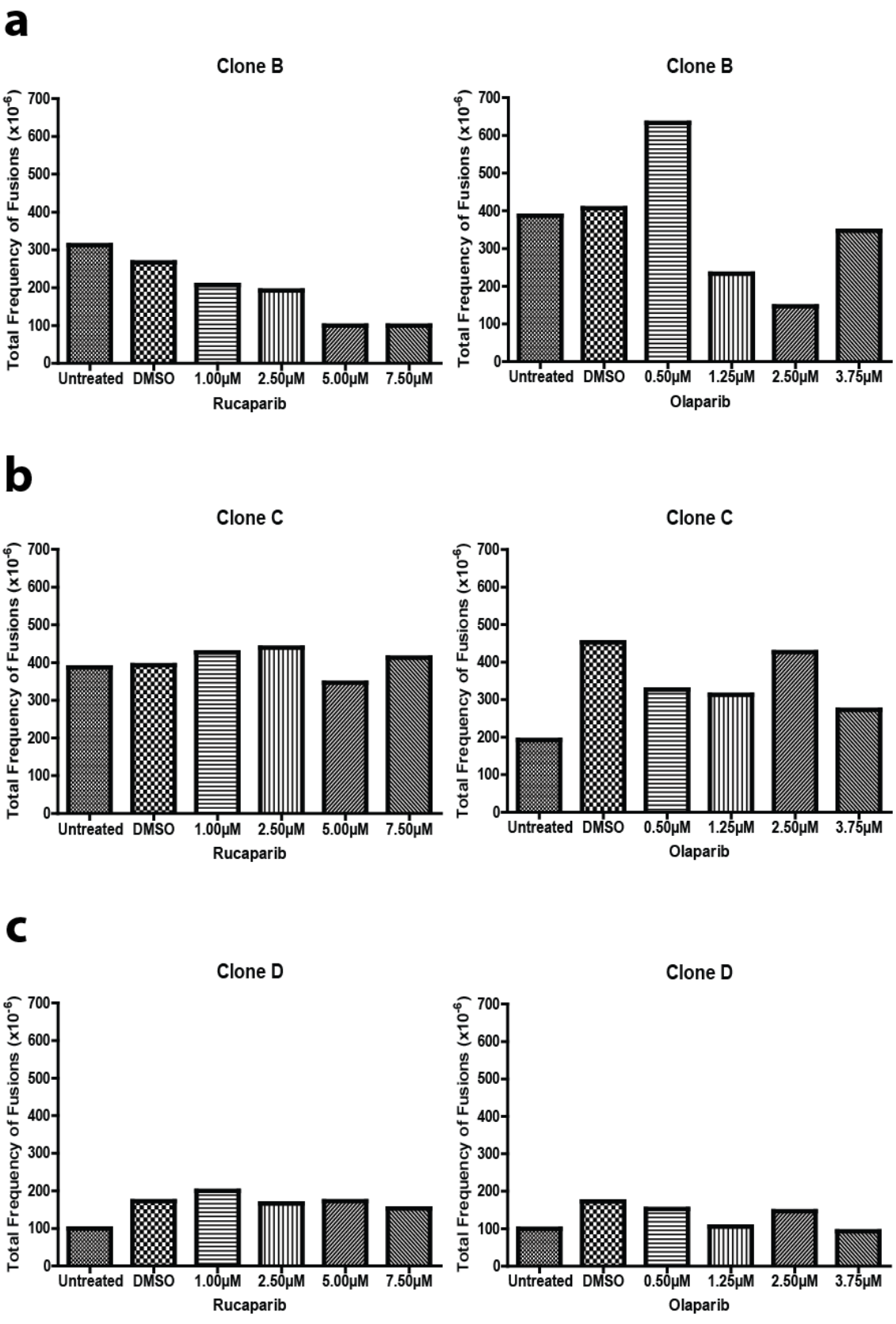

Figure 5.14 - The Change in the Frequency of Chromosomal Fusion Events for JJN-3 DN-hTERT Clones, Grown in the Presence of Either Rucaparib or Olaparib

Graphical representations of the fusion profiles depicted in *Figure 5.10*, *Figure 5.11* and *Figure 5.12*. Graphs depict the total frequency of all fusion events recorded for each JJN-3 DN-hTERT clone, treated with either Rucaparib or Olaparib. This includes 17p, XpYp, 16p-family and 21q-family of chromosomal ends.

fusion events, we could gain a clearer picture of any change Rucaparib- and Olaparib-treatment had on the clone D subpopulations (***Figure 5.14c***). From this, we identified that the untreated and DMSO-treated clone D subpopulations had total fusion frequencies of $100x10^{-6}$/cell and $173x10^{-6}$/cell respectively. The total fusion frequency of the 2.50μM, 5.00μM and 7.50μM Rucaparib-treated subpopulations all lay between these values ($167x10^{-6}$, $173x10^{-6}$ and $153x10^{-6}$/cell respectively). Meanwhile, only the 3.75μM Olaparib-treated subpopulation had a total frequency of fusion which was below the value of $100x10^{-6}$/cell recorded in the untreated subpopulation. The 0.50μM, 1.25μM and 2.50μM Olaparib-treated subpopulations each had a frequency of fusion which was below the value of $173x10^{-6}$/cell recorded in the DMSO-treated control.

5.5 Discussion

5.5.1 PARP Inhibition and the Ability of JJN-3 Cells to Escape from a Telomere-Driven Crisis

In the previous chapter, we attempted to demonstrate that the presence of critically shortened telomeres was associated with an increased frequency of chromosomal end-end fusion. By forcing clonal populations of JJN-3 cells to divide in the absence of telomerase (DN-hTERT), they entered a state of telomere-driven crisis which resulted in a period of increased fusion-frequency, followed by an escape from crisis. In this chapter, we have attempted to prevent the escape of these cells from a telomere-driven crisis by using the PARP inhibitors Rucaparib and Olaparib. Due to the essential roles played by PARP family proteins in repairing DNA damage, we hypothesised that PARP inhibition may limit the capacity of JJN-3 cells to repair single- and double-strand DNA breaks. By disrupting the alt-NHEJ pathway, and potentially altering the balance between intra- and interchromosomal fusion events, we anticipated that PARP inhibition would prevent the escape of cells from a telomere-driven crisis. It is in this way that we wished to highlight the potential therapeutic use of PARP inhibitors in treating MM.

As we saw in the previous chapter, untreated subpopulations of clonal JJN-3 DN-hTERT cells could escape from a telomere-driven crisis after a period of stalled growth. Treating each clone with either 7.50μM Rucaparib or 3.75μM Olaparib completely inhibited population growth and prevented an escape from a telomere-driven crisis. This contrasted with the control JJN-3 clonal population, whereby treatment with 7.50μM Rucaparib or 3.75μM Olaparib alone was not enough to completely inhibit growth.

Our result shared similarities with Neri et al. (2011), whose research documented that treatment with the PARP inhibitor Veliparib alone was not enough to impact on the viability of MM cell lines. For Veliparib to be effective, it was necessary to combine it

with the proteasome inhibitor Bortezomib. With Veliparib preventing the repair of single-strand breaks, MM cells would have to rely on the HR pathway to repair the resulting double-strand breaks. Bortezomib was found to be indirectly impairing the HR pathway, resulting in an accumulation of catastrophic DNA damage.

HR activity is thought to be elevated in MM (Shammas et al. 2009). It has also previously been shown that reactivation of telomerase occurs in late-stage MM, limiting the capacity of a telomere-driven crisis to work in tandem with PARP inhibitors (Shiratsuchi et al. 2002). For these reasons, PARP inhibition alone in late-stage MM may simply increase the frequency of double-strand DNA breaks and produce further genomic instability (Ito et al. 2016). The rate of tumour formation is thought to be significantly increased in mice which are both PARP1$^{-/-}$ and p53$^{-/-}$, an important consideration as 13% of newly diagnosed MM cases present with p53 abnormalities (Tong et al. 2003; Tong et al. 2007; Chng et al. 2008). For PARP inhibitors to be considered safe and effective, it may be necessary to at least combine their use with telomerase inhibition which would prevent telomere maintenance and induce a telomere-driven crisis.

However, the current use of PARP inhibition as a cancer treatment does not require a telomere-driven crisis. PARP inhibitors are mostly limited to breast and ovarian cancers which contain mutations in either BRCA1 or BRCA2, genes which are necessary for a functional homologous recombination pathway (Venkitaraman 2002). Further work should therefore focus on determining whether the effective concentration of PARP inhibition, during a telomere-driven crisis, can be reduced through co-treatment with compounds that suppress the homologous recombination pathway. Fortunately, Bortezomib is already commonly prescribed in the treatment of MM and has been shown to indirectly suppress homologous recombination (Palumbo et al. 2014; Murakawa et al. 2007). It will therefore be necessary to assess the effectiveness of combining Rucaparib/Olaparib treatment with Bortezomib during a telomere-driven crisis.

Also, previous studies have demonstrated that Olaparib has the capacity to slow the growth of CLL cell lines which fail to express a functional ATM protein (Weston et al., 2010). This effect was not seen in ATM^{wt} cell lines, but could be induced using retroviral knockdown of ATM. In either case, cell death was thought to occur due to mitotic catastrophe. Olaparib was also found to sensitise ATM-mutated CLL cell lines to cytotoxic agents such as alkylating agents and histone deacetylase inhibitors. This observation was later repeated using colorectal cancer cell lines, with Olaparib selectively killing those cells that expressed a dysfunctional ATM protein (Wang et al., 2017). However, the JJN-3 cell line has not been shown to express a dysfunctional ATM protein, and trisomy of chromosome 11 (the ATM gene is located at 11q22.3) has also been commonly described in MM (Rajan and Rajkumar, 2015). This may mean that PARP inhibitors, such as Olaparib, may fail to effectively treat MM and may instead induce genetic damage which could drive progression of the disease.

Further work should also be carried out to try and understand why different concentrations of Rucaparib and Olaparib were required to prevent an escape from a telomere-driven crisis. In the case of each JJN-3 clone, twice the concentration of Rucaparib (7.50μM) was required to produce the same effect as Olaparib (3.75μM). This pattern shared similarities with the recommended doses identified in phase II clinical trials which investigated the use of Rucaparib and Olaparib in treating BRCA-mutated breast and ovarian cancer. The suggested dose of Olaparib in each case was 400mg twice a day (Tutt et al. 2010; Ledermann et al. 2014). While the recommended dose of Rucaparib for treatment of the same cancer was greater at 600mg twice a day (Drew et al. 2016; Swisher et al. 2017). Although this does not answer the question of why a difference exists, and may even simply be explained by the maximum tolerated dose of each drug in the respective patient cohorts, it could also point towards differing mechanisms of action for each of these PARP inhibitors.

Wahlberg et al. (2012) characterised the targets of Rucaparib and Olaparib, demonstrating that each bound with the same affinity to the catalytic domains of PARP1, PARP2, PARP3, PARP4, PARP15 and PARP16. Olaparib also bound with weak affinity to PARP12, while Rucaparib bound with moderate affinity to PARP10, strong affinity to PARP5a and weak affinity to PARP5b.

Given these additional targets of Rucaparib, it would be expected that Olaparib would be the less effective PARP inhibitor but this does not appear to be the case. One possible explanation for this concerns the targets not analysed by the Wahlberg et al. (2012) study (PARP6, PARP7, PARP8 and PARP11). As only 13 of the 17 PARP family members were examined, the potential for Rucaparib and Olaparib to bind the remaining four PARP family members is unknown. Vyas et al. (2013) showed that knockdown of PARP6 or PARP7 in HeLa cells did not have a significant effect on viability. However, knockdown of PARP8 almost completely inhibited their growth. Therefore, work should now be carried out to assess whether Rucaparib or Olaparib can inhibit PARP8 and whether the activity of this PARP family protein is necessary for MM cell viability and/or growth.

A further explanation could be that the drugs behave differently *in vivo*. The results of Wahlberg et al. (2012) were generated by synthetically producing the catalytic domain fragments of the 13 PARP family members, before exposing them to commercially available PARP inhibitors. However, this assay only demonstrated the affinity each compound had for each catalytic domain of the PARP family members, but did not assess the effect that binding to each catalytic domain had on MAR/PAR synthesis and phenotypic changes to a cell. For this reason, it is still not possible to describe the exact mechanisms by which Rucaparib and Olaparib work in our JJN-3 cells. Future research should therefore focus on determining how these PARP inhibitors act, as well as the target PARP family member(s) whose inhibition is responsible for triggering cell death in MM. As many of the catalytic subunits of the PARP family members share a certain

homology (Ame, Spenlehauer, and de Murcia 2004), attempting to inhibit individual PARP proteins may prove difficult. Instead, identifying and inhibiting the upstream/downstream targets of each PARP protein may prove more selective.

5.5.2 Determining the Efficiency of PARP Inhibition in JJN-3 Clonal Populations

We attempted to demonstrate that treating JJN-3 clonal populations with either Rucaparib or Olaparib reduced the activity of the PARP family proteins. Western blotting was performed to measure PAR expression, a protein which is produced by some of the PARP family members, in response to Rucaparib or Olaparib. We hypothesised that PARP inhibition would simply lead to a reduction in the quantities of PAR produced, as observed in similar experiments in HCT116 cells (Greg Ngo, personal communication). However, we were unable to detect PAR in any of the JJN-3 clonal populations analysed. In response to this, the quantities of the retinoblastoma protein and checkpoint kinase 1 (Chk-1) protein were also measured to try and detect a DNA damage response within the cells. It was thought that these proteins could have been used to indirectly detect a change in the frequency of single- or double-strand DNA breaks.

While the presence of a positive control for PAR proved that the assay appeared to be working correctly, we were also able to use Chk-1 as a positive control for H_2O_2 treatment. H_2O_2 was added to the cells, 24 hours after treatment with either Rucaparib or Olaparib, to induce single-strand DNA breaks and increase PAR synthesis by PARP family proteins. From examination of the Western blots, each clonal subpopulation of JJN-3 cells that had not been exposed to H_2O_2 expressed less Chk-1 than those subpopulations that had been exposed to H_2O_2. As Chk-1 expression is upregulated in response to single- and double-strand DNA breaks, this suggested that the addition of H_2O_2 was successfully triggering a DNA damage response within the cells.

However, little change was seen in the expression of Chk-1 after the addition of Rucaparib or Olaparib. While it could be argued that increasing the concentration of PARP inhibitor might have resulted in a greater number of single-strand DNA breaks going unrepaired, and so greater Chk-1 expression in response to accumulating genetic damage, this was not apparent in these experiments. Instead, Chk-1 expression remained unchanged even as the concentration of Rucaparib or Olaparib increased. It was possible that, having been exposed to H_2O_2 for 30 minutes, Chk-1 expression was already at its peak and no further increase was possible. It may therefore be necessary to repeat this experiment, reducing the time that cells are exposed to H_2O_2 so as to detect more subtle changes in Chk-1 expression as a response to PARP inhibition.

Little change was also seen in the expression of the retinoblastoma protein after the addition of Rucaparib or Olaparib. While this protein is not directly involved with PARP signalling or DNA repair, it is eventually involved with the initiation of cell cycle arrest in response to single- and double-strand DNA breaks (Burkhart and Sage 2008). Unlike Chk-1, retinoblastoma protein expression was unaffected by the addition of H_2O_2. This lack of change in response to H_2O_2-driven DNA damage may mean that the cells were able to repair the single- and/or double-strand DNA breaks that resulted, preventing the need for a retinoblastoma-facilitated cell cycle arrest. However, it is also possible that more subtle changes in retinoblastoma protein expression were missed due to the use of Western blotting. In this case, cell cycle analysis might have identified differences in the proportion of cells undergoing cell cycle arrest in response to treatment with H_2O_2 and Rucaparib/Olaparib. It could be expected that increasing concentrations of Rucaparib or Olaparib would lead to an increasing frequency of double-strand DNA breaks, resulting in a greater number of cells undergoing apoptosis.

The lack of PAR was unexpected as it has been well documented that JJN-3 cells express PARP family proteins (Teoh et al. 2014; Tunquist, Woessner, and Walker 2010). It is therefore possible that one or more of these proteins are either not expressed or not

functional in the JJN-3 cell line. As the most abundantly expressed PAR-producing PARP family member, loss of a functional PARP1 protein might have meant that the cells were unable to produce PAR in the quantities necessary for quantification using the method employed here. This inactivity may also explain the increased homologous recombination activity detected in the JJN-3 cell line by Shammas et al. (2009), with the cells relying on this pathway to repair double-strand DNA breaks that arise from a defective PARP1-led single-strand DNA break repair pathway.

Although it is possible that further assays could be used to try and detect a change in PAR expression after treatment with either Rucaparib or Olaparib, many of these are still based the use of a PAR antibody. If PAR is not produced in sufficient quantities within the JJN-3 cell line, then these assays may simply yield the same result as our Western blot. The use of a PAR antibody also fails to account for the activity of those PARP family members which are targeted by Rucaparib and Olaparib, but do not produce PAR. Kleine et al. (2008) have demonstrated that it is possible to detect the activity of all PARP family members using ^{32}P-NAD^{+}, regardless of whether they have MAR or PAR activity. NAD^{+} is used as a substrate by PARP family members when attaching ADP-ribose units to proteins, meaning that proteins expressing MAR or PAR which have incorporated ^{32}P can be detected by autoradiography. This would allow the activity of all PARP family members to be examined within the context of Rucaparib or Olaparib treatment, without biasing the assay towards PARP1. However, the time required to develop and optimise this assay for use with our JJN-3 experiment was beyond the scope of this study. It therefore became necessity to rely on previously reported data regarding the efficiency of PARP inhibition by Rucaparib and Olaparib (Murai et al. 2014).

5.5.3 PARP Inhibition and the Effect on Mean XpYp Telomere Length

Just before the JJN-3 DN-hTERT clones entered a state of telomere-driven crisis, samples of each subpopulation were harvested for DNA extraction. STELA was then

used to identify any changes in mean XpYp telomere length that occurred due to treatment with either Rucaparib or Olaparib. Surprisingly, PARP inhibition appeared to result in certain subpopulations of cells having a longer mean telomere length than controls. In the case of each JJN-3 clone, 3.75μM Olaparib treatment lead to a significantly longer mean XpYp telomere length than the control subpopulations. However, this was not the case when cells were treated with Rucaparib. In each case, 1.00μM – 7.50μM Rucaparib had no significant effect on mean XpYp telomere length.

Of the 17 PARP family proteins, only PARP5a and PARP5b are thought to play a role in telomere length maintenance. Each works by attaching PAR to TRF1, a subunit of the shelterin complex (Ye and de Lange 2004). This inhibits the activity of TRF1 and prevents it from binding to the telomere, thus allowing telomerase to bind instead which then results in telomere elongation (Kulak et al. 2015). It should therefore follow that inhibition of PARP5a and PARP5b would allow TRF1 binding at the telomere and result in telomeric shortening. With regards to our data, the opposite is true. Only the addition of 3.75μM Olaparib led to a significant longer mean XpYp telomere length. However, PARP5a and PARP5b activity would have had little effect on telomere length even without the presence of Rucaparib or Olaparib. As each JJN-3 clonal population expresses DN-hTERT, telomerase would be unable to elongate telomeres and mean XpYp telomere length would decrease regardless of whether PARP5a and PARP5b were activated or inhibited. Also, only Rucaparib was shown to bind to PARP5a and PARP5b (Wahlberg et al. 2012). This prevents these PARP family proteins from being used to explain the difference in mean XpYp telomere length seen upon treatment with Olaparib.

It is therefore unlikely that the difference in mean XpYp telomere length which we observed was the result of direct action/inaction by PARP family proteins at the telomere. Instead, it could be argued that Olaparib was somehow changing the rate of population growth. It was suggested in the previous chapter that the chromosomal instability witnessed during a telomere-driven crisis led to the eventual reactivation of telomerase

in these clonal populations of JJN-3 cells. This resulted in mean XpYp telomere length increasing as the cells escaped from crisis. If PARP inhibition increased the rate of cell division, Olaparib-treated cells would enter and escape from crisis sooner than the untreated controls. Theoretically, this could result in these cells eventually having an increased mean XpYp telomere length, relative to that of the slower-growing pre-crisis control subpopulations.

Reducing the rate of population growth would also be a possible explanation, with 3.75μM Olaparib-treated subpopulations simply having a longer mean XpYp telomere length because they had undergone fewer cell divisions. This may be caused by PARP inhibition restricting the ability of a cell to repair single- and double-strand DNA breaks, delaying cell division as cell cycle checkpoints are activated. Nile et al. (2016) have shown that treating human neuroblastoma and glioblastoma cell lines with either Rucaparib or Olaparib increases the proportion of cells in the G_2/M phase of the cell cycle. The G_2/M cell cycle checkpoint is responsible for ensuring that DNA damage has been repaired before initiating mitosis (Yarden et al. 2002).

Apoptosis may also play a role here, with PARP inhibition selectively killing cells that have shorter telomeres and thus greater genomic instability. Several examples from other researchers exist which also demonstrate the anti-proliferative and pro-apoptotic effects of PARP inhibitors. Albert et al. (2007) used Veliparib to reduce the rate of growth and increase the rate of apoptosis in populations of H460 lung cancer cells. Meanwhile, Ihnen et al. (2013) showed increased rates of apoptosis in ovarian cancer cell lines treated with Rucaparib. This explanation for the difference in mean XpYp telomere length would also correlate with the growth recorded for each JJN-3 DN-hTERT subpopulation, whereby those cells treated with either Rucaparib and Olaparib took longer to reach the same PD as the untreated controls. However, it fails to explain why a change in mean telomere length was not also observed in Rucaparib-treated subpopulations.

5.5.4 PARP Inhibition and the Effect on Chromosomal Fusion

PARP1, PARP2 and PARP3 are all involved in the repair of single- or double-strand DNA breaks. We therefore hypothesised that treatment with Rucaparib or Olaparib would inhibit the activity of these PARP family proteins, preventing erroneous DNA repair and reducing the frequency of chromosomal end-end fusion. Specifically, we expected PARP inhibition to disrupt the alt-NHEJ pathway and reduce the frequency of intrachromosomal fusion events. However, Rucaparib and Olaparib had little effect on the incidence of chromosomal fusion. In almost all cases, the difference between the control subpopulations and the treated subpopulations appeared to be negligible. The only exception was JJN-3 DN-hTERT clone B, whereby Rucaparib and Olaparib both caused a minor reduction in chromosomal end-end fusion, with greater concentrations of each drug further decreasing the number of fusion events recorded.

This observation in clone B could be caused by PARP inhibition preventing the cells from recognising and repairing telomere-deficient chromosomal ends as double-strand DNA breaks. PARP1 is thought to promote double-strand DNA break repair via the alternative-NHEJ pathway (Mansour et al. 2013). Meanwhile, PARP3 has been shown to have a role in promoting the classical-NHEJ pathway (Rulten et al. 2011). It might therefore follow that inhibition of these PARP family proteins would impair the NHEJ pathways and lead to fewer chromosomal end-end fusion events. However, it has been shown that PARP1$^{-/-}$ and PARP3$^{-/-}$ cells are still able to repair DNA damage via the homologous recombination and NHEJ pathways (Yang et al. 2004; Beck et al. 2014). This suggests that PARP1 and PARP3 are active in double-strand DNA break repair, but not strictly necessary. This explanation also fails to account for the results of clone C and clone D, whereby the addition of Rucaparib and Olaparib had little effect on the frequency of fusion observed.

Instead, the reduction in chromosomal end-end fusion may simply be the result of increased telomere length. We previously discussed the fact that treating clone B cells with Olaparib caused an apparent increase in mean XpYp telomere length. In chapter 4, we also demonstrated that a longer mean telomere length correlated with a reduced frequency of chromosomal end-end fusion. It could therefore be argued that, as PARP inhibition resulted in an increased mean XpYp telomere length, fewer chromosomal ends had critically shortened telomeres that would result in fusion. However, this fails to explain the results obtained for clone C and clone D. When the cells were treated with 3.75μM Olaparib, a longer mean XpYp telomere length was recorded. However, there was no corresponding change in the frequency of fusion observed, relative to the control subpopulations.

It may therefore by possible that the ability of Rucaparib and Olaparib to prevent the escape of JJN-3 cells from crisis is not a direct consequence of changes to telomere dynamics or end-end fusion frequency. Instead, PARP inhibitors may simply generate significant genetic damage by inhibiting single-strand DNA repair pathways (Murai et al. 2012). This, combined with the additional genetic instability bought on by a telomere-driven crisis, may overwhelm the cells ability to repair DNA damage. In this way, Rucaparib and Olaparib are likely to promote apoptosis by increasing genetic instability, rather than specifically targeting the formation of intrachromosomal fusion by the alt-NHEJ pathway as was originally thought.

5.5.5 Conclusions

Here, we have demonstrated that treating clonal populations of JJN-3 DN-hTERT cells with either 7.50μM Rucaparib or 3.75μM Olaparib prevented their escape from a telomere-driven crisis. While we have also provided some evidence to suggest that Olaparib modulates mean XpYp telomere length, we have been unable to explain the mechanism involved. We were also unable to determine whether Rucaparib or Olaparib

played any role in limiting the frequency of chromosomal end-end fusion. Future work should therefore focus on determining the mechanism by which PARP inhibition prevented the escape of cells from a telomere-driven crisis. As the effects of Rucaparib and Olaparib on telomere length and fusion frequency are inconsistent and inconclusive, focus should instead shift towards the role that PARP inhibitors have in promoting apoptosis. We now hypothesise that the increased genetic damage caused by Rucaparib and Olaparib, combined with a telomere-driven crisis, overwhelms the cells capacity for DNA repair. It is in this way that PARP inhibitors may create catastrophic genetic damage, stimulating apoptosis in genetically unstable cells.

A new method for determining the effectiveness of PARP inhibition by Rucaparib and Olaparib in the JJN-3 cell line should also be utilised, with focus placed on techniques that avoid the requirement for the use of a PAR antibody. Further work should be conducted to identify whether the PARP1 protein is functional within the JJN-3 cell line. Doing so may explain why PAR could not be detected in these cells via western blot, as well as further charactering an important and widely-used MM cell line. Regardless, we feel that we have begun to demonstrate the importance of PARP inhibition as a treatment for MM. While we believe that administering PARP inhibitors alone may increase the risk of DNA damage and chromosomal instability, Rucaparib and Olaparib should be able to complement existing cancer treatments. We therefore suggest that further experiments are carried out to assess the effectiveness of combining PARP inhibition with bortezomib and telomerase inhibition as a novel treatment for MM.

Chapter 6

General Discussion and Future Directions

6.1 Summary

This study set out determine whether mean XpYp telomere length measurements held prognostic value within the context of MM. Having shown that it did, we then attempted to use our findings to increase the prognostic resolution of the ISS. By isolating $CD138^+$ cells from the whole bone marrow aspirates of three MM patients, we demonstrated that critical telomeric erosion appeared to be confined to the plasma cells. Telomere length measurements, using DNA extracted from the whole bone marrow aspirates of 141 MM patients, identified a mean XpYp telomere length threshold of 3.92kb which could be used to stratify patients as either low- or high-risk. Combining this threshold with a serum β2 microglobulin concentration threshold of 5.5mg/L allowed each prognostic subset to be further risk-stratified. We therefore argued for the inclusion of telomere length measurements within the ISS, either to complement or replace measurements of serum albumin concentration. However, a prospective study of patients stratified according to the revised ISS (R-ISS) is now warranted to establish whether telomere length can add prognostic value within cytogenetic risk groups.

Having demonstrated that a shorter mean XpYp telomere length (<3.92kb) was associated with inferior patient outcome in MM, we next sought to identify a potential cause for this observation. Chromosomal end-end fusion events, a type of genetic instability commonly associated with critically shortened telomeres (Capper et al. 2007), were detected in the whole bone marrow aspirates of MM patients. We then used clonal populations of the JJN-3 cell line to highlight a relationship between telomere length and the frequency of these fusion events in MM. In this case, telomeric shortening resulted in greater fusion frequency and the initiation of a telomere-driven crisis. Cells were

eventually able to escape crisis, driven by the spontaneous reactivation of telomerase which led to an increased mean telomere length and decreased frequency of fusion.

It has been well documented that the genetic instability triggered by chromosomal end-end fusion is crucial for the escape of cells from a telomere-driven crisis (Jones et al. 2014). Telomere-deficient chromosomal ends are subject to repair by the NHEJ pathways (Liddiard et al. 2016), resulting in the genomic deletions and rearrangements that drive cancer progression and characterise high-risk MM. We therefore attempted to disrupt these pathways by targeting those PARP family proteins which play a role in the repair of single- and double-strand DNA breaks. Exposing pre-crisis clonal populations of JJN-3 DN-hTERT cells to the PARP inhibitors Rucaparib (7.50μM) or Olaparib (3.75μM) prevented their escape from crisis, although we were unable to determine the exact cause of this observation.

During the course of this study, we also laid the foundation for future work in a number of key areas. The first of these regards our attempt to address whether telomere length correlated with fusion frequency in unsorted bone marrow aspirates from MM patients. Although a correlation between telomere length and fusion frequency was established using the JJN-3 cell line, the next logical step would have been to ensure that this relationship held true in primary cells. Unfortunately, having access to the bone marrow aspirates of only 16 MM patients made this task difficult. It was therefore concluded that greater patient numbers, as well as isolating plasma cells from whole bone marrow, might hold the key to determining why telomere length measurements held prognostic value in MM.

Progress was also made on defining the role of p53 abnormalities during the escape of cells from a telomere-driven crisis. We observed that the $p53^{-/-}$ JJN-3 cell line could escape crisis, while the $p53^{+/+}$ NCI-H929 cell line could not. However, this is clearly

insufficient to conclude that the presence or absence of a functional p53 protein defines the response of cells to crisis. We therefore reasoned that a greater number of $p53^{-/-}$ and $p53^{wt}$ cell lines should be examined, with a view to extending this work to primary plasma cells extracted from MM patients.

Finally, while we could demonstrate that exposing pre-crisis JJN-3 cells to either Rucaparib or Olaparib prevented their escape from a telomere-driven crisis, we could not explain why this might have been. Attempts to link PARP inhibition to changes in telomere length or fusion frequency proved inconclusive, although exposure to 3.75μM Olaparib appeared to result in a longer mean XpYp telomere length when compared to controls. While it was still felt that future work should involve a greater exploration of the mechanisms involved, the focus should be on combining PARP inhibitors with other drugs such as Bortezomib (Neri et al. 2011; Weiss et al. 2012). It is in this way that we would hope to improve the efficiency of MM treatment, directly targeting the genetic instability which is thought to drive cancer progression.

6.2 Comparisons to Current Knowledge

It has long been considered that telomeric shortening acts as a tumour suppressive mechanism, leading countless researchers to explore the role of telomere dysfunction during cancer formation (Deng, Chan, and Chang 2008). A significant body of research exists to explain the mechanisms underlying telomere dysfunction, with much of this work forming a basis for the discovery of prognostic indicators and novel cancer treatments (Ding et al. 2012; Lin et al. 2014; Burchett, Yan, and Ouellette 2014). While telomeres have also been discussed within the context of MM, little progress has been made in translating this work into clinical practice (Cottliar et al. 2003; Wu et al. 2003). We therefore set out to utilise our understanding of telomere dysfunction and genetic instability to identify new prognostic markers and treatment options for MM.

6.2.1 The Prognostic Value of Telomere Length Measurements in MM

The clinical course of MM can vary significantly (Kyle, Remstein, et al. 2007; Greipp et al. 2005), with reliable prognostic markers being necessary to provide accurate risk stratification and aid in clinical decision making (Palumbo et al. 2015). Although previous studies involving CLL and breast cancer had demonstrated that a shorter mean telomere length correlated with a poorer patient outcome (Lin et al. 2014; Simpson et al. 2015), little was known about whether these findings translated to MM. Meanwhile, both Wu et al. (2003) and Cottliar et al. (2003) had established that telomeric shortening occurred in MM, with the mean telomere length of plasma cells and bone marrow aspirates being shorter in MM patients than in healthy controls. Our study was the first to combine these findings and demonstrate that the telomeric shortening observed in MM held prognostic value.

However, we were not the first to explore a relationship between telomere dynamics and disease progression in MM. Klewes et al. (2013) observed that both mean telomere length and the frequency of chromosomal aggregates correlated with cancer progression. The plasma cells of MGUS patients were associated with longer telomeres and a decreased frequency of aggregates, relative to the plasma cells of MM patients whose telomeres were shorter and more prone to aggregate formation. This result mirrored our own finding, whereby the mean XpYp telomere length of MGUS patients was significantly longer than that of MM patients. Our study even went a step further, demonstrating that the mean XpYp telomere length of stage I patients was significantly longer than that of stage II and stage III patients. It was thought that this relationship was the result of clonal plasma cell growth, whereby a cell with shorter telomeres gave rise to a mass of cells with equivalently short telomeres. The proliferation of these genetically unstable cells would then increase the risk of disease progression, a concept which was explored by Roger et al. (2013). They concluded that telomere length was

likely established before the progression of the cancer, rather than being dynamically regulated throughout the course of the disease.

Meanwhile, Campa et al. (2015) observed that the circulating leukocytes of MM patients had a longer mean telomere length than matched controls. It was determined that a longer leukocyte telomere length was associated with an increased risk of MM, while single-nucleotide polymorphisms (SNP) which reduced the efficiency of the telomerase enzyme were associated with a decreased risk of MM. With regard to telomerase, this result was supported by Wu et al. (2003) which identified an increased overall survival for those MM patients whose $CD138^{+}$ cells had a lower telomerase activity. However, it is well known that abnormal plasma cells primarily reside within the bone marrow. Therefore, in the absence of purified malignant plasma cells, it is logical that telomere length measurements in MM bone marrow samples will more accurately reflect the tumour telomere length and tumour burden (Billadeau et al. 1993; Rasmussen et al. 1999) when compared to peripheral blood samples.

Our results concerning the prognostic value of telomere length measurements in MM closely resembled the results of a similar study involving CLL. Lin et al. (2014) examined the relationship between mean telomere length and the frequency of chromosomal end-end fusion in the peripheral blood mononuclear cells (PBMCs) of CLL patients, identifying two key thresholds. The first of these, 3.81kb, was termed the upper threshold of telomere dysfunction; chromosomal fusion events were only observed in a patient sample when the mean XpYp telomere length was <3.81kb. It was also demonstrated that this threshold held significant prognostic value. Our results identified a prognostic threshold of 3.92kb in MM, strikingly close to the upper threshold of telomere dysfunction described in CLL.

However, it was the 2.26kb threshold identified by Lin et al. (2014) that held the greatest prognostic value in CLL. 2.26kb was the mean telomere length of all those samples in which fusion events were detected. This result was mirrored by Simpson et al. (2015), whereby the most significant mean XpYp telomere length threshold used to stratify low- and high-risk breast cancer patients was also 2.26kb. Unfortunately, we were unable to assess the prognostic value of this threshold in MM as only four patients from our cohort had a mean XpYp telomere length below 2.26kb. However, when we first isolated plasma cells from the bone marrow aspirates of three MM patients, the average XpYp telomere length was found to be 2.40kb. This suggests that a 2.26kb threshold may hold greater prognostic value in MM than the 3.92kb threshold used here, but exploring this hypothesis would require the positive isolation and specific telomere length analysis of malignant plasma cells.

Another key limitation of this study was the lack of data regarding cytogenetics for each MM patient. Although we were able to successfully incorporate telomere length measurements into the ISS, increasing the prognostic resolution of this staging system, the ISS has recently been updated to include the presence of high-risk genetic abnormalities such as del(17p), t(4;14) or t(14;16). We were therefore unable to explore the role of telomere length measurements in the revised ISS, combining our 3.92kb threshold with data regarding serum lactate dehydrogenase (LDH) concentrations or the cytogenetics of each patient (Palumbo et al. 2015).

6.2.2 Telomere-Driven Genomic Instability in MM

It has long been known that critically shortened telomeres, particularly within the context of compromised cell cycle checkpoints, have a detrimental effect on genomic stability (Maciejowski and de Lange 2017). Telomeric shortening has been associated with chromosomal end-end fusion which can result in the deletion, translocation or gain of genetic material (Capper et al. 2007; Maciejowski and de Lange 2017). Examples of

genetic instability in MM include IgH translocations and hyperdiploidy which are thought to act as initiating events (Avet-Loiseau et al. 2002; Smadja et al. 2001), with TP53 deletion and MYC upregulation following as secondary events (Avet-Loiseau et al. 2007). However, ours was the first study to demonstrate a causal link between telomeric shortening and increased fusion frequency in MM.

Although we were able to sequence chromosomal end-end fusions from the whole bone marrow aspirates of MM patients, we could not claim that $CD138^+$ plasma cells were the source of this genetic instability. A necessary future step would therefore be to prove the existence of these fusion events in isolated plasma cells. Although Klewes et al. (2013) had demonstrated that telomeric aggregates were a common feature of the $CD138^+$ cells of MM patients, an aggregate is not necessarily the same as a chromosomal end-end fusion event. Regardless, it was observed that the frequency of these telomeric aggregates increased with disease progression, with MGUS patients having fewer aggregates than MM patients. However, no attempt was made to link telomeric shortening with increased aggregate formation or fusion frequency. Meanwhile, our study tried to use the whole bone marrow aspirates of 16 MM patients to demonstrate that a shorter mean telomere length was linked to a greater frequency of chromosomal end-end fusion.

While we could not identify a direct link between mean XpYp telomere length and fusion frequency, we were able to conclude that a significant relationship existed between the standard deviation of each patient's STELA profile and the frequency of fusion observed. It was thought that the standard deviation offered an estimation of the extent to which the telomere length of the plasma cell population differed from that of the remaining marrow cells. It will therefore be necessary to examine this theory by first isolating $CD138^+$ plasma cells from the whole bone marrow aspirates of MM patients. By measuring mean telomere length and fusion frequency in these isolated cells, it may offer an explanation as to whether the telomeric shortening observed in plasma cells is

responsible for the genetic instability associated with MM. However, clinical samples are inherently diverse and harbour numerous cytogenetic abnormalities. It was therefore concluded that establishing any mechanistic basis for the relationship between telomere length and fusion frequency would require the use of MM cells lines

By driving clonal populations of JJN-3 cells into a telomere-driven crisis, we could offer an explanation for why telomere length measurements might hold prognostic value in MM. At least in this cell line, telomeric shortening was associated with increased fusion frequency and the reactivation of telomerase, likely facilitating cell survival. Our study shared similarities with Capper et al. (2007) and Lin et al. (2014), both of whom identified an identical relationship between telomere length and fusion frequency in fibroblast and CLL cells respectively. Unlike Lin et al. (2014), however, we were unable to go a step further and demonstrate that the frequency of chromosomal end-end fusion increased during disease progression.

The identification of inter- and intrachromosomal fusion was critical in explaining why JJN-3 cells could escape from a telomere-driven crisis. Jones et al. (2014) demonstrated that the escape of HCT116 cells from crisis was ligase III-dependent, with a higher ratio of intra- to interchromosomal fusion thought to be primarily responsible for localised gene amplification. This included the TERT locus which is one of the most distal genes on the short (p) arm of chromosome 5. Our study observed that telomerase was reactivated in clonal populations of JJN-3 cells, each expressing DN-hTERT, following a period of telomere-driven crisis and increased fusion frequency. This appeared to correlate with several studies examining telomerase expression in MM, with most identifying increased telomerase activity in the $CD138^+$ cells of patients (Shiratsuchi et al. 2002). Wu et al. (2003) not only demonstrated that telomerase was reactivated in abnormal $CD138^+$ cells, but that greater telomerase activity correlated with a significantly reduced overall survival.

We therefore concluded that telomeric shortening in the abnormal plasma cells of MM patients would likely lead to an increased frequency of chromosomal end-end fusion. A possible consequence of this genomic instability is the reactivation of telomerase, resulting in an increased mean XpYp telomere length which might prolong the survival of the abnormal cells. Telomerase inhibition alone, particularly within the context of compromised cell cycle checkpoints, might simply lead to further genomic instability (Jones et al. 2014). Instead, novel treatments should focus on preventing the escape of cells from a telomere-driven crisis, possibly by combining telomerase inhibition with drugs that are known to prevent chromosomal end-end fusion.

6.2.3 Preventing the Escape of Cells from a Telomere-Driven Crisis

PARP inhibitors, such as Rucaparib and Olaparib, are currently used during the treatment of BRCA-deficient breast and ovarian cancers (Venkitaraman 2002). They are thought to work by trapping PARP family proteins at the site of single-strand DNA breaks, preventing their repair and leading to the formation of double-strand DNA breaks (Konecny and Kristeleit 2016). When HR is compromised, such as in BRCA-deficient cancers, cells must rely on the error-prone NHEJ pathways to repair these double-strand DNA breaks. This eventually results in catastrophic DNA damage and apoptosis. However, PARP family proteins have also been implicated in DNA repair mechanisms, most notably the alt-NHEJ pathway which is known to be necessary for the escape of abnormal cells from a telomere-driven crisis (Mansour et al. 2013; Jones et al. 2014). We therefore sought to utilise Rucaparib and Olaparib to prevent the repair of single- and double-strand DNA breaks during a telomere-driven crisis, with the aim of prohibiting cells from escaping.

However, our study demonstrated that treating a JJN-3 clonal population (not expressing DN-hTERT) with either Rucaparib or Olaparib failed to prevent cell growth. This result shared similarities with Neri et al. (2011), whose research documented that treatment

with the PARP inhibitor Veliparib alone was not enough to impact on the viability of MM cell lines. In our study, PARP inhibition was only effective when combined with a reduction in telomerase activity which brought about a telomere-driven crisis. After entering crisis, continued exposure to either 7.50μM Rucaparib or 3.75μM Olaparib prevented clonal populations of the JJN-3 cell line from escaping.

In this *in vitro* study, we had to drive JJN-3 cells into a telomere-driven crisis by forcing the expression of a DN-hTERT construct, in order for PARP inhibition to be effective. However, effective use of PARP inhibitors for the treatment of MM may not be so dependent on the dual genetic knock-down of telomerase. Alagpulinsa et al. (2016) demonstrated that Dinaciclib, a CDK inhibitor, sensitised MM cell lines to Veliparib by impairing the HR pathway. It was observed that treating mouse MM xenograft models with a combination of Dinaciclib and Veliparib significantly increased overall survival. This is in comparison to mice treated with Veliparib alone, which unsurprisingly had the same overall survival as untreated controls. Fortunately, the additional step of combining PARP inhibition with Dinaciclib may not be necessary. Neri et al. (2011) demonstrated that MM cell lines could be sensitised to the effects of Veliparib by co-treating with Bortezomib, a drug which is already commonly used during the treatment of MM.

Although Neri et al. (2011) found that Bortezomib indirectly impaired the HR pathway, Weiss et al. (2012) observed that Bortezomib was also responsible for downregulating telomerase activity in both MM cell lines and primary cells. It is therefore possible that combining Bortezomib with PARP inhibition may have a similar effect to that observed in our study. This could be tested *in vitro* and in mouse models of MM whereby a reduction in telomerase activity is combined with a PARP inhibitor like Rucaparib and Olaparib.

However, the greatest limitation of this study was our inability to explain why PARP inhibition prevented clonal populations of JJN-3 cells from escaping a telomere-driven

crisis. Although we could demonstrate that Rucaparib and Olaparib were effective in preventing the escape of JJN-3 cells from crisis, we had also anticipated that PARP inhibition would suppress the alt-NHEJ pathway and reduce the frequency of chromosomal end-end fusion observed. Frustratingly, fusion frequency remained relatively unchanged during treatment. Not only this, but PARP activity could not be detected in JJN-3 cells using the methods utilised here. A significant amount of further work would therefore be necessary to understand the mechanism by which PARP inhibition prevents the escape of cells from a telomere-driven crisis in these MM cell lines.

6.3 Future Directions

One of the core aims of this study was to determine whether telomere length measurements held prognostic value within the context of MM. Having demonstrated that a mean XpYp telomere length threshold of 3.92kb could be used to stratify low- and high-risk patients, and that this threshold could be further used to increase the prognostic resolution of the ISS, we next turned our attention to explaining why telomere length measurements held prognostic value. Although we observed a relationship between telomere length and the frequency of chromosomal end-end fusion in the JJN-3 cell line, we were unable to replicate this exact relationship using the whole bone marrow aspirates of MM patients. Instead, we could only identify a relationship between the variance of each patient's STELA profile and the frequency of fusion, suggesting that a subset of critically shortened telomers may be responsible for the genomic instability and rearrangement that defines MM.

The next step would therefore involve isolating $CD138^{+}$ plasma cells from the whole bone marrow aspirates of a large well-characterised cohort of MM patients. From this, we would seek to identify whether the prognostic resolution of telomere length measurements could be further increased, in much the same way as Lin et al. (2014)

and Simpson et al. (2015) did with purified CLL and breast tumour samples. It is in this way that we could explore the value of a 2.26kb telomere length threshold in MM, as well using the cytogenetic data for each patient to establish its utility in the R-ISS. Using isolated plasma cells would also allow for a more targeted exploration of the relationship between telomere length and fusion frequency in MM primary cells. Not only would we hope to demonstrate that shorter telomeres correlated with increased fusion frequency, but we would also aim to identify a telomere dysfunction threshold for MM. This would involve defining the mean telomere length at which chromosomal end-end fusion could first be observed in plasma cells, as well whether the frequency of fusion could be used as an indicator of patient outcome.

Isolating $CD138^{+}$ plasma cells from MM patients may also help to explore the role that TP53 abnormalities play during the onset of a telomere-driven crisis. TP53 abnormalities are estimated to be present in around 13% of MM cases at diagnosis, limiting the ability of a cell to trigger cell cycle checkpoints when telomeres become critically shortened (Chng et al. 2007). We observed that the $p53^{-/-}$ JJN-3 cell line could escape from a telomere-driven crisis, while the $p53^{wt}$ NCI-H929 cell line could not. Other researchers have also observed that inhibiting telomerase activity causes apoptosis in $p53^{wt}$ MM cell lines (Shammas et al. 2003; Akiyama et al. 2003). Further work is clearly necessary explore the role that p53 expression plays during the escape of an abnormal plasma cell from a telomere-driven crisis. This work could also extend to haploinsufficient ($p53^{+/-}$) cells and those with genetic abnormalities which are known to result in a compromised DNA damage response.

We would likely begin by reducing the expression of p53 in the NCI-H929 cell line, before using DN-hTERT expression to drive the cells into a telomere-driven crisis. A reduction in p53 expression could be achieved by inhibiting translation of the p53 mRNA via RNA interference (He et al. 2005). We hypothesise that, with a compromised senescent pathway, the cells may be able to escape from crisis in a similar manor to the JJN-3 cell

line. If this were the case, and could be repeated in other $p53^{wt}$ MM cell lines, then it may be worth exploring the relationship between p53 expression and the frequency of chromosomal end-end fusion in the $CD138^{+}$ plasma cells of MM patients. This might further explain why del(17p) is consider a high-risk genetic abnormality in MM, with a compromised senescent pathway leading to an increased frequency of fusion which drives progression of the disease.

One of the most important areas of future work should be exploring the use of PARP inhibitors as a treatment for MM. Although we have demonstrated that exposing JJN-3 cells to 7.50μM Rucaparib or 3.75μM Olaparib through a telomere-driven crisis was sufficient to prevent their escape, focus should now shift towards combining PARP inhibitors with Bortezomib. Not only is Bortezomib commonly used during the treatment of MM, but it has also been shown to sensitise abnormal plasma cells to the effects of PARP inhibition by impairing both the HR pathway and telomerase activity (Neri et al. 2011; Weiss et al. 2012). Work should also be carried out to replicate these findings using other MM cell lines and eventually $CD138^{+}$ plasma cells obtained from patients. This would be to ensure that the effects of PARP inhibition are not localised to the JJN-3 cell line. This isolation of $CD138^{+}$ cells from MM patients could also be performed alongside the stratification of patients based on mean telomere length, assessing the prognostic value of a 2.26kb threshold.

Although it would also be interesting to understand why PARP inhibition prevents the escape of JJN-3 cells from a telomere-driven crisis, this is not nearly as important as further exploring the use of PARP inhibitors as a treatment for MM. However, understanding why PARP inhibition prevents cells from escaping crisis may still influence how we perceive and treat the disease. It may therefore be necessary to explore the effects of these drugs on cell cycle progression and single-strand DNA break repair mechanisms. It is in this way that we would wish to identify PARP inhibition as a novel treatment for MM, while simultaneously offering an explanation for its effectiveness.

6.4 Conclusions

During the course of this study, we have determined the prognostic value of telomere length measurements in patients with MM. By using STELA to measure the mean XpYp telomere length in 141 MM patients, we have identified a telomere length threshold of 3.92kb which could be used to stratify patients as either low- or high-risk. Combining this threshold with a serum β2 microglobulin concentration threshold of 5.5mg/L allowed each prognostic subset to be further risk-stratified, establishing an argument for the incorporation of telomere length measurements into the ISS. We have also offered an explanation for the prognostic value of telomere length measurements in MM, identifying $CD138^{+}$ plasma cells as the source of critically shortened telomeres in three patients with the disease.

Clonal populations of JJN-3 cells were then used to show that telomeric shortening in this MM cell line would generate genetic instability in the form of chromosomal end-end fusion. DN-hTERT expression forced the cells into a telomere-driven crisis, resulting in telomeric erosion that correlated with an increased frequency of fusion. Each clonal JJN-3 population was then able to escape crisis, accompanied by an increase in telomerase activity and gradual telomeric elongation. By exposing these cells to Rucaparib or Olaparib, we were able to prevent this escape from crisis and highlight the potential for PARP inhibitors to be used as a treatment option for MM.

Appendix

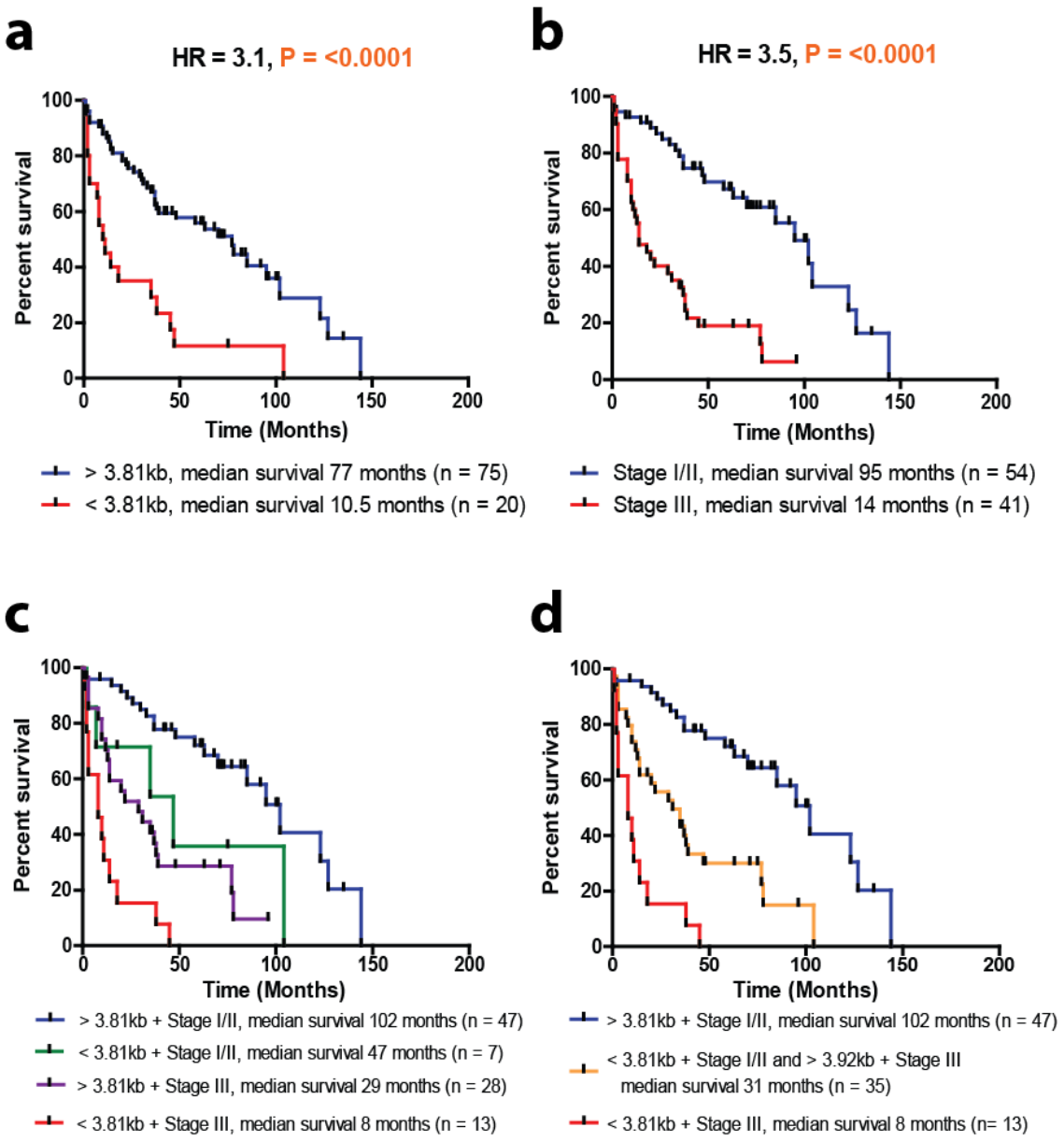

Supplementary Figure 1 - Prognostic Resolution can be Increased by Incorporating Mean Telomere Length into the ISS

Of the 131-patient cohort, ISS staging was also available for 95 of these patients. **(a)** Kaplan Meier curve which stratifies patients using a 3.81kb threshold. **(b)** Kaplan Meier curve which stratifies patients based on their ISS staging. **(c)** Kaplan Meier curve which used a combination of the 3.81kb threshold and ISS staging to stratify patients. This resulted in both the ISS I/II and ISS III cohorts splitting into two further sub-groups. **(d)** Kaplan Meier curve which also uses a combination of the 3.81kb threshold and ISS staging, but combines the **< 3.81kb + Stage I/II** and **> 3.81kb + Stage III** patient groups. Significance was defined as $P<0.05$

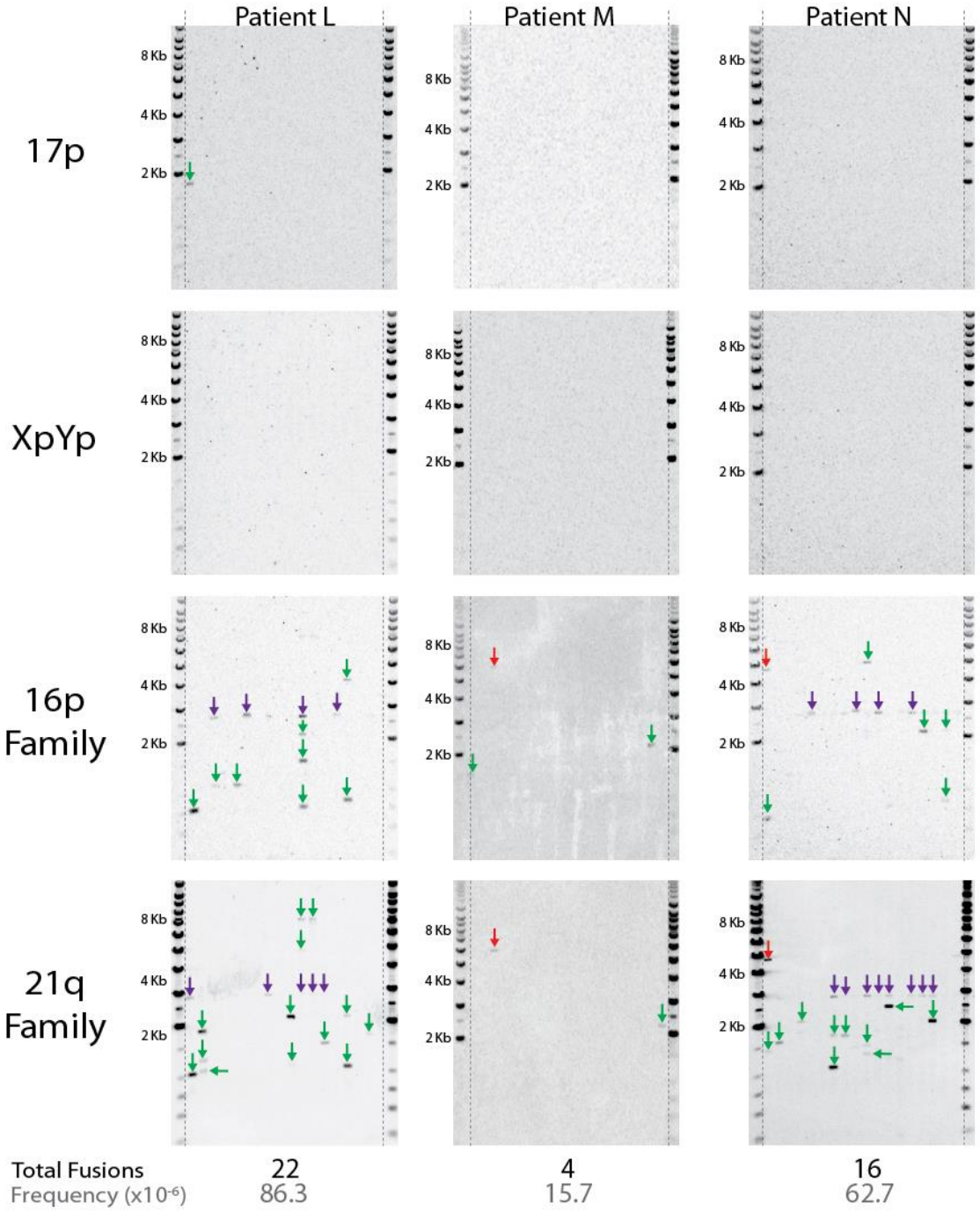

Supplementary Figure 2 - Bone Marrow Cells of MM Patients Show Evidence of Chromosomal Fusion

(a) Three MM patients whose DNA was examined for the presence of chromosomal fusion events. In total, 1530ng of DNA was analysed per patient. The frequency of chromosomal fusion was estimated by dividing the number of observable fusion bands by the number of input molecules (around 255,000 cells). Bands representing possible intrachromosomal fusion events were highlighted in green, while interchromosomal fusion events were highlighted in red. Purple arrows were used to highlight bands that were located in areas known for backgrounds bands (these were not included in the final analysis).

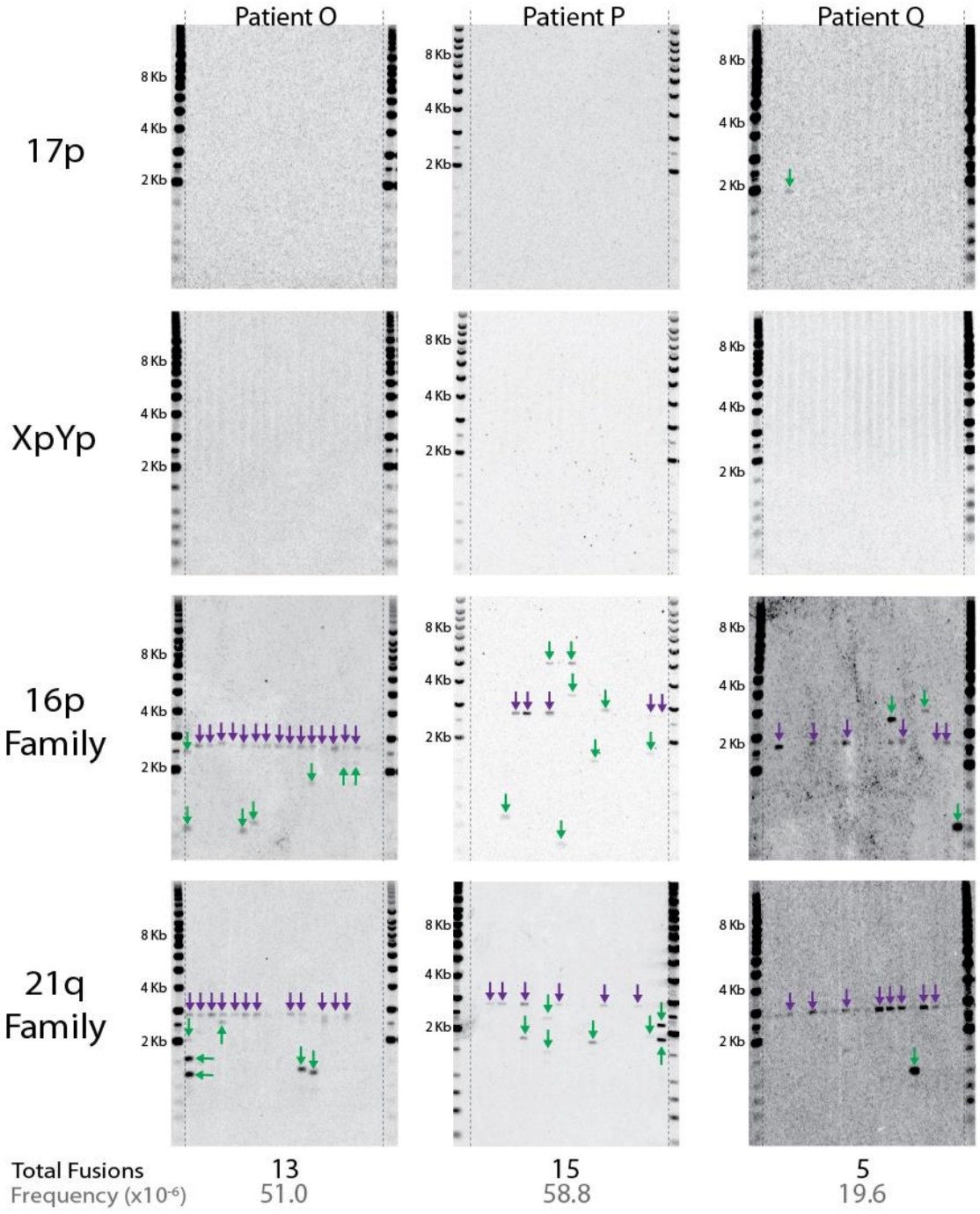

Supplementary Figure 3 - Bone Marrow Cells of MM Patients Show Evidence of Chromosomal Fusion

(a) Three MM patients whose DNA was examined for the presence of chromosomal fusion events. In total, 1530ng of DNA was analysed per patient. The frequency of chromosomal fusion was estimated by dividing the number of observable fusion bands by the number of input molecules (around 255,000 cells). Bands representing possible intrachromosomal fusion events were highlighted in green, while interchromosomal fusion events were highlighted in red. Purple arrows were used to highlight bands that were located in areas known for backgrounds bands (these were not included in the final analysis).

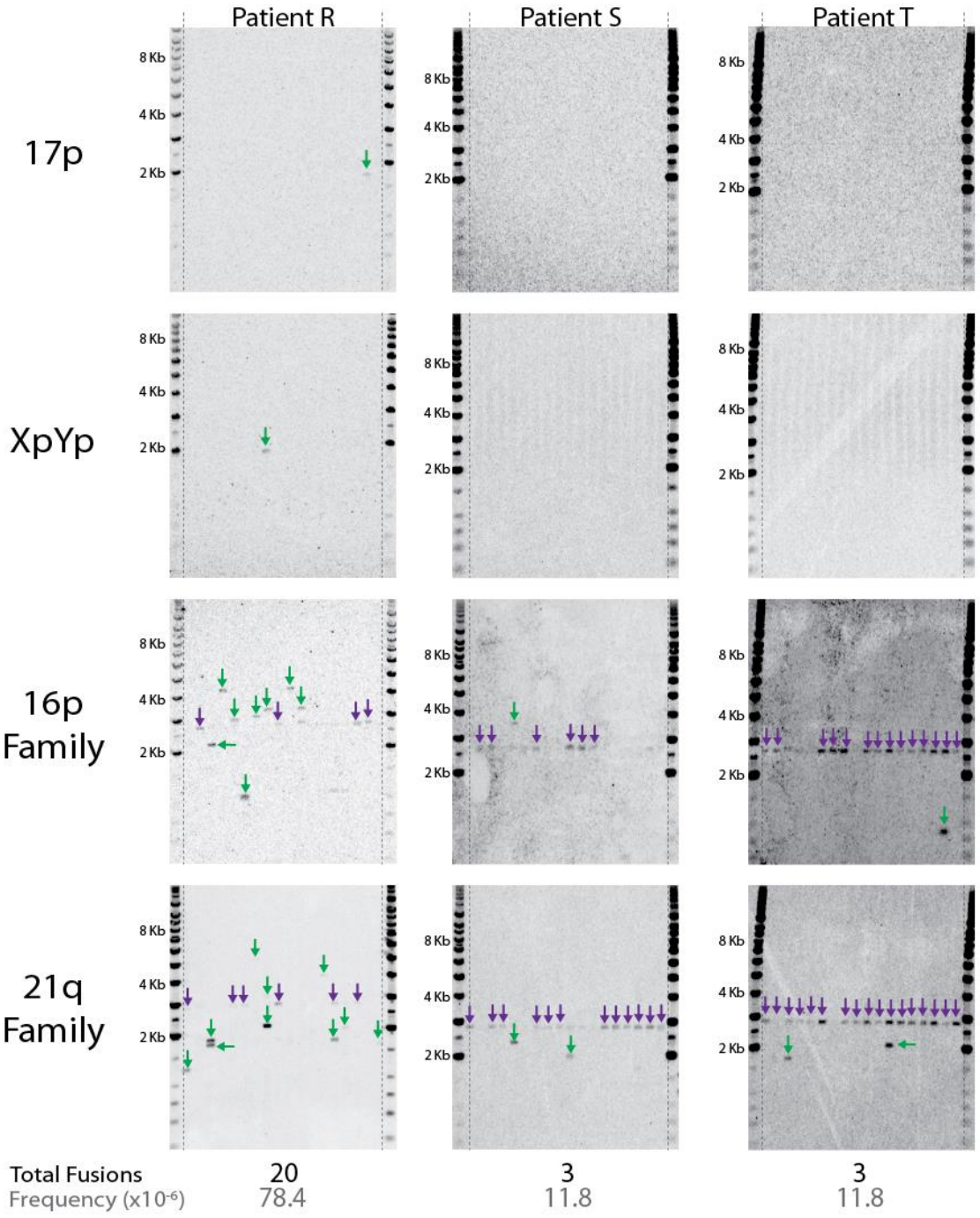

Supplementary Figure 4 - Bone Marrow Cells of MM Patients Show Evidence of Chromosomal Fusion

(a) Three MM patients whose DNA was examined for the presence of chromosomal fusion events. In total, 1530ng of DNA was analysed per patient. The frequency of chromosomal fusion was estimated by dividing the number of observable fusion bands by the number of input molecules (around 255,000 cells). Bands representing possible intrachromosomal fusion events were highlighted in green, while interchromosomal fusion events were highlighted in red. Purple arrows were used to highlight bands that were located in areas known for backgrounds bands (these were not included in the final analysis).

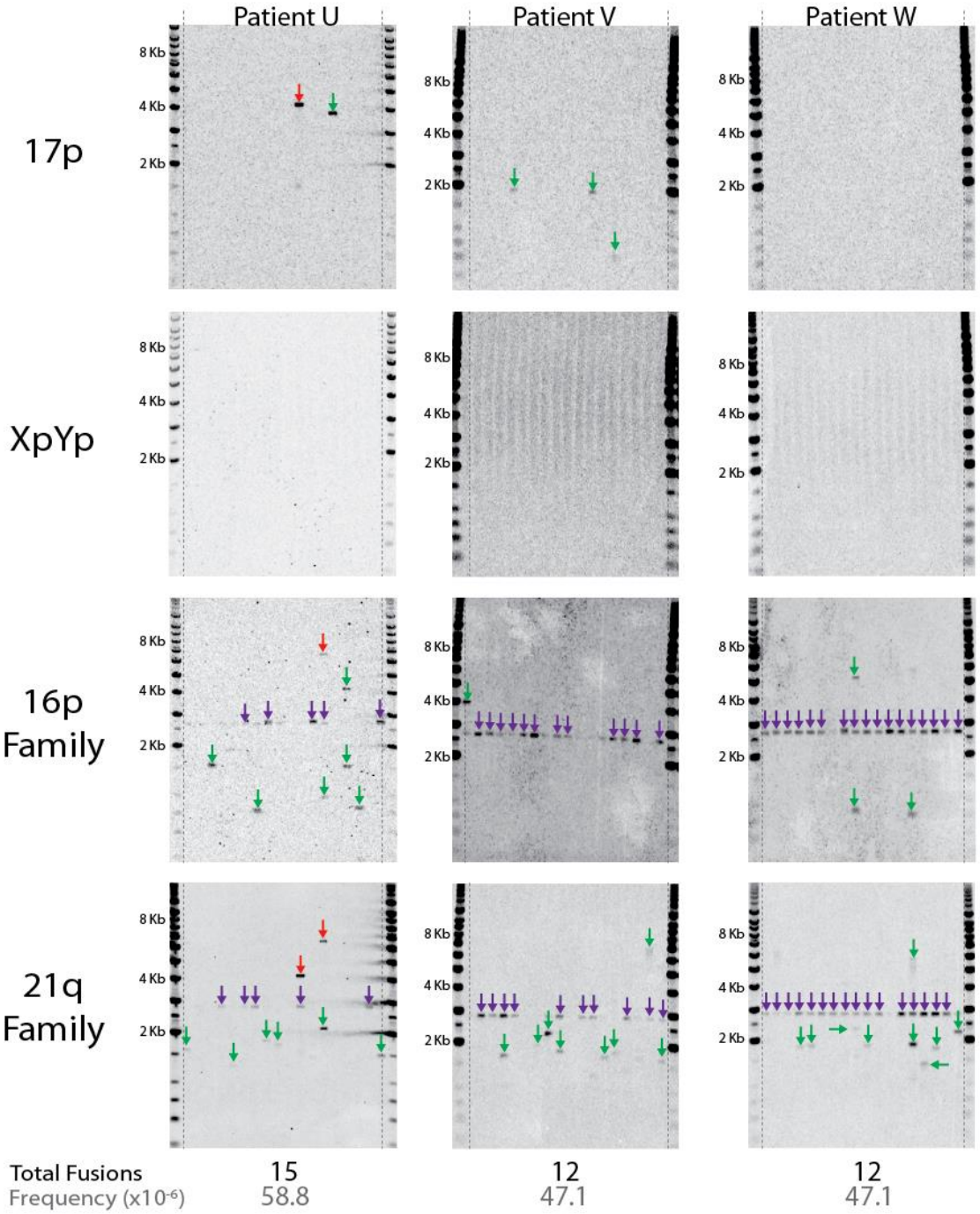

Supplementary Figure 5 - Bone Marrow Cells of MM Patients Show Evidence of Chromosomal Fusion

(a) Three MM patients whose DNA was examined for the presence of chromosomal fusion events. In total, 1530ng of DNA was analysed per patient. The frequency of chromosomal fusion was estimated by dividing the number of observable fusion bands by the number of input molecules (around 255,000 cells). Bands representing possible intrachromosomal fusion events were highlighted in green, while interchromosomal fusion events were highlighted in red. Purple arrows were used to highlight bands that were located in areas known for backgrounds bands (these were not included in the final analysis).

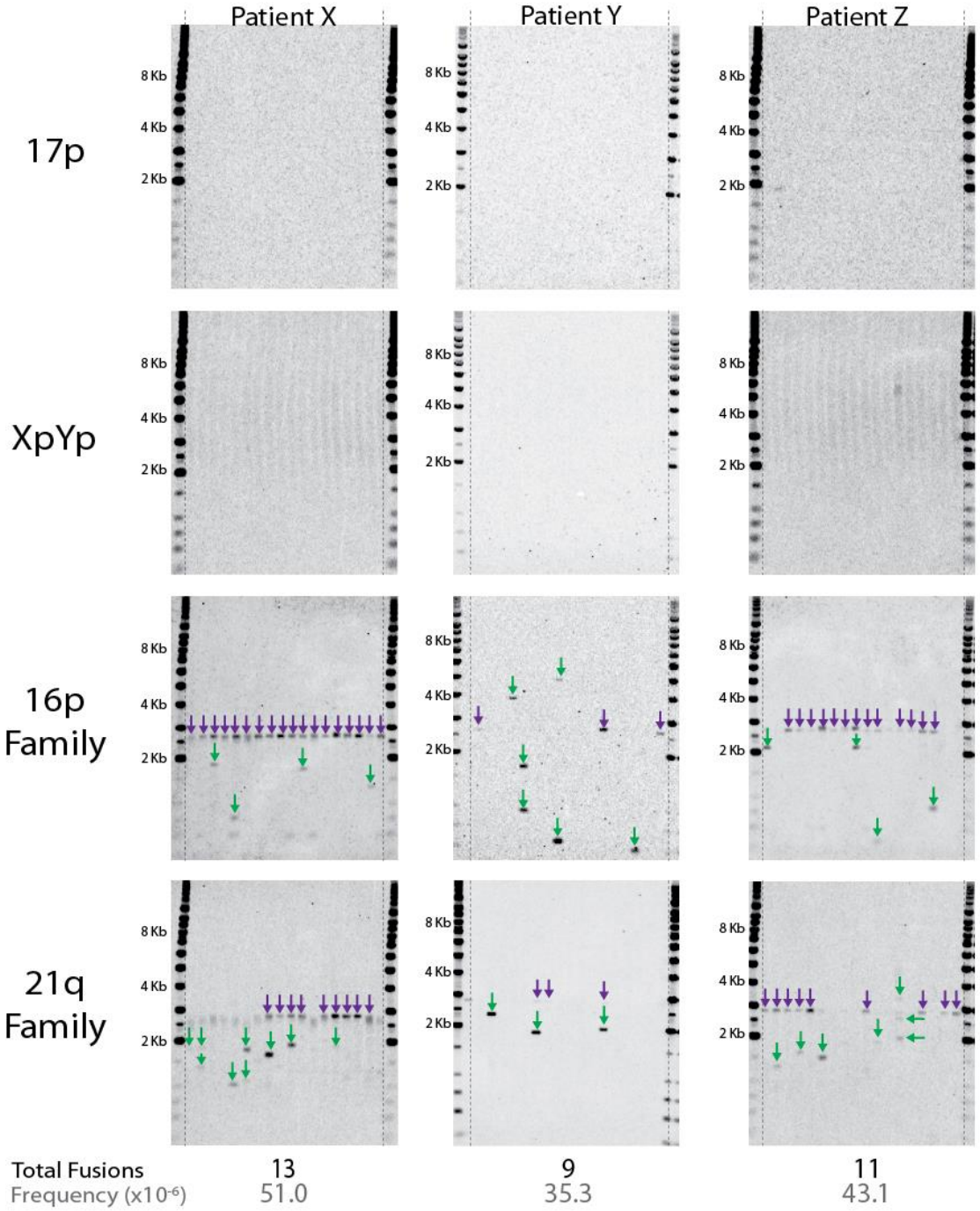

Supplementary Figure 6 - Bone Marrow Cells of MM Patients Show Evidence of Chromosomal Fusion

(a) Three MM patients whose DNA was examined for the presence of chromosomal fusion events. In total, 1530ng of DNA was analysed per patient. The frequency of chromosomal fusion was estimated by dividing the number of observable fusion bands by the number of input molecules (around 255,000 cells). Bands representing possible intrachromosomal fusion events were highlighted in green, while interchromosomal fusion events were highlighted in red. Purple arrows were used to highlight bands that were located in areas known for backgrounds bands (these were not included in the final analysis).

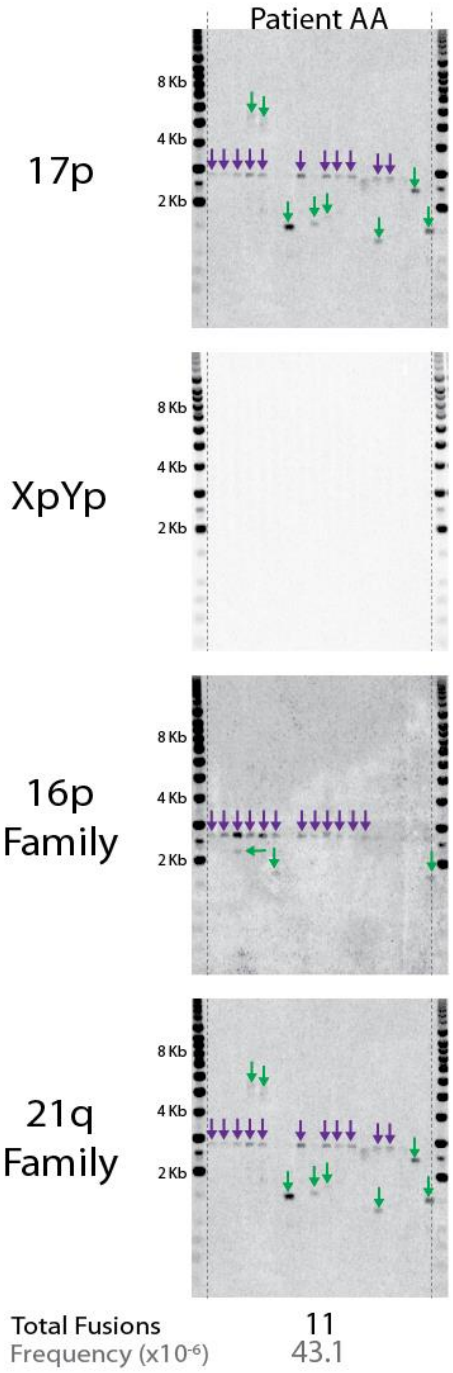

Supplementary Figure 7 - Bone Marrow Cells of MM Patients Show Evidence of Chromosomal Fusion

(a) A MM patient whose DNA was examined for the presence of chromosomal fusion events. In total, 1530ng of DNA was analysed per patient. The frequency of chromosomal fusion was estimated by dividing the number of observable fusion bands by the number of input molecules (around 255,000 cells). Bands representing possible intrachromosomal fusion events were highlighted in green, while interchromosomal fusion events were highlighted in red. Purple arrows were used to highlight bands that were located in areas known for backgrounds bands (these were not included in the final analysis).

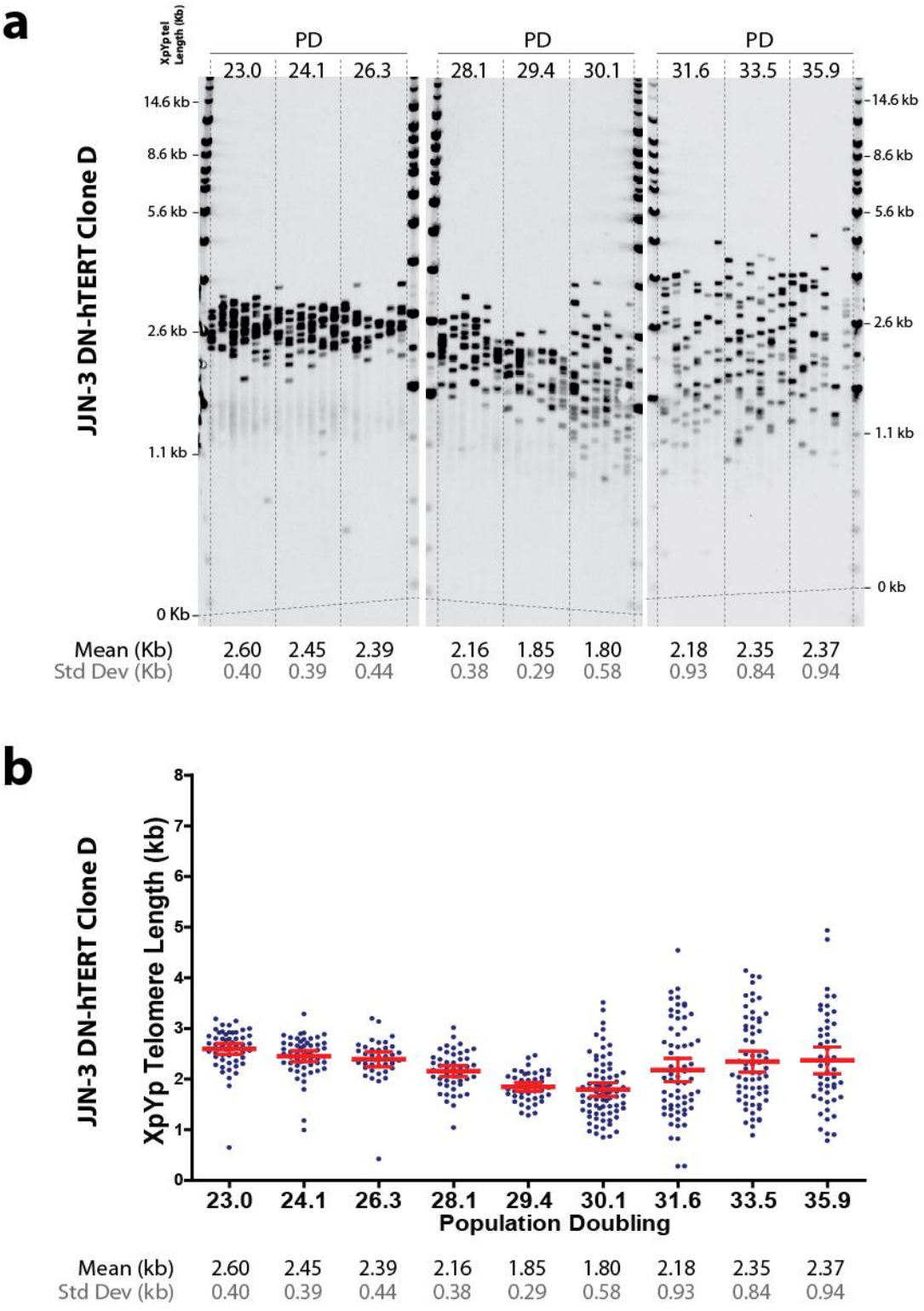

Supplementary Figure 8 - The Change in the XpYp Telomere Length of JJN-3 Clone D During a Period of Telomere-Driven Crisis

A clonal population of JJN-3 cells expressing DN-hTERT were grown over a period of 35.9 population doublings. Samples of cells were taken at 9 time points during this period, with STELA being performed as a way to measure the resulting XpYp telomere length. **(a)** STELA profiles showing the XpYp telomere lengths, during a period of telomere-driven crisis, in a clonal population of JJN-3 cells expressing DN-hTERT. **(b)** Graphical representation of the STELA profiles. The mean telomere length for each time point is shown in red alongside the uper and lower 95% confidance intervals.

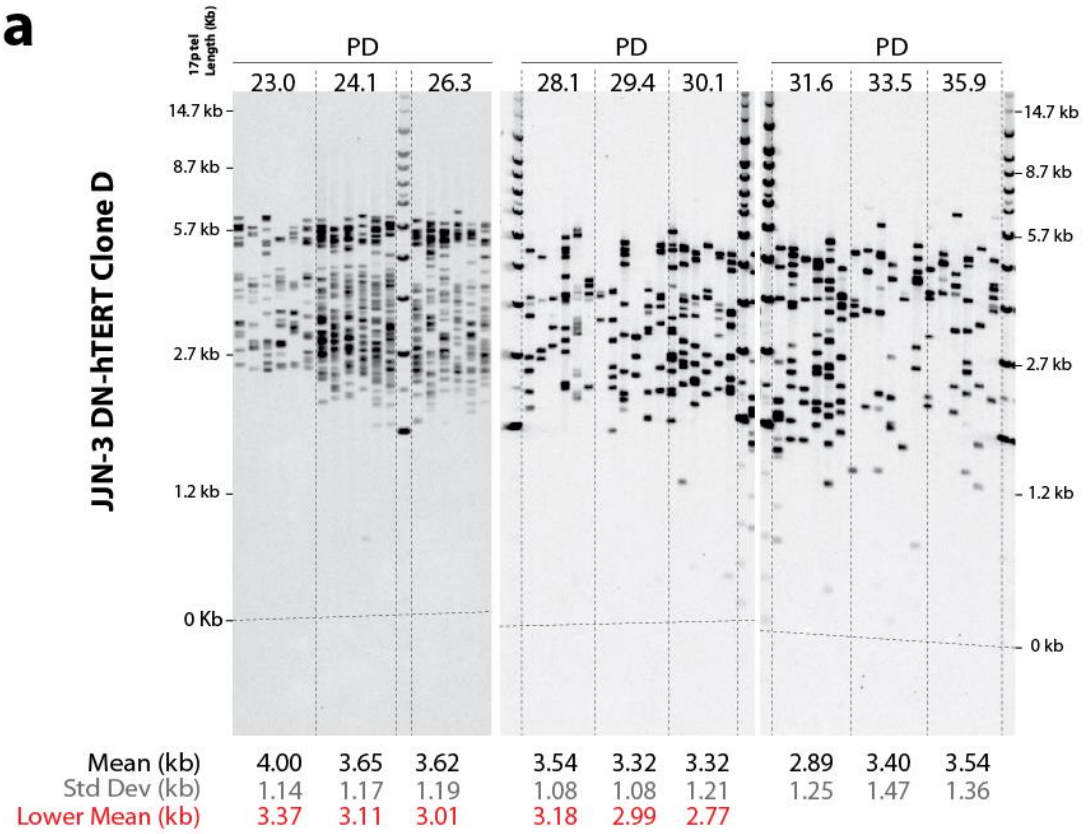

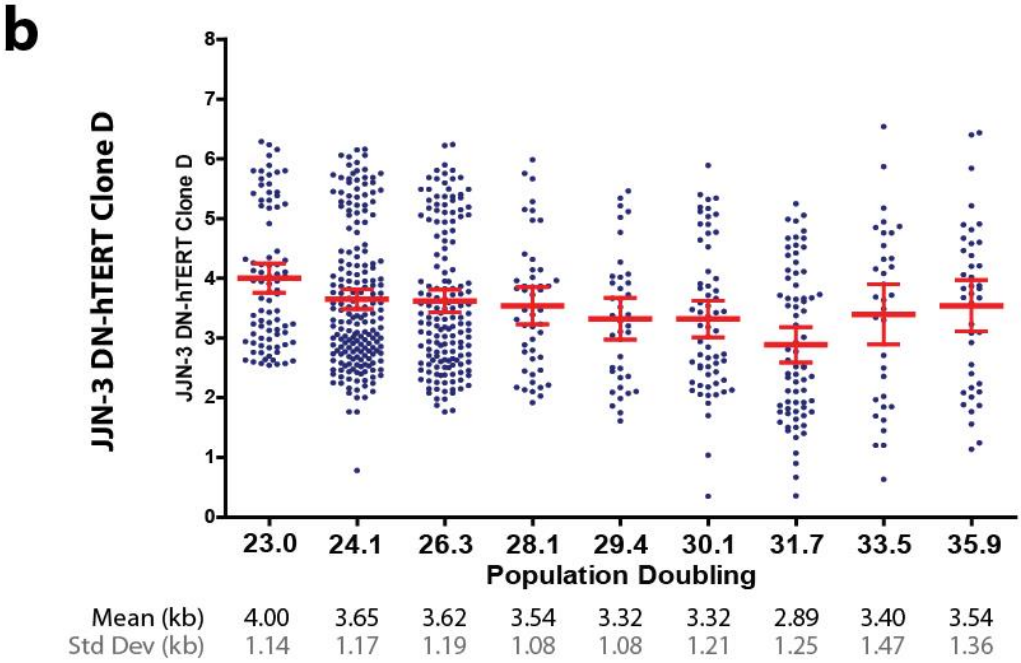

Supplementary Figure 9 - The Change in the 17p Telomere Length of JJN-3 Clone D During a Period of Telomere-Driven Crisis

A clonal population of JJN-3 cells expressing DN-hTERT were grown over a period of 35.9 population doublings. Samples of cells were taken at 9 time points during this period, with STELA being performed as a way to measure the resulting 17p telomere length. **(a)** STELA profiles showing the 17p telomere lengths, during a period of telomere-driven crisis, in a clonal population of JJN-3 cells expressing DN-hTERT. **(b)** Graphical representation of the STELA profiles. The mean telomere length for each time point is shown in red alongside the uper and lower 95% confidance intervals.

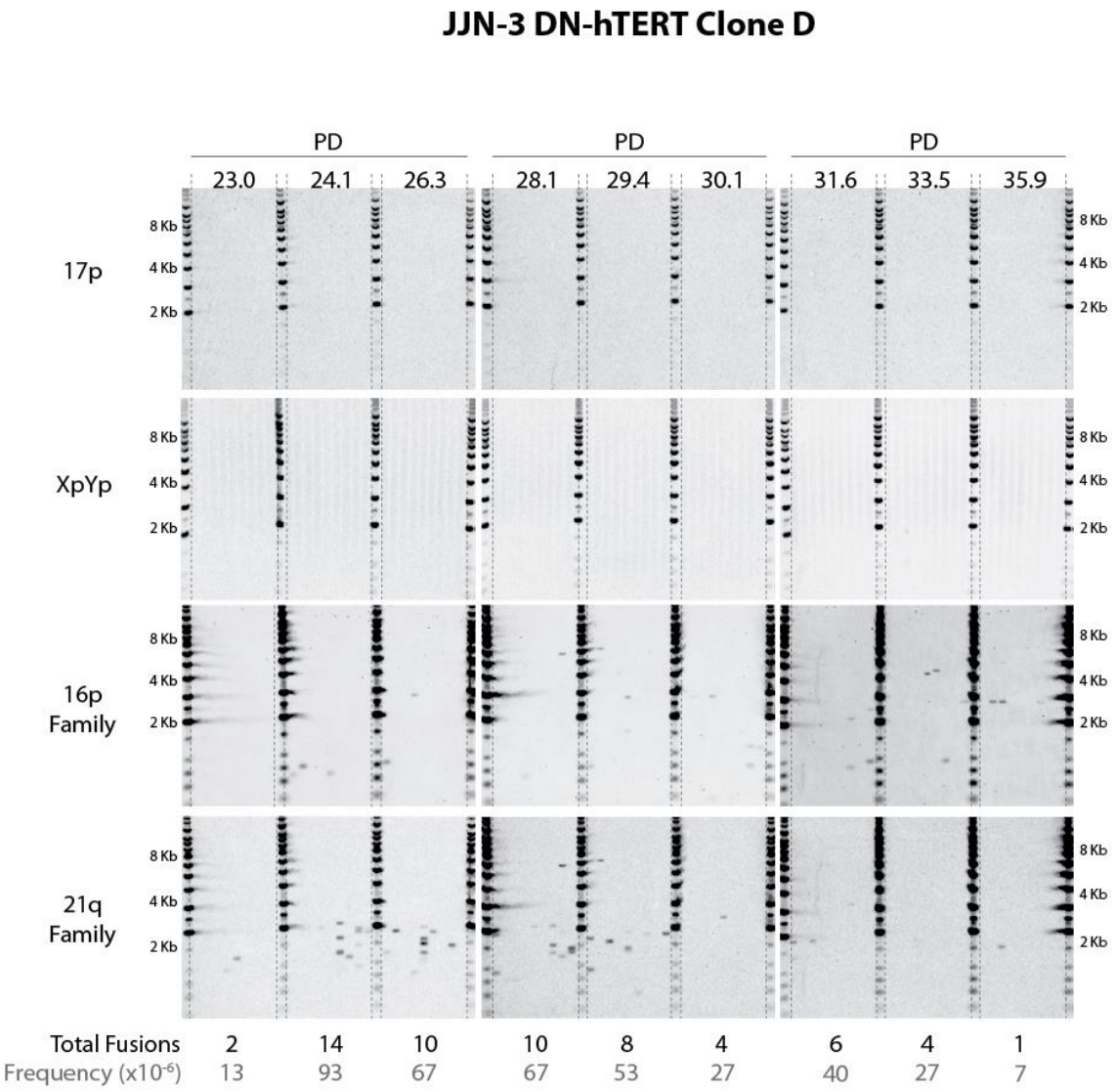

Supplementary Figure 10 - The Change in the Frequency of Chromosomal Fusion Events for JJN-3 Clone D During a Period of Telomere-Driven Crisis

The frequency of chromosomal fusion events in clone D was monitored during a period of telomere-dirven crisis. In total, 900ng of DNA were examined per time point. The frequency of chromosomal fusion was estimated by dividing the number of observable fusion bands by the number of input molecules (around 150,000 cells). Visualisation of these events was performed using the oligonucleotide probes 17p6, XpYpO-G, 16p1 and 21q1.

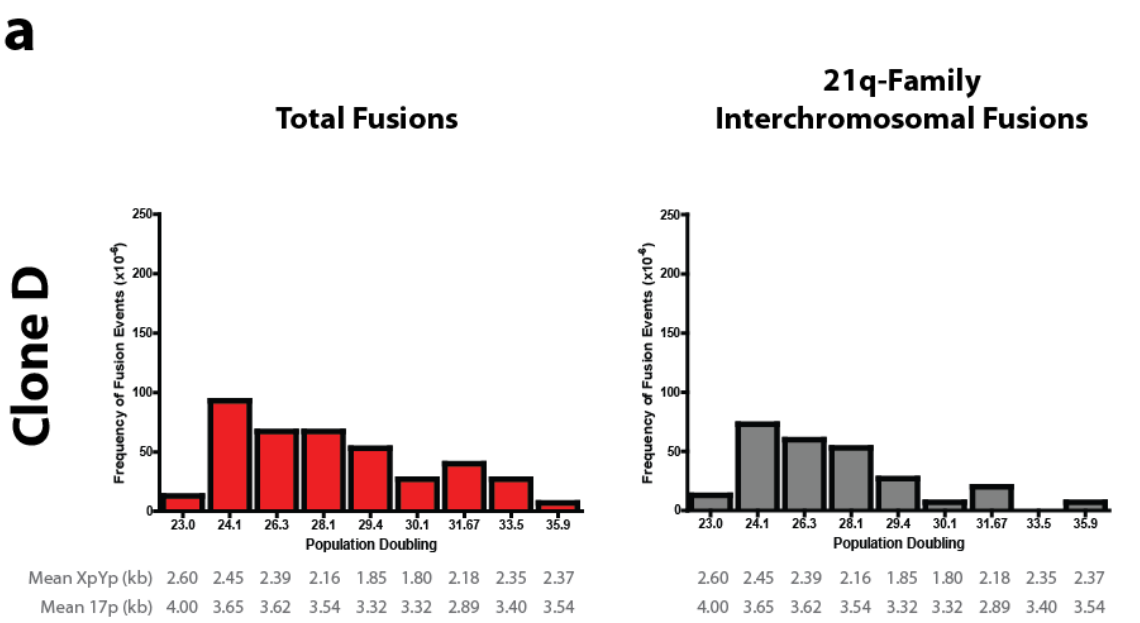

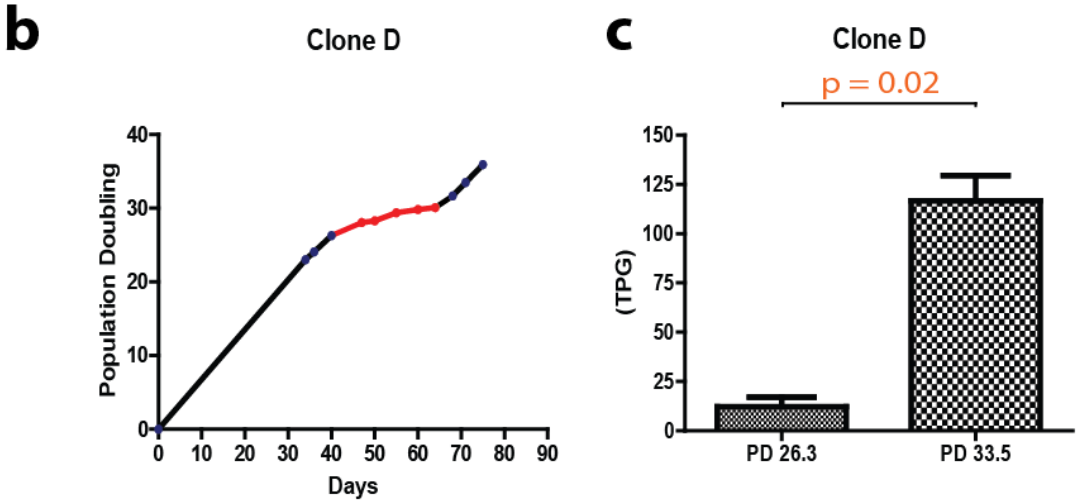

Supplementary Figure 11 - Characteristics of JJN-3 DN-hTERT Clone D
(a) Graphs showing either the total frequency of fusion events or the fusion events involving the 21q-family of chromosome ends. In total, 900ng of DNA were examined per time point. The frequency of chromosomal fusion was estimated by dividing the number of observable fusion bands by the number of input molecules (around 150,000 cells). Visualisation of these events was performed using the oligonucleotide probes 17p6, XpYpO-G, 16p1 and 21q1. The mean XpYp and 17p telomere lengths have been listed for each time point, underneath each graph. **(b)** A clonal population of the JJN-3 cell line, expressing the DN-hTERT protein, had its growth monitored over a period of weeks. During this time, the clonal population experienced a period of stalled growth which was thought to be caused by a telomere-induced crisis (highlighted in red). Eventually, the clonal population managed to escape from this period of crisis and resume the level of growth seen pre-crisis. **(c)** The telomerase activity of a JJN-3 clonal population was monitored before and after crisis. Total Product Generated (**TPG**) is a unit specific to the TRAPeze detection kit used to measure telomerase activity. Significance was determined using a paired t-test and defined as <0.05

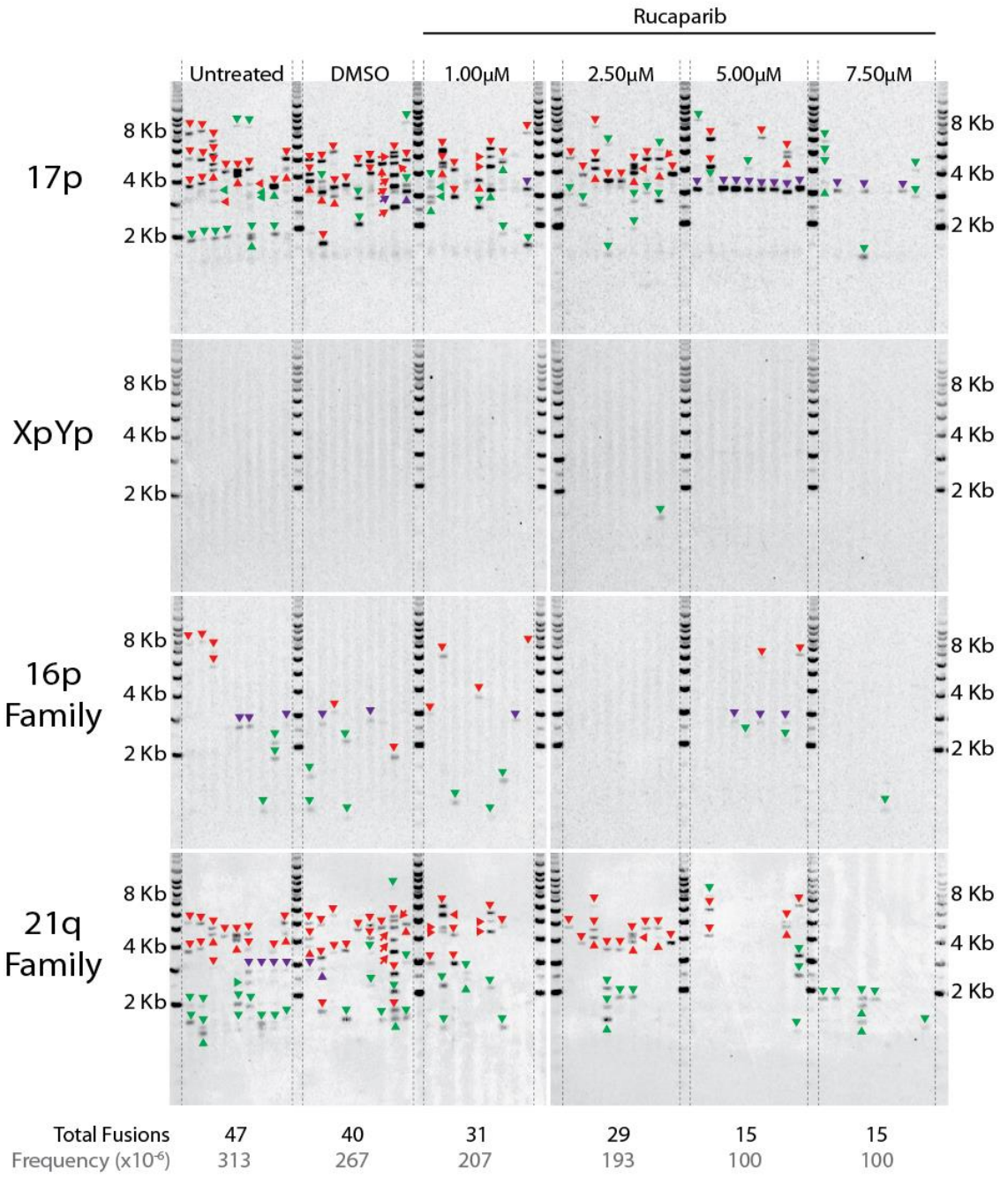

Supplementary Figure 12 - The Change in the Frequency of Chromosomal Fusion Events for JJN-3 DN-hTERT Clone B, Grown in the Presence of Rucaparib

JJN-3 DN-hTERT clone B was grown in the presence of Rucaparib. On day 52 (see ***figure 5.1a***) samples of cells were taken for DNA extraction. In total, 900ng of DNA were examined per time point. The frequency of chromosomal fusion was estimated by dividing the number of observable fusion bands by the number of input molecules (around 150,000 cells). Visualisation of these events was performed using the oligonucleotide probes 17p6, XpYpO-G, 16p1 and 21q1. Bands representing possible intrachromosomal fusion events were highlighted in green, while interchromosomal fusion events were highlighted in red. Purple arrows were used to highlight bands that were located in areas known for backgrounds bands (these were not included in the final analysis).

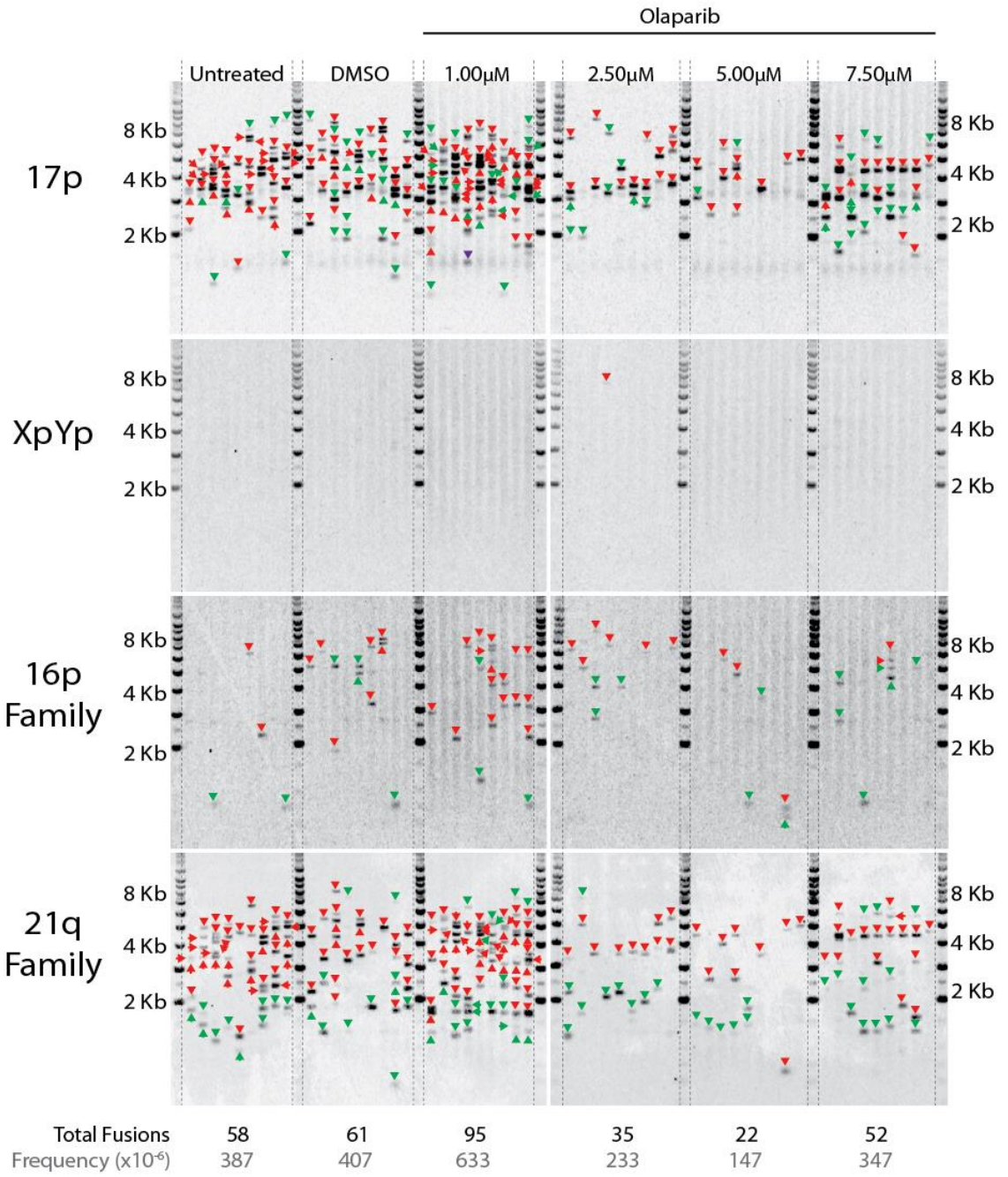

Supplementary Figure 13 - The Change in the Frequency of Chromosomal Fusion Events for JJN-3 DN-hTERT Clone B, Grown in the Presence of Olaparib

JJN-3 DN-hTERT clone B was grown in the presence of Olaparib. On day 56 (see ***figure 5.1b***) samples of cells were taken for DNA extraction. In total, 900ng of DNA were examined per time point. The frequency of chromosomal fusion was estimated by dividing the number of observable fusion bands by the number of input molecules (around 150,000 cells). Visualisation of these events was performed using the oligonucleotide probes 17p6, XpYpO-G, 16p1 and 21q1. Bands representing possible intrachromosomal fusion events were highlighted in green, while interchromosomal fusion events were highlighted in red. Purple arrows were used to highlight bands that were located in areas known for backgrounds bands (these were not included in the final analysis).

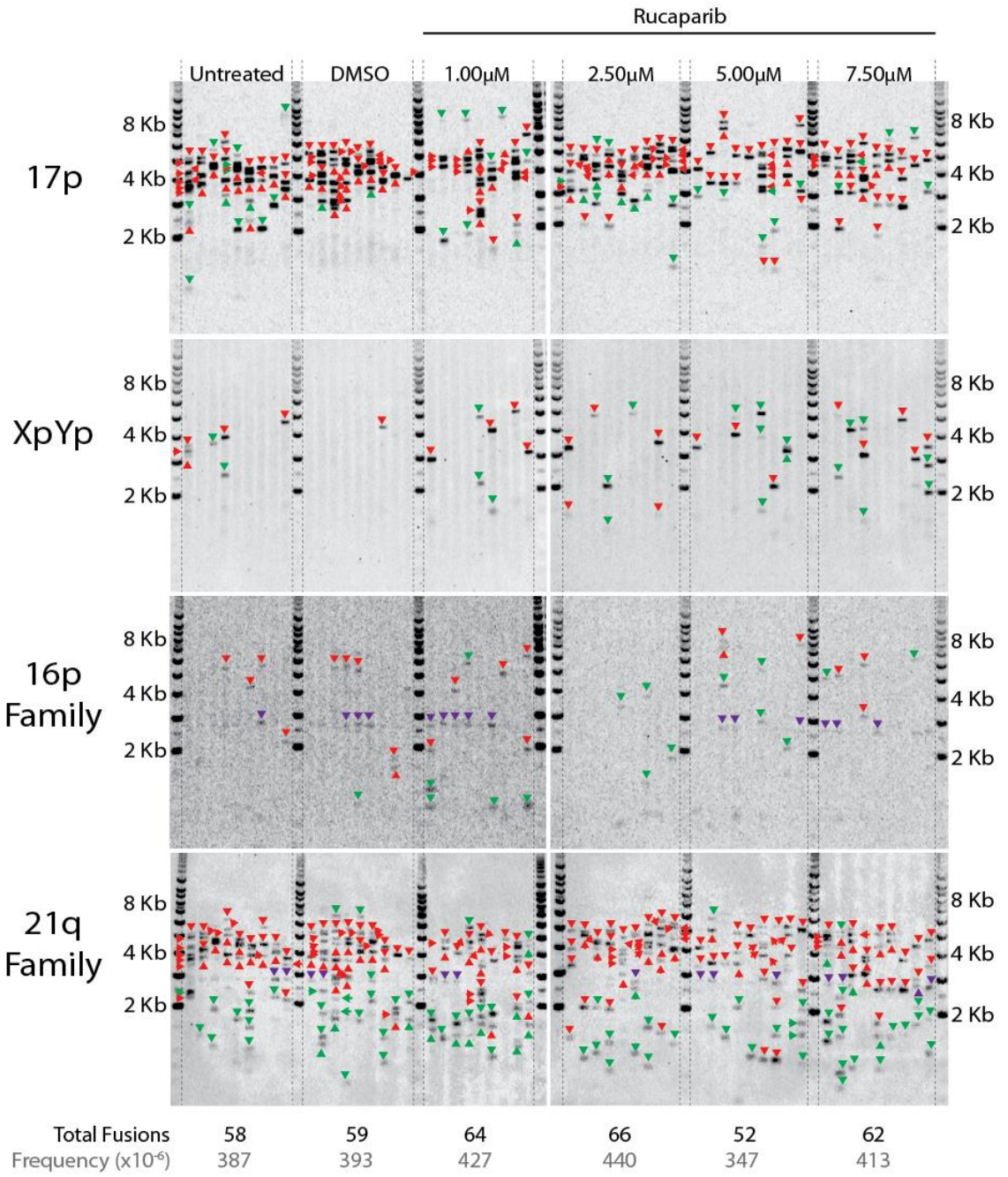

Supplementary Figure 14 - The Change in the Frequency of Chromosomal Fusion Events for JJN-3 DN-hTERT Clone C, Grown in the Presence of Rucaparib

JJN-3 DN-hTERT clone C was grown in the presence of Rucaparib. On day 67 (see ***figure 5.2a***) samples of cells were taken for DNA extraction. In total, 900ng of DNA were examined per time point. The frequency of chromosomal fusion was estimated by dividing the number of observable fusion bands by the number of input molecules (around 150,000 cells). Visualisation of these events was performed using the oligonucleotide probes 17p6, XpYpO-G, 16p1 and 21q1. Bands representing possible intrachromosomal fusion events were highlighted in green, while interchromosomal fusion events were highlighted in red. Purple arrows were used to highlight bands that were located in areas known for backgrounds bands (these were not included in the final analysis).

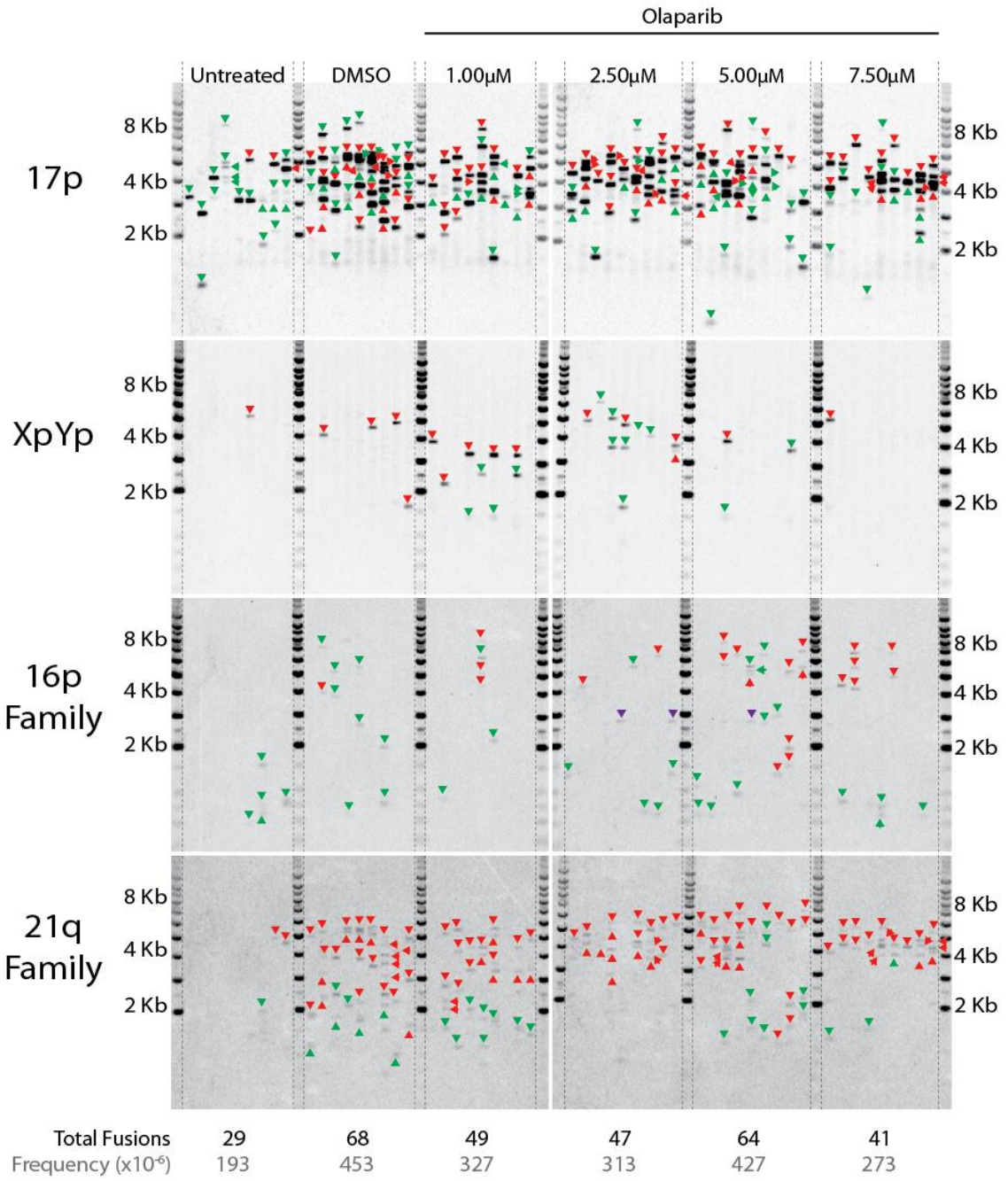

Supplementary Figure 15 - The Change in the Frequency of Chromosomal Fusion Events for JJN-3 DN-hTERT Clone C, Grown in the Presence of Olaparib

JJN-3 DN-hTERT clone C was grown in the presence of Rucaparib. On day 61 (see ***figure 5.2b***) samples of cells were taken for DNA extraction. In total, 900ng of DNA were examined per time point. The frequency of chromosomal fusion was estimated by dividing the number of observable fusion bands by the number of input molecules (around 150,000 cells). Visualisation of these events was performed using the oligonucleotide probes 17p6, XpYpO-G, 16p1 and 21q1. Bands representing possible intrachromosomal fusion events were highlighted in green, while interchromosomal fusion events were highlighted in red. Purple arrows were used to highlight bands that were located in areas known for backgrounds bands (these were not included in the final analysis).

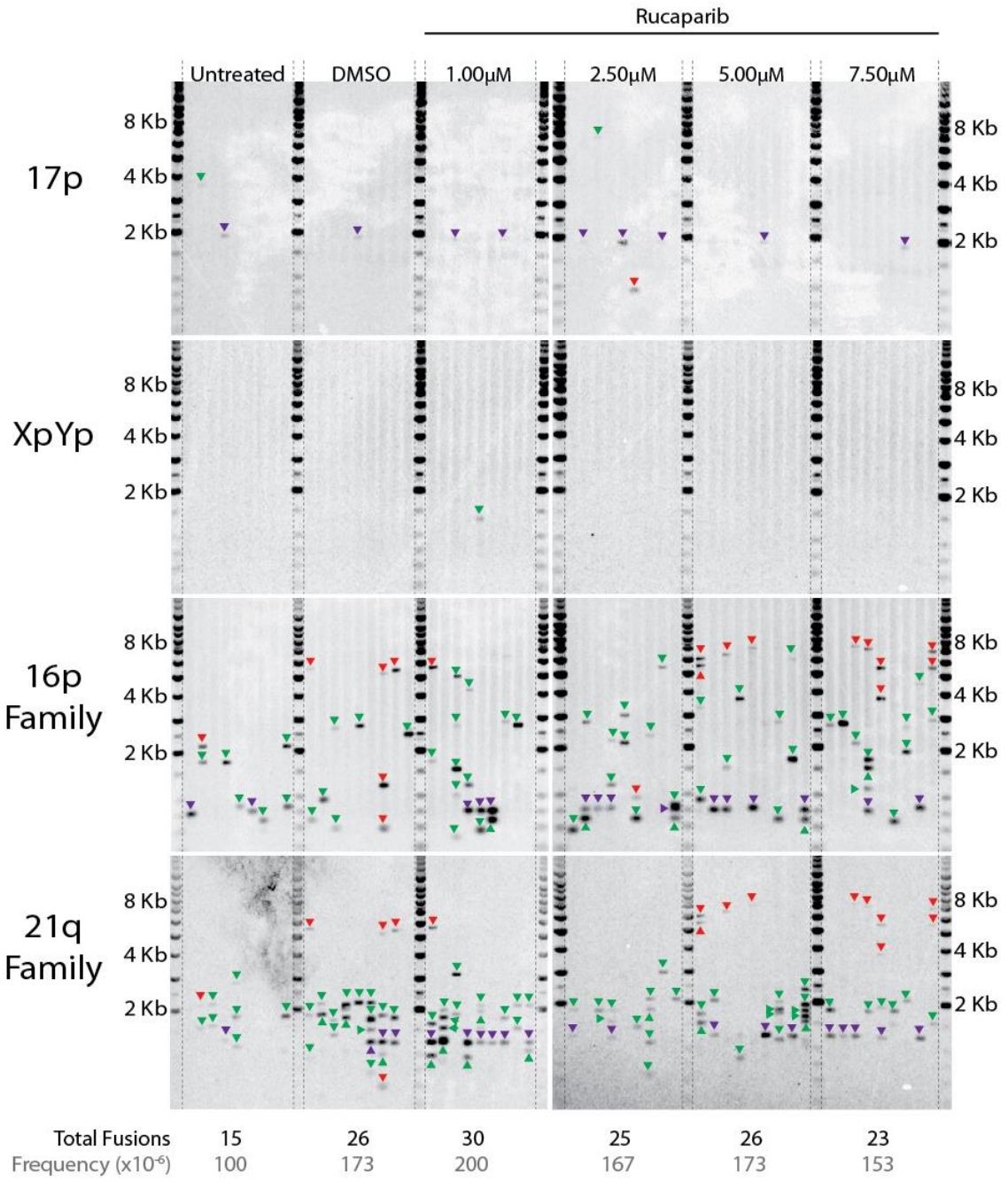

Supplementary Figure 16 - The Change in the Frequency of Chromosomal Fusion Events for JJN-3 DN-hTERT Clone D, Grown in the Presence of Rucaparib

JJN-3 DN-hTERT clone D was grown in the presence of Rucaparib. On day 58 (see ***figure 5.3a***) samples of cells were taken for DNA extraction. In total, 900ng of DNA were examined per time point. The frequency of chromosomal fusion was estimated by dividing the number of observable fusion bands by the number of input molecules (around 150,000 cells). Visualisation of these events was performed using the oligonucleotide probes 17p6, XpYpO-G, 16p1 and 21q1. Bands representing possible intrachromosomal fusion events were highlighted in green, while interchromosomal fusion events were highlighted in red. Purple arrows were used to highlight bands that were located in areas known for backgrounds bands (these were not included in the final analysis).

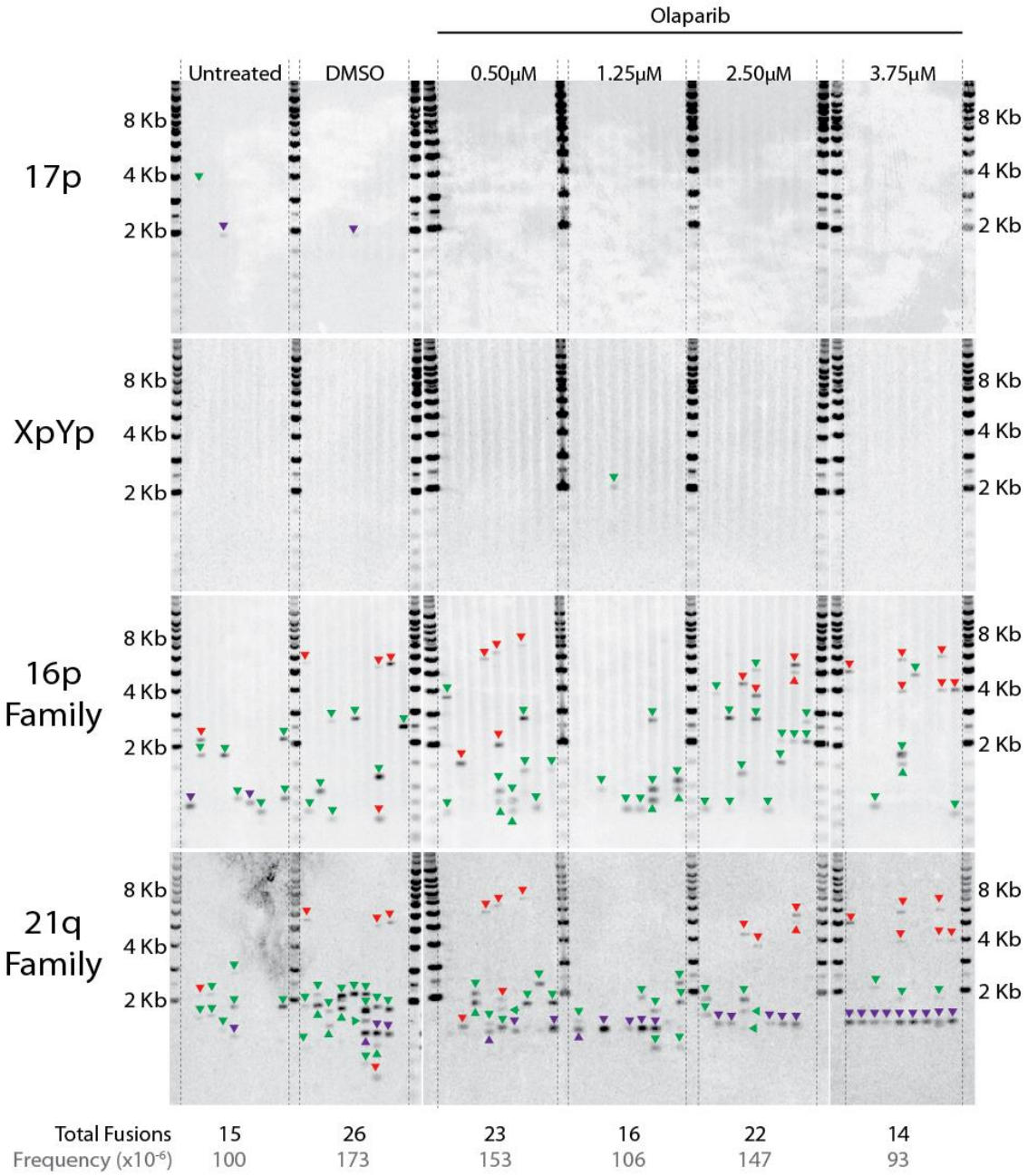

Supplementary Figure 17 - The Change in the Frequency of Chromosomal Fusion Events for JJN-3 DN-hTERT Clone D, Grown in the Presence of Olaparib

JJN-3 DN-hTERT clone D was grown in the presence of Olaparib. On day 58 (see ***figure 5.3b***) samples of cells were taken for DNA extraction. In total, 900ng of DNA were examined per time point. The frequency of chromosomal fusion was estimated by dividing the number of observable fusion bands by the number of input molecules (around 150,000 cells). Visualisation of these events was performed using the oligonucleotide probes 17p6, XpYpO-G, 16p1 and 21q1. Bands representing possible intrachromosomal fusion events were highlighted in green, while interchromosomal fusion events were highlighted in red. Purple arrows were used to highlight bands that were located in areas known for backgrounds bands (these were not included in the final analysis).

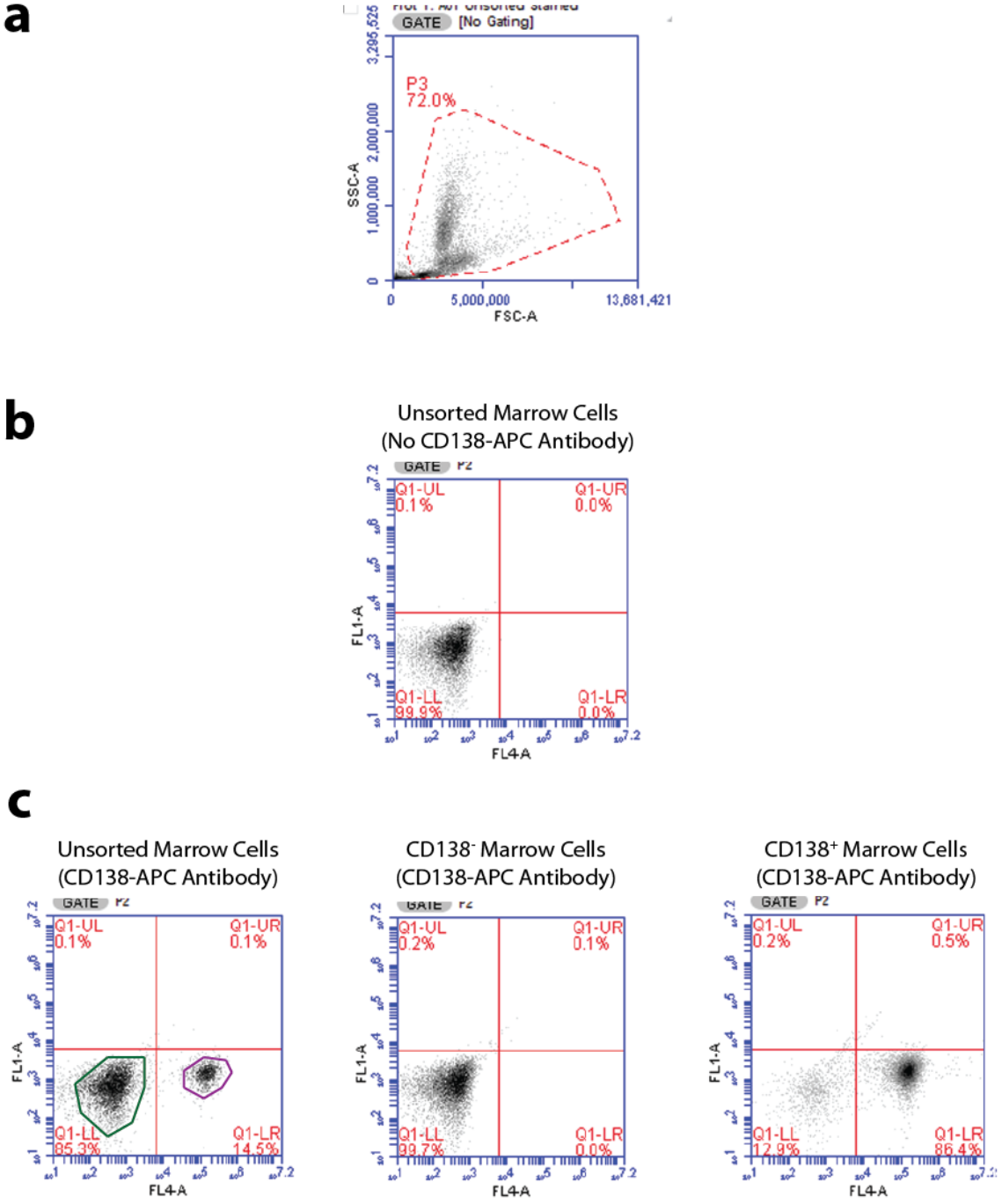

Supplementary Figure 18 - Flow Cytometric Analysis of CD138-Sorted Marrow Cells
Flow cytomety was used to determine the purity of the CD138$^-$ and CD138$^+$ sorted bone marrow samples. In total, 10,000 events were recorded per sample **(a)** Each sample was analysed using FCS-A against SSC-A. Appropriate gating was then used to isolate the cell debris and dead cells **(b)** A sample of the unsorted marrow cells was analysed using FLA-4 and FLA-1. This sample was not treated with the CD138-APC antibody and so was used as a control. **(c)** A sample of unsorted marrow cells, CD138$^-$ sorted cells and CD138$^+$ sorted cells were analysed using FL4-A against FL1-A. In each case, the purity of the sample was >80%. In the unsorted sample, the CD138$^-$ cells have been highlighted in green, while the CD138$^+$ cells have been highlighted in purple.

References

Adams, S. P., T. P. Hartman, K. Y. Lim, M. W. Chase, M. D. Bennett, I. J. Leitch, and A. R. Leitch. 2001. 'Loss and recovery of Arabidopsis-type telomere repeat sequences 5'-(TTTAGGG)(n)-3' in the evolution of a major radiation of flowering plants', *Proc Biol Sci*, 268: 1541-6.

Akiyama, M., T. Hideshima, M. A. Shammas, T. Hayashi, M. Hamasaki, Y. T. Tai, P. Richardson, S. Gryaznov, N. C. Munshi, and K. C. Anderson. 2003. 'Effects of oligonucleotide N3'-->P5' thio-phosphoramidate (GRN163) targeting telomerase RNA in human multiple myeloma cells', *Cancer Res*, 63: 6187-94.

Al-Quran, S. Z., L. Yang, J. M. Magill, R. C. Braylan, and V. K. Douglas-Nikitin. 2007. 'Assessment of bone marrow plasma cell infiltrates in multiple myeloma: the added value of CD138 immunohistochemistry', *Hum Pathol*, 38: 1779-87.

Alagpulinsa, D. A., S. Ayyadevara, S. Yaccoby, and R. J. Shmookler Reis. 2016. 'A Cyclin-Dependent Kinase Inhibitor, Dinaciclib, Impairs Homologous Recombination and Sensitizes Multiple Myeloma Cells to PARP Inhibition', *Mol Cancer Ther*, 15: 241-50.

Albanell, J., F. Lonardo, V. Rusch, M. Engelhardt, J. Langenfeld, W. Han, D. Klimstra, E. Venkatraman, M. A. Moore, and E. Dmitrovsky. 1997. 'High telomerase activity in primary lung cancers: association with increased cell proliferation rates and advanced pathologic stage', *J Natl Cancer Inst*, 89: 1609-15.

Albert, J. M., C. Cao, K. W. Kim, C. D. Willey, L. Geng, D. Xiao, H. Wang, A. Sandler, D. H. Johnson, A. D. Colevas, J. Low, M. L. Rothenberg, and B. Lu. 2007. 'Inhibition of poly(ADP-ribose) polymerase enhances cell death and improves tumor growth delay in irradiated lung cancer models', *Clin Cancer Res*, 13: 3033-42.

Alderton, G. K., H. Joenje, R. Varon, A. D. Borglum, P. A. Jeggo, and M. O'Driscoll. 2004. 'Seckel syndrome exhibits cellular features demonstrating defects in the ATR-signalling pathway', *Hum Mol Genet*, 13: 3127-38.

Allen, C. D., T. Okada, and J. G. Cyster. 2007. 'Germinal-center organization and cellular dynamics', *Immunity*, 27: 190-202.

Allsopp, R. C., H. Vaziri, C. Patterson, S. Goldstein, E. V. Younglai, A. B. Futcher, C. W. Greider, and C. B. Harley. 1992. 'Telomere length predicts replicative capacity of human fibroblasts', *Proc Natl Acad Sci U S A*, 89: 10114-8.

Alter, B. P., G. M. Baerlocher, S. A. Savage, S. J. Chanock, B. B. Weksler, J. P. Willner, J. A. Peters, N. Giri, and P. M. Lansdorp. 2007. 'Very short telomere length by flow fluorescence in situ hybridization identifies patients with dyskeratosis congenita', *Blood*, 110: 1439-47.

Alter, B. P., N. Giri, S. A. Savage, and P. S. Rosenberg. 2009. 'Cancer in dyskeratosis congenita', *Blood*, 113: 6549-57.

Ame, J. C., C. Spenlehauer, and G. de Murcia. 2004. 'The PARP superfamily', *Bioessays*, 26: 882-93.

Amodio, N., M. T. Di Martino, U. Foresta, E. Leone, M. Lionetti, M. Leotta, A. M. Gulla, M. R. Pitari, F. Conforti, M. Rossi, V. Agosti, M. Fulciniti, G. Misso, F. Morabito, M. Ferrarini, A. Neri, M. Caraglia, N. C. Munshi, K. C. Anderson, P. Tagliaferri, and P. Tassone. 2012. 'miR-29b sensitizes multiple myeloma cells to bortezomib-induced apoptosis through the activation of a feedback loop with the transcription factor Sp1', *Cell Death Dis*, 3: e436.

Amorim, J. P., G. Santos, J. Vinagre, and P. Soares. 2016. 'The Role of ATRX in the Alternative Lengthening of Telomeres (ALT) Phenotype', *Genes (Basel)*, 7.

Ancelin, K., M. Brunori, S. Bauwens, C. E. Koering, C. Brun, M. Ricoul, J. P. Pommier, L. Sabatier, and E. Gilson. 2002. 'Targeting assay to study the cis functions of human telomeric proteins: evidence for inhibition of telomerase by TRF1 and for activation of telomere degradation by TRF2', *Mol Cell Biol*, 22: 3474-87.

Antoniou, A. C., A. B. Spurdle, O. M. Sinilnikova, S. Healey, K. A. Pooley, R. K. Schmutzler, B. Versmold, C. Engel, A. Meindl, N. Arnold, W. Hofmann, C. Sutter, D. Niederacher, H. Deissler, T. Caldes, K. Kampjarvi, H. Nevanlinna, J. Simard, J. Beesley, X. Chen, Cancer Kathleen Cuningham Consortium for Research into Familial Breast, S. L. Neuhausen, T. R. Rebbeck, T. Wagner, H. T. Lynch, C. Isaacs, J. Weitzel, P. A. Ganz, M. B. Daly, G. Tomlinson, O. I. Olopade, J. L. Blum, F. J. Couch, P. Peterlongo, S. Manoukian, M. Barile, P. Radice, C. I. Szabo, L. H. Pereira, M. H. Greene, G. Rennert, F. Lejbkowicz, O. Barnett-Griness, I. L. Andrulis, H. Ozcelik, Ocgn, A. M. Gerdes, M. A. Caligo, Y. Laitman, B. Kaufman, R. Milgrom, E. Friedman, Brca Swedish, Brca study collaborators, S. M. Domchek, K. L. Nathanson, A. Osorio, G. Llort, R. L. Milne, J. Benitez, U. Hamann, F. B. Hogervorst, P. Manders, M. J. Ligtenberg, A. M. van den Ouweland, Dna-Hebon collaborators, S. Peock, M. Cook, R. Platte, D. G. Evans, R. Eeles, G. Pichert, C. Chu, D. Eccles, R. Davidson, F. Douglas, Embrace, A. K. Godwin, L. Barjhoux, S. Mazoyer, H. Sobol, V. Bourdon, F. Eisinger, A. Chompret, C. Capoulade, B. Bressac-de Paillerets, G. M. Lenoir, M. Gauthier-Villars, C. Houdayer, D. Stoppa-Lyonnet, Gemo, G. Chenevix-Trench, D. F. Easton, and Cimba. 2008. 'Common breast cancer-predisposition alleles are associated with breast cancer risk in BRCA1 and BRCA2 mutation carriers', *Am J Hum Genet*, 82: 937-48.

Antoniou, A., P. D. Pharoah, S. Narod, H. A. Risch, J. E. Eyfjord, J. L. Hopper, N. Loman, H. Olsson, O. Johannsson, A. Borg, B. Pasini, P. Radice, S. Manoukian, D. M. Eccles, N. Tang, E. Olah, H. Anton-Culver, E. Warner, J. Lubinski, J. Gronwald, B. Gorski, H. Tulinius, S. Thorlacius, H. Eerola, H. Nevanlinna, K. Syrjakoski, O. P. Kallioniemi, D. Thompson, C. Evans, J. Peto, F. Lalloo, D. G. Evans, and D. F. Easton. 2003. 'Average risks of breast and ovarian cancer associated with BRCA1 or BRCA2 mutations detected in case Series unselected for family history: a combined analysis of 22 studies', *Am J Hum Genet*, 72: 1117-30.

Arndt, G. M., and K. L. MacKenzie. 2016. 'New prospects for targeting telomerase beyond the telomere', *Nat Rev Cancer*, 16: 508-24.

Arnoult, N., and J. Karlseder. 2015. 'Complex interactions between the DNA-damage response and mammalian telomeres', *Nat Struct Mol Biol*, 22: 859-66.

Aubert, G., M. Hills, and P. M. Lansdorp. 2012. 'Telomere length measurement-caveats and a critical assessment of the available technologies and tools', *Mutat Res*, 730: 59-67.

Audebert, M., B. Salles, and P. Calsou. 2004. 'Involvement of poly(ADP-ribose) polymerase-1 and XRCC1/DNA ligase III in an alternative route for DNA double-strand breaks rejoining', *J Biol Chem*, 279: 55117-26.

Augustson, B. M., G. Begum, J. A. Dunn, N. J. Barth, F. Davies, G. Morgan, J. Behrens, A. Smith, J. A. Child, and M. T. Drayson. 2005. 'Early mortality after diagnosis of multiple myeloma: analysis of patients entered onto the United kingdom Medical Research Council trials between 1980 and 2002--Medical Research Council Adult Leukaemia Working Party', *J Clin Oncol*, 23: 9219-26.

Avet-Loiseau, H., M. Attal, P. Moreau, C. Charbonnel, F. Garban, C. Hulin, S. Leyvraz, M. Michallet, I. Yakoub-Agha, L. Garderet, G. Marit, L. Michaux, L. Voillat, M. Renaud, B. Grosbois, G. Guillerm, L. Benboubker, M. Monconduit, C. Thieblemont, P. Casassus, D. Caillot, A. M. Stoppa, J. J. Sotto, M. Wetterwald, C. Dumontet, J. G. Fuzibet, I. Azais, V. Dorvaux, M. Zandecki, R. Bataille, S. Minvielle, J. L. Harousseau, T. Facon, and C. Mathiot. 2007. 'Genetic abnormalities and survival in multiple myeloma: the experience of the Intergroupe Francophone du Myelome', *Blood*, 109: 3489-95.

Avet-Loiseau, H., T. Facon, B. Grosbois, F. Magrangeas, M. J. Rapp, J. L. Harousseau, S. Minvielle, R. Bataille, and Myelome Intergroupe Francophone du. 2002. 'Oncogenesis of multiple myeloma: 14q32 and 13q chromosomal abnormalities are not randomly distributed, but correlate with natural history, immunological features, and clinical presentation', *Blood*, 99: 2185-91.

Avet-Loiseau, H., F. Gerson, F. Magrangeas, S. Minvielle, J. L. Harousseau, R. Bataille, and Myelome Intergroupe Francophone du. 2001. 'Rearrangements of the c-myc oncogene are present in 15% of primary human multiple myeloma tumors', *Blood*, 98: 3082-6.

Aviv, A., S. C. Hunt, J. Lin, X. Cao, M. Kimura, and E. Blackburn. 2011. 'Impartial comparative analysis of measurement of leukocyte telomere length/DNA content by Southern blots and qPCR', *Nucleic Acids Res*, 39: e134.

Azzalin, C. M., and J. Lingner. 2015. 'Telomere functions grounding on TERRA firma', *Trends Cell Biol*, 25: 29-36.

Bailey, S. M., M. A. Brenneman, and E. H. Goodwin. 2004. 'Frequent recombination in telomeric DNA may extend the proliferative life of telomerase-negative cells', *Nucleic Acids Res*, 32: 3743-51.

Bainbridge, M. N., G. N. Armstrong, M. M. Gramatges, A. A. Bertuch, S. N. Jhangiani, H. Doddapaneni, L. Lewis, J. Tombrello, S. Tsavachidis, Y. Liu, A. Jalali, S. E. Plon, C. C. Lau, D. W. Parsons, E. B. Claus, J. Barnholtz-Sloan, D. Il'yasova, J. Schildkraut, F. Ali-Osman, S. Sadetzki, C. Johansen, R. S. Houlston, R. B. Jenkins, D. Lachance, S. H. Olson, J. L. Bernstein, R. T. Merrell, M. R. Wrensch, K. M. Walsh, F. G. Davis, R. Lai, S. Shete, K. Aldape, C. I. Amos, P. A. Thompson, D. M. Muzny, R. A. Gibbs, B. S. Melin, M. L. Bondy, and Consortium Gliogene. 2015. 'Germline mutations in shelterin complex genes are associated with familial glioma', *J Natl Cancer Inst*, 107: 384.

Baird, D. M., J. Coleman, Z. H. Rosser, and N. J. Royle. 2000. 'High levels of sequence polymorphism and linkage disequilibrium at the telomere of 12q: implications for telomere biology and human evolution', *Am J Hum Genet*, 66: 235-50.

Baird, D. M., T. Davis, J. Rowson, C. J. Jones, and D. Kipling. 2004. 'Normal telomere erosion rates at the single cell level in Werner syndrome fibroblast cells', *Hum Mol Genet*, 13: 1515-24.

Baird, D. M., J. Rowson, D. Wynford-Thomas, and D. Kipling. 2003. 'Extensive allelic variation and ultrashort telomeres in senescent human cells', *Nat Genet*, 33: 203-7.

Bakkenist, C. J., and M. B. Kastan. 2003. 'DNA damage activates ATM through intermolecular autophosphorylation and dimer dissociation', *Nature*, 421: 499-506.

Barata, P., A. K. Sood, and D. S. Hong. 2016. 'RNA-targeted therapeutics in cancer clinical trials: Current status and future directions', *Cancer Treat Rev*, 50: 35-47.

Barnetson, R. A., A. Tenesa, S. M. Farrington, I. D. Nicholl, R. Cetnarskyj, M. E. Porteous, H. Campbell, and M. G. Dunlop. 2006. 'Identification and survival of carriers of mutations in DNA mismatch-repair genes in colon cancer', *N Engl J Med*, 354: 2751-63.

Batista, L. F., M. F. Pech, F. L. Zhong, H. N. Nguyen, K. T. Xie, A. J. Zaug, S. M. Crary, J. Choi, V. Sebastiano, A. Cherry, N. Giri, M. Wernig, B. P. Alter, T. R. Cech, S. A. Savage, R. A. Reijo Pera, and S. E. Artandi. 2011. 'Telomere shortening and loss of self-renewal in dyskeratosis congenita induced pluripotent stem cells', *Nature*, 474: 399-402.

Baumann, P., and T. R. Cech. 2001. 'Pot1, the putative telomere end-binding protein in fission yeast and humans', *Science*, 292: 1171-5.

Beck, C., C. Boehler, J. Guirouilh Barbat, M. E. Bonnet, G. Illuzzi, P. Ronde, L. R. Gauthier, N. Magroun, A. Rajendran, B. S. Lopez, R. Scully, F. D. Boussin, V. Schreiber, and F. Dantzer. 2014. 'PARP3 affects the relative contribution of homologous recombination and nonhomologous end-joining pathways', *Nucleic Acids Res*, 42: 5616-32.

Benarroch-Popivker, D., S. Pisano, A. Mendez-Bermudez, L. Lototska, P. Kaur, S. Bauwens, N. Djerbi, C. M. Latrick, V. Fraisier, B. Pei, A. Gay, E. Jaune, K. Foucher, J. Cherfils-Vicini, E. Aeby, S. Miron, A. Londono-Vallejo, J. Ye, M. H. Le Du, H. Wang, E. Gilson, and M. J. Giraud-Panis. 2016. 'TRF2-Mediated Control of Telomere DNA Topology as a Mechanism for Chromosome-End Protection', *Mol Cell*, 61: 274-86.

Berenson, J., R. Pflugmacher, P. Jarzem, J. Zonder, K. Schechtman, J. B. Tillman, L. Bastian, T. Ashraf, F. Vrionis, and Investigators Cancer Patient Fracture Evaluation. 2011. 'Balloon kyphoplasty versus non-surgical fracture management for treatment of painful vertebral body compression fractures in patients with cancer: a multicentre, randomised controlled trial', *Lancet Oncol*, 12: 225-35.

Bergsagel, P. L., and W. M. Kuehl. 2001. 'Chromosome translocations in multiple myeloma', *Oncogene*, 20: 5611-22.

Bergsagel, P. L., and W. M. Kuehl. 2003. 'Critical roles for immunoglobulin translocations and cyclin D dysregulation in multiple myeloma', *Immunol Rev*, 194: 96-104.

Bergsagel, P. L., and W. M. Kuehl. 2005. 'Molecular pathogenesis and a consequent classification of multiple myeloma', *J Clin Oncol*, 23: 6333-8.

Billadeau, D., G. Ahmann, P. Greipp, and B. Van Ness. 1993. 'The bone marrow of multiple myeloma patients contains B cell populations at different stages of differentiation that are clonally related to the malignant plasma cell', *J Exp Med*, 178: 1023-31.

Blackburn, E. H., and K. Collins. 2011. 'Telomerase: an RNP enzyme synthesizes DNA', *Cold Spring Harb Perspect Biol*, 3.

Blimark, C., E. Holmberg, U. H. Mellqvist, O. Landgren, M. Bjorkholm, M. Hultcrantz, C. Kjellander, I. Turesson, and S. Y. Kristinsson. 2015. 'Multiple myeloma and infections: a population-based study on 9253 multiple myeloma patients', *Haematologica*, 100: 107-13.

Bohnhorst, J., T. Rasmussen, S. H. Moen, M. Flottum, L. Knudsen, M. Borset, T. Espevik, and A. Sundan. 2006. 'Toll-like receptors mediate proliferation and survival of multiple myeloma cells', *Leukemia*, 20: 1138-44.

Boulton, S. J., and S. P. Jackson. 1998. 'Components of the Ku-dependent non-homologous end-joining pathway are involved in telomeric length maintenance and telomeric silencing', *EMBO J*, 17: 1819-28.

Bower, K., C. E. Napier, S. L. Cole, R. A. Dagg, L. M. Lau, E. L. Duncan, E. L. Moy, and R. R. Reddel. 2012. 'Loss of wild-type ATRX expression in somatic cell hybrids segregates with activation of Alternative Lengthening of Telomeres', *PLoS One*, 7: e50062.

Brennan, S. K., Q. Wang, R. Tressler, C. Harley, N. Go, E. Bassett, C. A. Huff, R. J. Jones, and W. Matsui. 2010. 'Telomerase inhibition targets clonogenic multiple myeloma cells through telomere length-dependent and independent mechanisms', *PLoS One*, 5.

Breslin, C., P. Hornyak, A. Ridley, S. L. Rulten, H. Hanzlikova, A. W. Oliver, and K. W. Caldecott. 2015. 'The XRCC1 phosphate-binding pocket binds poly (ADP-ribose) and is required for XRCC1 function', *Nucleic Acids Res*, 43: 6934-44.

Britt-Compton, B., J. Rowson, M. Locke, I. Mackenzie, D. Kipling, and D. M. Baird. 2006. 'Structural stability and chromosome-specific telomere length is governed by cis-acting determinants in humans', *Hum Mol Genet*, 15: 725-33.

Broberg, K., J. Bjork, K. Paulsson, M. Hoglund, and M. Albin. 2005. 'Constitutional short telomeres are strong genetic susceptibility markers for bladder cancer', *Carcinogenesis*, 26: 1263-71.

Brown, E. J., and D. Baltimore. 2000. 'ATR disruption leads to chromosomal fragmentation and early embryonic lethality', *Genes Dev*, 14: 397-402.

Bryan, T. M., A. Englezou, L. Dalla-Pozza, M. A. Dunham, and R. R. Reddel. 1997. 'Evidence for an alternative mechanism for maintaining telomere length in human tumors and tumor-derived cell lines', *Nat Med*, 3: 1271-4.

Bryan, T. M., A. Englezou, J. Gupta, S. Bacchetti, and R. R. Reddel. 1995. 'Telomere elongation in immortal human cells without detectable telomerase activity', *EMBO J*, 14: 4240-8.

Bryant, H. E., E. Petermann, N. Schultz, A. S. Jemth, O. Loseva, N. Issaeva, F. Johansson, S. Fernandez, P. McGlynn, and T. Helleday. 2009. 'PARP is activated at stalled forks to mediate Mre11-dependent replication restart and recombination', *EMBO J*, 28: 2601-15.

Bundock, P., H. van Attikum, and P. Hooykaas. 2002. 'Increased telomere length and hypersensitivity to DNA damaging agents in an Arabidopsis KU70 mutant', *Nucleic Acids Res*, 30: 3395-400.

Burchett, K. M., Y. Yan, and M. M. Ouellette. 2014. 'Telomerase inhibitor Imetelstat (GRN163L) limits the lifespan of human pancreatic cancer cells', *PLoS One*, 9: e85155.

Burgers, P. M. 2009. 'Polymerase dynamics at the eukaryotic DNA replication fork', *J Biol Chem*, 284: 4041-5.

Burkhart, D. L., and J. Sage. 2008. 'Cellular mechanisms of tumour suppression by the retinoblastoma gene', *Nat Rev Cancer*, 8: 671-82.

Buseman, C. M., W. E. Wright, and J. W. Shay. 2012. 'Is telomerase a viable target in cancer?', *Mutat Res*, 730: 90-7.

Calabrese, C. R., R. Almassy, S. Barton, M. A. Batey, A. H. Calvert, S. Canan-Koch, B. W. Durkacz, Z. Hostomsky, R. A. Kumpf, S. Kyle, J. Li, K. Maegley, D. R. Newell, E. Notarianni, I. J. Stratford, D. Skalitzky, H. D. Thomas, L. Z. Wang, S. E. Webber, K. J. Williams, and N. J. Curtin. 2004. 'Anticancer chemosensitization and radiosensitization by the novel poly(ADP-ribose) polymerase-1 inhibitor AG14361', *J Natl Cancer Inst*, 96: 56-67.

Caldecott, K. W. 2008. 'Single-strand break repair and genetic disease', *Nat Rev Genet*, 9: 619-31.

Caldecott, K. W. 2014. 'DNA single-strand break repair', *Exp Cell Res*, 329: 2-8.

Campa, D., A. Martino, J. Varkonyi, F. Lesueur, K. Jamroziak, S. Landi, A. Jurczyszyn, H. Marques, V. Andersen, M. Jurado, H. Brenner, M. Petrini, U. Vogel, R. Garcia-Sanz, G. Buda, F. Gemignani, R. Rios, A. J. Vangsted, C. Dumontet, J. Martinez-Lopez, M. J. Moreno, A. Stepien, M. Watek, V. Moreno, A. K. Dieffenbach, A. M. Rossi, K. Butterbach, S. E. Jacobsen, H. Goldschmidt, J. Sainz, J. Hillengass, E. Orciuolo, M. Dudzinski, N. Weinhold, R. M. Reis, and F. Canzian. 2015. 'Risk of multiple myeloma is associated with polymorphisms within telomerase genes and telomere length', *Int J Cancer*, 136: E351-8.

Campisi, J. 2001. 'Cellular senescence as a tumor-suppressor mechanism', *Trends Cell Biol*, 11: S27-31.

Campisi, J., and F. d'Adda di Fagagna. 2007. 'Cellular senescence: when bad things happen to good cells', *Nat Rev Mol Cell Biol*, 8: 729-40.

Canela, A., E. Vera, P. Klatt, and M. A. Blasco. 2007. 'High-throughput telomere length quantification by FISH and its application to human population studies', *Proc Natl Acad Sci U S A*, 104: 5300-5.

Cao, Y., T. M. Bryan, and R. R. Reddel. 2008. 'Increased copy number of the TERT and TERC telomerase subunit genes in cancer cells', *Cancer Sci*, 99: 1092-9.

Capper, R., B. Britt-Compton, M. Tankimanova, J. Rowson, B. Letsolo, S. Man, M. Haughton, and D. M. Baird. 2007. 'The nature of telomere fusion and a definition of the critical telomere length in human cells', *Genes Dev*, 21: 2495-508.

Cavo, M., L. Pantani, A. Pezzi, M. T. Petrucci, F. Patriarca, F. Di Raimondo, G. Marzocchi, M. Galli, V. Montefusco, E. Zamagni, B. Gamberi, P. Tacchetti, A. Brioli, A. Palumbo, and P. Sonneveld. 2015. 'Bortezomib-thalidomide-dexamethasone (VTD) is superior to bortezomib-cyclophosphamide-dexamethasone (VCD) as induction therapy prior to autologous stem cell transplantation in multiple myeloma', *Leukemia*, 29: 2429-31.

Cavo, M., P. Tacchetti, F. Patriarca, M. T. Petrucci, L. Pantani, M. Galli, F. Di Raimondo, C. Crippa, E. Zamagni, A. Palumbo, M. Offidani, P. Corradini, F. Narni, A. Spadano, N. Pescosta, G. L. Deliliers, A. Ledda, C. Cellini, T. Caravita, P. Tosi, M. Baccarani, and Gimema Italian Myeloma Network. 2010. 'Bortezomib with thalidomide plus dexamethasone compared with thalidomide plus dexamethasone as induction therapy before, and consolidation therapy after, double autologous stem-cell transplantation in newly diagnosed multiple myeloma: a randomised phase 3 study', *Lancet*, 376: 2075-85.

Cawthon, R. M. 2002. 'Telomere measurement by quantitative PCR', *Nucleic Acids Res*, 30: e47.

Cawthon, R. M. 2009. 'Telomere length measurement by a novel monochrome multiplex quantitative PCR method', *Nucleic Acids Res*, 37: e21.

Celli, G. B., and T. de Lange. 2005. 'DNA processing is not required for ATM-mediated telomere damage response after TRF2 deletion', *Nat Cell Biol*, 7: 712-8.

Cesare, A. J., and J. D. Griffith. 2004. 'Telomeric DNA in ALT cells is characterized by free telomeric circles and heterogeneous t-loops', *Mol Cell Biol*, 24: 9948-57.

Cesare, A. J., and R. R. Reddel. 2010. 'Alternative lengthening of telomeres: models, mechanisms and implications', *Nat Rev Genet*, 11: 319-30.

Chanan-Khan, A., B. Holkova, M. A. Perle, E. Reich, C. D. Wu, G. Inghirami, and K. Takeshita. 2003. 'T-cell clonality and myelodysplasia without chromosomal fragility in a patient with features of Seckel syndrome', *Haematologica*, 88: ECR14.

Chapman, J. R., M. R. Taylor, and S. J. Boulton. 2012. 'Playing the end game: DNA double-strand break repair pathway choice', *Mol Cell*, 47: 497-510.

Chauhan, D., M. Velankar, M. Brahmandam, T. Hideshima, K. Podar, P. Richardson, R. Schlossman, I. Ghobrial, N. Raje, N. Munshi, and K. C. Anderson. 2007. 'A novel Bcl-2/Bcl-X(L)/Bcl-w inhibitor ABT-737 as therapy in multiple myeloma', *Oncogene*, 26: 2374-80.

Cheema, P. K., S. Zadeh, V. Kukreti, D. Reece, C. Chen, S. Trudel, and J. Mikhael. 2009. 'Age 40 years and under does not confer superior prognosis in patients with multiple myeloma undergoing upfront autologous stem cell transmplant', *Biol Blood Marrow Transplant*, 15: 686-93.

Chen, L., C. J. Nievera, A. Y. Lee, and X. Wu. 2008. 'Cell cycle-dependent complex formation of BRCA1.CtIP.MRN is important for DNA double-strand break repair', *J Biol Chem*, 283: 7713-20.

Chen, L., K. Trujillo, P. Sung, and A. E. Tomkinson. 2000. 'Interactions of the DNA ligase IV-XRCC4 complex with DNA ends and the DNA-dependent protein kinase', *J Biol Chem*, 275: 26196-205.

Chen, Y., H. Liu, H. Zhang, C. Sun, Z. Hu, Q. Tian, C. Peng, P. Jiang, H. Hua, X. Li, and H. Pei. 2017. 'And-1 coordinates with CtIP for efficient homologous recombination and DNA damage checkpoint maintenance', *Nucleic Acids Res*, 45: 2516-30.

Chiappori, A. A., T. Kolevska, D. R. Spigel, S. Hager, M. Rarick, S. Gadgeel, N. Blais, J. Von Pawel, L. Hart, M. Reck, E. Bassett, B. Burington, and J. H. Schiller. 2015. 'A randomized phase II study of the telomerase inhibitor imetelstat as maintenance therapy for advanced non-small-cell lung cancer', *Ann Oncol*, 26: 354-62.

Chiecchio, L., R. K. Protheroe, A. H. Ibrahim, K. L. Cheung, C. Rudduck, G. P. Dagrada, E. D. Cabanas, T. Parker, M. Nightingale, A. Wechalekar, K. H. Orchard, C. J. Harrison, N. C. Cross, G. J. Morgan, and F. M. Ross. 2006. 'Deletion of chromosome 13 detected by conventional cytogenetics is a critical prognostic factor in myeloma', *Leukemia*, 20: 1610-7.

Chin, L., S. E. Artandi, Q. Shen, A. Tam, S. L. Lee, G. J. Gottlieb, C. W. Greider, and R. A. DePinho. 1999. 'p53 deficiency rescues the adverse effects of telomere loss and cooperates with telomere dysfunction to accelerate carcinogenesis', *Cell*, 97: 527-38.

Chng, W. J., N. Gonzalez-Paz, T. Price-Troska, S. Jacobus, S. V. Rajkumar, M. M. Oken, R. A. Kyle, K. J. Henderson, S. Van Wier, P. Greipp, B. Van Ness, and R. Fonseca. 2008. 'Clinical and biological significance of RAS mutations in multiple myeloma', *Leukemia*, 22: 2280-4.

Chng, W. J., T. Price-Troska, N. Gonzalez-Paz, S. Van Wier, S. Jacobus, E. Blood, K. Henderson, M. Oken, B. Van Ness, P. Greipp, S. V. Rajkumar, and R. Fonseca. 2007. 'Clinical significance of TP53 mutation in myeloma', *Leukemia*, 21: 582-4.

Choi, S. J., J. C. Cruz, F. Craig, H. Chung, R. D. Devlin, G. D. Roodman, and M. Alsina. 2000. 'Macrophage inflammatory protein 1-alpha is a potential osteoclast stimulatory factor in multiple myeloma', *Blood*, 96: 671-5.

Chow, T. T., Y. Zhao, S. S. Mak, J. W. Shay, and W. E. Wright. 2012. 'Early and late steps in telomere overhang processing in normal human cells: the position of the final RNA primer drives telomere shortening', *Genes Dev*, 26: 1167-78.

Chretien, M. L., J. Corre, V. Lauwers-Cances, F. Magrangeas, A. Cleynen, E. Yon, C. Hulin, X. Leleu, F. Orsini-Piocelle, J. S. Blade, C. Sohn, L. Karlin, X. Delbrel, B. Hebraud, M. Roussel, G. Marit, L. Garderet, M. Mohty, P. Rodon, L. Voillat, B. Royer, A. Jaccard, K. Belhadj, J. Fontan, D. Caillot, A. M. Stoppa, M. Attal, T. Facon, P. Moreau, S. Minvielle, and H. Avet-Loiseau. 2015. 'Understanding the role of hyperdiploidy in myeloma prognosis: which trisomies really matter?', *Blood*, 126: 2713-9.

Chun, H. H., and R. A. Gatti. 2004. 'Ataxia-telangiectasia, an evolving phenotype', *DNA Repair (Amst)*, 3: 1187-96.

Cimprich, K. A., and D. Cortez. 2008. 'ATR: an essential regulator of genome integrity', *Nat Rev Mol Cell Biol*, 9: 616-27.

Coleman, J., D. M. Baird, and N. J. Royle. 1999. 'The plasticity of human telomeres demonstrated by a hypervariable telomere repeat array that is located on some copies of 16p and 16q', *Hum Mol Genet*, 8: 1637-46.

Colgin, L. M., K. Baran, P. Baumann, T. R. Cech, and R. R. Reddel. 2003. 'Human POT1 facilitates telomere elongation by telomerase', *Curr Biol*, 13: 942-6.

Conomos, D., M. D. Stutz, M. Hills, A. A. Neumann, T. M. Bryan, R. R. Reddel, and H. A. Pickett. 2012. 'Variant repeats are interspersed throughout the telomeres and recruit nuclear receptors in ALT cells', *J Cell Biol*, 199: 893-906.

Cook, B. D., J. N. Dynek, W. Chang, G. Shostak, and S. Smith. 2002. 'Role for the related poly(ADP-Ribose) polymerases tankyrase 1 and 2 at human telomeres', *Mol Cell Biol*, 22: 332-42.

Cook, G., C. Williams, J. M. Brown, D. A. Cairns, J. Cavenagh, J. A. Snowden, A. J. Ashcroft, M. Fletcher, C. Parrish, K. Yong, J. Cavet, H. Hunter, J. M. Bird, A. Chalmers, S. O'Connor, M. T. Drayson, T. C. Morris, and Group National Cancer Research Institute Haemato-oncology Clinical Studies. 2014. 'High-dose chemotherapy plus autologous stem-cell transplantation as consolidation therapy in patients with relapsed multiple myeloma after previous autologous stem-cell transplantation (NCRI Myeloma X Relapse [Intensive trial]): a randomised, open-label, phase 3 trial', *Lancet Oncol*, 15: 874-85.

Cortez, D., S. Guntuku, J. Qin, and S. J. Elledge. 2001. 'ATR and ATRIP: partners in checkpoint signaling', *Science*, 294: 1713-6.

Cottliar, A., E. Pedrazzini, C. Corrado, M. I. Engelberger, M. Narbaitz, and I. Slavutsky. 2003. 'Telomere shortening in patients with plasma cell disorders', *Eur J Haematol*, 71: 334-40.

Crawley, C., S. Iacobelli, B. Bjorkstrand, J. F. Apperley, D. Niederwieser, and G. Gahrton. 2007. 'Reduced-intensity conditioning for myeloma: lower nonrelapse mortality but higher relapse rates compared with myeloablative conditioning', *Blood*, 109: 3588-94.

Cristofari, G., and J. Lingner. 2006. 'Telomere length homeostasis requires that telomerase levels are limiting', *EMBO J*, 25: 565-74.

Daniali, L., A. Benetos, E. Susser, J. D. Kark, C. Labat, M. Kimura, K. Desai, M. Granick, and A. Aviv. 2013. 'Telomeres shorten at equivalent rates in somatic tissues of adults', *Nat Commun*, 4: 1597.

De Boeck, G., R. G. Forsyth, M. Praet, and P. C. Hogendoorn. 2009. 'Telomere-associated proteins: cross-talk between telomere maintenance and telomere-lengthening mechanisms', *J Pathol*, 217: 327-44.

Delhommeau, F., A. Thierry, D. Feneux, E. Lauret, E. Leclercq, M. H. Courtier, F. Sainteny, W. Vainchenker, and A. Bennaceur-Griscelli. 2002. 'Telomere dysfunction and telomerase reactivation in human leukemia cell lines after telomerase inhibition by the expression of a dominant-negative hTERT mutant', *Oncogene*, 21: 8262-71.

Denchi, E. L., and T. de Lange. 2007. 'Protection of telomeres through independent control of ATM and ATR by TRF2 and POT1', *Nature*, 448: 1068-71.

Deng, Y., S. S. Chan, and S. Chang. 2008. 'Telomere dysfunction and tumour suppression: the senescence connection', *Nat Rev Cancer*, 8: 450-8.

Deng, Z., J. Norseen, A. Wiedmer, H. Riethman, and P. M. Lieberman. 2009. 'TERRA RNA binding to TRF2 facilitates heterochromatin formation and ORC recruitment at telomeres', *Mol Cell*, 35: 403-13.

Dicker, F., H. Herholz, S. Schnittger, A. Nakao, N. Patten, L. Wu, W. Kern, T. Haferlach, and C. Haferlach. 2009. 'The detection of TP53 mutations in chronic lymphocytic leukemia independently predicts rapid disease progression and is highly correlated with a complex aberrant karyotype', *Leukemia*, 23: 117-24.

Dimopoulos, M. A., E. Kastritis, L. Rosinol, J. Blade, and H. Ludwig. 2008. 'Pathogenesis and treatment of renal failure in multiple myeloma', *Leukemia*, 22: 1485-93.

Dimopoulos, M. A., E. Terpos, A. Chanan-Khan, N. Leung, H. Ludwig, S. Jagannath, R. Niesvizky, S. Giralt, J. P. Fermand, J. Blade, R. L. Comenzo, O. Sezer, A. Palumbo, J. L. Harousseau, P. G. Richardson, B. Barlogie, K. C. Anderson, P. Sonneveld, P. Tosi, M. Cavo, S. V. Rajkumar, B. G. Durie, and J. San Miguel. 2010. 'Renal impairment in patients with multiple myeloma: a consensus statement on behalf of the International Myeloma Working Group', *J Clin Oncol*, 28: 4976-84.

Ding, Z., C. J. Wu, M. Jaskelioff, E. Ivanova, M. Kost-Alimova, A. Protopopov, G. C. Chu, G. Wang, X. Lu, E. S. Labrot, J. Hu, W. Wang, Y. Xiao, H. Zhang, J. Zhang, J. Zhang, B. Gan, S. R. Perry, S. Jiang, L. Li, J. W. Horner, Y. A. Wang, L. Chin, and R. A. DePinho. 2012. 'Telomerase reactivation following telomere dysfunction yields murine prostate tumors with bone metastases', *Cell*, 148: 896-907.

Diotti, R., and D. Loayza. 2011. 'Shelterin complex and associated factors at human telomeres', *Nucleus*, 2: 119-35.

Dispenzieri, A., R. A. Kyle, J. A. Katzmann, T. M. Therneau, D. Larson, J. Benson, R. J. Clark, L. J. Melton, 3rd, M. A. Gertz, S. K. Kumar, R. Fonseca, D. F. Jelinek, and S. V. Rajkumar. 2008. 'Immunoglobulin free light chain ratio is an independent risk factor for progression of smoldering (asymptomatic) multiple myeloma', *Blood*, 111: 785-9.

Dispenzieri, A., R. Kyle, G. Merlini, J. S. Miguel, H. Ludwig, R. Hajek, A. Palumbo, S. Jagannath, J. Blade, S. Lonial, M. Dimopoulos, R. Comenzo, H. Einsele, B. Barlogie, K. Anderson, M. Gertz, J. L. Harousseau, M. Attal, P. Tosi, P. Sonneveld, M. Boccadoro, G. Morgan, P. Richardson, O. Sezer, M. V. Mateos, M. Cavo, D. Joshua, I. Turesson, W. Chen, K. Shimizu, R. Powles, S. V. Rajkumar, B. G. Durie, and Group International Myeloma Working. 2009. 'International Myeloma Working Group guidelines for serum-free light chain analysis in multiple myeloma and related disorders', *Leukemia*, 23: 215-24.

Doheny, J. G., R. Mottus, and T. A. Grigliatti. 2008. 'Telomeric position effect--a third silencing mechanism in eukaryotes', *PLoS One*, 3: e3864.

Doksani, Y., and T. de Lange. 2014. 'The role of double-strand break repair pathways at functional and dysfunctional telomeres', *Cold Spring Harb Perspect Biol*, 6: a016576.

Doksani, Y., J. Y. Wu, T. de Lange, and X. Zhuang. 2013. 'Super-resolution fluorescence imaging of telomeres reveals TRF2-dependent T-loop formation', *Cell*, 155: 345-56.

Donawho, C. K., Y. Luo, Y. Luo, T. D. Penning, J. L. Bauch, J. J. Bouska, V. D. Bontcheva-Diaz, B. F. Cox, T. L. DeWeese, L. E. Dillehay, D. C. Ferguson, N. S. Ghoreishi-Haack, D. R. Grimm, R. Guan, E. K. Han, R. R. Holley-Shanks, B. Hristov, K. B. Idler, K. Jarvis, E. F. Johnson, L. R. Kleinberg, V. Klinghofer, L. M. Lasko, X. Liu, K. C. Marsh, T. P. McGonigal, J. A. Meulbroek, A. M. Olson, J. P. Palma, L. E. Rodriguez, Y. Shi, J. A. Stavropoulos, A. C. Tsurutani, G. D. Zhu, S. H. Rosenberg, V. L. Giranda, and D. J. Frost. 2007. 'ABT-888, an orally active poly(ADP-ribose) polymerase inhibitor that potentiates DNA-damaging agents in preclinical tumor models', *Clin Cancer Res*, 13: 2728-37.

Drew, Y., J. Ledermann, G. Hall, D. Rea, R. Glasspool, M. Highley, G. Jayson, J. Sludden, J. Murray, D. Jamieson, S. Halford, G. Acton, Z. Backholer, R. Mangano, A. Boddy, N. Curtin, and R. Plummer. 2016. 'Phase 2 multicentre trial investigating intermittent and continuous dosing schedules of the poly(ADP-ribose) polymerase inhibitor rucaparib in germline BRCA mutation carriers with advanced ovarian and breast cancer', *Br J Cancer*, 114: 723-30.

Dunham, M. A., A. A. Neumann, C. L. Fasching, and R. R. Reddel. 2000. 'Telomere maintenance by recombination in human cells', *Nat Genet*, 26: 447-50.

Durie, B. G., R. A. Kyle, A. Belch, W. Bensinger, J. Blade, M. Boccadoro, J. A. Child, R. Comenzo, B. Djulbegovic, D. Fantl, G. Gahrton, J. L. Harousseau, V. Hungria, D. Joshua, H. Ludwig, J. Mehta, A. R. Morales, G. Morgan, A. Nouel, M. Oken, R. Powles, D. Roodman, J. San Miguel, K. Shimizu, S. Singhal, B. Sirohi, P. Sonneveld, G. Tricot, B. Van Ness, and Foundation Scientific Advisors of the International Myeloma. 2003. 'Myeloma management guidelines: a consensus report from the Scientific Advisors of the International Myeloma Foundation', *Hematol J*, 4: 379-98.

Durie, B. G., and S. E. Salmon. 1975. 'A clinical staging system for multiple myeloma. Correlation of measured myeloma cell mass with presenting clinical features, response to treatment, and survival', *Cancer*, 36: 842-54.

Egan, E. D., and K. Collins. 2010. 'Specificity and stoichiometry of subunit interactions in the human telomerase holoenzyme assembled in vivo', *Mol Cell Biol*, 30: 2775-86.

Ellebaek, E., L. Engell-Noerregaard, T. Z. Iversen, T. M. Froesig, S. Munir, S. R. Hadrup, M. H. Andersen, and I. M. Svane. 2012. 'Metastatic melanoma patients treated with dendritic cell vaccination, Interleukin-2 and metronomic cyclophosphamide: results from a phase II trial', *Cancer Immunol Immunother*, 61: 1791-804.

Ernst, A., D. T. Jones, K. K. Maass, A. Rode, K. I. Deeg, B. M. Jebaraj, A. Korshunov, V. Hovestadt, M. A. Tainsky, K. W. Pajtler, S. Bender, S. Brabetz, S. Grobner, M. Kool, F. Devens, J. Edelmann, C. Zhang, P. Castelo-Branco, U. Tabori, D. Malkin, K. Rippe, S. Stilgenbauer, S. M. Pfister, M. Zapatka, and P. Lichter. 2016. 'Telomere dysfunction and chromothripsis', *Int J Cancer*, 138: 2905-14.

Facon, T., J. Y. Mary, C. Hulin, L. Benboubker, M. Attal, B. Pegourie, M. Renaud, J. L. Harousseau, G. Guillerm, C. Chaleteix, M. Dib, L. Voillat, H. Maisonneuve, J. Troncy, V. Dorvaux, M. Monconduit, C. Martin, P. Casassus, J. Jaubert, H. Jardel, C. Doyen, B. Kolb, B. Anglaret, B. Grosbois, I. Yakoub-Agha, C. Mathiot, H. Avet-Loiseau, and Myelome Intergroupe Francophone du. 2007. 'Melphalan and prednisone plus thalidomide versus melphalan and prednisone alone or reduced-intensity autologous stem cell transplantation in elderly patients with multiple myeloma (IFM 99-06): a randomised trial', *Lancet*, 370: 1209-18.

Faiman, B. M., P. Mangan, J. Spong, J. D. Tariman, and Board The International Myeloma Foundation Nurse Leadership. 2011. 'Renal complications in multiple myeloma and related disorders: survivorship care plan of the International Myeloma Foundation Nurse Leadership Board', *Clin J Oncol Nurs*, 15 Suppl: 66-76.

Farmer, H., N. McCabe, C. J. Lord, A. N. Tutt, D. A. Johnson, T. B. Richardson, M. Santarosa, K. J. Dillon, I. Hickson, C. Knights, N. M. Martin, S. P. Jackson, G. C. Smith, and A. Ashworth. 2005. 'Targeting the DNA repair defect in BRCA mutant cells as a therapeutic strategy', *Nature*, 434: 917-21.

Fechtner, K., J. Hillengass, S. Delorme, C. Heiss, K. Neben, H. Goldschmidt, H. U. Kauczor, and M. A. Weber. 2010. 'Staging monoclonal plasma cell disease: comparison of the Durie-Salmon and the Durie-Salmon PLUS staging systems', *Radiology*, 257: 195-204.

Fenoglio, D., P. Traverso, A. Parodi, L. Tomasello, S. Negrini, F. Kalli, F. Battaglia, F. Ferrera, S. Sciallero, G. Murdaca, M. Setti, A. Sobrero, F. Boccardo, G. Cittadini, F. Puppo, D. Criscuolo, G. Carmignani, F. Indiveri, and G. Filaci. 2013. 'A multi-peptide, dual-adjuvant telomerase vaccine (GX301) is highly immunogenic in patients with prostate and renal cancer', *Cancer Immunol Immunother*, 62: 1041-52.

Fitch, M. E., S. Nakajima, A. Yasui, and J. M. Ford. 2003. 'In vivo recruitment of XPC to UV-induced cyclobutane pyrimidine dimers by the DDB2 gene product', *J Biol Chem*, 278: 46906-10.

Fong, P. C., D. S. Boss, T. A. Yap, A. Tutt, P. Wu, M. Mergui-Roelvink, P. Mortimer, H. Swaisland, A. Lau, M. J. O'Connor, A. Ashworth, J. Carmichael, S. B. Kaye, J. H. Schellens, and J. S. de Bono. 2009. 'Inhibition of poly(ADP-ribose) polymerase in tumors from BRCA mutation carriers', *N Engl J Med*, 361: 123-34.

Friedberg, E. C. 2001. 'How nucleotide excision repair protects against cancer', *Nat Rev Cancer*, 1: 22-33.

Friedrich, U., E. Griese, M. Schwab, P. Fritz, K. Thon, and U. Klotz. 2000. 'Telomere length in different tissues of elderly patients', *Mech Ageing Dev*, 119: 89-99.

Fujimori, J., T. Matsuo, S. Shimose, T. Kubo, M. Ishikawa, Y. Yasunaga, and M. Ochi. 2011. 'Antitumor effects of telomerase inhibitor TMPyP4 in osteosarcoma cell lines', *J Orthop Res*, 29: 1707-11.

Ghobrial, I. M., M. A. Gertz, and R. Fonseca. 2003. 'Waldenstrom macroglobulinaemia', *Lancet Oncol*, 4: 679-85.

Gilson, E., and V. Geli. 2007. 'How telomeres are replicated', *Nat Rev Mol Cell Biol*, 8: 825-38.

Gisselsson, D., T. Jonson, A. Petersen, B. Strombeck, P. Dal Cin, M. Hoglund, F. Mitelman, F. Mertens, and N. Mandahl. 2001. 'Telomere dysfunction triggers extensive DNA fragmentation and evolution of complex chromosome abnormalities in human malignant tumors', *Proc Natl Acad Sci U S A*, 98: 12683-8.

Giuliani, N., R. Bataille, C. Mancini, M. Lazzaretti, and S. Barille. 2001. 'Myeloma cells induce imbalance in the osteoprotegerin/osteoprotegerin ligand system in the human bone marrow environment', *Blood*, 98: 3527-33.

Giuliani, N., S. Colla, and V. Rizzoli. 2004. 'New insight in the mechanism of osteoclast activation and formation in multiple myeloma: focus on the receptor activator of NF-kappaB ligand (RANKL)', *Exp Hematol*, 32: 685-91.

Goldberg, A. D., L. A. Banaszynski, K. M. Noh, P. W. Lewis, S. J. Elsaesser, S. Stadler, S. Dewell, M. Law, X. Guo, X. Li, D. Wen, A. Chapgier, R. C. DeKelver, J. C. Miller, Y. L. Lee, E. A. Boydston, M. C. Holmes, P. D. Gregory, J. M. Greally, S. Rafii, C. Yang, P. J. Scambler, D. Garrick, R. J. Gibbons, D. R. Higgs, I. M. Cristea, F. D. Urnov, D. Zheng, and C. D. Allis. 2010. 'Distinct factors control histone variant H3.3 localization at specific genomic regions', *Cell*, 140: 678-91.

Gonsalves, W. I., N. Leung, S. V. Rajkumar, A. Dispenzieri, M. Q. Lacy, S. R. Hayman, F. K. Buadi, D. Dingli, P. Kapoor, R. S. Go, Y. Lin, S. J. Russell, J. A. Lust, S. Zeldenrust, R. A. Kyle, M. A. Gertz, and S. K. Kumar. 2015. 'Improvement in renal function and its impact on survival in patients with newly diagnosed multiple myeloma', *Blood Cancer J*, 5: e296.

Gooding, R. P., A. Bybee, F. Cooke, A. Little, S. G. Marsh, E. Coelho, D. Gupta, D. Samson, and J. F. Apperley. 1999. 'Phenotypic and molecular analysis of six human cell lines derived from patients with plasma cell dyscrasia', *Br J Haematol*, 106: 669-81.

Gorgun, G., E. Calabrese, T. Hideshima, J. Ecsedy, G. Perrone, M. Mani, H. Ikeda, G. Bianchi, Y. Hu, D. Cirstea, L. Santo, Y. T. Tai, S. Nahar, M. Zheng, M. Bandi, R. D. Carrasco, N. Raje, N. Munshi, P. Richardson, and K. C. Anderson. 2010. 'A novel Aurora-A kinase inhibitor MLN8237 induces cytotoxicity and cell-cycle arrest in multiple myeloma', *Blood*, 115: 5202-13.

Grand, C. L., H. Han, R. M. Munoz, S. Weitman, D. D. Von Hoff, L. H. Hurley, and D. J. Bearss. 2002. 'The cationic porphyrin TMPyP4 down-regulates c-MYC and human telomerase reverse transcriptase expression and inhibits tumor growth in vivo', *Mol Cancer Ther*, 1: 565-73.

Greipp, P. R., J. San Miguel, B. G. Durie, J. J. Crowley, B. Barlogie, J. Blade, M. Boccadoro, J. A. Child, H. Avet-Loiseau, R. A. Kyle, J. J. Lahuerta, H. Ludwig, G. Morgan, R. Powles, K. Shimizu, C. Shustik, P. Sonneveld, P. Tosi, I. Turesson, and J. Westin. 2005. 'International staging system for multiple myeloma', *J Clin Oncol*, 23: 3412-20.

Greten, T. F., A. Forner, F. Korangy, G. N'Kontchou, N. Barget, C. Ayuso, L. A. Ormandy, M. P. Manns, M. Beaugrand, and J. Bruix. 2010. 'A phase II open label trial evaluating safety and efficacy of a telomerase peptide vaccination in patients with advanced hepatocellular carcinoma', *BMC Cancer*, 10: 209.

Griffith, J. D., L. Comeau, S. Rosenfield, R. M. Stansel, A. Bianchi, H. Moss, and T. de Lange. 1999. 'Mammalian telomeres end in a large duplex loop', *Cell*, 97: 503-14.

Guo, X., Y. Deng, Y. Lin, W. Cosme-Blanco, S. Chan, H. He, G. Yuan, E. J. Brown, and S. Chang. 2007. 'Dysfunctional telomeres activate an ATM-ATR-dependent DNA damage response to suppress tumorigenesis', *EMBO J*, 26: 4709-19.

Haferlach, C., F. Dicker, H. Herholz, S. Schnittger, W. Kern, and T. Haferlach. 2008. 'Mutations of the TP53 gene in acute myeloid leukemia are strongly associated with a complex aberrant karyotype', *Leukemia*, 22: 1539-41.

Halverson, R., R. M. Torres, and R. Pelanda. 2004. 'Receptor editing is the main mechanism of B cell tolerance toward membrane antigens', *Nat Immunol*, 5: 645-50.

Hanzlikova, H., W. Gittens, K. Krejcikova, Z. Zeng, and K. W. Caldecott. 2017. 'Overlapping roles for PARP1 and PARP2 in the recruitment of endogenous XRCC1 and PNKP into oxidized chromatin', *Nucleic Acids Res*, 45: 2546-57.

Hayani, A., C. R. Suarez, Z. Molnar, M. LeBeau, and J. Godwin. 1994. 'Acute myeloid leukaemia in a patient with Seckel syndrome', *J Med Genet*, 31: 148-9.

Hayflick, L. 1965. 'The Limited in Vitro Lifetime of Human Diploid Cell Strains', *Exp Cell Res*, 37: 614-36.

He, Z., J. Li, C. Zhen, L. Feng, and X. Ding. 2005. 'Knockdown of p53 by RNAi in ES cells facilitates RA-induced differentiation into muscle cells', *Biochem Biophys Res Commun*, 335: 676-83.

Heaphy, C. M., G. S. Yoon, S. B. Peskoe, C. E. Joshu, T. K. Lee, E. Giovannucci, L. A. Mucci, S. A. Kenfield, M. J. Stampfer, J. L. Hicks, A. M. De Marzo, E. A. Platz, and A. K. Meeker. 2013. 'Prostate cancer cell telomere length variability and stromal cell telomere length as prognostic markers for metastasis and death', *Cancer Discov*, 3: 1130-41.

Hegde, M. L., T. K. Hazra, and S. Mitra. 2008. 'Early steps in the DNA base excision/single-strand interruption repair pathway in mammalian cells', *Cell Res*, 18: 27-47.

Helleday, T., S. Eshtad, and S. Nik-Zainal. 2014. 'Mechanisms underlying mutational signatures in human cancers', *Nat Rev Genet*, 15: 585-98.

Hemann, M. T., M. A. Strong, L. Y. Hao, and C. W. Greider. 2001. 'The shortest telomere, not average telomere length, is critical for cell viability and chromosome stability', *Cell*, 107: 67-77.

Henson, J. D., Y. Cao, L. I. Huschtscha, A. C. Chang, A. Y. Au, H. A. Pickett, and R. R. Reddel. 2009. 'DNA C-circles are specific and quantifiable markers of alternative-lengthening-of-telomeres activity', *Nat Biotechnol*, 27: 1181-5.

Henson, J. D., A. A. Neumann, T. R. Yeager, and R. R. Reddel. 2002. 'Alternative lengthening of telomeres in mammalian cells', *Oncogene*, 21: 598-610.

Henson, J. D., and R. R. Reddel. 2010. 'Assaying and investigating Alternative Lengthening of Telomeres activity in human cells and cancers', *FEBS Lett*, 584: 3800-11.

Herbig, U., W. A. Jobling, B. P. Chen, D. J. Chen, and J. M. Sedivy. 2004. 'Telomere shortening triggers senescence of human cells through a pathway involving ATM, p53, and p21(CIP1), but not p16(INK4a)', *Mol Cell*, 14: 501-13.

Hirashima, K., and H. Seimiya. 2015. 'Telomeric repeat-containing RNA/G-quadruplex-forming sequences cause genome-wide alteration of gene expression in human cancer cells in vivo', *Nucleic Acids Res*, 43: 2022-32.

Hombauer, H., C. S. Campbell, C. E. Smith, A. Desai, and R. D. Kolodner. 2011. 'Visualization of eukaryotic DNA mismatch repair reveals distinct recognition and repair intermediates', *Cell*, 147: 1040-53.

Hultdin, M., E. Gronlund, K. Norrback, E. Eriksson-Lindstrom, T. Just, and G. Roos. 1998. 'Telomere analysis by fluorescence in situ hybridization and flow cytometry', *Nucleic Acids Res*, 26: 3651-6.

Hurt, E. M., S. B. Thomas, B. Peng, and W. L. Farrar. 2006. 'Reversal of p53 epigenetic silencing in multiple myeloma permits apoptosis by a p53 activator', *Cancer Biol Ther*, 5: 1154-60.

Hutchison, C. A., P. Cockwell, S. Reid, K. Chandler, G. P. Mead, J. Harrison, J. Hattersley, N. D. Evans, M. J. Chappell, M. Cook, H. Goehl, M. Storr, and A. R. Bradwell. 2007. 'Efficient removal of immunoglobulin free light chains by hemodialysis for multiple myeloma: in vitro and in vivo studies', *J Am Soc Nephrol*, 18: 886-95.

Hyatt, S., R. E. Jones, N. H. Heppel, J. W. Grimstead, C. Fegan, G. H. Jackson, R. Hills, J. M. Allan, G. Pratt, C. Pepper, and D. M. Baird. 2017. 'Telomere length is a critical determinant for survival in multiple myeloma', *Br J Haematol*.

Ibrahim, Y. H., C. Garcia-Garcia, V. Serra, L. He, K. Torres-Lockhart, A. Prat, P. Anton, P. Cozar, M. Guzman, J. Grueso, O. Rodriguez, M. T. Calvo, C. Aura, O. Diez, I. T. Rubio, J. Perez, J. Rodon, J. Cortes, L. W. Ellisen, M. Scaltriti, and J. Baselga. 2012. 'PI3K inhibition impairs BRCA1/2 expression and sensitizes BRCA-proficient triple-negative breast cancer to PARP inhibition', *Cancer Discov*, 2: 1036-47.

Ihnen, M., C. zu Eulenburg, T. Kolarova, J. W. Qi, K. Manivong, M. Chalukya, J. Dering, L. Anderson, C. Ginther, A. Meuter, B. Winterhoff, S. Jones, V. E. Velculescu, N. Venkatesan, H. M. Rong, S. Dandekar, N. Udar, F. Janicke, G. Los, D. J. Slamon, and G. E. Konecny. 2013. 'Therapeutic potential of the poly(ADP-ribose) polymerase inhibitor rucaparib for the treatment of sporadic human ovarian cancer', *Mol Cancer Ther*, 12: 1002-15.

Inoue, K., H. Osaka, V. C. Thurston, J. T. Clarke, A. Yoneyama, L. Rosenbarker, T. D. Bird, M. E. Hodes, L. G. Shaffer, and J. R. Lupski. 2002. 'Genomic rearrangements resulting in PLP1 deletion occur by nonhomologous end joining and cause different dysmyelinating phenotypes in males and females', *Am J Hum Genet*, 71: 838-53.

International Myeloma Working, Group. 2003. 'Criteria for the classification of monoclonal gammopathies, multiple myeloma and related disorders: a report of the International Myeloma Working Group', *Br J Haematol*, 121: 749-57.

Ito, S., C. G. Murphy, E. Doubrovina, M. Jasin, and M. E. Moynahan. 2016. 'PARP Inhibitors in Clinical Use Induce Genomic Instability in Normal Human Cells', *PLoS One*, 11: e0159341.

Iwanaga, M., M. Tagawa, K. Tsukasaki, T. Matsuo, K. Yokota, Y. Miyazaki, T. Fukushima, T. Hata, Y. Imaizumi, D. Imanishi, J. Taguchi, S. Momita, S. Kamihira, and M. Tomonaga. 2009. 'Relationship between monoclonal gammopathy of undetermined significance and radiation exposure in Nagasaki atomic bomb survivors', *Blood*, 113: 1639-50.

Jacob, J., G. Kelsoe, K. Rajewsky, and U. Weiss. 1991. 'Intraclonal generation of antibody mutants in germinal centres', *Nature*, 354: 389-92.

Jacobson, J. L., M. A. Hussein, B. Barlogie, B. G. Durie, J. J. Crowley, and Group Southwest Oncology. 2003. 'A new staging system for multiple myeloma patients based on the Southwest Oncology Group (SWOG) experience', *Br J Haematol*, 122: 441-50.

Janouskova, E., I. Necasova, J. Pavlouskova, M. Zimmermann, M. Hluchy, V. Marini, M. Novakova, and C. Hofr. 2015. 'Human Rap1 modulates TRF2 attraction to telomeric DNA', *Nucleic Acids Res*, 43: 2691-700.

Javle, M., and N. J. Curtin. 2011. 'The role of PARP in DNA repair and its therapeutic exploitation', *Br J Cancer*, 105: 1114-22.

Jazayeri, A., J. Falck, C. Lukas, J. Bartek, G. C. Smith, J. Lukas, and S. P. Jackson. 2006. 'ATM- and cell cycle-dependent regulation of ATR in response to DNA double-strand breaks', *Nat Cell Biol*, 8: 37-45.

Jeon, H. S., Y. Y. Choi, J. E. Choi, W. K. Lee, E. Lee, S. S. Yoo, S. Y. Lee, J. Lee, S. I. Cha, C. H. Kim, and J. Y. Park. 2014. 'Telomere length of tumor tissues and survival in patients with early stage non-small cell lung cancer', *Mol Carcinog*, 53: 272-9.

Jimenez-Zepeda, V. H., and V. J. Dominguez-Martinez. 2009. 'Plasma cell leukemia: a highly aggressive monoclonal gammopathy with a very poor prognosis', *Int J Hematol*, 89: 259-68.

Jimenez-Zepeda, V. H., P. Duggan, P. Neri, F. Rashid-Kolvear, J. Tay, and N. J. Bahlis. 2016. 'Revised International Staging System Applied to Real World Multiple Myeloma Patients', *Clin Lymphoma Myeloma Leuk*, 16: 511-18.

Jiricny, J. 2006. 'The multifaceted mismatch-repair system', *Nat Rev Mol Cell Biol*, 7: 335-46.

Jones, R. E., S. Oh, J. W. Grimstead, J. Zimbric, L. Roger, N. H. Heppel, K. E. Ashelford, K. Liddiard, E. A. Hendrickson, and D. M. Baird. 2014. 'Escape from telomere-driven crisis is DNA ligase III dependent', *Cell Rep*, 8: 1063-76.

Jourdan, M., M. Cren, N. Robert, K. Bollore, T. Fest, C. Duperray, F. Guilloton, D. Hose, K. Tarte, and B. Klein. 2014. 'IL-6 supports the generation of human long-lived plasma cells in combination with either APRIL or stromal cell-soluble factors', *Leukemia*, 28: 1647-56.

Kabir, S., D. Hockemeyer, and T. de Lange. 2014. 'TALEN gene knockouts reveal no requirement for the conserved human shelterin protein Rap1 in telomere protection and length regulation', *Cell Rep*, 9: 1273-80.

Kamileri, I., I. Karakasilioti, and G. A. Garinis. 2012. 'Nucleotide excision repair: new tricks with old bricks', *Trends Genet*, 28: 566-73.

Kang, J. U., S. H. Koo, K. C. Kwon, J. W. Park, and J. M. Kim. 2008. 'Gain at chromosomal region 5p15.33, containing TERT, is the most frequent genetic event in early stages of non-small cell lung cancer', *Cancer Genet Cytogenet*, 182: 1-11.

Karlseder, J., K. Hoke, O. K. Mirzoeva, C. Bakkenist, M. B. Kastan, J. H. Petrini, and T. de Lange. 2004. 'The telomeric protein TRF2 binds the ATM kinase and can inhibit the ATM-dependent DNA damage response', *PLoS Biol*, 2: E240.

Kaufman, B., R. Shapira-Frommer, R. K. Schmutzler, M. W. Audeh, M. Friedlander, J. Balmana, G. Mitchell, G. Fried, S. M. Stemmer, A. Hubert, O. Rosengarten, M. Steiner, N. Loman, K. Bowen, A. Fielding, and S. M. Domchek. 2015. 'Olaparib monotherapy in patients with advanced cancer and a germline BRCA1/2 mutation', *J Clin Oncol*, 33: 244-50.

Kelleher, C., I. Kurth, and J. Lingner. 2005. 'Human protection of telomeres 1 (POT1) is a negative regulator of telomerase activity in vitro', *Mol Cell Biol*, 25: 808-18.

Khalil, D. N., E. L. Smith, R. J. Brentjens, and J. D. Wolchok. 2016. 'The future of cancer treatment: immunomodulation, CARs and combination immunotherapy', *Nat Rev Clin Oncol*, 13: 273-90.

Kim, G., G. Ison, A. E. McKee, H. Zhang, S. Tang, T. Gwise, R. Sridhara, E. Lee, A. Tzou, R. Philip, H. J. Chiu, T. K. Ricks, T. Palmby, A. M. Russell, G. Ladouceur, E. Pfuma, H. Li, L. Zhao, Q. Liu, R. Venugopal, A. Ibrahim, and R. Pazdur. 2015. 'FDA Approval Summary: Olaparib Monotherapy in Patients with Deleterious Germline BRCA-Mutated Advanced Ovarian Cancer Treated with Three or More Lines of Chemotherapy', *Clin Cancer Res*, 21: 4257-61.

Kim, J. E., C. Yoo, D. H. Lee, S. W. Kim, J. S. Lee, and C. Suh. 2010. 'Serum albumin level is a significant prognostic factor reflecting disease severity in symptomatic multiple myeloma', *Ann Hematol*, 89: 391-7.

Kim, M. Y., M. Gleason-Guzman, E. Izbicka, D. Nishioka, and L. H. Hurley. 2003. 'The different biological effects of telomestatin and TMPyP4 can be attributed to their selectivity for interaction with intramolecular or intermolecular G-quadruplex structures', *Cancer Res*, 63: 3247-56.

Kim, S. H., C. Beausejour, A. R. Davalos, P. Kaminker, S. J. Heo, and J. Campisi. 2004. 'TIN2 mediates functions of TRF2 at human telomeres', *J Biol Chem*, 279: 43799-804.

Kim, S. H., P. Kaminker, and J. Campisi. 1999. 'TIN2, a new regulator of telomere length in human cells', *Nat Genet*, 23: 405-12.

Kim, W., A. T. Ludlow, J. Min, J. D. Robin, G. Stadler, I. Mender, T. P. Lai, N. Zhang, W. E. Wright, and J. W. Shay. 2016. 'Regulation of the Human Telomerase Gene TERT by Telomere Position Effect-Over Long Distances (TPE-OLD): Implications for Aging and Cancer', *PLoS Biol*, 14: e2000016.

Kimura, M., and A. Aviv. 2011. 'Measurement of telomere DNA content by dot blot analysis', *Nucleic Acids Res*, 39: e84.

Kleine, H., E. Poreba, K. Lesniewicz, P. O. Hassa, M. O. Hottiger, D. W. Litchfield, B. H. Shilton, and B. Luscher. 2008. 'Substrate-assisted catalysis by PARP10 limits its activity to mono-ADP-ribosylation', *Mol Cell*, 32: 57-69.

Klewes, L., R. Vallente, E. Dupas, C. Brand, D. Grun, A. Guffei, C. Sathitruangsak, J. A. Awe, A. Kuzyk, D. Lichtensztejn, P. Tammur, T. Ilus, A. Tamm, M. Punab, M. Rubinger, A. Olujohungbe, and S. Mai. 2013. 'Three-dimensional Nuclear Telomere Organization in Multiple Myeloma', *Transl Oncol*, 6: 749-56.

Knepper, T. C., J. Saller, and C. M. Walko. 2017. 'Novel and Expanded Oncology Drug Approvals of 2016-PART 1: New Options in Solid Tumor Management', *Oncology (Williston Park)*, 31: 110-21.

Kocak, H., B. J. Ballew, K. Bisht, R. Eggebeen, B. D. Hicks, S. Suman, A. O'Neil, N. Giri, Nci Dceg Cancer Genomics Research Laboratory, Nci Dceg Cancer Sequencing Working Group, I. Maillard, B. P. Alter, C. E. Keegan, J. Nandakumar, and S. A. Savage. 2014. 'Hoyeraal-Hreidarsson syndrome caused by a germline mutation in the TEL patch of the telomere protein TPP1', *Genes Dev*, 28: 2090-102.

Konecny, G. E., and R. S. Kristeleit. 2016. 'PARP inhibitors for BRCA1/2-mutated and sporadic ovarian cancer: current practice and future directions', *Br J Cancer*, 115: 1157-73.

Kotsakis, A., E. K. Vetsika, S. Christou, D. Hatzidaki, N. Vardakis, D. Aggouraki, G. Konsolakis, V. Georgoulias, Ch Christophyllakis, P. Cordopatis, K. Kosmatopoulos, and D. Mavroudis. 2012. 'Clinical outcome of patients with various advanced cancer types vaccinated with an optimized cryptic human telomerase reverse transcriptase (TERT) peptide: results of an expanded phase II study', *Ann Oncol*, 23: 442-9.

Krejci, L., V. Altmannova, M. Spirek, and X. Zhao. 2012. 'Homologous recombination and its regulation', *Nucleic Acids Res*, 40: 5795-818.

Kretzner, L., A. Scuto, P. M. Dino, C. M. Kowolik, J. Wu, P. Ventura, R. Jove, S. J. Forman, Y. Yen, and M. H. Kirschbaum. 2011. 'Combining histone deacetylase inhibitor vorinostat with aurora kinase inhibitors enhances lymphoma cell killing with repression of c-Myc, hTERT, and microRNA levels', *Cancer Res*, 71: 3912-20.

Krokan, H. E., and M. Bjoras. 2013. 'Base excision repair', *Cold Spring Harb Perspect Biol*, 5: a012583.

Kuchen, S., R. Robbins, G. P. Sims, C. Sheng, T. M. Phillips, P. E. Lipsky, and R. Ettinger. 2007. 'Essential role of IL-21 in B cell activation, expansion, and plasma cell generation during CD4+ T cell-B cell collaboration', *J Immunol*, 179: 5886-96.

Kuehl, W. M., and P. L. Bergsagel. 2005. 'Early genetic events provide the basis for a clinical classification of multiple myeloma', *Hematology Am Soc Hematol Educ Program*: 346-52.

Kulak, O., H. Chen, B. Holohan, X. Wu, H. He, D. Borek, Z. Otwinowski, K. Yamaguchi, L. A. Garofalo, Z. Ma, W. Wright, C. Chen, J. W. Shay, X. Zhang, and L. Lum. 2015. 'Disruption of Wnt/beta-Catenin Signaling and Telomeric Shortening Are Inextricable Consequences of Tankyrase Inhibition in Human Cells', *Mol Cell Biol*, 35: 2425-35.

Kumagai, A., J. Lee, H. Y. Yoo, and W. G. Dunphy. 2006. 'TopBP1 activates the ATR-ATRIP complex', *Cell*, 124: 943-55.

Kumar, S. K., B. LaPlant, W. J. Chng, J. Zonder, N. Callander, R. Fonseca, B. Fruth, V. Roy, C. Erlichman, A. K. Stewart, and Consortium Mayo Phase. 2015. 'Dinaciclib, a novel CDK inhibitor, demonstrates encouraging single-agent activity in patients with relapsed multiple myeloma', *Blood*, 125: 443-8.

Kupiec, M. 2014. 'Biology of telomeres: lessons from budding yeast', *FEMS Microbiol Rev*, 38: 144-71.

Kyle, R. A., B. G. Durie, S. V. Rajkumar, O. Landgren, J. Blade, G. Merlini, N. Kroger, H. Einsele, D. H. Vesole, M. Dimopoulos, J. San Miguel, H. Avet-Loiseau, R. Hajek, W. M. Chen, K. C. Anderson, H. Ludwig, P. Sonneveld, S. Pavlovsky, A. Palumbo, P. G. Richardson, B. Barlogie, P. Greipp, R. Vescio, I. Turesson, J. Westin, M. Boccadoro, and Group International Myeloma Working. 2010. 'Monoclonal gammopathy of undetermined significance (MGUS) and smoldering (asymptomatic) multiple myeloma: IMWG consensus perspectives risk factors for progression and guidelines for monitoring and management', *Leukemia*, 24: 1121-7.

Kyle, R. A., and S. V. Rajkumar. 2008. 'Multiple myeloma', *Blood*, 111: 2962-72.

Kyle, R. A., E. D. Remstein, T. M. Therneau, A. Dispenzieri, P. J. Kurtin, J. M. Hodnefield, D. R. Larson, M. F. Plevak, D. F. Jelinek, R. Fonseca, L. J. Melton, 3rd, and S. V. Rajkumar. 2007. 'Clinical course and prognosis of smoldering (asymptomatic) multiple myeloma', *N Engl J Med*, 356: 2582-90.

Kyle, R. A., T. M. Therneau, S. V. Rajkumar, J. R. Offord, D. R. Larson, M. F. Plevak, and L. J. Melton, 3rd. 2002. 'A long-term study of prognosis in monoclonal gammopathy of undetermined significance', *N Engl J Med*, 346: 564-9.

Kyle, R. A., T. M. Therneau, S. V. Rajkumar, E. D. Remstein, J. R. Offord, D. R. Larson, M. F. Plevak, and L. J. Melton, 3rd. 2003. 'Long-term follow-up of IgM monoclonal gammopathy of undetermined significance', *Blood*, 102: 3759-64.

Kyle, R. A., G. C. Yee, M. R. Somerfield, P. J. Flynn, S. Halabi, S. Jagannath, R. Z. Orlowski, D. G. Roodman, P. Twilde, K. Anderson, and Oncology American Society of Clinical. 2007. 'American Society of Clinical Oncology 2007 clinical practice guideline update on the role of bisphosphonates in multiple myeloma', *J Clin Oncol*, 25: 2464-72.

Kyo, S., M. Takakura, T. Fujiwara, and M. Inoue. 2008. 'Understanding and exploiting hTERT promoter regulation for diagnosis and treatment of human cancers', *Cancer Sci*, 99: 1528-38.

Kyo, S., M. Takakura, T. Taira, T. Kanaya, H. Itoh, M. Yutsudo, H. Ariga, and M. Inoue. 2000. 'Sp1 cooperates with c-Myc to activate transcription of the human telomerase reverse transcriptase gene (hTERT)', *Nucleic Acids Res*, 28: 669-77.

Landau, H. J., S. C. McNeely, J. S. Nair, R. L. Comenzo, T. Asai, H. Friedman, S. C. Jhanwar, S. D. Nimer, and G. K. Schwartz. 2012. 'The checkpoint kinase inhibitor AZD7762 potentiates chemotherapy-induced apoptosis of p53-mutated multiple myeloma cells', *Mol Cancer Ther*, 11: 1781-8.

Landgren, O., G. Gridley, I. Turesson, N. E. Caporaso, L. R. Goldin, D. Baris, T. R. Fears, R. N. Hoover, and M. S. Linet. 2006. 'Risk of monoclonal gammopathy of undetermined significance (MGUS) and subsequent multiple myeloma among African American and white veterans in the United States', *Blood*, 107: 904-6.

Landgren, O., R. A. Kyle, J. A. Hoppin, L. E. Beane Freeman, J. R. Cerhan, J. A. Katzmann, S. V. Rajkumar, and M. C. Alavanja. 2009. 'Pesticide exposure and risk of monoclonal gammopathy of undetermined significance in the Agricultural Health Study', *Blood*, 113: 6386-91.

Lansdorp, P. M., N. P. Verwoerd, F. M. van de Rijke, V. Dragowska, M. T. Little, R. W. Dirks, A. K. Raap, and H. J. Tanke. 1996. 'Heterogeneity in telomere length of human chromosomes', *Hum Mol Genet*, 5: 685-91.

Ledermann, J., P. Harter, C. Gourley, M. Friedlander, I. Vergote, G. Rustin, C. L. Scott, W. Meier, R. Shapira-Frommer, T. Safra, D. Matei, A. Fielding, S. Spencer, B. Dougherty, M. Orr, D. Hodgson, J. C. Barrett, and U. Matulonis. 2014. 'Olaparib maintenance therapy in patients with platinum-sensitive relapsed serous ovarian cancer: a preplanned retrospective analysis of outcomes by BRCA status in a randomised phase 2 trial', *Lancet Oncol*, 15: 852-61.

Lee, J. H., P. Khadka, S. H. Baek, and I. K. Chung. 2010. 'CHIP promotes human telomerase reverse transcriptase degradation and negatively regulates telomerase activity', *J Biol Chem*, 285: 42033-45.

Lee, J. H., and T. T. Paull. 2007. 'Activation and regulation of ATM kinase activity in response to DNA double-strand breaks', *Oncogene*, 26: 7741-8.

Lei, M., E. R. Podell, and T. R. Cech. 2004. 'Structure of human POT1 bound to telomeric single-stranded DNA provides a model for chromosome end-protection', *Nat Struct Mol Biol*, 11: 1223-9.

Li, B., S. Oestreich, and T. de Lange. 2000. 'Identification of human Rap1: implications for telomere evolution', *Cell*, 101: 471-83.

Liang, F., M. Han, P. J. Romanienko, and M. Jasin. 1998. 'Homology-directed repair is a major double-strand break repair pathway in mammalian cells', *Proc Natl Acad Sci U S A*, 95: 5172-7.

Liddiard, K., B. Ruis, T. Takasugi, A. Harvey, K. E. Ashelford, E. A. Hendrickson, and D. M. Baird. 2016. 'Sister chromatid telomere fusions, but not NHEJ-mediated inter-chromosomal telomere fusions, occur independently of DNA ligases 3 and 4', *Genome Res*, 26: 588-600.

Lin, T. T., B. T. Letsolo, R. E. Jones, J. Rowson, G. Pratt, S. Hewamana, C. Fegan, C. Pepper, and D. M. Baird. 2010. 'Telomere dysfunction and fusion during the progression of chronic lymphocytic leukemia: evidence for a telomere crisis', *Blood*, 116: 1899-907.

Lin, T. T., K. Norris, N. H. Heppel, G. Pratt, J. M. Allan, D. J. Allsup, J. Bailey, L. Cawkwell, R. Hills, J. W. Grimstead, R. E. Jones, B. Britt-Compton, C. Fegan, D. M. Baird, and C. Pepper. 2014. 'Telomere dysfunction accurately predicts clinical outcome in chronic lymphocytic leukaemia, even in patients with early stage disease', *Br J Haematol*, 167: 214-23.

Ling, S. C., E. K. Lau, A. Al-Shabeeb, A. Nikolic, A. Catalano, H. Iland, N. Horvath, P. J. Ho, S. Harrison, S. Fleming, D. E. Joshua, and J. D. Allen. 2012. 'Response of myeloma to the proteasome inhibitor bortezomib is correlated with the unfolded protein response regulator XBP-1', *Haematologica*, 97: 64-72.

Liu, D., M. S. O'Connor, J. Qin, and Z. Songyang. 2004. 'Telosome, a mammalian telomere-associated complex formed by multiple telomeric proteins', *J Biol Chem*, 279: 51338-42.

Loayza, D., H. Parsons, J. Donigian, K. Hoke, and T. de Lange. 2004. 'DNA binding features of human POT1: a nonamer 5'-TAGGGTTAG-3' minimal binding site, sequence specificity, and internal binding to multimeric sites', *J Biol Chem*, 279: 13241-8.

Lobrich, M., and P. A. Jeggo. 2007. 'The impact of a negligent G2/M checkpoint on genomic instability and cancer induction', *Nat Rev Cancer*, 7: 861-9.

Lode, L., M. Eveillard, V. Trichet, T. Soussi, S. Wuilleme, S. Richebourg, F. Magrangeas, N. Ifrah, L. Campion, C. Traulle, F. Guilhot, D. Caillot, G. Marit, C. Mathiot, T. Facon, M. Attal, J. L. Harousseau, P. Moreau, S. Minvielle, and H. Avet-Loiseau. 2010. 'Mutations in TP53 are exclusively associated with del(17p) in multiple myeloma', *Haematologica*, 95: 1973-6.

Lokhorst, H., H. Einsele, D. Vesole, B. Bruno, J. San Miguel, J. A. Perez-Simon, N. Kroger, P. Moreau, G. Gahrton, C. Gasparetto, S. Giralt, W. Bensinger, and Group International Myeloma Working. 2010. 'International Myeloma Working Group consensus statement regarding the current status of allogeneic stem-cell transplantation for multiple myeloma', *J Clin Oncol*, 28: 4521-30.

Lonial, S., M. Dimopoulos, A. Palumbo, D. White, S. Grosicki, I. Spicka, A. Walter-Croneck, P. Moreau, M. V. Mateos, H. Magen, A. Belch, D. Reece, M. Beksac, A. Spencer, H. Oakervee, R. Z. Orlowski, M. Taniwaki, C. Rollig, H. Einsele, K. L. Wu, A. Singhal, J. San-Miguel, M. Matsumoto, J. Katz, E. Bleickardt, V. Poulart, K. C. Anderson, P. Richardson, and Eloquent- Investigators. 2015. 'Elotuzumab Therapy for Relapsed or Refractory Multiple Myeloma', *N Engl J Med*, 373: 621-31.

Lonial, S., B. Durie, A. Palumbo, and J. San-Miguel. 2016. 'Monoclonal antibodies in the treatment of multiple myeloma: current status and future perspectives', *Leukemia*, 30: 526-35.

Lopes-Carvalho, T., and J. F. Kearney. 2004. 'Development and selection of marginal zone B cells', *Immunol Rev*, 197: 192-205.

Lundblad, V. 2012. 'Telomere end processing: unexpected complexity at the end game', *Genes Dev*, 26: 1123-7.

Maciejowski, J., and T. de Lange. 2017. 'Telomeres in cancer: tumour suppression and genome instability', *Nat Rev Mol Cell Biol*, 18: 175-86.

Maciejowski, J., Y. Li, N. Bosco, P. J. Campbell, and T. de Lange. 2015. 'Chromothripsis and Kataegis Induced by Telomere Crisis', *Cell*, 163: 1641-54.

Maes, K., E. Nemeth, G. D. Roodman, A. Huston, F. Esteve, C. Freytes, N. Callander, E. Katodritou, L. Tussing-Humphreys, S. Rivera, K. Vanderkerken, A. Lichtenstein, and T. Ganz. 2010. 'In anemia of multiple myeloma, hepcidin is induced by increased bone morphogenetic protein 2', *Blood*, 116: 3635-44.

Mailand, N., J. Falck, C. Lukas, R. G. Syljuasen, M. Welcker, J. Bartek, and J. Lukas. 2000. 'Rapid destruction of human Cdc25A in response to DNA damage', *Science*, 288: 1425-9.

Makarov, V. L., Y. Hirose, and J. P. Langmore. 1997. 'Long G tails at both ends of human chromosomes suggest a C strand degradation mechanism for telomere shortening', *Cell*, 88: 657-66.

Maloisel, L., F. Fabre, and S. Gangloff. 2008. 'DNA polymerase delta is preferentially recruited during homologous recombination to promote heteroduplex DNA extension', *Mol Cell Biol*, 28: 1373-82.

Maltseva, E. A., N. I. Rechkunova, M. V. Sukhanova, and O. I. Lavrik. 2015. 'Poly(ADP-ribose) Polymerase 1 Modulates Interaction of the Nucleotide Excision Repair Factor XPC-RAD23B with DNA via Poly(ADP-ribosyl)ation', *J Biol Chem*, 290: 21811-20.

Mansour, W. Y., K. Borgmann, C. Petersen, E. Dikomey, and J. Dahm-Daphi. 2013. 'The absence of Ku but not defects in classical non-homologous end-joining is required to trigger PARP1-dependent end-joining', *DNA Repair (Amst)*, 12: 1134-42.

Marteijn, J. A., H. Lans, W. Vermeulen, and J. H. Hoeijmakers. 2014. 'Understanding nucleotide excision repair and its roles in cancer and ageing', *Nat Rev Mol Cell Biol*, 15: 465-81.

Martin-Ruiz, C. M., D. Baird, L. Roger, P. Boukamp, D. Krunic, R. Cawthon, M. M. Dokter, P. van der Harst, S. Bekaert, T. de Meyer, G. Roos, U. Svenson, V. Codd, N. J. Samani, L. McGlynn, P. G. Shiels, K. A. Pooley, A. M. Dunning, R. Cooper, A. Wong, A. Kingston, and T. von Zglinicki. 2015. 'Reproducibility of telomere length assessment: an international collaborative study', *Int J Epidemiol*, 44: 1673-83.

Mateos, M. V., M. T. Hernandez, P. Giraldo, J. de la Rubia, F. de Arriba, L. L. Corral, L. Rosinol, B. Paiva, L. Palomera, J. Bargay, A. Oriol, F. Prosper, J. Lopez, J. M. Arguinano, N. Quintana, J. L. Garcia, J. Blade, J. J. Lahuerta, and J. F. Miguel. 2016. 'Lenalidomide plus dexamethasone versus observation in patients with high-risk smouldering multiple myeloma (QuiRedex): long-term follow-up of a randomised, controlled, phase 3 trial', *Lancet Oncol*, 17: 1127-36.

McClintock, B. 1941. 'The Stability of Broken Ends of Chromosomes in Zea Mays', *Genetics*, 26: 234-82.

McEachern, M. J., and E. H. Blackburn. 1994. 'A conserved sequence motif within the exceptionally diverse telomeric sequences of budding yeasts', *Proc Natl Acad Sci U S A*, 91: 3453-7.

Mead, G. P., H. D. Carr-Smith, M. T. Drayson, G. J. Morgan, J. A. Child, and A. R. Bradwell. 2004. 'Serum free light chains for monitoring multiple myeloma', *Br J Haematol*, 126: 348-54.

Mefford, H. C., and B. J. Trask. 2002. 'The complex structure and dynamic evolution of human subtelomeres', *Nat Rev Genet*, 3: 91-102.

Mehle, C., B. Ljungberg, and G. Roos. 1994. 'Telomere shortening in renal cell carcinoma', *Cancer Res*, 54: 236-41.

Mello Filho, A. C., and R. Meneghini. 1984. 'In vivo formation of single-strand breaks in DNA by hydrogen peroxide is mediated by the Haber-Weiss reaction', *Biochim Biophys Acta*, 781: 56-63.

Mendez-Bermudez, A., M. Hills, H. A. Pickett, A. T. Phan, J. L. Mergny, J. F. Riou, and N. J. Royle. 2009. 'Human telomeres that contain (CTAGGG)n repeats show replication dependent instability in somatic cells and the male germline', *Nucleic Acids Res*, 37: 6225-38.

Mergny, J. L., and C. Helene. 1998. 'G-quadruplex DNA: a target for drug design', *Nat Med*, 4: 1366-7.

Middleton, G., P. Silcocks, T. Cox, J. Valle, J. Wadsley, D. Propper, F. Coxon, P. Ross, S. Madhusudan, T. Roques, D. Cunningham, S. Falk, N. Wadd, M. Harrison, P. Corrie, T. Iveson, A. Robinson, K. McAdam, M. Eatock, J. Evans, C. Archer, T. Hickish, A. Garcia-Alonso, M. Nicolson, W. Steward, A. Anthoney, W. Greenhalf, V. Shaw, E. Costello, D. Naisbitt, C. Rawcliffe, G. Nanson, and J. Neoptolemos. 2014. 'Gemcitabine and capecitabine with or without telomerase peptide vaccine GV1001 in patients with locally advanced or metastatic pancreatic cancer (TeloVac): an open-label, randomised, phase 3 trial', *Lancet Oncol*, 15: 829-40.

Mimitou, E. P., and L. S. Symington. 2009. 'Nucleases and helicases take center stage in homologous recombination', *Trends Biochem Sci*, 34: 264-72.

Mishima, Y., L. Santo, H. Eda, D. Cirstea, N. Nemani, A. J. Yee, E. O'Donnell, M. K. Selig, S. N. Quayle, S. Arastu-Kapur, C. Kirk, L. H. Boise, S. S. Jones, and N. Raje. 2015. 'Ricolinostat (ACY-1215) induced inhibition of aggresome formation accelerates carfilzomib-induced multiple myeloma cell death', *Br J Haematol*, 169: 423-34.

Mishra, K., and D. Shore. 1999. 'Yeast Ku protein plays a direct role in telomeric silencing and counteracts inhibition by rif proteins', *Curr Biol*, 9: 1123-6.

Mitchell, J. R., and K. Collins. 2000. 'Human telomerase activation requires two independent interactions between telomerase RNA and telomerase reverse transcriptase', *Mol Cell*, 6: 361-71.

Mitchell, J. R., E. Wood, and K. Collins. 1999. 'A telomerase component is defective in the human disease dyskeratosis congenita', *Nature*, 402: 551-5.

Mittelman, M. 2003. 'The implications of anemia in multiple myeloma', *Clin Lymphoma*, 4 Suppl 1: S23-9.

Mocellin, S., K. A. Pooley, and D. Nitti. 2013. 'Telomerase and the search for the end of cancer', *Trends Mol Med*, 19: 125-33.

Modrich, P. 2006. 'Mechanisms in eukaryotic mismatch repair', *J Biol Chem*, 281: 30305-9.

Montpetit, A. J., A. A. Alhareeri, M. Montpetit, A. R. Starkweather, L. W. Elmore, K. Filler, L. Mohanraj, C. W. Burton, V. S. Menzies, D. E. Lyon, and C. K. Jackson-Cook. 2014. 'Telomere length: a review of methods for measurement', *Nurs Res*, 63: 289-99.

Moreau, P., T. Masszi, N. Grzasko, N. J. Bahlis, M. Hansson, L. Pour, I. Sandhu, P. Ganly, B. W. Baker, S. R. Jackson, A. M. Stoppa, D. R. Simpson, P. Gimsing, A. Palumbo, L. Garderet, M. Cavo, S. Kumar, C. Touzeau, F. K. Buadi, J. P. Laubach, D. T. Berg, J. Lin, A. Di Bacco, A. M. Hui, H. van de Velde, P. G. Richardson, and Tourmaline-Mm Study Group. 2016. 'Oral Ixazomib, Lenalidomide, and Dexamethasone for Multiple Myeloma', *N Engl J Med*, 374: 1621-34.

Moriarty, T. J., D. T. Marie-Egyptienne, and C. Autexier. 2004. 'Functional organization of repeat addition processivity and DNA synthesis determinants in the human telomerase multimer', *Mol Cell Biol*, 24: 3720-33.

Moser, J., H. Kool, I. Giakzidis, K. Caldecott, L. H. Mullenders, and M. I. Fousteri. 2007. 'Sealing of chromosomal DNA nicks during nucleotide excision repair requires XRCC1 and DNA ligase III alpha in a cell-cycle-specific manner', *Mol Cell*, 27: 311-23.

Moynahan, M. E., and M. Jasin. 2010. 'Mitotic homologous recombination maintains genomic stability and suppresses tumorigenesis', *Nat Rev Mol Cell Biol*, 11: 196-207.

Munoz-Espin, D., and M. Serrano. 2014. 'Cellular senescence: from physiology to pathology', *Nat Rev Mol Cell Biol*, 15: 482-96.

Muntoni, A., A. A. Neumann, M. Hills, and R. R. Reddel. 2009. 'Telomere elongation involves intra-molecular DNA replication in cells utilizing alternative lengthening of telomeres', *Hum Mol Genet*, 18: 1017-27.

Murai, J., S. Y. Huang, B. B. Das, A. Renaud, Y. Zhang, J. H. Doroshow, J. Ji, S. Takeda, and Y. Pommier. 2012. 'Trapping of PARP1 and PARP2 by Clinical PARP Inhibitors', *Cancer Res*, 72: 5588-99.

Murai, J., S. Y. Huang, A. Renaud, Y. Zhang, J. Ji, S. Takeda, J. Morris, B. Teicher, J. H. Doroshow, and Y. Pommier. 2014. 'Stereospecific PARP trapping by BMN 673 and comparison with olaparib and rucaparib', *Mol Cancer Ther*, 13: 433-43.

Murakawa, Y., E. Sonoda, L. J. Barber, W. Zeng, K. Yokomori, H. Kimura, A. Niimi, A. Lehmann, G. Y. Zhao, H. Hochegger, S. J. Boulton, and S. Takeda. 2007. 'Inhibitors of the proteasome suppress homologous DNA recombination in mammalian cells', *Cancer Res*, 67: 8536-43.

Murnane, J. P. 2006. 'Telomeres and chromosome instability', *DNA Repair (Amst)*, 5: 1082-92.

Musgrove, E. A., C. E. Caldon, J. Barraclough, A. Stone, and R. L. Sutherland. 2011. 'Cyclin D as a therapeutic target in cancer', *Nat Rev Cancer*, 11: 558-72.

Nabetani, A., and F. Ishikawa. 2009. 'Unusual telomeric DNAs in human telomerase-negative immortalized cells', *Mol Cell Biol*, 29: 703-13.

Nam, E. A., and D. Cortez. 2011. 'ATR signalling: more than meeting at the fork', *Biochem J*, 436: 527-36.

Napier, C. E., L. I. Huschtscha, A. Harvey, K. Bower, J. R. Noble, E. A. Hendrickson, and R. R. Reddel. 2015. 'ATRX represses alternative lengthening of telomeres', *Oncotarget*, 6: 16543-58.

Nardiello, T., A. A. Jungbluth, A. Mei, M. Diliberto, X. Huang, A. Dabrowski, V. C. Andrade, R. Wasserstrum, S. Ely, R. Niesvizky, R. Pearse, M. Coleman, D. S. Jayabalan, N. Bhardwaj, L. J. Old, S. Chen-Kiang, and H. J. Cho. 2011. 'MAGE-A inhibits apoptosis in proliferating myeloma cells through repression of Bax and maintenance of survivin', *Clin Cancer Res*, 17: 4309-19.

Nelson, W. G., and M. B. Kastan. 1994. 'DNA strand breaks: the DNA template alterations that trigger p53-dependent DNA damage response pathways', *Mol Cell Biol*, 14: 1815-23.

Neri, P., L. Ren, K. Gratton, E. Stebner, J. Johnson, A. Klimowicz, P. Duggan, P. Tassone, A. Mansoor, D. A. Stewart, S. Lonial, L. H. Boise, and N. J. Bahlis. 2011. 'Bortezomib-induced "BRCAness" sensitizes multiple myeloma cells to PARP inhibitors', *Blood*, 118: 6368-79.

Nguyen, B. N., L. W. Elmore, and S. E. Holt. 2009. 'Mechanism of dominant-negative telomerase function', *Cell Cycle*, 8: 3227-33.

Nice. 2016. 'Myeloma: Diagnosis and Management', NICE Guidelines, 9-18.

Nile, D. L., C. Rae, I. J. Hyndman, M. N. Gaze, and R. J. Mairs. 2016. 'An evaluation in vitro of PARP-1 inhibitors, rucaparib and olaparib, as radiosensitisers for the treatment of neuroblastoma', *BMC Cancer*, 16: 621.

Nishida, K., A. Tamura, N. Nakazawa, Y. Ueda, T. Abe, F. Matsuda, K. Kashima, and M. Taniwaki. 1997. 'The Ig heavy chain gene is frequently involved in chromosomal translocations in multiple myeloma and plasma cell leukemia as detected by in situ hybridization', *Blood*, 90: 526-34.

Nussey, D. H., D. Baird, E. Barrett, W. Boner, J. Fairlie, N. Gemmell, N. Hartmann, T. Horn, M. Haussmann, M. Olsson, C. Turbill, S. Verhulst, S. Zahn, and P. Monaghan. 2014. 'Measuring telomere length and telomere dynamics in evolutionary biology and ecology', *Methods Ecol Evol*, 5: 299-310.

O'Sullivan, R. J., and J. Karlseder. 2010. 'Telomeres: protecting chromosomes against genome instability', *Nat Rev Mol Cell Biol*, 11: 171-81.

Oh, S., Y. H. Song, J. Yim, and T. K. Kim. 2000. 'Identification of Mad as a repressor of the human telomerase (hTERT) gene', *Oncogene*, 19: 1485-90.

Oh, S., Y. Song, J. Yim, and T. K. Kim. 1999. 'The Wilms' tumor 1 tumor suppressor gene represses transcription of the human telomerase reverse transcriptase gene', *J Biol Chem*, 274: 37473-8.

Okamoto, K., C. Bartocci, I. Ouzounov, J. K. Diedrich, J. R. Yates, 3rd, and E. L. Denchi. 2013. 'A two-step mechanism for TRF2-mediated chromosome-end protection', *Nature*, 494: 502-5.

Oracki, S. A., J. A. Walker, M. L. Hibbs, L. M. Corcoran, and D. M. Tarlinton. 2010. 'Plasma cell development and survival', *Immunol Rev*, 237: 140-59.

Ottaviani, A., E. Gilson, and F. Magdinier. 2008. 'Telomeric position effect: from the yeast paradigm to human pathologies?', *Biochimie*, 90: 93-107.

Otto, T., and P. Sicinski. 2017. 'Cell cycle proteins as promising targets in cancer therapy', *Nat Rev Cancer*, 17: 93-115.

Paino, T., M. E. Sarasquete, B. Paiva, P. Krzeminski, L. San-Segundo, L. A. Corchete, A. Redondo, M. Garayoa, R. Garcia-Sanz, N. C. Gutierrez, E. M. Ocio, and J. F. San-Miguel. 2014. 'Phenotypic, genomic and functional characterization reveals no differences between CD138++ and CD138low subpopulations in multiple myeloma cell lines', *PLoS One*, 9: e92378.

Palumbo, A., H. Avet-Loiseau, S. Oliva, H. M. Lokhorst, H. Goldschmidt, L. Rosinol, P. Richardson, S. Caltagirone, J. J. Lahuerta, T. Facon, S. Bringhen, F. Gay, M. Attal, R. Passera, A. Spencer, M. Offidani, S. Kumar, P. Musto, S. Lonial, M. T. Petrucci, R. Z. Orlowski, E. Zamagni, G. Morgan, M. A. Dimopoulos, B. G. Durie, K. C. Anderson, P. Sonneveld, J. San Miguel, M. Cavo, S. V. Rajkumar, and P. Moreau. 2015. 'Revised International Staging System for Multiple Myeloma: A Report From International Myeloma Working Group', *J Clin Oncol*, 33: 2863-9.

Palumbo, A., A. Chanan-Khan, K. Weisel, A. K. Nooka, T. Masszi, M. Beksac, I. Spicka, V. Hungria, M. Munder, M. V. Mateos, T. M. Mark, M. Qi, J. Schecter, H. Amin, X. Qin, W. Deraedt, T. Ahmadi, A. Spencer, P. Sonneveld, and Castor Investigators. 2016. 'Daratumumab, Bortezomib, and Dexamethasone for Multiple Myeloma', *N Engl J Med*, 375: 754-66.

Palumbo, A., T. Facon, P. Sonneveld, J. Blade, M. Offidani, F. Gay, P. Moreau, A. Waage, A. Spencer, H. Ludwig, M. Boccadoro, and J. L. Harousseau. 2008. 'Thalidomide for treatment of multiple myeloma: 10 years later', *Blood*, 111: 3968-77.

Palumbo, A., S. V. Rajkumar, J. F. San Miguel, A. Larocca, R. Niesvizky, G. Morgan, O. Landgren, R. Hajek, H. Einsele, K. C. Anderson, M. A. Dimopoulos, P. G. Richardson, M. Cavo, A. Spencer, A. K. Stewart, K. Shimizu, S. Lonial, P. Sonneveld, B. G. Durie, P. Moreau, and R. Z. Orlowski. 2014. 'International Myeloma Working Group consensus statement for the management, treatment, and supportive care of patients with myeloma not eligible for standard autologous stem-cell transplantation', *J Clin Oncol*, 32: 587-600.

Pannunzio, N. R., S. Li, G. Watanabe, and M. R. Lieber. 2014. 'Non-homologous end joining often uses microhomology: implications for alternative end joining', *DNA Repair (Amst)*, 17: 74-80.

Papapoulos, S. 2008. 'Bisphosphonates: how do they work?' *Best Prac & Reas Clin Endo & Met*, 22: 831-847

Pascucci, B., M. Stucki, Z. O. Jonsson, E. Dogliotti, and U. Hubscher. 1999. 'Long patch base excision repair with purified human proteins. DNA ligase I as patch size mediator for DNA polymerases delta and epsilon', *J Biol Chem*, 274: 33696-702.

Patel, A. G., J. N. Sarkaria, and S. H. Kaufmann. 2011. 'Nonhomologous end joining drives poly(ADP-ribose) polymerase (PARP) inhibitor lethality in homologous recombination-deficient cells', *Proc Natl Acad Sci U S A*, 108: 3406-11.

Peifer, M., F. Hertwig, F. Roels, D. Dreidax, M. Gartlgruber, R. Menon, A. Kramer, J. L. Roncaioli, F. Sand, J. M. Heuckmann, F. Ikram, R. Schmidt, S. Ackermann, A. Engesser, Y. Kahlert, W. Vogel, J. Altmuller, P. Nurnberg, J. Thierry-Mieg, D. Thierry-Mieg, A. Mariappan, S. Heynck, E. Mariotti, K. O. Henrich, C. Gloeckner, G. Bosco, I. Leuschner, M. R. Schweiger, L. Savelyeva, S. C. Watkins, C. Shao, E. Bell, T. Hofer, V. Achter, U. Lang, J. Theissen, R. Volland, M. Saadati, A. Eggert, B. de Wilde, F. Berthold, Z. Peng, C. Zhao, L. Shi, M. Ortmann, R. Buttner, S. Perner, B. Hero, A. Schramm, J. H. Schulte, C. Herrmann, R. J. O'Sullivan, F. Westermann, R. K. Thomas, and M. Fischer. 2015. 'Telomerase activation by genomic rearrangements in high-risk neuroblastoma', *Nature*, 526: 700-4.

Podlevsky, J. D., and J. J. Chen. 2012. 'It all comes together at the ends: telomerase structure, function, and biogenesis', *Mutat Res*, 730: 3-11.

Porro, A., S. Feuerhahn, and J. Lingner. 2014. 'TERRA-reinforced association of LSD1 with MRE11 promotes processing of uncapped telomeres', *Cell Rep*, 6: 765-76.

Porro, A., S. Feuerhahn, P. Reichenbach, and J. Lingner. 2010. 'Molecular dissection of telomeric repeat-containing RNA biogenesis unveils the presence of distinct and multiple regulatory pathways', *Mol Cell Biol*, 30: 4808-17.

Powell, S. N., and L. A. Kachnic. 2003. 'Roles of BRCA1 and BRCA2 in homologous recombination, DNA replication fidelity and the cellular response to ionizing radiation', *Oncogene*, 22: 5784-91.

Qi, X., M. Xie, A. F. Brown, C. J. Bley, J. D. Podlevsky, and J. J. Chen. 2012. 'RNA/DNA hybrid binding affinity determines telomerase template-translocation efficiency', *EMBO J*, 31: 150-61.

Qiang, Y. W., Y. Chen, O. Stephens, N. Brown, B. Chen, J. Epstein, B. Barlogie, and J. D. Shaughnessy, Jr. 2008. 'Myeloma-derived Dickkopf-1 disrupts Wnt-regulated osteoprotegerin and RANKL production by osteoblasts: a potential mechanism underlying osteolytic bone lesions in multiple myeloma', *Blood*, 112: 196-207.

Rahman, R., L. Mo, and W. Cui. 2006. 'Telomerase with mutated catalytic motifs has dominant negative effects on telomerase activity and inhibits cell growth', *Biochem Biophys Res Commun*, 350: 796-802.

Rai, R., H. Zheng, H. He, Y. Luo, A. Multani, P. B. Carpenter, and S. Chang. 2010. 'The function of classical and alternative non-homologous end-joining pathways in the fusion of dysfunctional telomeres', *EMBO J*, 29: 2598-610.

Rajan, A. and Rajkumar, S. 2015. 'Interpretation of cytogenetic results in multiple myeloma for clinical practice', Blood Cancer J, 5: e365

Rajkumar, S. V., M. A. Dimopoulos, A. Palumbo, J. Blade, G. Merlini, M. V. Mateos, S. Kumar, J. Hillengass, E. Kastritis, P. Richardson, O. Landgren, B. Paiva, A. Dispenzieri, B. Weiss, X. LeLeu, S. Zweegman, S. Lonial, L. Rosinol, E. Zamagni, S. Jagannath, O. Sezer, S. Y. Kristinsson, J. Caers, S. Z. Usmani, J. J. Lahuerta, H. E. Johnsen, M. Beksac, M. Cavo, H. Goldschmidt, E. Terpos, R. A. Kyle, K. C. Anderson, B. G. Durie, and J. F. Miguel. 2014. 'International Myeloma Working Group updated criteria for the diagnosis of multiple myeloma', *Lancet Oncol*, 15: e538-48.

Rajkumar, S. V., V. Gupta, R. Fonseca, A. Dispenzieri, W. I. Gonsalves, D. Larson, R. P. Ketterling, J. A. Lust, R. A. Kyle, and S. K. Kumar. 2013. 'Impact of primary molecular cytogenetic abnormalities and risk of progression in smoldering multiple myeloma', *Leukemia*, 27: 1738-44.

Rajkumar, S. V., D. Larson, and R. A. Kyle. 2011. 'Diagnosis of smoldering multiple myeloma', *N Engl J Med*, 365: 474-5.

Rasmussen, T., J. Kastrup, L. M. Knudsen, and H. E. Johnsen. 1999. 'High numbers of clonal CD19+ cells in the peripheral blood of a patient with multiple myeloma', *Br J Haematol*, 105: 265-7.

Redon, S., P. Reichenbach, and J. Lingner. 2010. 'The non-coding RNA TERRA is a natural ligand and direct inhibitor of human telomerase', *Nucleic Acids Res*, 38: 5797-806.

Reynolds, P., S. Cooper, M. Lomax, and P. O'Neill. 2015. 'Disruption of PARP1 function inhibits base excision repair of a sub-set of DNA lesions', *Nucleic Acids Res*, 43: 4028-38.

Riballo, E., M. Kuhne, N. Rief, A. Doherty, G. C. Smith, M. J. Recio, C. Reis, K. Dahm, A. Fricke, A. Krempler, A. R. Parker, S. P. Jackson, A. Gennery, P. A. Jeggo, and M. Lobrich. 2004. 'A pathway of double-strand break rejoining dependent upon ATM, Artemis, and proteins locating to gamma-H2AX foci', *Mol Cell*, 16: 715-24.

Richardson, P. G., P. Sonneveld, M. W. Schuster, D. Irwin, E. A. Stadtmauer, T. Facon, J. L. Harousseau, D. Ben-Yehuda, S. Lonial, H. Goldschmidt, D. Reece, J. F. San-Miguel, J. Blade, M. Boccadoro, J. Cavenagh, W. S. Dalton, A. L. Boral, D. L. Esseltine, J. B. Porter, D. Schenkein, K. C. Anderson, and Investigators Assessment of Proteasome Inhibition for Extending Remissions. 2005. 'Bortezomib or high-dose dexamethasone for relapsed multiple myeloma', *N Engl J Med*, 352: 2487-98.

Riethman, H., A. Ambrosini, C. Castaneda, J. Finklestein, X. L. Hu, U. Mudunuri, S. Paul, and J. Wei. 2004. 'Mapping and initial analysis of human subtelomeric sequence assemblies', *Genome Res*, 14: 18-28.

Robin, J. D., A. T. Ludlow, K. Batten, F. Magdinier, G. Stadler, K. R. Wagner, J. W. Shay, and W. E. Wright. 2014. 'Telomere position effect: regulation of gene expression with progressive telomere shortening over long distances', *Genes Dev*, 28: 2464-76.

Roger, L., R. E. Jones, N. H. Heppel, G. T. Williams, J. R. Sampson, and D. M. Baird. 2013. 'Extensive telomere erosion in the initiation of colorectal adenomas and its association with chromosomal instability', *J Natl Cancer Inst*, 105: 1202-11.

Roodman, G. D. 2004. 'Pathogenesis of myeloma bone disease', *Blood Cells Mol Dis*, 32: 290-2.

Rooney, P. H., G. I. Murray, D. A. Stevenson, N. E. Haites, J. Cassidy, and H. L. McLeod. 1999. 'Comparative genomic hybridization and chromosomal instability in solid tumours', *Br J Cancer*, 80: 862-73.

Rossi, D., M. Fangazio, L. De Paoli, A. Puma, P. Riccomagno, V. Pinto, P. Zigrossi, A. Ramponi, G. Monga, and G. Gaidano. 2010. 'Beta-2-microglobulin is an independent predictor of progression in asymptomatic multiple myeloma', *Cancer*, 116: 2188-200.

Rothkamm, K., I. Kruger, L. H. Thompson, and M. Lobrich. 2003. 'Pathways of DNA double-strand break repair during the mammalian cell cycle', *Mol Cell Biol*, 23: 5706-15.

Rouleau, M., A. Patel, M. J. Hendzel, S. H. Kaufmann, and G. G. Poirier. 2010. 'PARP inhibition: PARP1 and beyond', *Nat Rev Cancer*, 10: 293-301.

Rubin, H. 2002. 'The disparity between human cell senescence in vitro and lifelong replication in vivo', *Nat Biotechnol*, 20: 675-81.

Rufer, N., W. Dragowska, G. Thornbury, E. Roosnek, and P. M. Lansdorp. 1998. 'Telomere length dynamics in human lymphocyte subpopulations measured by flow cytometry', *Nat Biotechnol*, 16: 743-7.

Rulten, S. L., A. E. Fisher, I. Robert, M. C. Zuma, M. Rouleau, L. Ju, G. Poirier, B. Reina-San-Martin, and K. W. Caldecott. 2011. 'PARP-3 and APLF function together to accelerate nonhomologous end-joining', *Mol Cell*, 41: 33-45.

Russo, A., F. Modica, S. Guarrera, G. Fiorito, B. Pardini, C. Viberti, A. Allione, R. Critelli, A. Bosio, G. Casetta, G. Cucchiarale, P. Destefanis, P. Gontero, L. Rolle, A. Zitella, D. Fontana, B. Frea, P. Vineis, C. Sacerdote, and G. Matullo. 2014. 'Shorter leukocyte telomere length is independently associated with poor survival in patients with bladder cancer', *Cancer Epidemiol Biomarkers Prev*, 23: 2439-46.

Ruzankina, Y., C. Pinzon-Guzman, A. Asare, T. Ong, L. Pontano, G. Cotsarelis, V. P. Zediak, M. Velez, A. Bhandoola, and E. J. Brown. 2007. 'Deletion of the developmentally essential gene ATR in adult mice leads to age-related phenotypes and stem cell loss', *Cell Stem Cell*, 1: 113-26.

Sagawa, Y., H. Nishi, K. Isaka, A. Fujito, and M. Takayama. 2001. 'The correlation of TERT expression with c-myc expression in cervical cancer', *Cancer Lett*, 168: 45-50.

Samassekou, O. 2013. 'Dynamic length changes of telomeres and their nuclear organization in chronic myeloid leukemia', *Cancers (Basel)*, 5: 1086-102.

San-Miguel, J. F., V. T. Hungria, S. S. Yoon, M. Beksac, M. A. Dimopoulos, A. Elghandour, W. W. Jedrzejczak, A. Gunther, T. N. Nakorn, N. Siritanaratkul, P. Corradini, S. Chuncharunee, J. J. Lee, R. L. Schlossman, T. Shelekhova, K. Yong, D. Tan, T. Numbenjapon, J. D. Cavenagh, J. Hou, R. LeBlanc, H. Nahi, L. Qiu, H. Salwender, S. Pulini, P. Moreau, K. Warzocha, D. White, J. Blade, W. Chen, J. de la Rubia, P. Gimsing, S. Lonial, J. L. Kaufman, E. M. Ocio, L. Veskovski, S. K. Sohn, M. C. Wang, J. H. Lee, H. Einsele, M. Sopala, C. Corrado, B. R. Bengoudifa, F. Binlich, and P. G. Richardson. 2014. 'Panobinostat plus bortezomib and dexamethasone versus placebo plus bortezomib and dexamethasone in patients with relapsed or relapsed and refractory multiple myeloma: a multicentre, randomised, double-blind phase 3 trial', *Lancet Oncol*, 15: 1195-206.

San Miguel, J., K. Weisel, P. Moreau, M. Lacy, K. Song, M. Delforge, L. Karlin, H. Goldschmidt, A. Banos, A. Oriol, A. Alegre, C. Chen, M. Cavo, L. Garderet, V. Ivanova, J. Martinez-Lopez, A. Belch, A. Palumbo, S. Schey, P. Sonneveld, X. Yu, L. Sternas, C. Jacques, M. Zaki, and M. Dimopoulos. 2013. 'Pomalidomide plus low-dose dexamethasone versus high-dose dexamethasone alone for patients with relapsed and refractory multiple myeloma (MM-003): a randomised, open-label, phase 3 trial', *Lancet Oncol*, 14: 1055-66.

Sarek, G., J. B. Vannier, S. Panier, J. H. Petrini, and S. J. Boulton. 2015. 'TRF2 recruits RTEL1 to telomeres in S phase to promote t-loop unwinding', *Mol Cell*, 57: 622-35.

Savage, S. A., N. Giri, G. M. Baerlocher, N. Orr, P. M. Lansdorp, and B. P. Alter. 2008. 'TINF2, a component of the shelterin telomere protection complex, is mutated in dyskeratosis congenita', *Am J Hum Genet*, 82: 501-9.

Schmidt, J. C., and T. R. Cech. 2015. 'Human telomerase: biogenesis, trafficking, recruitment, and activation', *Genes Dev*, 29: 1095-105.

Schoeftner, S., and M. A. Blasco. 2008. 'Developmentally regulated transcription of mammalian telomeres by DNA-dependent RNA polymerase II', *Nat Cell Biol*, 10: 228-36.

Schreiber, V., J. C. Ame, P. Dolle, I. Schultz, B. Rinaldi, V. Fraulob, J. Menissier-de Murcia, and G. de Murcia. 2002. 'Poly(ADP-ribose) polymerase-2 (PARP-2) is required for efficient base excision DNA repair in association with PARP-1 and XRCC1', *J Biol Chem*, 277: 23028-36.

Sealey, D. C., L. Zheng, M. A. Taboski, J. Cruickshank, M. Ikura, and L. A. Harrington. 2010. 'The N-terminus of hTERT contains a DNA-binding domain and is required for telomerase activity and cellular immortalization', *Nucleic Acids Res*, 38: 2019-35.

Shammas, M. A., H. Koley, R. C. Bertheau, P. Neri, M. Fulciniti, P. Tassone, S. Blotta, A. Protopopov, C. Mitsiades, R. B. Batchu, K. C. Anderson, A. Chin, S. Gryaznov, and N. C. Munshi. 2008. 'Telomerase inhibitor GRN163L inhibits myeloma cell growth in vitro and in vivo', *Leukemia*, 22: 1410-8.

Shammas, M. A., R. J. Shmookler Reis, M. Akiyama, H. Koley, D. Chauhan, T. Hideshima, R. K. Goyal, L. H. Hurley, K. C. Anderson, and N. C. Munshi. 2003. 'Telomerase inhibition and cell growth arrest by G-quadruplex interactive agent in multiple myeloma', *Mol Cancer Ther*, 2: 825-33.

Shammas, M. A., R. J. Shmookler Reis, H. Koley, R. B. Batchu, C. Li, and N. C. Munshi. 2009. 'Dysfunctional homologous recombination mediates genomic instability and progression in myeloma', *Blood*, 113: 2290-7.

Shapiro-Shelef, M., and K. Calame. 2005. 'Regulation of plasma-cell development', *Nat Rev Immunol*, 5: 230-42.

Sharma, S., E. Nemeth, Y. H. Chen, J. Goodnough, A. Huston, G. D. Roodman, T. Ganz, and A. Lichtenstein. 2008. 'Involvement of hepcidin in the anemia of multiple myeloma', *Clin Cancer Res*, 14: 3262-7.

Shaughnessy, J., J. Jacobson, J. Sawyer, J. McCoy, A. Fassas, F. Zhan, K. Bumm, J. Epstein, E. Anaissie, S. Jagannath, D. Vesole, D. Siegel, R. Desikan, N. Munshi, A. Badros, E. Tian, M. Zangari, G. Tricot, J. Crowley, and B. Barlogie. 2003. 'Continuous absence of metaphase-defined cytogenetic abnormalities, especially of chromosome 13 and hypodiploidy, ensures long-term survival in multiple myeloma treated with Total Therapy I: interpretation in the context of global gene expression', *Blood*, 101: 3849-56.

Shay, J. W., and W. E. Wright. 2000. 'Hayflick, his limit, and cellular ageing', *Nat Rev Mol Cell Biol*, 1: 72-6.

Shay, J. W., and W. E. Wright. 2005. 'Senescence and immortalization: role of telomeres and telomerase', *Carcinogenesis*, 26: 867-74.

Shi, J., X. R. Yang, B. Ballew, M. Rotunno, D. Calista, M. C. Fargnoli, P. Ghiorzo, B. Bressac-de Paillerets, E. Nagore, M. F. Avril, N. E. Caporaso, M. L. McMaster, M. Cullen, Z. Wang, X. Zhang, Nci Dceg Cancer Sequencing Working Group, Nci Dceg Cancer Genomics Research Laboratory, Group French Familial Melanoma Study, W. Bruno, L. Pastorino, P. Queirolo, J. Banuls-Roca, Z. Garcia-Casado, A. Vaysse, H. Mohamdi, Y. Riazalhosseini, M. Foglio, F. Jouenne, X. Hua, P. L. Hyland, J. Yin, H. Vallabhaneni, W. Chai, P. Minghetti, C. Pellegrini, S. Ravichandran, A. Eggermont, M. Lathrop, K. Peris, G. B. Scarra, G. Landi, S. A. Savage, J. N. Sampson, J. He, M. Yeager, L. R. Goldin, F. Demenais, S. J. Chanock, M. A. Tucker, A. M. Goldstein, Y. Liu, and M. T. Landi. 2014. 'Rare missense variants in POT1 predispose to familial cutaneous malignant melanoma', *Nat Genet*, 46: 482-6.

Shiratsuchi, M., K. Muta, Y. Abe, S. Motomura, F. Taguchi, H. Takatsuki, N. Uike, T. Umemura, H. Nawata, and J. Nishimura. 2002. 'Clinical significance of telomerase activity in multiple myeloma', *Cancer*, 94: 2232-8.

Shlomchik, M. J., and F. Weisel. 2012. 'Germinal center selection and the development of memory B and plasma cells', *Immunol Rev*, 247: 52-63.

Shrivastav, M., L. P. De Haro, and J. A. Nickoloff. 2008. 'Regulation of DNA double-strand break repair pathway choice', *Cell Res*, 18: 134-47.

Simpson, K., R. E. Jones, J. W. Grimstead, R. Hills, C. Pepper, and D. M. Baird. 2015. 'Telomere fusion threshold identifies a poor prognostic subset of breast cancer patients', *Mol Oncol*, 9: 1186-93.

Smadja, N. V., C. Bastard, C. Brigaudeau, D. Leroux, C. Fruchart, and Hematologique Groupe Francais de Cytogenetique. 2001. 'Hypodiploidy is a major prognostic factor in multiple myeloma', *Blood*, 98: 2229-38.

Smith, K. G., T. D. Hewitson, G. J. Nossal, and D. M. Tarlinton. 1996. 'The phenotype and fate of the antibody-forming cells of the splenic foci', *Eur J Immunol*, 26: 444-8.

Smith, S. 2001. 'The world according to PARP', *Trends Biochem Sci*, 26: 174-9.

Smith, S., and T. de Lange. 2000. 'Tankyrase promotes telomere elongation in human cells', *Curr Biol*, 10: 1299-302.

Smogorzewska, A., B. van Steensel, A. Bianchi, S. Oelmann, M. R. Schaefer, G. Schnapp, and T. de Lange. 2000. 'Control of human telomere length by TRF1 and TRF2', *Mol Cell Biol*, 20: 1659-68.

Soboleski, M. R., J. Oaks, and W. P. Halford. 2005. 'Green fluorescent protein is a quantitative reporter of gene expression in individual eukaryotic cells', *FASEB J*, 19: 440-2.

Sommerfeld, H. J., A. K. Meeker, M. A. Piatyszek, G. S. Bova, J. W. Shay, and D. S. Coffey. 1996. 'Telomerase activity: a prevalent marker of malignant human prostate tissue', *Cancer Res*, 56: 218-22.

Speedy, H. E., B. Kinnersley, D. Chubb, P. Broderick, P. J. Law, K. Litchfield, S. Jayne, M. J. Dyer, C. Dearden, G. A. Follows, D. Catovsky, and R. S. Houlston. 2016. 'Germline mutations in shelterin complex genes are associated with familial chronic lymphocytic leukemia', *Blood*.

Sprung, C. N., L. Sabatier, and J. P. Murnane. 1996. 'Effect of telomere length on telomeric gene expression', *Nucleic Acids Res*, 24: 4336-40.

Stagno D'Alcontres, M., A. Mendez-Bermudez, J. L. Foxon, N. J. Royle, and P. Salomoni. 2007. 'Lack of TRF2 in ALT cells causes PML-dependent p53 activation and loss of telomeric DNA', *J Cell Biol*, 179: 855-67.

Stavnezer, J., J. Guikema and C. Schrader. 2009. 'Mechanism and Regulation of Class Switch Recombination', *Annu Rev Immunol*, 26: 261-293

Stewart, A. K., S. V. Rajkumar, M. A. Dimopoulos, T. Masszi, I. Spicka, A. Oriol, R. Hajek, L. Rosinol, D. S. Siegel, G. G. Mihaylov, V. Goranova-Marinova, P. Rajnics, A. Suvorov, R. Niesvizky, A. J. Jakubowiak, J. F. San-Miguel, H. Ludwig, M. Wang, V. Maisnar, J. Minarik, W. I. Bensinger, M. V. Mateos, D. Ben-Yehuda, V. Kukreti, N. Zojwalla, M. E. Tonda, X. Yang, B. Xing, P. Moreau, A. Palumbo, and Aspire Investigators. 2015. 'Carfilzomib, lenalidomide, and dexamethasone for relapsed multiple myeloma', *N Engl J Med*, 372: 142-52.

Strefford, J. C., L. Kadalayil, J. Forster, M. J. Rose-Zerilli, A. Parker, T. T. Lin, N. Heppel, K. Norris, A. Gardiner, Z. Davies, D. Gonzalez de Castro, M. Else, A. J. Steele, H. Parker, T. Stankovic, C. Pepper, C. Fegan, D. Baird, A. Collins, D. Catovsky, and D. G. Oscier. 2015. 'Telomere length predicts progression and overall survival in chronic lymphocytic leukemia: data from the UK LRF CLL4 trial', *Leukemia*, 29: 2411-4.

Sun, H., L. He, H. Wu, F. Pan, X. Wu, J. Zhao, Z. Hu, C. Sekhar, H. Li, L. Zheng, H. Chen, B. H. Shen, and Z. Guo. 2017. 'The FEN1 L209P mutation interferes with long-patch base excision repair and induces cellular transformation', *Oncogene*, 36: 194-207.

Surget, S., G. Descamps, C. Brosseau, V. Normant, S. Maiga, P. Gomez-Bougie, N. Gouy-Colin, C. Godon, M. C. Bene, P. Moreau, S. Le Gouill, M. Amiot, and C. Pellat-Deceunynck. 2014. 'RITA (Reactivating p53 and Inducing Tumor Apoptosis) is efficient against TP53abnormal myeloma cells independently of the p53 pathway', *BMC Cancer*, 14: 437.

Svenson, U., K. Nordfjall, D. Baird, L. Roger, P. Osterman, M. L. Hellenius, and G. Roos. 2011. 'Blood cell telomere length is a dynamic feature', *PLoS One*, 6: e21485.

Swisher, E. M., K. K. Lin, A. M. Oza, C. L. Scott, H. Giordano, J. Sun, G. E. Konecny, R. L. Coleman, A. V. Tinker, D. M. O'Malley, R. S. Kristeleit, L. Ma, K. M. Bell-McGuinn, J. D. Brenton, J. M. Cragun, A. Oaknin, I. Ray-Coquard, M. I. Harrell, E. Mann, S. H. Kaufmann, A. Floquet, A. Leary, T. C. Harding, S. Goble, L. Maloney, J. Isaacson, A. R. Allen, L. Rolfe, R. Yelensky, M. Raponi, and I. A. McNeish. 2017. 'Rucaparib in relapsed, platinum-sensitive high-grade ovarian carcinoma (ARIEL2 Part 1): an international, multicentre, open-label, phase 2 trial', *Lancet Oncol*, 18: 75-87.

Syed, Y. Y. 2017. 'Rucaparib: First Global Approval', *Drugs*, 77: 585-92.

Takai, K. K., S. Hooper, S. Blackwood, R. Gandhi, and T. de Lange. 2010. 'In vivo stoichiometry of shelterin components', *J Biol Chem*, 285: 1457-67.

Tanaka, Y., M. Abe, M. Hiasa, A. Oda, H. Amou, A. Nakano, K. Takeuchi, K. Kitazoe, S. Kido, D. Inoue, K. Moriyama, T. Hashimoto, S. Ozaki, and T. Matsumoto. 2007. 'Myeloma cell-osteoclast interaction enhances angiogenesis together with bone resorption: a role for vascular endothelial cell growth factor and osteopontin', *Clin Cancer Res*, 13: 816-23.

Tefferi, A., T. L. Lasho, K. H. Begna, M. M. Patnaik, D. L. Zblewski, C. M. Finke, R. R. Laborde, E. Wassie, L. Schimek, C. A. Hanson, N. Gangat, X. Wang, and A. Pardanani. 2015. 'A Pilot Study of the Telomerase Inhibitor Imetelstat for Myelofibrosis', *N Engl J Med*, 373: 908-19.

Tentori, L., C. Leonetti, M. Scarsella, A. Muzi, E. Mazzon, M. Vergati, O. Forini, R. Lapidus, W. Xu, A. S. Dorio, J. Zhang, S. Cuzzocrea, and G. Graziani. 2006. 'Inhibition of poly(ADP-ribose) polymerase prevents irinotecan-induced intestinal damage and enhances irinotecan/temozolomide efficacy against colon carcinoma', *FASEB J*, 20: 1709-11.

Teoh, P. J., T. H. Chung, S. Sebastian, S. N. Choo, J. Yan, S. B. Ng, R. Fonseca, and W. J. Chng. 2014. 'p53 haploinsufficiency and functional abnormalities in multiple myeloma', *Leukemia*, 28: 2066-74.

Terpos, E., E. Katodritou, M. Roussou, A. Pouli, E. Michalis, S. Delimpasi, A. Parcharidou, Z. Kartasis, A. Zomas, A. Symeonidis, N. A. Viniou, N. Anagnostopoulos, T. Economopoulos, K. Zervas, M. A. Dimopoulos, and Greece Greek Myeloma Study Group. 2010. 'High serum lactate dehydrogenase adds prognostic value to the international myeloma staging system even in the era of novel agents', *Eur J Haematol*, 85: 114-9.

Terpos, E., L. A. Moulopoulos, and M. A. Dimopoulos. 2011. 'Advances in imaging and the management of myeloma bone disease', *J Clin Oncol*, 29: 1907-15.

Tesmer, V. M., L. P. Ford, S. E. Holt, B. C. Frank, X. Yi, D. L. Aisner, M. Ouellette, J. W. Shay, and W. E. Wright. 1999. 'Two inactive fragments of the integral RNA cooperate to assemble active telomerase with the human protein catalytic subunit (hTERT) in vitro', *Mol Cell Biol*, 19: 6207-16.

Thanasoula, M., J. M. Escandell, N. Suwaki, and M. Tarsounas. 2012. 'ATM/ATR checkpoint activation downregulates CDC25C to prevent mitotic entry with uncapped telomeres', *EMBO J*, 31: 3398-410.

Therneau, T. M., R. A. Kyle, L. J. Melton, 3rd, D. R. Larson, J. T. Benson, C. L. Colby, A. Dispenzieri, S. Kumar, J. A. Katzmann, J. R. Cerhan, and S. V. Rajkumar. 2012. 'Incidence of monoclonal gammopathy of undetermined significance and estimation of duration before first clinical recognition', *Mayo Clin Proc*, 87: 1071-9.

Tiedemann, R. E., N. Gonzalez-Paz, R. A. Kyle, R. Santana-Davila, T. Price-Troska, S. A. Van Wier, W. J. Chng, R. P. Ketterling, M. A. Gertz, K. Henderson, P. R. Greipp, A. Dispenzieri, M. Q. Lacy, S. V. Rajkumar, P. L. Bergsagel, A. K. Stewart, and R. Fonseca. 2008. 'Genetic aberrations and survival in plasma cell leukemia', *Leukemia*, 22: 1044-52.

Tong, W. M., H. Ohgaki, H. Huang, C. Granier, P. Kleihues, and Z. Q. Wang. 2003. 'Null mutation of DNA strand break-binding molecule poly(ADP-ribose) polymerase causes medulloblastomas in p53(-/-) mice', *Am J Pathol*, 162: 343-52.

Tong, W. M., Y. G. Yang, W. H. Cao, D. Galendo, L. Frappart, Y. Shen, and Z. Q. Wang. 2007. 'Poly(ADP-ribose) polymerase-1 plays a role in suppressing mammary tumourigenesis in mice', *Oncogene*, 26: 3857-67.

Truong, L. N., Y. Li, L. Z. Shi, P. Y. Hwang, J. He, H. Wang, N. Razavian, M. W. Berns, and X. Wu. 2013. 'Microhomology-mediated End Joining and Homologous Recombination share the initial end resection step to repair DNA double-strand breaks in mammalian cells', *Proc Natl Acad Sci U S A*, 110: 7720-5.

Tunquist, B. J., R. D. Woessner, and D. H. Walker. 2010. 'Mcl-1 stability determines mitotic cell fate of human multiple myeloma tumor cells treated with the kinesin spindle protein inhibitor ARRY-520', *Mol Cancer Ther*, 9: 2046-56.

Tutt, A., M. Robson, J. E. Garber, S. M. Domchek, M. W. Audeh, J. N. Weitzel, M. Friedlander, B. Arun, N. Loman, R. K. Schmutzler, A. Wardley, G. Mitchell, H. Earl, M. Wickens, and J. Carmichael. 2010. 'Oral poly(ADP-ribose) polymerase inhibitor olaparib in patients with BRCA1 or BRCA2 mutations and advanced breast cancer: a proof-of-concept trial', *Lancet*, 376: 235-44.

Unsal-Kacmaz, K., and A. Sancar. 2004. 'Quaternary structure of ATR and effects of ATRIP and replication protein A on its DNA binding and kinase activities', *Mol Cell Biol*, 24: 1292-300.

Uziel, T., Y. Lerenthal, L. Moyal, Y. Andegeko, L. Mittelman, and Y. Shiloh. 2003. 'Requirement of the MRN complex for ATM activation by DNA damage', *EMBO J*, 22: 5612-21.

Vachon, C. M., R. A. Kyle, T. M. Therneau, B. J. Foreman, D. R. Larson, C. L. Colby, T. K. Phelps, A. Dispenzieri, S. K. Kumar, J. A. Katzmann, and S. V. Rajkumar. 2009. 'Increased risk of monoclonal gammopathy in first-degree relatives of patients with multiple myeloma or monoclonal gammopathy of undetermined significance', *Blood*, 114: 785-90.

Valentijn, L. J., J. Koster, D. A. Zwijnenburg, N. E. Hasselt, P. van Sluis, R. Volckmann, M. M. van Noesel, R. E. George, G. A. Tytgat, J. J. Molenaar, and R. Versteeg. 2015. 'TERT rearrangements are frequent in neuroblastoma and identify aggressive tumors', *Nat Genet*, 47: 1411-4.

van Karnebeek, C. D., S. Quik, S. Sluijter, M. M. Hulsbeek, J. M. Hoovers, and R. C. Hennekam. 2002. 'Further delineation of the chromosome 14q terminal deletion syndrome', *Am J Med Genet*, 110: 65-72.

van Steensel, B., and T. de Lange. 1997. 'Control of telomere length by the human telomeric protein TRF1', *Nature*, 385: 740-3.

van Steensel, B., A. Smogorzewska, and T. de Lange. 1998. 'TRF2 protects human telomeres from end-to-end fusions', *Cell*, 92: 401-13.

Vekemans, M. C., L. Michaux, E. Van Den Neste, and A. Ferrant. 2014. 'Long-term survival after allogeneic stem cell transplantation for advanced stage multiple myeloma', *Br J Haematol*, 166: 616-8.

Veldman, T., K. T. Etheridge, and C. M. Counter. 2004. 'Loss of hPot1 function leads to telomere instability and a cut-like phenotype', *Curr Biol*, 14: 2264-70.

Venkitaraman, A. R. 2002. 'Cancer susceptibility and the functions of BRCA1 and BRCA2', *Cell*, 108: 171-82.

Vera, E. and M. Blasco. 2012. 'Beyond average: potential for measurement of short telomeres.' *Aging*, 4:379-392

Vulliamy, T., R. Beswick, M. Kirwan, A. Marrone, M. Digweed, A. Walne, and I. Dokal. 2008. 'Mutations in the telomerase component NHP2 cause the premature ageing syndrome dyskeratosis congenita', *Proc Natl Acad Sci U S A*, 105: 8073-8.

Vyas, S., and P. Chang. 2014. 'New PARP targets for cancer therapy', *Nat Rev Cancer*, 14: 502-9.

Vyas, S., M. Chesarone-Cataldo, T. Todorova, Y. H. Huang, and P. Chang. 2013. 'A systematic analysis of the PARP protein family identifies new functions critical for cell physiology', *Nat Commun*, 4: 2240.

Wadhera, R. K., and S. V. Rajkumar. 2010. 'Prevalence of monoclonal gammopathy of undetermined significance: a systematic review', *Mayo Clin Proc*, 85: 933-42.

Wahlberg, E., T. Karlberg, E. Kouznetsova, N. Markova, A. Macchiarulo, A. G. Thorsell, E. Pol, A. Frostell, T. Ekblad, D. Oncu, B. Kull, G. M. Robertson, R. Pellicciari, H. Schuler, and J. Weigelt. 2012. 'Family-wide chemical profiling and structural analysis of PARP and tankyrase inhibitors', *Nat Biotechnol*, 30: 283-8.

Walker, B. A., P. E. Leone, L. Chiecchio, N. J. Dickens, M. W. Jenner, K. D. Boyd, D. C. Johnson, D. Gonzalez, G. P. Dagrada, R. K. Protheroe, Z. J. Konn, D. M. Stockley, W. M. Gregory, F. E. Davies, F. M. Ross, and G. J. Morgan. 2010. 'A compendium of myeloma-associated chromosomal copy number abnormalities and their prognostic value', *Blood*, 116: e56-65.

Walne, A. J., T. Vulliamy, A. Marrone, R. Beswick, M. Kirwan, Y. Masunari, F. H. Al-Qurashi, M. Aljurf, and I. Dokal. 2007. 'Genetic heterogeneity in autosomal recessive dyskeratosis congenita with one subtype due to mutations in the telomerase-associated protein NOP10', *Hum Mol Genet*, 16: 1619-29.

Wang, C., N. Jette, D. Moussienko, D. Bebb, S. Lees-Miller. 2017. 'ATM-deficient colorectal cancer cells are sensitive to the PARP inhibitor olaparib', *Trans Oncol,* 10: 190-196

Wang, R. C., A. Smogorzewska, and T. de Lange. 2004. 'Homologous recombination generates T-loop-sized deletions at human telomeres', *Cell*, 119: 355-68.

Wang, Y., J. W. Huang, P. Calses, C. J. Kemp, and T. Taniguchi. 2012. 'MiR-96 downregulates REV1 and RAD51 to promote cellular sensitivity to cisplatin and PARP inhibition', *Cancer Res*, 72: 4037-46.

Wei, W., U. Herbig, S. Wei, A. Dutriaux, and J. M. Sedivy. 2003. 'Loss of retinoblastoma but not p16 function allows bypass of replicative senescence in human fibroblasts', *EMBO Rep*, 4: 1061-6.

Weiss, C., O. Uziel, O. Wolach, J. Nordenberg, E. Beery, S. Bulvick, G. Kanfer, O. Cohen, R. Ram, M. Bakhanashvili, H. Magen-Nativ, N. Shilo, and M. Lahav. 2012. 'Differential downregulation of telomerase activity by bortezomib in multiple myeloma cells-multiple regulatory pathways in vitro and ex vivo', *Br J Cancer*, 107: 1844-52.

Wenz, C., B. Enenkel, M. Amacker, C. Kelleher, K. Damm, and J. Lingner. 2001. 'Human telomerase contains two cooperating telomerase RNA molecules', *EMBO J*, 20: 3526-34.

Weston, V., C. Oldreive, A. Skowronska, D. Oscier, G. Pratt, M. Dyer, G. Smith, J. Powell, Z. Rubzki, P. Kearns, P. Moss, M. Tayler, and T. Stankovic. 2010. 'The PARP inhibitor olaparib induces significant killing of ATM-deficient lymphoid tumour cells in vitro and in vivo', Blood. 116:4578-4587

Weterings, E., and D. J. Chen. 2008. 'The endless tale of non-homologous end-joining', *Cell Res*, 18: 114-24.

Williams, J., N. H. Heppel, B. Britt-Compton, J. W. Grimstead, R. E. Jones, S. Tauro, D. T. Bowen, S. Knapper, M. Groves, R. K. Hills, C. Pepper, D. M. Baird, and C. Fegan. 2017. 'Telomere length is an independent prognostic marker in MDS but not in de novo AML', *Br J Haematol*.

Williams, R. S., G. Moncalian, J. S. Williams, Y. Yamada, O. Limbo, D. S. Shin, L. M. Groocock, D. Cahill, C. Hitomi, G. Guenther, D. Moiani, J. P. Carney, P. Russell, and J. A. Tainer. 2008. 'Mre11 dimers coordinate DNA end bridging and nuclease processing in double-strand-break repair', *Cell*, 135: 97-109.

Win, A. K., J. P. Young, N. M. Lindor, K. M. Tucker, D. J. Ahnen, G. P. Young, D. D. Buchanan, M. Clendenning, G. G. Giles, I. Winship, F. A. Macrae, J. Goldblatt, M. C. Southey, J. Arnold, S. N. Thibodeau, S. R. Gunawardena, B. Bapat, J. A. Baron, G. Casey, S. Gallinger, L. Le Marchand, P. A. Newcomb, R. W. Haile, J. L. Hopper, and M. A. Jenkins. 2012. 'Colorectal and other cancer risks for carriers and noncarriers from families with a DNA mismatch repair gene mutation: a prospective cohort study', *J Clin Oncol*, 30: 958-64.

Wright, W. E., V. M. Tesmer, K. E. Huffman, S. D. Levene, and J. W. Shay. 1997. 'Normal human chromosomes have long G-rich telomeric overhangs at one end', *Genes Dev*, 11: 2801-9.

Wu, K. D., L. M. Orme, J. Shaughnessy, Jr., J. Jacobson, B. Barlogie, and M. A. Moore. 2003. 'Telomerase and telomere length in multiple myeloma: correlations with disease heterogeneity, cytogenetic status, and overall survival', *Blood*, 101: 4982-9.

Xin, H., D. Liu, M. Wan, A. Safari, H. Kim, W. Sun, M. S. O'Connor, and Z. Songyang. 2007. 'TPP1 is a homologue of ciliate TEBP-beta and interacts with POT1 to recruit telomerase', *Nature*, 445: 559-62.

Xu, D., N. Popov, M. Hou, Q. Wang, M. Bjorkholm, A. Gruber, A. R. Menkel, and M. Henriksson. 2001. 'Switch from Myc/Max to Mad1/Max binding and decrease in histone acetylation at the telomerase reverse transcriptase promoter during differentiation of HL60 cells', *Proc Natl Acad Sci U S A*, 98: 3826-31.

Xu, D., C. Zheng, S. Bergenbrant, G. Holm, M. Bjorkholm, Q. Yi, and A. Gruber. 2001. 'Telomerase activity in plasma cell dyscrasias', *Br J Cancer*, 84: 621-5.

Xu, Y., Y. Suzuki, K. Ito, and M. Komiyama. 2010. 'Telomeric repeat-containing RNA structure in living cells', *Proc Natl Acad Sci U S A*, 107: 14579-84.

Xue, Y., R. Gibbons, Z. Yan, D. Yang, T. L. McDowell, S. Sechi, J. Qin, S. Zhou, D. Higgs, and W. Wang. 2003. 'The ATRX syndrome protein forms a chromatin-remodeling complex with Daxx and localizes in promyelocytic leukemia nuclear bodies', *Proc Natl Acad Sci U S A*, 100: 10635-40.

Yadav, P., C. Hutchison, K. Basnayake, S. Stringer, M. Jesky, L. Fifer, K. Snell, J. Pinney, M. Drayson, M. Cook, and P. Cockwell. 'Patients with multiple myeloma have excellent long-term outcomes after recovery from dialysis-dependent acute kidney injury', *Euro Jour Haem*, 96: 610-617

Yang, Y. G., U. Cortes, S. Patnaik, M. Jasin, and Z. Q. Wang. 2004. 'Ablation of PARP-1 does not interfere with the repair of DNA double-strand breaks, but compromises the reactivation of stalled replication forks', *Oncogene*, 23: 3872-82.

Yarden, R. I., S. Pardo-Reoyo, M. Sgagias, K. H. Cowan, and L. C. Brody. 2002. 'BRCA1 regulates the G2/M checkpoint by activating Chk1 kinase upon DNA damage', *Nat Genet*, 30: 285-9.

Ye, J. Z., and T. de Lange. 2004. 'TIN2 is a tankyrase 1 PARP modulator in the TRF1 telomere length control complex', *Nat Genet*, 36: 618-23.

Ye, J. Z., D. Hockemeyer, A. N. Krutchinsky, D. Loayza, S. M. Hooper, B. T. Chait, and T. de Lange. 2004. 'POT1-interacting protein PIP1: a telomere length regulator that recruits POT1 to the TIN2/TRF1 complex', *Genes Dev*, 18: 1649-54.

Yee, A. J., W. I. Bensinger, J. G. Supko, P. M. Voorhees, J. G. Berdeja, P. G. Richardson, E. N. Libby, E. E. Wallace, N. E. Birrer, J. N. Burke, D. L. Tamang, M. Yang, S. S. Jones, C. A. Wheeler, R. J. Markelewicz, and N. S. Raje. 2016. 'Ricolinostat plus lenalidomide, and dexamethasone in relapsed or refractory multiple myeloma: a multicentre phase 1b trial', *Lancet Oncol*, 17: 1569-78.

Ying, W. Z., and P. W. Sanders. 2001. 'Mapping the binding domain of immunoglobulin light chains for Tamm-Horsfall protein', *Am J Pathol*, 158: 1859-66.

Zhan, F., Y. Huang, S. Colla, J. P. Stewart, I. Hanamura, S. Gupta, J. Epstein, S. Yaccoby, J. Sawyer, B. Burington, E. Anaissie, K. Hollmig, M. Pineda-Roman, G. Tricot, F. van Rhee, R. Walker, M. Zangari, J. Crowley, B. Barlogie, and J. D. Shaughnessy, Jr. 2006. 'The molecular classification of multiple myeloma', *Blood*, 108: 2020-8.

Zhang, C., X. Chen, L. Li, Y. Zhou, C. Wang, and S. Hou. 2015. 'The Association between Telomere Length and Cancer Prognosis: Evidence from a Meta-Analysis', *PLoS One*, 10: e0133174.

Zhang, Y., L. Y. Chen, X. Han, W. Xie, H. Kim, D. Yang, D. Liu, and Z. Songyang. 2013. 'Phosphorylation of TPP1 regulates cell cycle-dependent telomerase recruitment', *Proc Natl Acad Sci U S A*, 110: 5457-62.

Zhang, Y., and M. Jasin. 2011. 'An essential role for CtIP in chromosomal translocation formation through an alternative end-joining pathway', *Nat Struct Mol Biol*, 18: 80-4.

Zhao, Y., E. Abreu, J. Kim, G. Stadler, U. Eskiocak, M. P. Terns, R. M. Terns, J. W. Shay, and W. E. Wright. 2011. 'Processive and distributive extension of human telomeres by telomerase under homeostatic and nonequilibrium conditions', *Mol Cell*, 42: 297-307.

Zhong, F. L., L. F. Batista, A. Freund, M. F. Pech, A. S. Venteicher, and S. E. Artandi. 2012. 'TPP1 OB-fold domain controls telomere maintenance by recruiting telomerase to chromosome ends', *Cell*, 150: 481-94.

Zhou, B. B., and J. Bartek. 2004. 'Targeting the checkpoint kinases: chemosensitization versus chemoprotection', *Nat Rev Cancer*, 4: 216-25.